Protein Engineering and Structural Characterisation Approaches Aimed Towards the Improvement of Biological Therapies

Esteban Cruz

This thesis is submitted in fulfilment of the requirements for the degree of Doctor of Philosophy

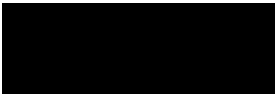School of Pharmacy

Faculty of Medicine and Health

The University of Sydney

2019

Statement of Authenticity

This thesis is submitted to the University of Sydney in fulfilment of the requirements for the degree of Doctor of Philosophy. The material included herein has not been submitted, either in full or in part, for another degree at this institution or any other. The content of this thesis is original except as acknowledged in the text accordingly.

Name: Esteban Cruz

Signature:

Date: 19$^{\text{th}}$ of August 2019

Acknowledgements

It is hard to believe that four years have already gone by since I moved all the way across the world from Costa Rica to undertake my PhD studies at the University of Sydney. It has been four years full of challenges and sacrifice, being away from my family and friends, yet I was fortunate enough to cross paths with amazing people along the way that I am now proud to call friends and mentors. I would like to first acknowledge my PhD supervisor, Associate Professor Veysel Kayser, for giving me the opportunity to embark on this journey and providing constant support and guidance throughout my candidature. I deeply appreciate the mentorship and research opportunities you provided. To my auxiliary supervisor Associate Professor Serdar Kuyucak. To my colleagues, Vicki, Mouhamad and Ziya, with whom I worked and learned extensively in the lab and shared a lot of fun moments. To our most valuable postdoc Zehra, whose contribution to the lab in the early days of our PhDs was invaluable. To Christina, who has been my friend since the start and I now consider my little sister. I'm so grateful to have met you and I'd like to thank you for all your support and all the fun we've had together. To our honours students, Jacky, Emma and Fahmi, it was great working with all of you guys. To all the new members of the group, Masoume, Qudsia, Barbaros, Mohammad, Candice, Mariam, Dua'A, Rina, and Abdul, I wish you all the best in your postgraduate studies. To all members of S114 for creating a great atmosphere to work in, especially to Ophelia who always had a bright smile (or sweets) to cheer me up, and to Luke who is a legend and taught me all about Australian culture.

I would like to express my sincerest gratitude to our Head of School, Professor Andrew MacLachlan, and our HDR coordinator, Dr. Ingrid Gelissen, with whom I've liaised constantly throughout my last year of candidature as an HDR student representative and member of the committee of the AAPS Student Chapter. The support you have provided has been spectacular and is truly inspiring for all students. To the incredible staff we have at the School of Pharmacy, who greatly facilitate our work as students. Special mention to Shane, Suley and Tim, absolute legends and some of the most generous and helpful people I've met.

Living abroad doing a PhD would have been extremely difficult without my friends' support. I would like to thank Ana and her family for their support at the start of my degree. To Ingrid, Astrid,

List of Publications

Published peer-reviewed journal articles in support of this thesis:

E. Cruz, J. Cain, B. Crossett, V. Kayser. Site-specific Glycosylation Profile of Influenza A (H1N1) Hemagglutinin Through Tandem Mass Spectrometry. Human Vaccines and Immunotherapeutics, 14(3) (2018), 508-517. [Chapter 2]

Z. Elgundi, M. Reslan, E. Cruz, V. Sifniotis, V. Kayser. The State-of-play and Future of Antibody Therapeutics. Advanced Drug Delivery Reviews, 122 (2017), 2-19. [Chapter 3]

E. Cruz, V. Kayser. Monoclonal Antibody Therapy of Solid Tumors: Clinical Limitations and Novel Strategies to Enhance Treatment Efficacy. Biologics: Targets and Therapy, 13 (2019), 33-51. [Chapter 6]

E. Cruz, V. Kayser. Synthesis and Enhanced Cellular Uptake *In Vitro* of Anti-HER2 Multifunctional Gold Nanoparticles. Cancers, 11 (2019), 870. [Chapter 7]

Submitted manuscripts in support of this thesis

M. Reslan, V. Sifniotis, E. Cruz, Z. Sumer-Bayraktar, S. Cordwell, V. Kayser (2019). Enhancing the Stability of Adalimumab by Engineering Additional Glycosylation Motifs. Biotechnology and Bioengineering. [Chapter 4]

Manuscripts prepared for submission in support of this thesis

E. Cruz, V. Sifniotis, Z. Sumer-Bayraktar, S. Cordwell, V. Kayser. (2019). Glycan Profile Analysis of Engineered Trastuzumab with Rationally Added Glycosylation Sequons for Enhanced Physical Stability. [Chapter 5]

Further published peer-reviewed publications during the candidature

V. Sifniotis, E. Cruz, B. Eroglu, V. Kayser. Currents Advancements in Addressing Key Challenges of Therapeutic Antibody Manufacture and Formulation. Antibodies. 8(2) (2019), 36.

Z. Elgundi, V. Sifniotis, M. Reslan, E. Cruz, V. Kayser. Laboratory Scale Production and Purification of a Therapeutic Antibody. Journal of Visualized Experiments, 2017 (119), 1-8.

Y. Moussa, Y. Ong, J. Perry, Z. Cheng, V. Kayser, E. Cruz, R. Kim, N. Sciortino, N. Wheate. Demonstration of *In Vitro* Host-guest Complex Formation and Safety of Para-sulfonatocalix[8]arene as a Delivery Vehicle for Two Antibiotic Drugs. Journal of Pharmaceutical Sciences, 107(12) (2018), 3105-3111.

Further manuscripts prepared for submission during the candidature

Cruz E, Kayser V. Major Classes of Biotherapeutics. In: Ramzan I, ed. Biologics, Biosimilars, and Biobetters: An Introduction for Pharmacists, Physicians and Other Health Practitioners. Wiley; To be published in 2020.

M. Reslan, E. Cruz, V. Kayser. Analysis of the aggregation kinetics of Herceptin® (trastuzumab).

Conference presentations

Cruz, E., Kayser, V. Multifunctional gold nanoparticles targeted against HER-2 amplified cells for selective delivery of cytotoxic payloads. 29th Annual Queenstown Molecular Biology Meeting. Queenstown, New Zealand. 2-4 September 2019. (Oral presentation).

Cruz, E., Kayser, V. Engineered Glycosylation Sites on Monoclonal Antibodies for Enhanced Stability. AAPS 2019 PharmSci 360. San Antonio, Texas, United States. 3-6 November 2019. (Oral presentation)

List of Abbreviations

HA	Hemagglutinin
RPLC	Reversed-phase liquid chromatography
MS	Mass spectrometry
ADC	Antibody-drug conjugate
WT	Wildtype
LC	Liquid chromatography
SE-HPLC	Size-exclusion high performance liquid chromatography
Tm	Melting temperature
Tagg	Onset temperature of aggregation
TNF-α	Tumor necrosis factor alpha
FcγR	Fc-gamma receptor
HER-2	Human epidermal growth factor receptor 2
Tmab	Trastuzumab
SH	Sulfhydryl
PEG	Polyethylene glycol
HIV	Human immunodeficiency virus
CPP	Cell-penetrating peptide
UV	Ultraviolet
Vis	Visible
DLS	Dynamic light scattering
ICP-MS	Inductively couple plasma mass spectrometry
TEM	Transmission electron microscope
DNA	Deoxyribonucleic acid
CDR	Complementarity determining regions
mAb	Monoclonal antibody
ADCC	Antibody-dependent cellular cytotoxicity

ESI	Electrospray ionisation
MALDI	Matrix-assisted laser desorption/ionisation
APCI	Atmospheric pressure chemical ionisation
DDA	Data-dependent acquisition
CID	Collision-induced dissociation
HCD	High-energy collision dissociation
ETD	Electron-transfer dissociation
ECD	Electron-capture dissociation
NA	Neuraminidase
RNA	Ribonucleic acid
NIAID	National Institute of Allergy and Infectious Disease
IRD	Influenza Research Database
PDB	Protein Data Bank
VMD	Visual Molecular Dynamics
PBS	Phosphate-buffered saline
FA	Formic acid
HPLC	High performance liquid chromatography
ER	Endoplasmic reticulum
RBS	Receptor binding site
TIC	Total ion current
FDA	United Stated Food and Drug Administration
MDCK	Madin-Darby Canine Kidney
SA	Sialic acid
EGFR	Epidermal growth factor receptor
RANK	Receptor activator of nuclear factor kappa-B
NGS	Next-generation sequencing
VH	Heavy chain
LH	Light chain
BLA	Biologics license application
IL	Interleukin

NSCLC	Non-small cell lung cancer
PD-L1	Programmed death-ligand 1
EPCAM	Epithelial cell adhesion molecule
CD	Cluster of differentiation
CFD	Complement factor D
ACVR	Activin receptor
CLL	Chronic lymphocytic leukemia
vWF	Von Willebrand factor
TTP	Thrombotic thrombocytopenic purpura
kDa	Kilodalton
sdAb	Single-domain antibody fragments
SC	Subcutaneous
CDC	Complement dependent cellular cytotoxicity
PK	Pharmacokinetics
CCR4	CC-chemokine receptor 4
PTCL	Peripheral T cell lymphoma
NK	Natural killer cells
MCC	N-maleimidomethyl cyclohexane-1-carboxylate
DVD-Ig	Dual variable domain immunoglobulin
DNL	Dock-and-Lock
BiTE	Bispecific T-cell engager
DART	Dual affinity re-targeting
MMAE	Monomethyl auristatin E
PSMA	Protein-specific membrane antigen
NHL	Non-Hodgkin's lymphoma
MMAF	Monomethyl auristatin F
DM	Maytansinoid
SMCC	N-succinimidyl-4-(N-maleimidomethyl) cyclohexane-1-carboxylate
DAR	Drug-to-antibody ratio
SEED	Strand-exchange engineered domain

DC	Dendritic cells
EMA	European Medicines Agency
HAMA	Human anti-mouse antibodies
ALL	Acute lymphoblastic leukemia
HLA	Human leukocyte antigen
TCR	Toll-like receptor
DAF	Dual-action Fab
IV	Intravenous
RSV	Respiratory syncytial virus
SAP	Surface Aggregation Propensity
BCC	Basal cell carcinoma
APR	Aggregation-prone region
AA	Amino acid
CH1	Heavy chain constant region domain 1
CH2	Heavy chain constant region domain 2
CH3	Heavy chain constant region domain 3
VH	Heavy chain variable domain
CL	Light chain constant region
VL	Light chain variable domain
PCR	Polymerase chain reaction
PEI	Polyethylenimine
SFM	Serum free media
GE	General Electric
PSM	Peptide spectrum matches
GF	Gel filtration
AUC	Area under the curve
SD	Standard deviation
SLS	Static light scattering
BC<	Barycentric mean
SPR	Surface plasmon resonance

Ka	Association rate constant
Kd	Dissociation rate constant
KD	Equilibrium dissociation constant
HEK	Human embryonic kidney
MWCO	Molecular weight cutoff
IAA	Iodoacetamide
TFA	Trifluoroacetic acid
DTT	Dithiothreitol
PVDF	Polyvinylidene difluoride
SPE	Solid-phase extraction
PGC	Porous graphitic carbon
EIC	Extracted ion chromatogram
SASA	Solvent accessible surface area
MD	Molecular dynamics
CHO	Chinese hamster ovary
ECM	Extracellular matrix
IFP	Interstitial fluid pressure
ADCP	Antibody-dependent cellular phagocytosis
MAPK	Mitogen activated protein kinase
CDK	Cyclin-dependent kinase
IGF-IR	Type 1 insulin-like growth factor receptor
TGF-α	Tumor growth factor alpha
VEGF	Vascular endothelial growth factor
AML	Acute myeloid leukemia
CTLA-4	Cytotoxic T-lymphocyte associated protein 4
TCR	T-cell receptor
APC	Antigen presenting cell
TGF-β	Tumor growth factor beta
IFN-γ	Interferon gamma
NP	Nanoparticle

EPR	Enhanced permeability and retention effect
AIDS	Acquired immunodeficiency syndrome
ICI	Immune checkpoint inhibitor
MRI	Magnetic resonance imaging
EDTA	Ethylenediaminetetraacetic acid
DTNB	5, 5'-dithiobis(2-nitrobenzoic acid)
DMSO	Dimethyl sulfoxide
TOF	Time-of-flight
FBS	Fetal bovine serum
GR	Growth rate
RES	Reticuloendothelial system
MW	Molecular weight
NHS	N-Hydroxysuccinimide
AuNP	Gold nanoparticles
PDI	Polydispersity index

Thesis Abstract

Biological therapies are currently at the forefront of pharmaceutical innovation and drug discovery. Seminal developments in molecular biology and recombinant technologies in the 1990's brought about a new era in biomedicine, inasmuch as they expanded the ability to manipulate the synthetic machinery of biological systems for the production of recombinant macromolecules with exquisite therapeutic potential and versatility. Most prominent among these developments were advances in the manufacture of humanised and human monoclonal antibodies in a streamlined fashion. Biotherapeutics then experienced a remarkable boom in the early 2000's and currently remain the fastest-growing class of therapeutics. As the field of molecular biology continues to advance at an accelerated pace, manifold opportunities are presented to implement new tools and technologies in the design of novel biotherapeutics and the refinement of existing biological therapies. The empirical research contained in this thesis reports on various approaches to address crucial aspects of the development of novel biotherapeutics, and demonstrates the application of modern mass spectrometry methods to gain insight into the complex structural features of macromolecules.

Three main aims were defined and addressed in this work. The first aim consisted in employing a tailored mass spectrometry method to acquire the site-specific glycan profile of an influenza surface glycoprotein that plays a crucial role in infectivity and antigenicity. The structural data obtained sheds light into antigenic properties of the virus that can aid in the design of recombinant vaccines. The second aim sought to evaluate a protein engineering strategy to improve the biophysical properties of monoclonal antibodies through the targeted insertion of glycosylation sites in strategic positions on the protein. The data reported demonstrates the capabilities of the technique to increase physical stability and underlines aspects that require further refinement moving forward. The final aim focused on the synthesis of a nanoparticle-based drug delivery platform that employs antibodies as targeting agents for increased treatment specificity. We demonstrated the feasibility of chemically modifying the antibody using concomitant protein functionalisation techniques to produce antibody-drug conjugates that bind to the surface of gold nanoparticles to serve as targeting agents. The synthesized nanocarrier is designed to accumulate preferentially in tumours through the enhanced permeability and retention effect, where it can subsequently engage in specific interactions with tumour cells via active-targeting of the antibody.

Altogether, the body of work presented in this thesis reports on novel experimental approaches that will aid in the design and production of next-generation biotherapeutics.

Table of Contents

Chapter 1 - Thesis Introduction

Preface

Reports of the use of biological therapies can be traced back to the 1st millennium BC, with the employment of variolation in various regions of Africa and Asia. Variolation consisted in the inoculation of patients with smallpox pathogens through the administration of dried smallpox scabs into the nose of patients to prompt immunological protection – a rudimentary form of vaccination [1, 2]. The technique eventually spread to other parts of the world and by the 18th century it had reached Europe and America. By this point, it was common knowledge in Europe that dairymaids that had been infected with cowpox (a closely related virus) from contact with the cow's udders could develop immunity against smallpox. Encouraged by this observation, English physician and scientist Edward Jenner hypothesized that cowpox could deliberately be inoculated into a patient to generate cross immunity against smallpox. Jenner tested his theory in a small subset of patients and published his work in a booklet in 1798; which, although initially criticised by the scientific community, eventually led to the spread of the technique of vaccination throughout Europe in the early 1800s [3, 4]. The medical community then devoted efforts into refining the method and developing vaccines against other infectious diseases. Louis Pasteur would later make the technique safer by introducing the principle of viral attenuation [5]. Vaccination has since become the clinical intervention with the most important contribution to global health, best reflected by the eradication of smallpox and dramatic reductions in the global incidence of polio and measles [6-8].

Biological therapies (otherwise known as biotherapeutics, biopharmaceutics, and biologics) have since come a long way. Presently, biologics comprise a wide spectrum of therapeutic classes including vaccines, monoclonal antibodies, blood components, viruses, gene therapy, enzymes, and cytokines. Seminal developments in molecular biology and recombinant DNA technologies in the 1980's and 1990's enabled the manipulation of the synthetic machinery of living organisms to efficiently produce engineered macromolecules. The field then experienced a remarkable expansion since the late 1990's with the approval of myriad recombinant products, and by 2016 biotherapeutics comprised 25% of the global pharmaceutical market [9, 10]. Most pivotal among these developments was the invention of phage display technologies and complementarity-

determining region (CDR) grafting for the production of humanised and fully-human monoclonal antibodies (mAbs) against predetermined molecular targets [11-13]. Therapeutic monoclonal antibodies now dominate the pharmaceutical market, featuring 7 of the top-10 best-selling drugs in 2018; and they continue to expand as the fastest growing class of therapeutics [14]. The astounding clinical success of mAbs has arisen from the structural and functional versatility of the molecule and the exquisite molecular specificity that they confer. On that account, tremendous research efforts are currently being devoted to implement recent technological advancements for the improvement of currently available therapeutic mAbs and the development of enhanced next-generation antibody therapeutics. Prime examples of next-generation mAbs that have already reached the clinic include antibody fragments, fusion proteins, glycoengineered antibodies, antibody-drug conjugates (ADC), and bispecific antibodies (described in further detail in chapters 3 and 6).

Most biotherapeutics are structurally complex macromolecules, among which proteins and peptides are strongly predominant. In the case of proteins, the intrinsic complexity of their primary and higher-order structures is further complicated by post-translational modifications (PTMs) (e.g., glycosylation, phosphorylation, sulfation, hydroxylation, alkylation, N-acetylation, C-terminal amidation) that have important implications in the biological activity and biophysical properties of the protein [15, 16]. Arguably the most tangible illustration of the latter is the case of mAb Fc glycosylation, wherein the absence of core fucosylation has been identified as a major determinant of antibody-dependent cellular cytotoxicity (ADCC), which has led to the development of cell lines engineered to have double knockout alleles of the enzyme responsible for fucose addition [17-19]. PTMs are mostly enzymatic processes sensitive to metabolic alterations, making it challenging to control structural heterogeneity and batch-to-batch variability. This poses significant hurdles in the analysis and characterisation of therapeutic proteins and can hinder the development of novel biotherapeutics.

In this context, mass spectrometry (MS) has become a cornerstone in structural biology and currently plays a central role in the development of protein pharmaceuticals, biological therapies and biomarker identification. Mass spectrometry methods are particularly suited for the detailed study of post-translation modifications and are hence ubiquitously employed in such quality analyses. Broadly, different MS techniques can be applied in the analysis of an extensive range of

biomolecules, ranging from small metabolites to large protein complexes [20-22]. The current prominence of MS technologies in proteomics and protein analysis stems from numerous recent advancements in instrumentation and methodologies, particularly the development of macromolecule ionisation methods, such as electrospray ionisation (ESI), matrix-assisted laser desorption/ionisation (MALDI), and atmospheric pressure chemical ionisation (APCI) [23, 24]. Modern mass spectrometers offer exquisite m/z resolution and sensitivity, being able to detect molecules in the attomolar scale (10-18). The ability to couple MS instruments online to molecule separation methods such as liquid and gas chromatography greatly improves the analysis of complex samples, which can be aided by data-dependent acquisition methods (DDA) and tailored sample preparation workflows [25-27]. DDA methods involve the selection of predetermined precursor ions within allowed m/z ranges in an initial survey scan to be subjected to a subsequent stage of mass spectrometry. This ion "filtering" step is particularly useful in the targeted detection of low-abundance analytes in complex biological samples. Moreover, analysis of the fragmentation patterns produced through various activation modes (e.g., collision-induced dissociation (CID), high-energy collision dissociation (HCD), electron-transfer dissociation (ETD) and electron-capture dissociation (ECD)) in tandem mass spectrometry allows the elucidation of highly detailed structural information, as it is showcased in the experimental work in this thesis [28, 29].

Considering the opportunities that the current wealth of knowledge in molecular biology and biotechnology provide, the overarching aim of this thesis was to implement innovative protein engineering approaches aimed towards the development of improved biotherapeutics. The following body of work compiles a series of research manuscripts that delve into key aspects of the development of new generation biological therapies, with a strong component of mass spectrometry as a pivotal tool in the structural analysis of biomolecules.

Aims and chapter description

Aim 1 (Chapter 2) – Studying the glycan profile of influenza hemagglutinin to contribute to the design of improved vaccine platforms

In contrast to the experience with antibody therapeutics and other biologicals, the development of rationally-designed recombinant vaccines for numerous infectious diseases remains elusive. In the

case of influenza, further elucidation of antigenic determinants and viral adaptation mechanisms are needed to improve rational design of recombinant platforms. Hence, we sought to make use of state-of-the-art mass spectrometry methods to study an important structural feature of the virus – the N-glycosylation profile.

Chapter 2 – "Site-specific Glycosylation Profile of Influenza A (H1N1) Hemagglutinin Through Tandem Mass Spectrometry" – of this thesis describes a mass spectrometry-based methodology for the analysis of the site-specific glycan microheterogeneity of an influenza H1N1 strain. Historically, the study of the evolution of the influenza virus dating back to the outbreak of the Spanish flu in 1918 has focused primarily on antigenic alterations in the surface glycoproteins (hemagglutinin and neuraminidase) caused by antigenic shift. These mechanisms indubitably play a critical role in viral adaptation to human immunogenic responses; however, recent reports have established that variations in the number and localisation of glycans on these proteins can have a significant contribution to antigenic masking and modulation of strain infectivity. We thus present a methodology that involves a simple preliminary fractionation and digestion step of the viral proteins obtained from whole inactivated viruses, followed by a tandem mass spectrometry setup that enables the analysis of digested glycopeptides. We employed this methodology on the hemagglutinin protein of an H1N1 strain as a proof of principle, and we were able to establish two important structural characteristics of the protein: (1) identification and confirmation of glycosylation sites, and (2) the monosaccharide composition of the glycans obtained from specific sites within the primary sequence. This site-specific analysis can easily be extended to the study of other relevant viral strains in order to obtain further insight into viral evolution and adaptation mechanisms. **Chapter 2** was published in the Human Vaccines and Immunotherapeutics journal as:

E. Cruz, J. Cain, B. Crossett, V. Kayser. Site-specific Glycosylation Profile of Influenza A (H1N1) Hemagglutinin Through Tandem Mass Spectrometry. Human Vaccines and Immunotherapeutics, 14(3) (2018), 508-517.

The implementation of state-of-the-art structural analysis techniques like the one discussed in **Chapter 2** will likely have pivotal contributions to the design of optimised treatment strategies and vaccine design. Importantly, mass spectrometry techniques can be utilized to study an extensive range of biomolecules, ranging from small metabolites to large protein assemblies. This

is further exemplified in **Chapters 4, 5 and 7,** where equivalent MS approaches were similarly employed in the development of novel antibody-based therapeutics as discussed hereafter.

Aim 2 (Chapters 3, 4, and 5) – Targeted insertion of N-glycosylation sites to improve the physical stability of antibody therapeutics

Chapter 3 – "**The State-of-play and Future of Antibody Therapeutics**" – is a comprehensive review on the current landscape of antibody therapeutics, and it serves as an introduction to **Chapter 4 – "Enhancing the Stability of Adalimumab by Engineering Additional Glycosylation Motifs" –** and **Chapter 5** – "**Glycan Profile Analysis of Engineered Trastuzumab with Rationally Added Glycosylation Sequons for Enhanced Physical Stability"** – that report on an innovative approach to produce improved "biobetter" antibodies. The chapter gives an overview of important recent developments in antibody discovery and protein engineering strategies that aim to improve the therapeutic potential of the conventional IgG molecules that predominate in the market. Special focus is given to the limitations that derive from the intrinsic propensity of antibody molecules to aggregate, which represents a recurring problem in manufacturing and development of novel antibody therapeutics. The manuscript then discusses recently developed computational tools to identify aggregation-prone regions, which can then be targeted for replacement through mutagenesis as a means to improve the intrinsic physical stability of the protein. The latter engineering approach was implemented in **Chapter 4 – "Enhancing the Stability of Adalimumab by Engineering Additional Glycosylation Motifs" –** and **Chapter 5 – "Glycan Profile Analysis of Engineered Trastuzumab with Rationally Added Glycosylation Sequons for Enhanced Physical Stability"** . This review was published in the Advanced Drug Delivery Reviews journal as:

> Z. Elgundi, M. Reslan, E. Cruz, V. Sifniotis, V. Kayser. The State-of-play and Future of Antibody Therapeutics. Advanced Drug Delivery Reviews, 122 (2017), 2-19.

The next chapter of this thesis (**Chapter 4 – "Enhancing the Stability of Adalimumab by Engineering Additional Glycosylation Motifs"**) explores a novel engineering approach to enhance the intrinsic stability of antibodies against aggregation, using the blockbuster antibody adalimumab (Humira®) as a proof-of-concept. The strategy involved the insertion of glycosylation sequons on the primary structure of adalimumab to yield "hyperglycosylated" antibodies,

possessing glycans on engineered sites where the carbohydrate can shield identified aggregation-prone regions. Various candidate mutants were produced and subsequently tested for their tendency to aggregate through accelerated stability studies. A variation of the MS method presented in **Chapter 2 – "Site-specific Glycosylation Profile of Influenza A (H1N1) Hemagglutinin Through Tandem Mass Spectrometry" –** was employed for structural characterisation of the mutants and confirmation of both the amino acid mutation and glycan attachment. Several of the tested mutants displayed enhanced thermodynamic stability, reflected by substantial increases in the melting temperature of the Fab domain where the glycan was introduced. Importantly, the mutations were performed on conserved regions of the antibody, meaning that they have potential for application on further IgG1 molecules. **Chapter 2** has been submitted to the Biotechnology and Bioengineering journal as:

M. Reslan, V. Sifniotis, E. Cruz, Z. Sumer-Bayraktar, S. Cordwell, V. Kayser (2019). Enhancing the Stability of Adalimumab by Engineering Additional Glycosylation Motifs. Biotechnology and Bioengineering.

Given the established potential of the "hyperglycosylation" approach presented in **Chapter 4 – "Enhancing the Stability of Adalimumab by Engineering Additional Glycosylation Motifs",** we sought to analyse the structural characteristics of the introduced glycans to better understand the conferred physicochemical properties. To achieve this, we performed equivalent mutations on another blockbuster antibody – trastuzumab (Herceptin®) – and carried out a detailed structural analysis of the glycan profile of the mutants. Once again, a mass spectrometry method similar to the ones presented in **Chapter 2 – "Site-specific Glycosylation Profile of Influenza A (H1N1) Hemagglutinin Through Tandem Mass Spectrometry"** and **Chapter 4 – "Enhancing the Stability of Adalimumab by Engineering Additional Glycosylation Motifs",** was employed, however the technique utilised herein was modified to obtain structural information of the carbohydrates, rather than glycopeptides. The global glycan profile of the "hyperglycosylated" mutants revealed that the added Fab glycosylation site greatly enhances the heterogeneity of glycan structures in contrast to the glycan microheterogeneity of the conserved Fc glycan. This observation reveals an important feature that will likely have to be addressed if this strategy is to be pursued in clinical development. Importantly, it was also established that most of these mutations on trastuzumab have only a minor impact on the binding affinity to biologically relevant

receptors. The latter was similarly reported for adalimumab, suggesting that the biological activity of antibodies that rely on effector functions is unlikely to be significantly altered through this strategy. **Chapter 5** is prepared for submission as:

E. Cruz, V. Sifniotis, Z. Sumer-Bayraktar, S. Cordwell, V. Kayser. (2019). Glycan Profile Analysis of Engineered Trastuzumab with Rationally Added Glycosylation Sequons for Enhanced Physical Stability.

Aim 3 (Chapter 6 and 7) – Chemical functionalisation of an antibody molecule for employment as a targeting agent in the design of a nanoparticle drug delivery platform

Chapter 6 – **"Monoclonal Antibody Therapy of Solid Tumours: Clinical Limitations and Novel Strategies to Enhance Treatment Efficacy"** – is a literature review that introduces the aim of **Chapter 7** – **"Synthesis and Enhanced Cellular Uptake In Vitro of Anti-HER2 Multifunctional Gold Nanoparticles"** – that reports on an alternative approach to harness the specificity of antibody molecules to produce antibody-targeted nanoparticle delivery systems. The manuscript outlines critical challenges in the treatment of non-haematological cancers with monoclonal antibodies related to the architectural features of solid tumours. It emphasizes the importance of improving tumour penetration and distribution upon systemic delivery of an anticancer agent to prevent exposure to sub-therapeutic concentrations. It then briefly describes various novel strategies currently implemented or undergoing preclinical development to address such challenges. These include: (1) antibody-drug conjugates that aim to enhance intrinsic potency while maintaining selectivity, (2) antibody-based immune checkpoint inhibitors that can release the breaks of the immune anti-cancer response, and (3) nanoparticle formats that preferentially accumulate in solid tumours and can be granted further tumour-selectivity through the attachment of antibody molecules. This chapter is published in the Biologics: Targets and Therapy journal as:

E. Cruz, V. Kayser. Monoclonal Antibody Therapy of Solid Tumours: Clinical Limitations and Novel Strategies to Enhance Treatment Efficacy. Biologics: Targets and Therapy. 13 (2019), 33-51.

Chapter 7 describes the synthesis of antibody-targeted nanoparticle formats designed for enhanced specificity towards HER2-positive tumours. Preferential accumulation of nanosized

materials has been validated in a wide range of mouse tumour models, and there is clinical evidence in human patients to support this effect. Enhanced localisation stems from the increased leakiness of tumour vasculature and concomitant impaired lymphatic drainage, leading to nanoparticles extravasation and accumulation, respectively. Hence, nanoparticles constitute an appealing vehicle for selective delivery of cytotoxic payloads to solid tumours. In this chapter, we employed gold nanoparticles as drug carriers due to their proven biocompatibility and ease of surface functionalisation. Taking advantage of the latter, the nanoparticles were granted further tumour specificity via surface-attachment of a trastuzumab (anti-HER2) antibody-drug conjugate. Trastuzumab was chemically modified to enable attachment of a potent cytotoxic agent (monomethyl auristatin E) via a cleavable linker for selective intracellular release. The antibody was then bound to the nanoparticle surface via a stable SH-gold bond through a polyethylene glycol linker. The nanoparticle format was tested in *in vitro* experiments, where it displayed enhanced cellular uptake and a potent cytotoxic activity in HER2-amplified cell lines. This manuscript demonstrates the feasibility of employing antibody-drug conjugates as a potentially superior active-targeting agent for payload delivery in solid tumours. **Chapter 7** is published in the Cancers journal as:

E. Cruz, V. Kayser. Synthesis and Enhanced Cellular Uptake *In Vitro* of Anti-HER2 Multifunctional Gold Nanoparticles. Cancers, 11 (2019), 870.

Notes on the format of the chapters

Chapters 2-7 have been published, submitted, or prepared for publication. In the case of published and submitted material, the content included is identical to that of the published article, with the exception that some formatting changes have been made to standardise the style throughout the thesis. These formatting changes include a rearrangement of the order of the sections in some chapters, so that all research manuscripts are organised in the following order:

1.   Introduction

2.   Methods

3.   Results

4.   Discussion

5.   Conclusions

The format of the references has also been modified, so that all chapters follow the same style.

References

[1] S. Riedel, Edward Jenner and the history of smallpox and vaccination, Proc (Bayl Univ Med Cent), 18 (2005) 21-25.

[2] A.J. Stewart, P.M. Devlin, The history of the smallpox vaccine, Journal of Infection, 52 (2006) 329-334.

[3] M.R. Hilleman, Vaccines in historic evolution and perspective: a narrative of vaccine discoveries, Vaccine, 18 (2000) 1436-1447.

[4] P. Bonanni, J.I. Santos, Vaccine evolution, Perspectives in Vaccinology, 1 (2011) 1-24.

[5] S.A. Plotkin, S.L. Plotkin, The development of vaccines: how the past led to the future, Nature Reviews Microbiology, 9 (2011) 889.

[6] B. Greenwood, The contribution of vaccination to global health: past, present and future, Philos Trans R Soc Lond B Biol Sci, 369 (2014) 20130433-20130433.

[7] G.A. Shchelkunova, S.N. Shchelkunov, 40 Years without Smallpox, Acta naturae, 9 (2017) 4-12.

[8] A.S. Bandyopadhyay, J. Garon, K. Seib, W.A. Orenstein, Polio vaccination: past, present and future, Future Microbiology, 10 (2015) 791-808.

[9] R.L. Lalonde, P. Honig, Clinical Pharmacology in the Era of Biotherapeutics, Clinical Pharmacology & Therapeutics, 84 (2008) 533-536.

[10] E. Moorkens, N. Meuwissen, I. Huys, P. Declerck, A.G. Vulto, S. Simoens, The Market of Biopharmaceutical Medicines: A Snapshot of a Diverse Industrial Landscape, Front Pharmacol, 8 (2017) 314-314.

[11] B. Kotlan, M.C. Glassy, Antibody phage display: overview of a powerful technology that has quickly translated to the clinic, Methods in molecular biology (Clifton, N.J.), 562 (2009) 1-15.

[12] P.T. Jones, P.H. Dear, J. Foote, M.S. Neuberger, G. Winter, Replacing the complementarity-determining regions in a human antibody with those from a mouse, Nature, 321 (1986) 522-525.

[13] A. Harding, Profile: Sir Greg Winter—humaniser of antibodies, The Lancet, 368 (2006) S50.

[14] L. Urquhart, Top drugs and companies by sales in 2018, Nature Reviews Drug Discovery, 18 (2019) 145.

[15] F.M. Klis, A.F.J. Ram, R.C. Montijn, J.C. Kapteyn, L.H.P. Caro, J.H. Vossen, M.A.A. Van Berkel, S.S.C. Brekelmans, H. Van den Ende, 13 Posttranslational Modifications of Secretory Proteins, in: A.J.P. Brown, M. Tuite (Eds.) Methods in Microbiology, Academic Press1998, pp. 223-238.

[16] G. Walsh, R. Jefferis, Post-translational modifications in the context of therapeutic proteins, Nature biotechnology, 24 (2006) 1241-1252.

[17] O. Popp, S. Moser, J. Zielonka, P. Ruger, S. Hansen, O. Plottner, Development of a pre-glycoengineered CHO-K1 host cell line for the expression of antibodies with enhanced Fc mediated effector function, mAbs, 10 (2018) 290-303.

[18] C. Ferrara, P. Brunker, T. Suter, S. Moser, U. Puntener, P. Umana, Modulation of therapeutic antibody effector functions by glycosylation engineering: influence of Golgi enzyme localization domain and co-expression of heterologous beta1, 4-N-acetylglucosaminyltransferase III and Golgi alpha-mannosidase II, Biotechnology and bioengineering, 93 (2006) 851-861.

[19] K. Garber, No added sugar: antibody makers find an upside to 'no fucose', Nature biotechnology, 36 (2018) 1025-1027.

[20] D. Rathore, A. Faustino, J. Schiel, E. Pang, M. Boyne, S. Rogstad, The role of mass spectrometry in the characterization of biologic protein products, Expert review of proteomics, 15 (2018) 431-449.

[21] N. Iwamoto, T. Shimada, Recent advances in mass spectrometry-based approaches for proteomics and biologics: Great contribution for developing therapeutic antibodies, Pharmacology & therapeutics, 185 (2018) 147-154.

[22] R. O'Flaherty, I. Trbojevic-Akmacic, G. Greville, P.M. Rudd, G. Lauc, The sweet spot for biologics: recent advances in characterization of biotherapeutic glycoproteins, Expert review of proteomics, 15 (2018) 13-29.

[23] J.B. Fenn, M. Mann, C.K. Meng, S.F. Wong, C.M. Whitehouse, Electrospray ionization for mass spectrometry of large biomolecules, Science (New York, N.Y.), 246 (1989) 64-71.

[24] R. Aebersold, D.R. Goodlett, Mass Spectrometry in Proteomics, Chemical Reviews, 101 (2001) 269-296.

[25] V. Vidova, Z. Spacil, A review on mass spectrometry-based quantitative proteomics: Targeted and data independent acquisition, Analytica Chimica Acta, 964 (2017) 7-23.

[26] A. Lesur, B. Domon, Advances in high-resolution accurate mass spectrometry application to targeted proteomics, 15 (2015) 880-890.

[27] L.C. Gillet, A. Leitner, R. Aebersold, Mass Spectrometry Applied to Bottom-Up Proteomics: Entering the High-Throughput Era for Hypothesis Testing, Annual review of analytical chemistry (Palo Alto, Calif.), 9 (2016) 449-472.

[28] P. Roepstorff, J. Fohlman, Proposal for a common nomenclature for sequence ions in mass spectra of peptides, Biomedical mass spectrometry, 11 (1984) 601.

[29] J.S. Brodbelt, Ion Activation Methods for Peptides and Proteins, Anal Chem, 88 (2016) 30-51.

Chapter 2

Site-specific Glycosylation Profile of Influenza A (H1N1) Hemagglutinin through Tandem Mass Spectrometry
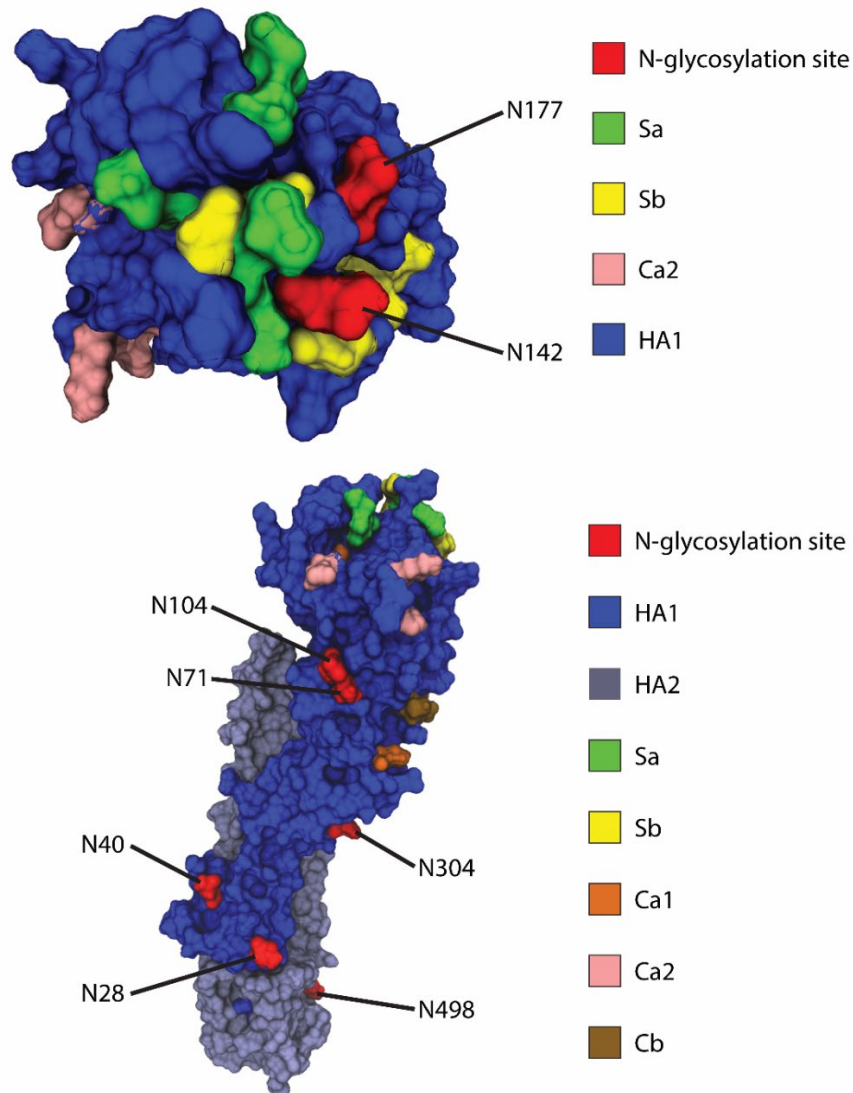
Chapter 2 – Authorship declaration statement

The following chapter is a full research article published in the journal Human Vaccines and Immunotherapeutics as:
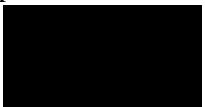
E. Cruz, J. Cain, B. Crossett, V. Kayser. Site-specific Glycosylation Profile of Influenza A (H1N1) Hemagglutinin Through Tandem Mass Spectrometry. Human Vaccines and Immunotherapeutics, 14(3) (2018), 508-517.

E. Cruz co-designed the study, performed all experimental work and data analysis and wrote the manuscript.

Permission to include the published material has been granted by the corresponding author.

Esteban Cruz, Signature: 19th of August, 2019

As corresponding author and supervisor for this candidature, I hereby confirm that this authorship declaration statement is complete and accurate

Veysel Kayser, Signature: 19th of August, 2019

Abstract

The study of influenza virus evolution in humans has revealed a significant role of glycosylation profile alterations in the viral glycoproteins – hemagglutinin (HA) and neuraminidase (NA), in the emergence of both seasonal and pandemic strains. Viral antigenic drift can modify the number and location of glycosylation sites, altering a wide range of biological activities and the antigenic properties of the strain. In view of the key role of glycans in determining antigenicity, elucidating the glycosylation profiles of influenza strains is a requirement towards the development of improved vaccines. Sequence-based analysis of viral RNA has provided great insight into the role of glycosite modifications in altering virulence and pathogenicity. Nonetheless, this sequence-based approach can only predict potential glycosylation sites. Due to experimental challenges, experimental confirmation of the occupation of predicted glycosylation sites has only been carried out for a few strains. Herein, we utilized HCD/CID-MS/MS tandem mass spectrometry to characterize the site-specific profile of HA of an egg-grown H1N1 reference strain (A/New Caledonia/20/1999). We confirmed experimentally the occupancy of glycosylation sites identified by primary sequence analysis and determined the heterogeneity of glycan structures. Four glycosylation sequons on the stalk region (N28, N40, N303 and N497) and four on the globular head (N71, N104, N142 and N177) of the protein are occupied. Our results revealed a broad glycan microheterogeneity, i.e., a great diversity of glycan compositions present on each glycosite. The present methodology can be applied to characterize other viruses, particularly different influenza strains, to better understand the impact of glycosylation on biological activities and aid the improvement of influenza vaccines.

Introduction

Influenza viruses undergo a high rate of antigenic drift, leading to gradual antigenic modifications that are responsible for the persistent emergence of seasonal influenza strains. Occasional antigenic shift (viral reassortments) can also lead to pandemic outbreaks that pose a serious public health threat [1, 2]. The production of immunological memory after a primary exposure (through infection or vaccination) to influenza is essential to trigger an accelerated and efficacious immune response to subsequent infection [3, 4]. For this reason, it is crucial to elucidate the mechanisms that prompt such response and determine the viral antigens that elicit the generation of immunological memory.

The selection of annual strains for influenza vaccines relies on detailed characterization of the genetic and antigenic features of circulating viruses [5]. Due to their surface exposure, the envelope glycoproteins NA and HA play a prominent role in host immune cell recognition and are considered to be the main antigenic determinants in the virus [6, 7]. Influenza A viruses are thus further classified into subtypes according to the antigenic variants of their surface glycoproteins – 18 HA (H1-H18) and 11 NA (N1-N11) subtypes [8]. HA is the most abundant protein in the viral envelope and is consequently also the focal point of virus surveillance [9].

The antigenic sites in HA are comprised mainly of polypeptide regions on the globular head; however, it has been demonstrated that the presence of glycans in the proximity of these sites can affect its biological activity, thereby altering immune cell recognition and receptor binding specificity [10, 11]. HA undergoes N-linked glycosylation (no O-glycosylation has been reported), whereby glycans are attached to asparagine residues within the consensus sequence Asn-Xaa-Ser (Xaa can be any amino acid except proline) [12, 13]. Hemagglutinin assembles as a homotrimer that displays a surface-exposed globular head formed by part of the HA1 chain, whereas the stalk region is comprised mostly of α-helix coils and a transmembrane domain from HA2 [9]. Both the stalk and the head region are often heavily glycosylated, and glycan attachment can affect a wide spectra of biological properties, such as immunogenicity, virulence and receptor specificity [14, 15]. Overall, glycan attachment on the stalk region is highly conserved, and glycans on this area play a critical role in correct protein folding and membrane transport [16, 17]. Conversely, the globular head of HA exhibits a considerably higher rate of variation. Most antigenic sites are found on the HA head, therefore modifications on this region usually impair immune recognition [18, 19].

Influenza subtype H1 has undergone extensive alteration over time in the number and position of glycans attached, mostly on the globular head [20]. These modifications are associated with adaptation mechanisms caused by antigenic drift, whereby novel virus subtypes avoid host cell immune recognition by masking antigenic regions through the variation in the localization or number of glycosites [20, 21].

The consensus sequons required for N-glycosylation make it possible to analyse glycosylation occupancy profiles by searching for potential acceptor sites in the primary sequence of proteins. Sequence-based analysis of potential glycosylation sites on H1 has revealed that in the early stages

of virus evolution after the outbreak of the 1918 pandemic, the H1N1 virus subtype predominantly increased the number of glycosylation sites on its globular head. However, following 1950, the number of sites remained somewhat constant and the alteration in position became the prominent feature [20]. Strikingly, the H1 of the 2009 swine flu pandemic virus resembles the 1918 pandemic H1 not only in its antigenic epitopes, but also in that they both lack glycosylation sites near the Sa antigenic site [22, 23]. This absence of shielding glycans was an important factor contributing to the pathogenicity of the 1918 pandemic strain [14].

Although sequence-based glycosylation analysis has substantially contributed to the understanding of virus evolution, the information obtained through this method is only limited, as the sequons it identifies are not necessarily occupied [24]. For this reason, there remains the need to confirm site occupancy experimentally. Moreover, it is important to assess whether differences in glycoforms exist among strains, and determine if the potential variations have an impact on biological properties. To this end, mass spectrometry based methods, especially those based on collision-induced dissociation (CID), higher-energy collision dissociation (HCD), electron-capture dissociation (ECD) and electron-transfer dissociation (ETD), are particularly suited to analyse protein posttranslational modifications [25, 26]. However, due to the experimental challenges that N-glycoproteomic analysis poses, characterization of site-specific glycosylation profiles has only been carried out for a few strains.

In this study, we employed HCD/CID tandem mass spectrometry to map glycosylation sites and characterize the glycan microheterogeneity (i.e., the subset of glycan structures on each particular position within the protein) of an egg-grown A/New Caledonia/20/1999 H1N1 reference strain. We confirmed the occupancy of eight glycosylation sites on this reference strain – four on the stalk and four on the globular head. This profile was consistent to the one obtained through sequence-based analysis using the NetNGlyc server for prediction of glycosylation potential. Moreover, a great diversity of glycan compositions was found on those positions close to the Sa antigenic site, which could have important implications on the antigenicity of the strain.

Materials and Methods

N-glycosylation sequon analysis of A/New Caledonia/20/1999 HA

The amino acid sequence for the A/New Caledonia/20/1999 HA was obtained from the National Institute of Allergy and Infectious Disease (NIAID) Influenza Research Database (IRD) [43]. through the web site at http://fludb.org. NetNGlyc 1.0 Server [24] was used for the prediction of potential glycosylation sites. NetNGlyc 1.0 Server utilizes several artificial neural networks that are able to predict the probability of an N-glycosylation motif to be occupied by analysing the adjacent primary sequence. The server sets a default threshold of 0.5, whereby a higher value indicates a predicted glycosylated residue.

Homology modelling of A/New Caledonia/20/1999 HA

The homology model of A/New Caledonia/20/1999 HA was created with Prime (Schrödinger) using H2 (PDB entry 2WR3, chain A) as a template. The molecular structures were generated using VMD 1.9.3.

Hemagglutinin isolation through polyacrylamide electrophoresis and in-gel trypsin digestion

Egg-grown A/New Caledonia/20/1999 virus samples were provided by Sanofi-Pasteur (PA-US). Viral proteins were separated by means of reducing SDS-PAGE by running whole virus samples (suspended in PBS) on a 10% home-made bis-acrylamide gel. The virus suspension was diluted with SDS-PAGE sample buffer containing 1% 2-Mercaptoethanol and 2% SDS. The samples were boiled at 95 °C for 10 minutes before loading onto the gel. The gel was stained with Coomassie Brilliant Blue R-250 overnight, and the bands corresponding to HA0 monomers, HA1 and HA2 were excised from the gel. The bands were subsequently destained using 40% (v/v) acetonitrile and dried using a vacuum concentrator prior to incubation with 5 μL 12 mg/mL trypsin (Promega) at 4 °C for 1 hour. 20 μL of NH_4HCO_3 50 mM pH 6.8 were added and incubated overnight to extract the proteins from the gel.

Analysis of tryptic peptides and glycopeptides by nanoRPLC-MS/MS

The tryptic peptide fraction was first desalted using a C18 ZipTip (Millipore) and eluted with 80% (v/v) acetonitrile. The desalted peptides were then dried by vacuum centrifugation and resuspended

in 0.1% formic acid (FA) prior to loading onto the nanoRPLC column. The glycopeptide solution was loaded onto an in-house packed 20 cm x 75 μm Reprosil-Pur C18AQ (3 μm, 120 A; Dr. Maisch GmbH) column/emitter using an easy nanoLC II HPLC (Proxeon). HPLC separation was carried out over 140 minutes at a flow rate of 250 nL/min using a 0-40% solvent B gradient, where solvent A consists in 0.1% (v/v) formic acid and solvent B is 90% (v/v) acetonitrile and 0.1% formic acid. Instrument parameters were set up as follows: source voltage = 2.0 kV, S-lens RF level = 68%, and capillary temperature = 275 °C. MS analysis was performed with an Orbitrap Velos Pro MS (Thermo Scientific). The initial MS scan was collected in the Orbitrap mass analyser (300-1,700 m/z; MS AGC = 1 x 10^{+6}) with a resolution of 30,000 at 300 m/z. The three most intense precursors were then selected for fragmentation using either data-dependent higher-energy collisional dissociation (HCD) or collision induced (CID) fragmentation. HCD parameters were as follows: activation time = 0.1 ms, resolution = 7,500, maximum injection time = 500 ms, dynamic exclusion = enabled with repeat count 1, normalized energy = 45, exclusion duration = 60 s, default charge state = 2, and MSn AGC 2 x 10,000. CID parameters as follows: activation time = 10 ms, maximum injection time = 300 ms, dynamic exclusion = enabled with repeat count 1, normalized energy = 35, exclusion duration = 30 s, default charge state = 2, and MSn AGC = 2 x 10^{+4}.

Analysis of MS/MS spectra of intact N-glycopeptides

The MS data was processed with Proteome Discoverer 2.0 (Thermo Scientific), with HCD scans searched using Byonic (Protein Metrics Inc.). The search was performed against an influenza A virus (A/New Caledonia/20/1999) and Chicken protein sequence databases using the following settings: Full trypsin specificity with a maximum of two missed cleavages, an MS tolerance of 20 ppm and a MS2 tolerance of 0.05 Da. A total of 3 common1 modifications (deamidation of asparagine and glutamine – +0.984016, cysteine propionamide – +71.037114 and asparagine glycosylation) were allowed and one total rare modification (oxidation of methionine – +15.994915 Da). The N-glycan database (309 mammalian no sodium) available in the Byonic search engine was chosen for N-linked modification. HCD spectra were manually inspected to confirm the matched glycopeptide fragmentation pattern and the presence of diagnostic HexNAc oxonium ions. CID spectra were manually inspected to validate the predicted glycan composition by manual annotation.

Results

Prediction of N-glycosylation sites

Prior to tandem mass spectrometry analysis, the amino acid sequence of the A/New Caledonia/20/1999 H1N1 strain was scanned to identify potential N-glycosylation sequons using the NetNGlyc 1.0 server. Figure 1 shows the predicted sites and table 1 displays the potential assigned for glycosylation for each sequon.
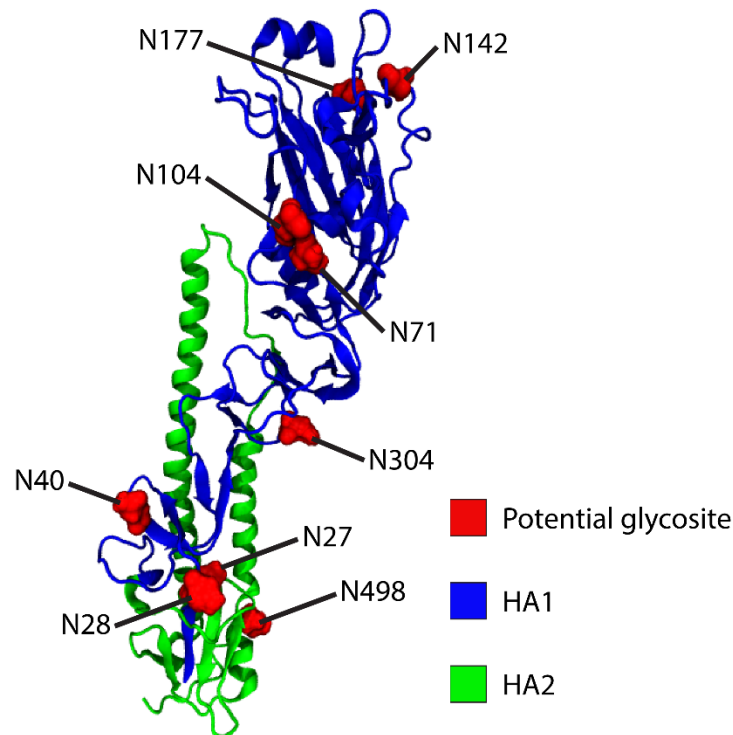
Figure 1. Location of potential N-glycosylation sites within A/New Caledonia/20/1999 H1. Monomeric H2 (PDB entry, 2WR3) was used as a template to generate the homology model of A/New Caledonia/20/1999 H1.

Table 1. Estimated glycosylation potential of the glycosylation sequons identified using the NetNGlyc 1.0 server

Residue number	Position	Sequence	Potential assigned
27	Stalk	NNST	0.4009
28	Stalk	NSTD	0.7964
40	Stalk	NVTV	0.7477
71	Side of head	NCSV	0.7470
104	Side of head	NGTC	0.6300
142	Top of head	NHTV	0.6911
177	Top of head	NLSK	0.7380
303	Stalk	NSSL	0.6707
498	Stalk	NGTY	0.5190
557	Cytoplasmic domain	NGSL	0.6833

A total of 10 sequons were identified within the amino acid sequence of the strain using the NetNGlyc 1.0 server. Four of these sites are located on the globular head (N71, N104, N142 and N177), five on the stalk (N27, N28, N71, N303 and N498) and one on the cytoplasmic tail (N557). With the exception of asparagine N27, all other sequons were predicted to be glycosylated (Fig. 1). The case of N27 is exceptional as its adjacent N28 residue is also a potential acceptor site, but only N28 yields a positive result (≥ 0.5).

Mass spectrometry analysis of electrophoretically-fractionated viral proteins

The first step in sample preparation for mass spectrometry involved a preliminary fractionation of the viral proteins from a whole inactivated virus sample suspension through SDS-PAGE. This isolation step was performed in order to reduce sample complexity prior to nanoLC-MS/MS analysis.

Following gel extraction and trypsin digestion, bands 1-6 (Fig. 2) were subjected to a preliminary nanoLC-MS/MS analysis to identify the bands where HA was present. The whole inactivated virus samples used in this analysis are produced in embryonated chicken eggs, thus the Byonic search was conducted against the strain's proteome database and then against a chicken proteome database. This last step allowed for the detection of remnant chicken proteins from the purification steps of the whole virus stock suspension, which also improves the confidence of viral protein matches in this case.
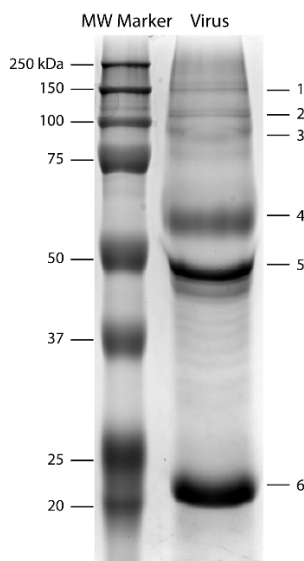
Figure 2. Reducing SDS-PAGE of whole inactivated A/New Caledonia/20/1999 H1N1 virus. The numbering on the virus lane indicates an arbitrarily-assigned order to identify the prominent protein bands obtained through viral fractionation that were subjected to nanoLC-MS/MS analysis.

HA was predominantly detected in band 4 (~60 kDa). This band also yielded the greater HA protein coverage (53%) among all the bands (supplementary table 1). Subunits HA1 and HA2 were detected in bands 5 (~50 kDa) and 6 (~22 kDa), respectively, and were subjected to glycopeptide analysis. Moreover, peptides from HA were identified in bands 1 and 2, likely due to the presence of hemagglutinin trimers and dimers. The overall protein coverage of HA across all bands was 71.5%.

Glycopeptide analysis

Bands 4-6 (Fig. 2) were then analysed to characterize the glycosylation profile of hemagglutinin. Precursor glycopeptide ions subjected to HCD yield several diagnostic oxonium ions. Diagnostic ions at 204.08 m/z (HexNAc + H) and 366.14 m/z (Hex(1)HexNAc(1) + H)) are typically present in HCD spectra of glycosylated peptides. The HCD spectra were used in this study to assign peptide identity. The higher dissociation energy of HCD allows for the fragmentation of the peptide backbone, whereby the presence of b and y ions in the spectrum is matched by Byonic to the theoretical fragmentation patterns of the tryptic peptides to score the PSMs (peptide spectral matches) and assign identity. Figure 3A shows a representative HCD spectra displaying the diagnostic oxonium ions at 186.076, 204.087 and 366.140 along with b and y ions for the reported peptide. Other peptide + fragmented glycan ions (Y ions, e.g., peptide+HexNAc, peptide+HexNAc(2)) detected through HCD can also be instrumental to manually validate the peptide identity assigned by the search engine. The peptide backbone mass can be inferred from the trimannosyl ions detected in the HCD/CID-MS/MS spectrum pairs. The theoretical Y ions are then matched to the HCD/CID-MS/MS spectrum pair to validate the spectral matches. Byonic derives the mass of the glycan by calculating the mass difference between the precursor ion (peptide + glycan) and the identified tryptic peptide, which is then used to predict the composition of the oligosaccharide by searching this value against the mammalian glycan database within the engine. Byonic is thus able to predict glycoforms to the level of monosaccharide composition.
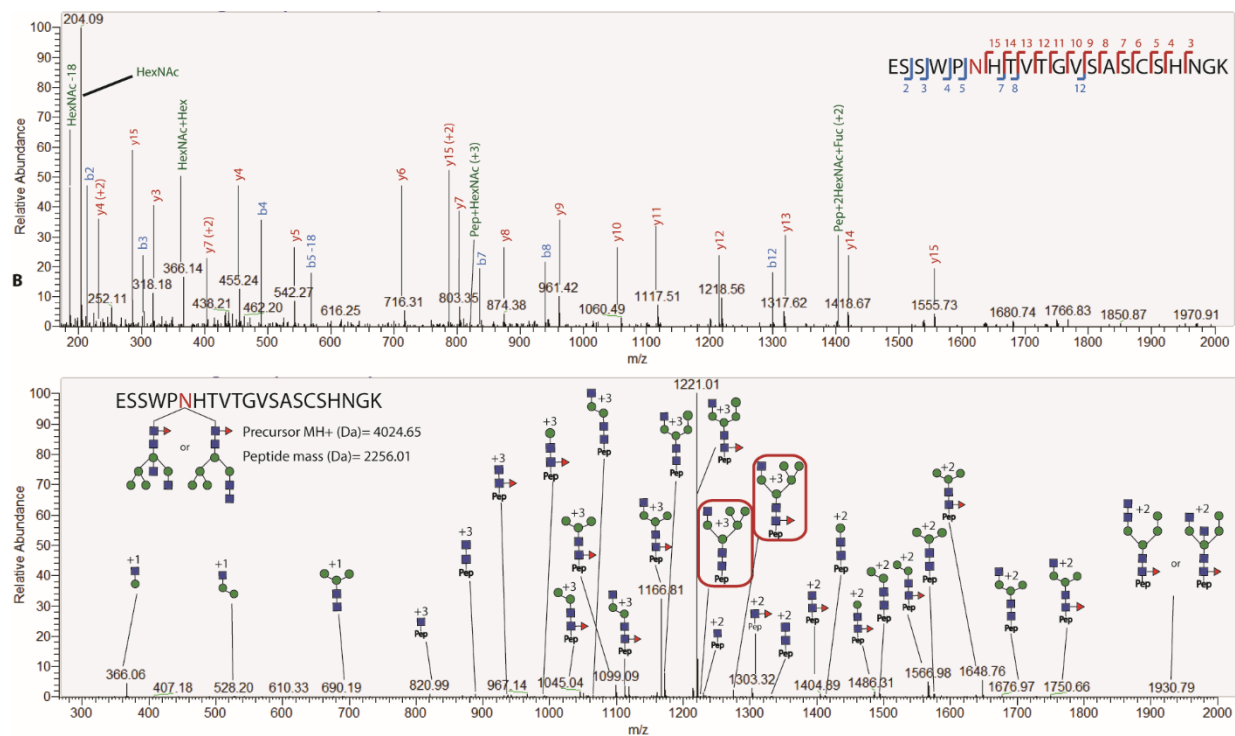
Figure 3. Representative CID and HCD spectra of H1 glycopeptides. (A) Annotated HCD spectrum of glycopeptide ESSWPNHTVTGVSASCSHNGK. The spectrum exhibits the diagnostic oxonium ion at 204.08 m/z and the presence of b and y ions derived from backbone fragmentation. (B) Annotated CID spectrum of glycopeptide ESSWPNHTVTGVSASCSHNGK with an attached glycan with a HexNAc(4)Hex(5)Fuc(1) composition. Sequential glycan fragmentation is predominant in the spectrum and allows for the validation of predicted glycan composition. The presence of a core fucose can be confirmed by the detection of ion Pep+2HexNAc-Fuc in both the HCD and CID spectra.

A complementary CID fragmentation of each precursor ion also allows for the validation of the predicted glycan composition from the Byonic server. Figure 3B displays the CID spectrum of the same precursor ion as the one used for HCD in figure 3A. In this HCD/CID setup, CID causes predominantly the cleavage of glycosidic bonds, resulting in the sequential fragmentation of the glycan. The glycan information derived from low-energy CID is limited, since it does not generate cross-ring fragmentation to elucidate linkage information, nor does it allow to differentiate between glycan isomers in many cases or elucidate topology. Still, the sequential fragmentation enables the elucidation of glycan monosaccharide compositions, by which the prediction from the engine can be manually validated. Consequently, predicted glycan compositions from

glycopeptides with a high byonic score for the HCD spectrum were subjected to manual interpretation.

Confirmation of glycosylated residues

Eight out of the nine predicted glycosylation sites were confirmed to be occupied. Four of these sites are on the stalk region (N28, N40, N304 and N498) and four on the globular head (N71, N104, N142 and N177). Figure 4 displays the location of these sequons on a 3D structure homology model of the hemagglutinin monomer. Prediction for asparagine 557 was positive, however, no peptide was detected for the cytosolic domain nor the transmembrane domain of HA, suggesting that only the ectodomain of the protein can be characterized using this sample preparation. Inasmuch as these domains are unlikely to play an important role in immunogenic response – since they are not exposed to the surface to influence in host cell recognition and have not been related to virulence, obtaining glycosylation information for N557 was deemed unnecessary. Furthermore, it is not expected for glycosylation site N557 to be occupied given its location in the cytosolic region of the protein.
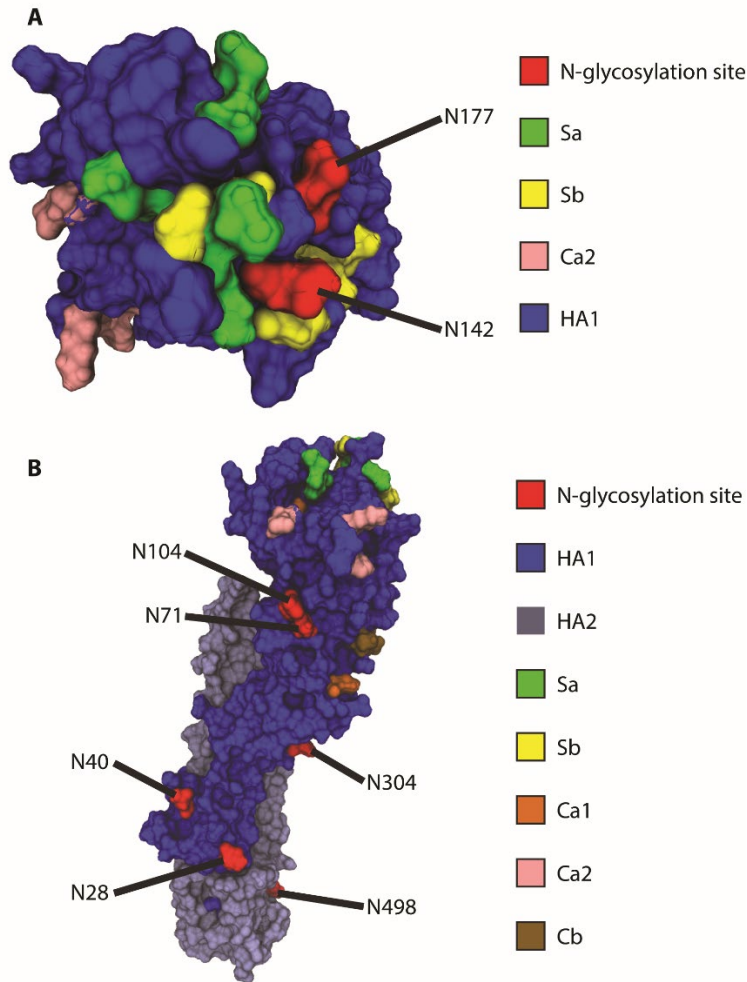
Figure 4. Location of confirmed glycosylation sites in relation to the most relevant antigenic sites on A/New Caledonia/20/1999 H1. (A) View of the globular head of H1 from the top. (B) View of H1 from the side to highlight the distribution of glycosites along the stalk region and the side of the globular head. Monomeric H2 (PDB entry, 2WR3) was used as a template to generate the homology model of A/New Caledonia/20/1999 H1.

Glycan microheterogeneity profile

Table 2 shows the glycan monomeric compositions found through HCD/CID-MS/MS on each glycosylation site within H1. Overall, glycan heterogeneity was quite broad, especially for sites N142 and N498.

Table 2. Microheterogeneity of A/New Caledonia/20/1999 H1.

Position of glycan attachment within the protein sequence	Predicted glycan composition	Ion detected (m/z)	Glycan mass (Da)	$\Delta_{m/z}$ (Da)
Site 1: Asparagine 28 (NSTD) Stalk	HexNAc(5)Hex(3)	1,389.59 (+6)	1, 501.55	-0.3369
Site 2: Asparagine 40 (NVTV) Stalk	HexNAc(5)Hex(8)Fuc(1)	1,474.63 (+3)	2, 457.87	0.0079
	HexNAc(5)Hex(6)	988.68 (+4)	1, 987.71	0.00022
Site 3: Asparagine 71 (NCSV) Side of the head	HexNAc(3)Hex(5)NeuGc(1)	1,564.69 (+3)	1, 726.59	-0.36158
Site 4: Asparagine 104 (NGTC) Side of the head	HexNAc(7)Hex(3)Fuc(1)	1,389.85 (+4)	2, 053.77	0.27418
	HexNAc(2)Hex(3)	1,081.43 (+4)	892.31	-0.001997
Site 5: Asparagine 142 (NHTV) Top of the head	HexNAc(6)Hex(6)Fuc(1)	1,149.22 (+4)	2, 336.85	0.00096
	HexNAc(6)Hex(5)	1,054.67 (+4)	2, 028.74	0.24239
	HexNAc(6)Hex(4)NeuAc(1)	1,104.64 (+4)	2, 157.78	0.25827
	HexNAc(6)Hex(4)Fuc(1)	1, 068.44 (4)	2, 012.74	0.24967

HexNAc(6)Hex(4)	953.60 (+5)	1, 866.68	0.00167
HexNAc(6)Hex(3)Fuc(1)NeuAc(1)	1,466.57 (+3)	2, 141.78	-0.35536
HexNAc(6)Hex(3)Fuc(2)	1,046.42 (+4)	1, 996.75	-0.00844
HexNAc(6)Hex(3)	991.16 (+4)	1, 704.63	0.00043
HexNAc(5)Hex(6)Fuc(2)	1,134.72 (+4)	2, 279.82	0.00087
HexNAc(5)Hex(6)Fuc(1)	1,098.45 (+4)	2, 133.77	0.00237
HexNAc(5)Hex(6)	1,061.70 (+4)	1, 987.71	-0.24352
HexNAc(5)Hex(5)Fuc(3)	1,130.96 (+4)	2, 263.83	0.00054
HexNAc(5)Hex(5)Fuc(2)	1,094.45 (+4)	2, 117.77	0.00123
HexNAc(5)Hex(5)Fuc(1)	1,057.94 (+4)	1, 971.71	0.0035
HexNAc(5)Hex(5)	1,021.42 (+4)	1, 825.66	-0.00022
HexNAc(5)Hex(4)NeuAc(1)	1,035.43 (+4)	1, 954.70	-0.24191
HexNAc(5)Hex(4)Fuc(1)	1,356.23 (+3)	1, 809.66	0.00052
HexNAc(5)Hex(4)	980.91 (+4)	1, 663.60	-0.00032
HexNAc(5)Hex(4)Fuc(2)	1,955.72 (+4)	1, 930.69	0.00039
HexNAc(5)Hex(3)Fuc(1)NeuGc(1)	1,404.24 (+3)	1, 954.70	-0.32956
HexNAc(5)Hex(3)Fuc(1)	976.91 (+4)	1, 647.61	-0.00067
HexNAc(4)Hex(7)	1,402.13 (+3)	1, 948.68	0.32814
HexNAc(4)Hex(6)NeuGc(1)	1,450.25 (+4)	2, 091.72	0.33191
HexNAc(4)Hex(6)NeuAc(1)	1,444.92 (+3)	2, 075.72	0.33262
HexNAc(4)Hex(6)Fuc(2)	1,084.19 (+4)	2, 076.75	0.00188

	HexNAc(4)Hex(6)Fuc(1)	1,047.93 (+4)	1, 930.69	0.2478
	HexNAc(4)Hex(6)	1,324.20 (+3)	1, 784.63	0.00147
	HexNAc(4)Hex(5)NeuGc(1)	1,047.18 (+4)	1, 926.67	0.00257
	HexNAc(4)Hex(5)NeuAc(1)	1,367.21 (+3)	1, 931.67	0.3165
	HexNAc(4)Hex(5)Fuc(3)	1,079.95 (+4)	2, 060.75	0.00052
	HexNAc(4)Hex(5)Fuc(2)	1,043.68 (+4)	1, 914.69	0.00044
	HexNAc(4)Hex(5)Fuc(1)	1,007.41 (+4)	1, 768.63	0.24923
	HexNAc(4)Hex(5)	970.65 (+4)	1, 622.58	-0.00094
	HexNAc(4)Hex(4)Fuc(2)NeuGc(1)	1,061.69 (+4)	2, 059.73	-0.24548
	HexNAc(4)Hex(4)Fuc(2)NeuAc(1)	1,057.69 (+4)	2, 043.74	-0.24382
	HexNAc(4)Hex(4)Fuc(1)NeuAc(1)	1,021.17 (+4)	1, 897.68	-0.24484
	HexNAc(4)Hex(4)NeuAc(1)	1,003.16 (+4)	1, 751.62	0.2533
	HexNAc(4)Hex(4)Fuc(2)	1,003.17 (+4)	1, 752.64	0.00223
	HexNAc(4)Hex(4)Fuc(1)	901.58 (+5)	1, 606.58	0.00127
	HexNAc(4)Hex(4)	929.89 (+4)	1, 460.52	0.00082
	HexNAc(4)Hex(3)Fuc(3)	981.16 (+4)	1, 736.64	-0.00291
	HexNAc(4)Hex(3)Fuc(1)	926.14 (+4)	1, 444.53	0.00019
	HexNAc(3)Hex(6)Fuc(1)NeuGc(1)	1,431.24 (+3)	2, 034.70	0.32942

	HexNAc(3)Hex(6)Fuc(1)NeuAc(1)	1,402.56 (+3)	2, 018.70	0.33363
	HexNAc(3)Hex(6)NeuGc(1)	1,037.41 (+4)	1, 888.64	0.24807
	HexNAc(3)Hex(6)Fuc(1)	996.91 (+4)	1, 727.61	0.00239
	HexNAc(3)Hex(6)	1,280.18 (+3)	1, 581.55	-0.01264
	HexNAc(3)Hex(5)Fuc(1)	956.39 (+4)	1, 565.56	0.00357
	HexNAc(3)Hex(5)	919.8 (+4)	1, 419.50	-0.00045
	HexNAc(3)Hex(4)Fuc(2)	915.88 (+4)	1, 549.56	0.00085
	HexNAc(3)Hex(4)Fuc(1)	915.64 (+4)	1, 403.50	0.00039
	HexNAc(3)Hex(3)Fuc(1)	875.37 (+4)	1, 241.45	-0.00017
	HexNAc(3)Hex(3)	838.85 (+4)	1, 095.39	0.00015
	HexNAc(2)Hex(5)	869.11 (+4)	1, 216.42	0.00035
	HexNAc(2)Hex(6)	909.62 (+4)	1, 378.47	0.00027
	HexNAc(2)Hex(7)	950.13 (+4)	1, 540.52	-0.00177
	HexNAc(2)Hex(8)	1,320.51 (+4)	1, 702.58	-0.01245
Site 6: Asparagine 177 (NLSK) Top of the head	HexNAc(5)Hex(4)Fuc(1)NeuAc(1)	1,553.65 (+2)	2, 100.76	-0.0034
	HexNAc(4)Hex(6)	1,166.17 (+3)	1, 784.63	0.00055
	HexNAc(2)Hex(8)	1,354.56 (+2)	1, 702.58	0.00196
	HexNAc(2)Hex(7)	1,273.53 (+2)	1, 540.52	0.00127
	HexNAc(2)Hex(6)	1,193.00 (+2)	1, 378.47	0.0015
	HexNAc(2)Hex(5)	1,111.98 (+2)	1, 216.42	0.00069
	HexNAc(2)	585.06 (+4)	406.15	-0.00064

Site 7: Asparagine 303 (NSSL) Stalk	HexNAc(6)Hex(4)	1,657.73 (+4)	1, 866.68	0.25101
	HexNAc(6)Hex(3)	1,621.22 (+4)	1, 704.63	0.25377
	HexNAc(4)Hex(5)NeuAc(1)	1,686.49 (+4)	1, 913.67	-0.24401
	HexNAc(4)Hex(4)NeuGc(1)	1,649.97 (+4)	1, 767.61	-0.25517
	HexNAc(3)Hex(6)NeuAc(1)	1,659.22 (+4)	1, 872.64	0.25161
	HexNAc(3)Hex(4)Fuc(1)NeuAc(1)	1,614.70 (+4)	1, 694.60	0.2467
Site 8: Asparagine 498 (NGTY) Stalk	HexNAc(8)Hex(8)Fuc(1)	1,342.18 (+3)	3, 067.11	-0.00606
	HexNAc(7)Hex(7)Fuc(1)NeuAc(2)	1,414.88 (+3)	3, 284.17	0.3354
	HexNAc(6)Hex(6)	1,050.08 (+3)	2, 190.79	0.00079
	HexNAc(6)Hex(5)Fuc(1)NeuAc(2)NeuGc(1)	1,341.19 (+3)	3, 064.07	0.02
	HexNAc(6)Hex(3)Fuc(2)NeuGc(1)	1,471.89 (+3)	2, 303.84	-0.34158
	HexNAc(5)Hex(7)	1,415.21 (+3)	2, 149.76	-0.33692
	HexNAc(5)Hex(5)Fuc(1)NeuAc(1)	1,458.23 (+3)	2, 262.81	-0.33147
	HexNAc(5)Hex(5)NeuGc(1)	1,409.55 (+3)	2, 132.75	-0.32933
	HexNAc(5)Hex(5)Fuc(1)	1,465.08 (+2)	1, 971.71	0.00223
	HexNAc(5)Hex(5)	1,307.84 (+3)	1, 825.66	0.00225
	HexNAc(5)Hex(4)Fuc(1)NeuAc(1)	1,401.21 (+3)	2, 100.76	-0.32961

HexNAc(5)Hex(4)Fuc(1)NeuGc(1)	1,409.55 (+3)	2, 116.75	-0.32763
HexNAc(5)Hex(4)NeuGc(1)	1,384.87 (+3)	1, 970.69	-0.00099
HexNAc(5)Hex(3)Fuc(1)NeuGc(1)	1,355.53 (+3)	1, 945.70	-0.32857
HexNAc(4)Hex(6)	1,293.83 (+3)	1, 784.63	-0.00351
HexNAc(4)Hex(5)Fuc(1)NeuGc(1)	1,390.54 (+4)	2, 075.72	-0.32938
HexNAc(4)Hex(5)NeuGc(1)	1,366.19 (+3)	1, 929.67	0.00128
HexNAc(4)Hex(5)Fuc(3)	1,386.20 (+3)	2, 060.75	-0.00084
HexNAc(4)Hex(5)Fuc(2)	1,006.74 (+3)	1, 914.69	0.00054
HexNAc(4)Hex(5)Fuc(1)	1,288.83 (+3)	1, 768.63	-0.00049
HexNAc(4)Hex(5)	1,101.78 (+3)	1, 622.58	0.00172
HexNAc(4)Hex(4)Fuc(2)NeuAc(1)	1,385.21 (+3)	2, 043.74	-0.32697
HexNAc(4)Hex(4)Fuc(1)NeuGc(1)	1,360.86 (+3)	1, 913.67	0.32938
HexNAc(4)Hex(4)Fuc(1)NeuAc(1)	1,336.52 (+3)	1, 987.68	-0.33167
HexNAc(4)Hex(4)Fuc(1)	943.87 (+4)	1, 606.58	-0.00836
HexNAc(3)Hex(6)Fuc(1)NeuGc(1)	1,382.18 (+3)	2, 034.70	-0.34415
HexNAc(3)Hex(6)Fuc(1)	1,343.03 (+2)	1, 727.61	0.00136

	HexNAc(3)Hex(5)NeuGc(1)	1,298.49 (+3)	1, 726.59	-0.00482
	HexNAc(3)Hex(4)Fuc(1)Neu Ac(1)	1,287.83 (+2)	1, 694.60	0.00233
	HexNAc(3)Hex(4)NeuAc(1)	1,239.15 (+3)	1, 548.54	0.00166
	HexNAc(3)Hex(4)Fuc(2)	1,239.15 (+3)	1, 549.56	-0.01108
	HexNAc(3)Hex(4)	1,107.95 (+2)	1, 257.44	0.00098
	HexNAc(2)Hex(8)	1,330.49 (+2)	1, 702.58	-0.02006

The structural information obtained through CID fragmentation, albeit limited, still allows to discriminate between high mannose, complex or hybrid glycans in some cases. A high mannose structure can be assigned to the monosaccharide compositions in the form HexNAc(2)Hex(5-12), as long as the sequential fragmentation confirms the neutral loss of only hexose residues in the antennae from the glycopeptide Y ion series. Complex and hybrid glycans can be distinguished when diagnostic Y ions are detected, such as Pep+HexNAc(2)Hex(4), for compositions with more than 2 HexNAc residues. In such cases, at least one of the HexNAc residues must be in the antennae, thus ruling out a high mannose glycan. Additionally, the Pep+HexNAc(2)Hex(4) fragment confirms that one hexose must be attached to one glucose residue from the trimannosyl core. Both these features combined can only occur in hybrid glycans, since only HexNAc residues are attached to the trymannosyl core in complex glycans. Figure 3B shows a representative CID spectrum with two diagnostic ions (Pep+HexNAc(3)Hex(5)+3 and Pep+HexNAc(3)Hex(5)Fuc(1)+3) for a hybrid structure.

Other diagnostic ions shed further structural information. A 512 m/z peak in the lower m/z range of the CID spectra corresponds to a Hex(1)HexNAc(1)Fuc(1) glycan B ion, characteristic of an outer arm fucose. Conversely, core fucosylation can be determined from the detection of Y ions such as Pep+HexNAc(1)Fuc(1) and Pep+HexNAc(2)Fuc(1). The latter fragments can also be observed in some HCD spectra to further confirm fucose attachment to the chitobiose core. Special consideration was given to glycans with a mass consistent with isobaric glycan compositions containing either Fuc+NeuGc or Hex+NeuAc. In these cases, not all spectra contained sufficient

information to derive the correct composition. Nonetheless, diagnostic ions (NeuAc (292.10 m/z), NeuAc-H2O (274.09 m/z), NeuGc (308.09 m/z), NeuGc-H2O (290.09 m/z)) were present in some HCD spectra and were used to identify the correct composition. Moreover, glycan B fragments corresponding to HexNAc-Gal-NeuAc (657 m/z) or HexNAc-Gal-NeuGc (673 m/z) detected in CID were also present in some spectra.

Residues N142 and N498 displayed a great variety of glycan monomeric compositions. Conversely, for sites N28, N40, N71 and N104, only a very limited number of compositions were detected. Overall, complex and hybrid glycans were predominantly found. Nonetheless, high mannose glycans are also present in N142 and N177, both located on the top of the globular head. Fucosylation was observed in most glycopeptides and was confirmed by the presence of fucose residues in the CID spectra or diagnostic ions in the HCD spectra. Core fucoses are predominant, but outer arm fucoses were also found in some glycoforms. Highly bulky complex glycans were found on N498.

Discussion

Sequence-based analysis has previously been employed by others to study the variation in the glycosylation profile of several strains during virus evolution [27, 28]. Although N-glycosylation prediction contributes greatly to the understanding of glycosite variation across strains, this method only provides a prediction that relies on primary sequence context, and the actual occupancy of glycosites must be confirmed experimentally. Moreover, it is known that the location of the sequon can affect glycan maturation, thereby resulting in different sets of glycoforms for each site depending on the accessibility of N-glycosyltransferases [29]. To this end, we used mass spectrometry analysis to confirm the occupancy of glycosites predicted by the NetNGlyc 1.0 Server for the A/New Caledonia/20/1999 H1 protein. Others have shown that hemagglutinin from egg-grown viruses and human cell lines display the same occupancy profile [30]. Therefore, the results obtained in this study are relevant to the understanding of influenza virus adaptation in humans.

The occupancy profile obtained through HCD/CID-MS/MS of tryptic glycopeptides was consistent with the prediction by the NetNGlyc 1.0 server. All eight sequons confirmed experimentally had been predicted by the server. Indeed, N28 (and not N27), was shown to be glycosylated as was predicted. The transfer of N-glycan precursors to asparagine residues in

endoplasmic reticulum (ER) bound ribosomes is affected by conformational constraints as well as inaccessibility due to steric hindrance from nearby residues. To this end, since N28 is occupied, it is unlikely that an olygosaccharyltransferase can act upon asparagine N27. The positive prediction for site N557 was not accurate, due to the location of the residue within the cytoplasmic domain of the protein. Nonetheless, such inaccuracies can easily be identified to prevent misleading interpretations when performing sequence-based analyses.

Glycosites N142 and N177 are of particular relevance for the study of immunogenicity and virulence. These residues are both located on the receptor binding site (RBS) and the attachment of oligosaccharides can mask the antigenic Sa region. Remarkably, both acceptor sites were absent in the 1918 and 2009 pandemic strains. Wei et al. showed that mice display cross-neutralization of 1918 and 2009 pandemic viruses after vaccination with the 1918 strain, whereas such antibodies did not protect against seasonal strains – providing evidence that the introduction of N-glycosylation sites on the vicinity of the RBS can mask antigenic recognition by pandemic antibodies [31].

A vast heterogeneity of glycan compositions was found on N142 (Table 2), which is even more notable taking into account that the predicted compositions can encompass several glycan isoforms; meaning that the actual heterogeneity is presumably broader. Among the predicted oligosaccharides attached to N142 are glycan compositions consistent with complex, high mannose and hybrid glycans. The vast complexity encountered on this asparagine residue can be attributed to the high surface exposure, providing accessibility for N-glycan processing and maturation (Fig. 4).

In the case of glycosite N177, a much narrower variety of glycoforms was detected. However, the intensities for these glycopeptides were much lower compared to those glycopeptides containing site N142. Therefore, many glycopeptides for N177 could have been suppressed and missed in the analysis, which constitutes a limitation of the method. Still, the MS/MS analysis predicted the occupancy of high mannose, hybrid and complex glycoforms.

The presence of terminal sialic acid residues in several of the predicted glycoforms attached to both N142 and N177 could play an important role in the immunogenicity of the strain. Ohuchi et al. suggested that the presence of terminal NeuAc and NeuGc on HA glycans in the vicinity of the receptor binding sites may impair binding to sialic acid-containing receptors [32]. Although the

effect of the presence of sialic acid residues on immune cell recognition in this case is unknown, the bulkiness and negative charge of NeuAc and NeuGc would likely further impair an immune response. Overall, terminal sialylation of both cell surfaces and glycoproteins has been shown to decrease antigenicity [33, 34]. Therefore, the attachment of negatively charged terminal residues in embryonated-egg vaccine production could be a drawback in terms of HA antigenicity compared to other recombinant hemagglutinin based vaccines, where sialylation can be controlled or non-existent, as is the case in the baculovirus expression system [35].

Glycosites N71 and N104 are located on the side of the globular head (Fig. 4). In the case of N71, only one glycan with a composition consistent with a non-fucosylated hybrid glycan was found (Table 2). For N104, one glycan with a complex-like composition was detected. Others have proposed that the occupancy of site N104 might be sterically hindered by glycan attachment on N71 due to their close proximity (Fig. 4) [20]. Moreover, it has been argued that since both glycosites are able to shield antigenic site Ca2, glycosylation on N71 could render the occupancy of N104 unnecessary to mask antigenic site Ca2 [20]. It was confirmed that both N71 and N104 are indeed glycosylated in egg-grown viruses. It was unexpected, however, to find such a limited set of glycan compositions in these sites, in contrast to other positions such as N142, N177 and N498. As discussed previously, these results are potentially due to a limited detection of the glycopeptides containing these acceptor sites. However, the close proximity of both residues also suggests that glycan processing might be impaired due to steric hindrance.

The detection of highly bulky complex glycans on N498 (e.g., HexNAc(8)Hex(8)Fuc(1) and HexNAc(7)Hex(7)Fuc(1)NeuAc(2)) suggests the presence of poly-N-acetyllactosamine groups, which are commonly found on membrane-proximal glycosites [36, 37]. The close proximity of N498 to the viral membrane (Fig. 4B) does not seem to decrease the degree of glycan maturation on this asparagine residue, resulting in a high complexity of structures.

In this mass spectrometry setup, some tryptic glycopeptides produce considerably higher intensities than others. This causes that more information on glycan microheterogeneity can be gathered on those glycopeptides that ionize with a higher efficiency and whose m/z value is better detected under these experimental conditions, whereas only limited information can be derived from other regions. This was likely the cause of the limited glycopeptide detection for sites N28, N40, N71 and N104. Unfortunately, this drawback prevents an appropriate comparison of glycan

microheterogeneity among glycosites. Obtaining a more comprehensive profile is required to better understand the role of glycan structures on the biological properties of the virus. Still, these results allowed to confirm glycan attachment on these sites.

An advantage of utilizing reducing SDS-PAGE as a preliminary fractionation step is that analysing HA0, HA1 and HA2 separately provides a more comprehensive characterization of glycan microheterogeneity, owing to the fact that the lower overall presence of non-glycosylated peptides in HA1 or HA2 isolated fractions (compared to HA0) could allow the detection of certain glycopeptides with low total ion current (TIC). In fact, most of the distinct glycan compositions detected on site N498 come from the analysis of HA2 and were not present in the analysis of HA0 (band 4 in figure 2). This is likely due to the large presence of non-glycosylated peptides in HA0, which can suppress the signal of N498 glycopeptides.

The experimental confirmation of glycosylation sites is highly important in the study of influenza viral evolution. Furthermore, there is evidence that egg and mammalian cell derived HA display the same occupancy profile [30]. Consequently, characterizing further egg-derived strains with this method would also yield site occupancy information relevant to other approved production platforms, such as cell-based and recombinant technologies. Currently, egg-based vaccines comprise the overwhelming majority of available influenza vaccine products. However, the FDA has recently approved the cell-based Flucelvax (Seqirus), produced in Madin-Darby Canine Kidney (MDCK) epithelial cells, and the recombinant Flublok (Protein Sciences Corporation), produced in insect cells [38-40]. It is noteworthy to mention that the glycan structures found on egg-derived viruses can differ significantly to those present on viruses that replicate in alternative cell substrates [30, 41, 42].

Conclusion

The results presented in this study confirmed the glycan occupancy profile of A/New Caledonia/20/1999 hemagglutinin, validated the prediction by the NetNGlyc 1.0 Server and characterized the site-specific structural heterogeneity of the attached glycans. The mass spectrometry approach employed was able to furnish information on sequon occupancy and glycan structures in a single run. This efficient strategy can be extended to study further influenza glycoproteins in order to attain deeper knowledge of the role of N-glycosylation in viral adaptation mechanisms. Site-specific mass spectrometry methods, however, typically provide only partial

information on the structure of the oligosaccharides. To this regard, additional work should be carried out to elucidate more detailed structural features to assess the impact of glycoforms on parameters such as antigen masking, immunogenicity, SA receptor binding affinity and viral membrane resistance to surfactant treatment. The latter is highly relevant for split-virus vaccine manufacturing, where a surfactant is employed to disrupt the viral membrane. Gaining further insight into the glycosylation characteristics of influenza viruses can therefore potentially improve the manufacturing process of split-virus vaccines, the selection of strains for the composition of seasonal vaccines and the development of recombinant products.

Disclosure of potential conflicts of interest

References

[1]. J.K. Taubenberger, J.C. Kash, Influenza Virus Evolution, Host Adaptation, and Pandemic Formation, Cell Host & Microbe, 7 (2010) 440-451. doi:410.1016/j.chom.2010.1005.1009.

[2]. M.I. Nelson, E.C. Holmes, The evolution of epidemic influenza, Nat Rev Genet, 8 (2007) 196-205. doi:110.1038/nrg2053.

[3]. C.W. Potter, J.S. Oxford, Determinants of immunity to influenza infection in man, British medical bulletin, 35 (1979) 69-75. PMID:367490.

[4]. N. Mancini, L. Solforosi, N. Clementi, D. De Marco, M. Clementi, R. Burioni, A potential role for monoclonal antibodies in prophylactic and therapeutic treatment of influenza, Antiviral research, 92 (2011) 15-26. doi:10.1016/j.antiviral.2011.1007.1013.

[5]. K. Stohr, D. Bucher, T. Colgate, J. Wood, Influenza virus surveillance, vaccine strain selection, and manufacture, Methods in molecular biology (Clifton, N.J.), 865 (2012) 147-162.

[6]. B.E. Johansson, D.J. Bucher, E.D. Kilbourne, Purified influenza virus hemagglutinin and neuraminidase are equivalent in stimulation of antibody response but induce contrasting types of immunity to infection, Journal of virology, 63 (1989) 1239-1246. PMID:2915381.

[7]. B.E. Johansson, T.M. Moran, C.A. Bona, S.W. Popple, E.D. Kilbourne, Immunologic response to influenza virus neuraminidase is influenced by prior experience with the associated viral hemagglutinin. II. Sequential infection of mice simulates human experience, Journal of immunology (Baltimore, Md. : 1950), 139 (1987) 2010-2014. PMID:3624874.

[8]. R.K. Virk, V. Gunalan, P.A. Tambyah, Influenza infection in human host: challenges in making a better influenza vaccine, Expert review of anti-infective therapy, 14 (2016) 365-375.

[9]. N. Sriwilaijaroen, Y. Suzuki, Molecular basis of the structure and function of H1 hemagglutinin of influenza virus, Proceedings of the Japan Academy. Series B, Physical and biological sciences, 88 (2012) 226-249. PMID:22728439.

[10]. C.C. Wang, J.R. Chen, Y.C. Tseng, C.H. Hsu, Y.F. Hung, S.W. Chen, C.M. Chen, K.H. Khoo, T.J. Cheng, Y.S. Cheng, J.T. Jan, C.Y. Wu, C. Ma, C.H. Wong, Glycans on influenza hemagglutinin affect receptor binding and immune response, Proceedings of the National Academy of Sciences of the United States of America, 106 (2009) 18137-18142. doi:18110.11073/pnas.0909696106.

[11]. K. Wanzeck, K.L. Boyd, J.A. McCullers, Glycan shielding of the influenza virus hemagglutinin contributes to immunopathology in mice, American journal of respiratory and critical care medicine, 183 (2011) 767-773. doi:710.1164/rccm.201007-201184OC.

[12]. W. Chen, Y. Zhong, Y. Qin, S. Sun, Z. Li, The Evolutionary Pattern of Glycosylation Sites in Influenza Virus (H5N1) Hemagglutinin and Neuraminidase, PLoS ONE, 7 (2012) e49224. doi:49210.41371/journal.pone.0049224.

[13]. J.I. Kim, M.S. Park, N-linked glycosylation in the hemagglutinin of influenza A viruses, Yonsei medical journal, 53 (2012) 886-893. doi:810.3349/ymj.2012.3353.3345.3886.

[14]. X. Sun, A. Jayaraman, P. Maniprasad, R. Raman, K.V. Houser, C. Pappas, H. Zeng, R. Sasisekharan, J.M. Katz, T.M. Tumpey, N-Linked Glycosylation of the Hemagglutinin Protein Influences Virulence and Antigenicity of the 1918 Pandemic and Seasonal H1N1 Influenza A Viruses, Journal of virology, 87 (2013) 8756-8766. doi:8710.1128/jvi.00593-00513.

[15]. R.P. de Vries, E. de Vries, B.J. Bosch, R.J. de Groot, P.J. Rottier, C.A. de Haan, The influenza A virus hemagglutinin glycosylation state affects receptor-binding specificity, Virology, 403 (2010) 17-25. doi:10.1016/j.virol.2010.1003.1047.

[16]. X. Zhang, S. Chen, D. Yang, X. Wang, J. Zhu, D. Peng, X. Liu, Role of stem glycans attached to haemagglutinin in the biological characteristics of H5N1 avian influenza virus, The Journal of general virology, 96 (2015) 1248-1257. doi:1210.1099/vir.1240.000082.

[17]. P.C. Roberts, W. Garten, H.D. Klenk, Role of conserved glycosylation sites in maturation and transport of influenza A virus hemagglutinin, Journal of virology, 67 (1993) 3048-3060. PMID:8497042.

[18]. P.L. Herve, V. Lorin, G. Jouvion, B. Da Costa, N. Escriou, Addition of N-glycosylation sites on the globular head of the H5 hemagglutinin induces the escape of highly pathogenic avian influenza A H5N1 viruses from vaccine-induced immunity, Virology, 486 (2015) 134-145. 110.1016/j.virol.2015.1008.1033.

[19]. R.A. Medina, S. Stertz, B. Manicassamy, P. Zimmermann, X. Sun, R.A. Albrecht, H. Uusi-Kerttula, O. Zagordi, R.B. Belshe, S.E. Frey, T.M. Tumpey, A. Garcia-Sastre, Glycosylations in the globular head of the hemagglutinin protein modulate the virulence and antigenic properties of the H1N1 influenza viruses, Science translational medicine, 5 (2013) 187ra170. doi:110.1126/scitranslmed.3005996.

[20]. S. Sun, Q. Wang, F. Zhao, W. Chen, Z. Li, Glycosylation Site Alteration in the Evolution of Influenza A (H1N1) Viruses, PLoS ONE, 6 (2011) e22844. doi:22810.21371/journal.pone.0022844.

[21]. M.D. Tate, E.R. Job, Y.M. Deng, V. Gunalan, S. Maurer-Stroh, P.C. Reading, Playing hide and seek: how glycosylation of the influenza virus hemagglutinin can modulate the immune response to infection, Viruses, 6 (2014) 1294-1316. doi:1210.3390/v6031294.

[22]. R. Xu, D.C. Ekiert, J.C. Krause, R. Hai, J.E. Crowe, I.A. Wilson, Structural basis of pre-existing immunity to the 2009 H1N1 pandemic influenza virus, Science (New York, N.Y.), 328 (2010) 357-360. doi:310.1126/science.1186430.

[23]. M. Igarashi, K. Ito, R. Yoshida, D. Tomabechi, H. Kida, A. Takada, Predicting the Antigenic Structure of the Pandemic (H1N1) 2009 Influenza Virus Hemagglutinin, PLoS ONE, 5 (2010) e8553. doi:8510.1371/journal.pone.0008553.

[24]. NetNGlyc, NetNGlyc 1.0 Server, 2015.

[25]. S. Doll, A.L. Burlingame, Mass spectrometry-based detection and assignment of protein posttranslational modifications, ACS chemical biology, 10 (2015) 63-71. doi:10.1021/cb500904b.

[26]. M. Thaysen-Andersen, N.H. Packer, Advances in LC–MS/MS-based glycoproteomics: Getting closer to system-wide site-specific mapping of the N- and O-glycoproteome, Biochim. Biophys. Acta, Proteins Proteomics, 1844 (2014) 1437-1452. doi:1410.1016/j.bbapap.2014.1405.1002.

[27]. S.R. Das, S.E. Hensley, A. David, L. Schmidt, J.S. Gibbs, P. Puigbò, W.L. Ince, J.R. Bennink, J.W. Yewdell, Fitness costs limit influenza A virus hemagglutinin glycosylation as an immune evasion strategy, Proceedings of the National Academy of Sciences of the United States of America, 108 (2011) E1417–E1422. doi:1410.1073/pnas.1108754108.

[28]. B.J. DeKosky, G.C. Ippolito, R.P. Deschner, J.J. Lavinder, Y. Wine, B.M. Rawlings, N. Varadarajan, C. Giesecke, T. Dorner, S.F. Andrews, P.C. Wilson, S.P. Hunicke-Smith, C.G. Willson, A.D. Ellington, G. Georgiou, High-throughput sequencing of the paired human immunoglobulin heavy and light chain repertoire, Nat Biotechnol 31 (2013) 166-169. doi:110.1038/nbt.2492.

[29]. M. Thaysen-Andersen, N.H. Packer, Site-specific glycoproteomics confirms that protein structure dictates formation of N-glycan type, core fucosylation and branching, Glycobiology, 22 (2012) 1440-1452. doi:1410.1093/glycob/cws1110.

[30]. Y. An, J.A. Rininger, D.L. Jarvis, X. Jing, Z. Ye, J.J. Aumiller, M. Eichelberger, J.F. Cipollo, Comparative Glycomics Analysis of Influenza Hemagglutinin (H5N1) Produced in Vaccine Relevant Cell Platforms, J Proteome Res, 12 (2013) 3707-3720. doi:3710.1021/pr400329k.

[31]. C.-J. Wei, J.C. Boyington, K. Dai, K.V. Houser, M.B. Pearce, W.-P. Kong, Z.-y. Yang, T.M. Tumpey, G.J. Nabel, Cross-Neutralization of 1918 and 2009 Influenza Viruses: Role of Glycans in Viral Evolution and Vaccine Design, Science translational medicine, 2 (2010) 24ra21-24ra21. doi:10.1126/scitranslmed.3000799.

[32]. M. Ohuchi, R. Ohuchi, A. Feldmann, H.D. Klenk, Regulation of receptor binding affinity of influenza virus hemagglutinin by its carbohydrate moiety, Journal of virology, 71 (1997) 8377-8384. PMID:9343193.

[33]. R. Schauer, Sialic acids as antigenic determinants of complex carbohydrates, Advances in experimental medicine and biology, 228 (1988) 47-72. PMID:2459931.

[34]. R. Schauer, Sialic acids as regulators of molecular and cellular interactions, Current opinion in structural biology, 19 (2009) 507-514. doi:510.1016/j.sbi.2009.1006.1003.

[35]. X. Shi, D.L. Jarvis, Protein N-Glycosylation in the Baculovirus-Insect Cell System, Curr drug targets, 8 (2007) 1116-1125. PMID:17979671.

[36]. S.Y. Mir-Shekari, D.A. Ashford, D.J. Harvey, R.A. Dwek, I.T. Schulze, The glycosylation of the influenza A virus hemagglutinin by mammalian cells. A site-specific study, The Journal of biological chemistry, 272 (1997) 4027-4036. doi:4010.1074/jbc.4272.4027.4027.

[37]. M. Fukuda, J.L. Guan, J.K. Rose, A membrane-anchored form but not the secretory form of human chorionic gonadotropin-alpha chain acquires polylactosaminoglycan, The Journal of biological chemistry, 263 (1988) 5314-5318. PMID:2451668.

[38]. P.C. Soema, R. Kompier, J.-P. Amorij, G.F.A. Kersten, Current and next generation influenza vaccines: Formulation and production strategies, Eur J Phar Biopharm, 94 (2015) 251-263.

[39]. I. Manini, A. Domnich, D. Amicizia, S. Rossi, T. Pozzi, R. Gasparini, D. Panatto, E. Montomoli, Flucelvax (Optaflu) for seasonal influenza, Expert review of vaccines, 14 (2015) 789-804.

[40]. L.P. Yang, Recombinant trivalent influenza vaccine (flublok((R))): a review of its use in the prevention of seasonal influenza in adults, Drugs, 73 (2013) 1357-1366.

[41]. S. Zhang, Comparative Characterization of the Glycosylation Profiles of an Influenza Hemagglutinin Produced in Plant and Insect Hosts, Proteomics, 12 (2012) 1269-1288.

[42]. M. Butler, M. Spearman, The choice of mammalian cell host and possibilities for glycosylation engineering, Curr Opin Biotechnol, 30 (2014) 107-112.

[43]. R.B. Squires, J. Noronha, V. Hunt, A. García-Sastre, C. Macken, N. Baumgarth, D. Suarez, B.E. Pickett, Y. Zhang, C.N. Larsen, A. Ramsey, L. Zhou, S. Zaremba, S. Kumar, J. Deitrich, E. Klem, R.H. Scheuermann, Influenza Research Database: an integrated bioinformatics resource for influenza research and surveillance, Influenza Other Respir Viruses, 6 (2012) 404-416. doi:410.1111/j.1750-2659.2011.00331.x.

Chapter 3

The State-of-Play and Future of Antibody Therapeutics

Graphical abstract
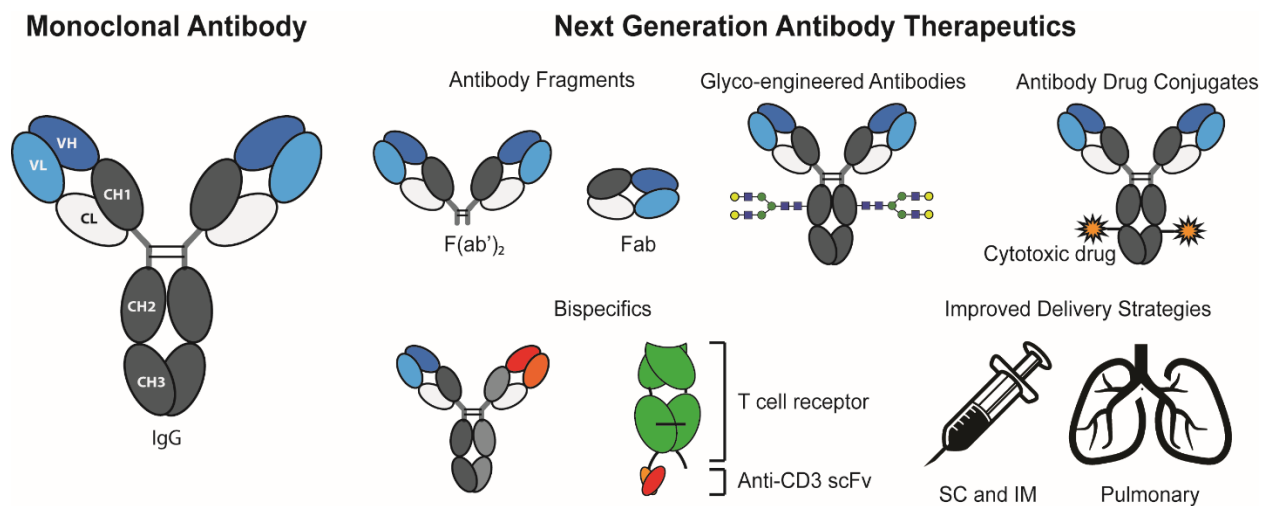
Chapter 3 – Authorship declaration statement

The following chapter is a literature review published in the journal Advanced Drug Delivery Reviews as:

Z. Elgundi, M. Reslan, E. Cruz, V. Sifniotis, V. Kayser. The State-of-play and Future of Antibody Therapeutics. Advanced Drug Delivery Reviews, 122 (2017), 2-19.
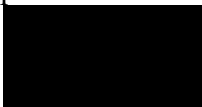
E. Cruz wrote the "Antibody-Drug Conjugates" and "Optimization of antibody bioavailability and delivery" sections, co-wrote the "Fc-engineered antibodies for enhanced effector functions" and contributed to the "Bispecifics" section and to writing the abstract and conclusions. E. Cruz created the figures featured in the review, including the graphical abstract. Additionally, the author provided critical review of the manuscript.

The section "Biosimilars, guidelines and challenges" contained in the original article has been omitted since it is not directly relevant to the subsequent chapters.

Permission to include the published material has been granted by the corresponding author.

Esteban Cruz, Signature: ██████████   19th of August, 2019

As corresponding author and supervisor for this candidature, I hereby confirm that this authorship declaration statement is complete and accurate

Veysel Kayser, Signature: ██████████   19th of August, 2019

Abstract

It has been over four decades since the development of monoclonal antibodies (mAbs) using a hybridoma cell line was first reported. Since then more than thirty therapeutic antibodies have been marketed, mostly as oncology, autoimmune and inflammatory therapeutics. While antibodies are very efficient, their cost-effectiveness has always been discussed owing to their high costs, accumulating to more than one billion dollars from preclinical development through to market approval. Because of this, therapeutic antibodies are inaccessible to some patients in both developed and developing countries. The growing interest in biosimilar antibodies as affordable versions of therapeutic antibodies may provide alternative treatment options as well potentially decreasing costs. As certain markets begin to capitalize on this opportunity, regulatory authorities continue to refine the requirements for demonstrating quality, efficacy and safety of biosimilar compared to originator products. In addition to biosimilars, innovations in antibody engineering are providing the opportunity to design biobetter antibodies with improved properties to maximize efficacy. Enhancing effector function, antibody drug conjugates (ADC) or targeting multiple disease pathways via multi-specific antibodies are being explored. The manufacturing process of antibodies is also moving forward with advancements relating to host cell production and purification processes. Studies into the physical and chemical degradation pathways of antibodies are contributing to the design of more stable proteins guided by computational tools. Moreover, the delivery and pharmacokinetics of antibody-based therapeutics are improving as optimized formulations are pursued through the implementation of recent innovations in the field.

Introduction

Over the past twenty years, therapeutic antibodies have rapidly become the leading product within the biopharmaceutical market. In 2013, therapeutic antibodies represented 50% of the $140 billion taken by the biopharmaceutical market with sales growing from $39 billion in 2008 to $75 billion in 2013 [1]. There are currently more than thirty therapeutic antibodies approved for established markets such as the United States and Europe with over three hundred antibody-based products in clinical development [1-3]. Therapeutic antibodies are no longer full-length, naked mouse antibodies; advancements in antibody engineering technologies, novel antigen discovery strategies and progress in deciphering disease pathways have all generated robust interest, resources and investment in antibody development. In this review, we will discuss developments in the field of

therapeutic antibodies, the growth of biosimilars and pay particular attention to targeting degradation pathways of antibodies to produce more stable biobetter antibodies and formulations.

Antibody discovery strategies

The generation of early antibodies relied on the immunization of mice or other mammals with the desired antigen target. This resulted in multiple antibodies directed at different epitopes of the antigen secreted by a mixed population of B cells with each cell secreting only one specific antibody (i.e. polyclonal). Unfortunately, secreting B cells can only replicate a limited number of times, therefore rendering mass production all but impossible. The ground-breaking hybridoma technology developed by Kohler and Milstein allowed antibody secreting cells from the spleen of immunized animals to be fused with immortalized non-antibody secreting cells, thus resulting in cells that would divide continuously when cultivated in permissive conditions [4, 5]. Although the first recombinant antibodies were produced using this technology, including the first approved therapeutic antibody muromonab-CD3 (Orthoclone OKT®3) in 1986 for preventing kidney transplant rejection, hybridoma production presented some drawbacks. Hybridomas can be labour intensive, low yielding or genetically unstable [6]. More importantly though, the antibody sequences originated from an immunized animal and consequently had the potential of triggering an immune response in humans. Therefore, further improvements were needed to yield antibodies more human-like and safe. These technologies have evolved from chimeric antibodies that is, grafting essential mouse amino acids needed for antigen binding onto a human antibody framework [7, 8] to both *in vitro* and *in vivo* techniques for generating humanized antibodies.

The XenoMouse™ (Abgenix) and HuMab-Mouse® (Medarex) are transgenic mice developed in parallel and in both, the endogenous murine heavy and kappa light chain genes are inactivated and replaced with the equivalent human germline sequences [9, 10]. Injection of antigens into these mice leads to development of 'fully human' antibodies that have undergone mouse somatic hypermutation and selection to relatively high affinity. Validation of this technology came with the regulatory approval of panitumumab (Vectibix®) in 2006; a fully human antibody directed against epidermal growth factor receptor (EGFR) as treatment for advanced colorectal cancer [11]. Since then, RANK ligand-specific denosumab (Prolia®) has been approved for bone loss and TNFα-specific golimumab (Simponi®) for rheumatoid arthritis.

An *in vitro* method for generating fully human antibodies can be accomplished by cloning and screening large libraries of sufficiently diverse human antibody genes in combination with display technology. The concept of display technology provides a direct physical link between a gene (genotype) and the encoding antibody fragment (phenotype) to allow selection of genes that encode a protein with the desired binding function. Phage display technology remains the most widely used *in vitro* method for the display of large repertoires and for the selection of high affinity antibodies to biologically relevant targets [6]. Phage display involves the expression of proteins on the surface of filamentous phage via fusion with phage coat protein with the genetic sequence packaged within, linking phenotype to genotype selection. When combined with antibody libraries, phage display allows for rapid *in vitro* selection of antigen-specific antibodies and recovery of their corresponding coding sequence [12-14]. This system is highly effective, robust and amenable to high throughput processes for screening of $>10^{+10}$ specificities [15]. The diversity of phage display libraries is distinguishable by source and design: naïve [16], immune [12], synthetic [17] and semi-synthetic [18]. The technology was first demonstrated for a single chain variable fragment (scFv) [13]. with screening of other formats also introduced including human antigen binding fragments (Fabs) [19], domain antibodies [20], camelid domain antibodies [21], single domain shark antibodies [22], diabodies [23] and even whole IgG [24]. The first approved human antibody isolated by phage display technology was adalimumab (Humira®) which binds the cytokine TNFα. This antibody was first selected as a scFv expressed on the surface of phage and was further engineered in human IgG1 format, providing major validation for phage display technologies [25]. Adalimumab remains the most lucrative antibody product generating global sales of $11 billion in 2013 [1]. The number of phage display-derived candidates currently in clinical development further demonstrates the value of phage display as an established and reliable drug discovery platform [26].

Other cell surface methodologies such as bacterial, baculovirus and yeast display present thousands of copies of the displayed protein on the cell surface thereby allowing for quantitative screening such as flow cytometry [27-29]. Yeast display has the additional feature of eukaryotic protein folding pathways and as a result, is perhaps the most ideally suited system for the surface display of mammalian secreted proteins such as antibodies. Alternatively, ribosome display is used to screen large scFv and single variable domain libraries containing up to $>10^{+13}$ mutant clones [30]. The main distinguishing feature of this method is that large libraries can be generated

because the entire procedure is performed *in vitro* without the need for cell transformations. The genotype and phenotype are linked through ribosomal complexes, consisting of messenger RNA (mRNA), ribosome and encoded protein. The *in vitro* selection of antibodies from antibody libraries based on target affinity is termed as "panning". The method is an iterative process whereby the population of target specific antibodies is enriched relative to the number of panning rounds.

With the advent of next-generation sequencing (NGS), analysis of the natural and synthetic repertoires from which libraries have been constructed has become possible [31-33]. In one application, NGS was used to identify antigen-specific IgG antibodies from polyclonal serum of immunized rabbits and mice when used in combination with affinity chromatography coupled to LC-MS/MS [34]. The technology has been used to demonstrate its utility in selecting antibodies with favourable properties. For example, Reddy et al. found that 21/27 (or 78%) of scFv they constructed could bind the target antigen with nanomolar affinity after using NGS data to pair together the most abundant variable heavy (VH) and variable light (VL) genes from immunized mice [35]. Other studies have seen similar findings with natural VH:VL pairing limitations [36]. and without the limitation [37]. Interestingly, the method of repertoire mining of VH and VL abundances using NGS of splenocytes isolated from immunized mice was compared with a phage panning approach of the same cDNA [38]. While both methods provided completely different sets of antibodies, specificity and affinities of the antibody clones were comparable.

Novel antibodies in approval and preclinical development stages

In 2015, eight therapeutic antibodies were granted market approval by the US Food and Drug Administration (FDA) (Table 1). While full-length and IgG1 antibodies still dominate, a humanized Fab also gained approval. Five of the eight approvals were to non-oncology indications with two antibodies entering 'first-in-class' for the treatment of hyperlipidemia. The outlook for 2016 has been positive with six antibodies approved (as of November 2016), including a first-in-class antibody to bacterial target Bacillus anthraxis. A number of full-length antibodies are currently under biologics license application (BLA) submission and awaiting FDA approval or have completed Phase III trials with endpoints met (Table 1).

Table 1. Novel full-length antibodies and fragments developed in recent years and their clinical status.

Name	Commercial Name	Company	Target	Indication (FDA approved)	Format
APPROVED BY FDA IN 2015					
Secukinumab	Costentyx®	Novartis	IL-17	Psoriasis	Whole IgG1 (fully human)
Dinutuximab	Unituxin®	United Therapeutics Corporation	GD2	Neuroblastoma (pediatric patients)	Whole IgG1 (chimeric)
Alirocumab	Praulent®	Sanofi	PCSK9	Hyperlipidemia	Whole IgG1 (fully human)
Evolocumab	Repatha®	Amgen	PCSK9	Hyperlipidemia	Whole IgG2 (fully human)
Idarucizumab	Praxbind®	Boehringer Ingelheim	Dabigatran	Anti-coagulation reversal	Fab fragment (humanized)
Mepolizumab	Nucala®	GlaxoSmithKline	IL-5	Asthma	Whole IgG1 (humanized)
Necitumumab	Portrazza®	Eli Lilly	EGFR	Non-small cell lung cancer (NSCLC)	Whole IgG1 (fully human)
Daratumumab	Darzalex®	Janssen Biotech	CD38	Multiple myeloma	Whole IgG1 (fully human)
APPROVED BY FDA IN 2016 (as of November)					
Reslizumab	Cinquil®	Teva	IL-5	Asthma	Whole IgG4 (humanized)
Ixekizumab	Taltz®	Eli Lilly	IL-17a	Psoriasis	Whole IgG4 (humanized)

Obiltoxaximab	Anthim®	Elusys Therapeutics	*Bacillus anthrax*	Anthrax	Whole IgG3 (humanized)
Atezolizumab	Tecentriq®	Genentech	PD-L1	NSCLC, Bladder cancer	Whole IgG1 (humanized)
Olaratumab (+ Doxorubicin)	Lartruvo®	Eli Lilly	PDGFRalpha	Soft tissue carcinoma	Whole IgG1
Bezlotoxumab	Zinplava®	Merck	*Clostridium difficile* toxin B	*Clostridium difficile* infection	Whole IgG1 (fully human)
NOT YET APPROVED, TRIALS COMPLETED					
Brodalumab		Valeant Pharmaceuticals	IL-17R	Psoriasis	Whole IgG1 (fully human)
Bimagrumab		Novartis	ACVR2B	Muscle loss and weakness	Whole IgG1 (fully human)
MABp1	Xilonix	XBiotech	IL-1alpha	Colorectal cancer, Cachexia	Whole IgG1 ('true' human)
Catumaxomab	Removab	Trion Pharma	EPCAM/CD3	Malignant ascites	Whole hybrid of rat IgG2 variable and mouse IgG2a Fc regions
Guselkumab		Janssen Biotech	IL-23/p19	Psoriasis	Whole IgG1 (fully human)
Dupilumab		Sanofi/Regeneron	IL-4R	Atopic Dermatitis	Whole IgG4 (fully human)
ONGOING PHASE III TRIALS					
Ocrelizumab	Ocrevus	Roche	CD20	Multiple Sclerosis	Whole IgG1

					(humanized)
Sirukumab		GlaxoSmithKline	IL-6	Rheumatoid arthritis	Whole IgG1
Sarilumab		Sanofi/Regeneron	IL-6R	Rheumatoid arthritis	Whole IgG1 (fully human)
Tildrakizumab		Sun Pharmaceutical	IL-23/p19	Psoriasis	Whole IgG1 (humanized)
Romosozumab		Amgen/UCB Pharma	Sclerostin	Osteoporosis	Whole IgG2 (humanized)
Racotumomab	Vaxira	Recombio	NGcGM3	NSCLC	Whole IgG1 (mouse)
Clivatuzumab tetraxetan	hPAM4-Cide	Immunomedics	Mucin1	Pancreatic cancer	Whole IgG1 (humanized)
Ublituximab		TG Therapeutics	CD20	Chronic Lymphocytic Leukemia	Whole IgG1 (chimeric)
Benralizumab		AstraZeneca	IL-5R	Asthma	Whole IgG1 (humanized)
Caplacizumab		Ablynx	vWF	Thrombotic thrombocytopenic purpura	VH-VH (humanized)
Lampalizumab		Roche	CFD	Macular degeneration	Fab fragment (humanized)
Avelumab		Merck/Pfizer	PD-L1	Merkel Cell Carcinoma	Whole IgG1 (fully human)
Aducanumab		Biogen	Beta amyloid	Alzheimer's Disease	Whole IgG1 (fully human)

Abbreviations: GD = disialoganglioside; PCSK = proprotein convertase subtilisin/kexin; EGFR = epidermal growth factor receptor; PD-L = programmed death-ligand; PDGFR = platelet-derived growth factor receptor; ACVR = activin receptor; EPCAM = epithelial cell adhesion molecule;

NGcGM = N-glycolyl (NGc) gangliosides; vWF = Von Willebrand factor; CF = complement factor.

There is expected to be an influx of antibodies in the coming years for the treatment of inflammatory skin conditions including psoriasis that encompass various cytokine targets or their respective receptors; IL-17a, IL-17R, IL-1α, IL-4R and IL-23 (Table 1). Other promising antibodies based on recent clinical trial results include ocrelizumab and atezolizumab. Ocrelizumab is a humanized antibody which selectively targets CD20-positive B cells which based on emerging evidence play a major role in activating T cells, the key cell type responsible for inflammatory damage within central nervous system lesions in multiple sclerosis (MS) [39]. Data from three Phase III studies (OPERA I, II and ORATORIO) show positive results in patients with relapsing MS and primary progressive MS (PPMS) with superiority to well-established therapy (Rebif®), by reducing the three major markers of disease activity. Atezolizumab is a monoclonal antibody designed to target PD-L1 expressed on T cells and tumour-infiltrating immune cells, preventing binding to PD-1 and B7.1 to mediate T cell immune responses. Positive results announced from two Phase II studies (POPLAR and BIRCH) in patients with advanced non-small cell lung cancer (NSCLC) show strong correlation between PD-L1 expression and response rates, suggesting that measuring PD-L1 may help identify people most likely to respond to antibody treatment. Atezolizumab has since been granted FDA approval (after priority review) for treatment of a specific type of bladder cancer and NSCLC.

A number of novel formats and treatment options are also likely to enter the market in 2017. Of note based on novelty, are racotumomab, ublituximab, MABp1 and caplacizumab. Racotumomab is an anti-idiotypic mouse monoclonal antibody that mimics N-glycolyl (NGc) gangliosides, thus triggering responses against tumor antigen NGcGM3 [40]. The idiotypic antibody acts as a therapeutic vaccine by inducing the immune system to elicit a specific response. A Phase III clinical trial is ongoing in advanced NSCLC patients.

Ublituximab is a chimeric monoclonal antibody which targets CD20 and has been fragment of crystallization (Fc) engineered with low fucose content to enhance affinity to all allelic variants of FcγIIIa receptors, demonstrating greater antibody dependent cell cytotoxicity (ADCC) than rituximab (Rituxan®) and ofatumumab (Arzerra®). This will see the second glyco-engineered antibody to enter the market (discussed later in Fc engineered section). Ublituximab is currently

being assessed in Phase III trials in combination with small molecule ibrutinib in patients with previously treated high-risk Chronic Lymphocytic Leukemia (CLL). Indeed, 2015 witnessed the first FDA approval of a combination regime of anti-PD-L1 antibodies nivolumab (Opdivo®) and ipilimumab (Yervoy®) and is quickly becoming a focus of ongoing research with both emerging and established therapeutics.

MABp1 is a 'natural' antibody cloned from an affinity-matured, *in vivo* human immune response, with no sequence modifications. The antibody was derived from Epstein-Barr-virus-immortalized B lymphocytes derived from an individual with circulating anti-interleukin-1α, a method previously described by Garrone and colleagues [41]. This potential breakthrough first-in-class 'true human™' monoclonal antibody targeting IL-1α is being assessed in Phase III clinical trials for late stage colorectal cancer. The safety results to date suggest a unique safety profile for this antibody, among the best tolerated therapies used in oncology making it ideally suited for treating advanced cancer patients with reduced tolerance for toxic therapy [42]. The antibody is also being investigated in a Phase II trial to correct the metabolic dysregulation underlying the wasting phenotype associated with malignancy by specifically targeting IL-1α signalling in the hypothalamus.

A Phase III clinical trial (HERCULES) has been initiated for bivalent nanobody® (or VHH) caplacizumab targeting anti-von Willebrand factor (vWF) to treat acquired Thrombotic Thrombocytopenic Purpura (TTP). This could see the first nanobody® to be approved and the smallest antibody fragment on the market at approximately fifteen kilodaltons (kDa).

Biobetter antibodies

Despite its success, antibody-based therapy still presents a long list of important shortcomings that need to be overcome to fully exploit their full therapeutic potential. Typical drawbacks in antibody-based therapy include limited efficacy due to poor tissue and tumor penetration, low *in vivo* efficacy, cumbersome administration, antibody aggregation, solubility as well as high production costs [43]. The use of antibody engineering to improve the properties of therapeutic antibodies has advanced greatly in the last decades giving rise to a varied set of novel formats that offer enhanced attributes for therapeutic and research purposes. These novel molecules are often referred to as biobetters or next-generation antibodies and include platforms such as: engineered antibodies for

enhanced effector functions, antibody drug-conjugates (ADC), multi-specific antibodies and single-domain antibody fragments (sdAb or nanobodies®) [44, 45].

A biobetter can have modifications to its chemical structure such as humanization, fusion/conjugation or be glyco-engineered to be less immunogenic or more efficacious. For instance, anti-CD20 ocrelizumab which is currently under review for FDA approval for MS is a humanized version of rituximab (Rituxan®). A biobetter may be modified to have an improved formulation for improved treatment regimen so treatment is less evasive or have a simplified manufacturing process. This was demonstrated with novel subcutaneous (SC) formulations of trastuzumab (Herceptin®) and rituximab (Mabthera®) developed by co-formulating the antibody with hyaluronidase, an enzyme that increases the absorption and distribution of the injected product [46]. A biobetter may be engineered to have higher target affinity, bind at a different epitope or stronger effector function to enhance efficacy and potentially reduce any off-target side effects. Any such improvement means that the therapeutic has been modified and incomparable to the original therapeutic; it is therefore classified as a new biological therapeutic and requires more laborious testing to obtain regulatory approval before market entry. In the next section, Fc engineering, ADC and multi-specific antibody-based therapies will be discussed.

Fc engineered antibodies for enhanced effector functions

Antibody engineering has sought to improve the effector function of antibodies via the Fc region; namely ADCC, complement dependent cytotoxicity (CDC) and PK profile. Specifically, this has been mostly explored through modifications in the amino acid sequence or the glycosylation pattern in the Fc region to enhance the affinity towards Fcγ receptors (FcγR) on effector cells [44, 47]. The most prominent and successful technology so far has been the glycosylation approach, which has seen nearly twenty glyco-engineered antibodies enter clinical trials with two already approved for clinical use [48-50]. The first success came with the approval of mogamulizumab (Poteligeo®) in Japan in 2012, developed using the POTELLIGENT (Kyowa Hakko Kirin) platform which is indicated for CC-chemokine receptor 4 (CCR4)-expressing T cell leukaemia-lymphoma and peripheral T cell lymphoma (PTCL) in adult patients [51].

An ADCC enhanced version of rituximab, obinituzumab (Gazyva®) gained approval by the FDA in 2013 under breakthrough therapy designation [52]. Obinituzumab is an anti-CD20 monoclonal antibody that was originated by GlycArt Biotechnology (now GlycoMAb) and is approved for

CCL [49]. Both POTELLIGENT® and GlycArt platforms are based on the manufacture of products using engineered cell lines that yield defucosylated antibodies; a structural modification that removes the core 1,6 fucose from the N-glycans attached to asparagine at amino acid position 297 of human IgG1 thereby greatly enhancing the affinity towards FcγRIII, and increasing ADCC induction by NK cells (Figure 1a) [53, 54]. NK cells are not abundant in the tumor site, and human endogenous IgG can inhibit the elicitation of ADCC by therapeutic antibodies [55] therefore, increasing the affinity towards FcγRIII to preferentially interact with the therapeutic antibody is a valuable approach to improve the efficacy profile. This approach was demonstrated by Zhang et al. by producing an anti-HER2 antibody with an identical sequence to trastuzumab but with superior binding affinity to FcγRIIIa and greater ADCC activity [56]. The antibody was produced using glyco-engineered Pichia pastoris and the differences were presumed to be due to absence of fucose in the N-glycans attached to the IgG1 product.
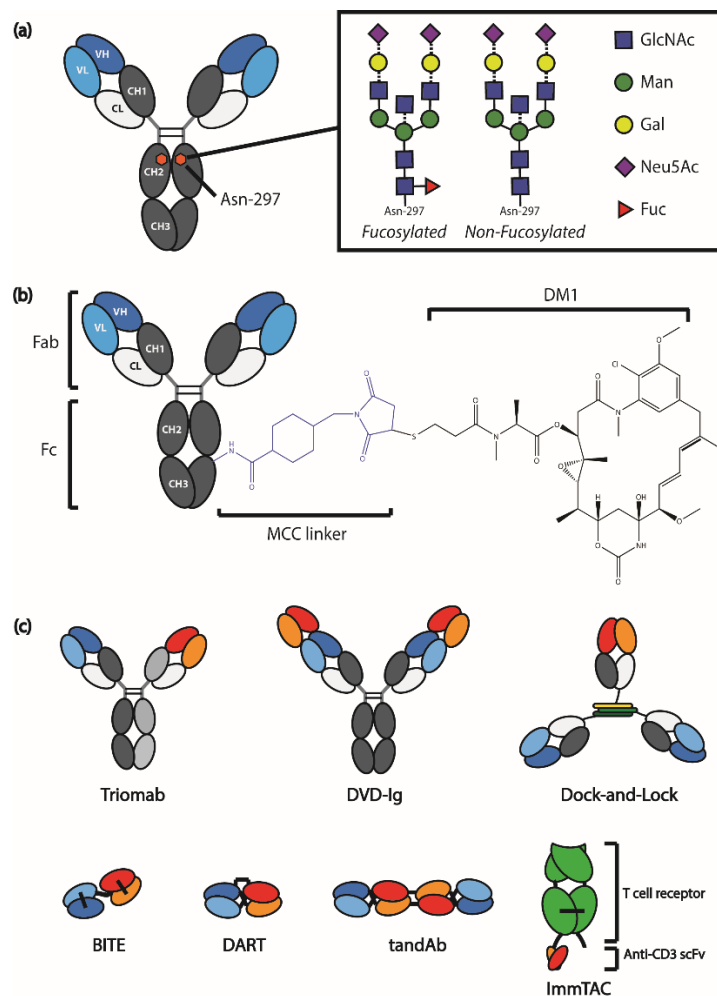
Figure 1. Schematic representation of biobetter antibody formats being pursued for clinical development. (a) Schematic structure of an IgG1 antibody with glycosylation sites at asparagine 297 (Asn-297) in CH2 domains indicated by hexagons. The general structure of N-linked glycosylation is shown inset; core structures indicated by solid lines and variable structures by dotted lines. Glyco-engineering of antibodies can involve defucosylation which refers to the removal of core fucose to enhance Fc-mediated effector functions. (b) Schematic structure of an antibody drug conjugate (ado-trastuzumab emtansine; Kadcyla®) including N-maleimidomethyl cyclohexane-1-carboxylate (MCC) linker and maytansinoid 1 (DM1) payload. (c) Prominent bispecific formats in development as discussed in the text including: Triomab or Trifunctional antibody, Dual variable domain immunoglobulin (DVD-Ig), Dock-and-Lock (DNL) antigen binding fragments (Fabs), Bispecific T cell engager (BITE), Dual affinity re-targeting (DART) molecule, Tandem diabody (tandAb) and Immune-mobilizing monoclonal TCRs against cancer (ImmTAC).

Whereas the glyco-engineering approach generates defucosylated antibodies with FcγRIIIa-specific affinity improvement, variants generated by mutagenesis of Fc amino acid sequence can be enhanced for multiple FcγR interactions. A number of publications have identified specific Fc mutations to improve binding to the activating receptor FcγIIIa and reduce binding to the inhibitory receptor FcγIIb with corresponding improvement to ADCC activity [57-59]. The XmAb® concept is currently being investigated as an anti-CD30 in Phase I trials for Hodgkin lymphoma.

In an alternative approach, aglycosylated antibodies (without glycan structures) can be engineered to display effector functions that are distinct from those of glycosylated counterparts [60-63]. The use of aglycosylated therapeutic antibodies offers manufacturing advantages by bypassing glycosylation and hence production can be performed in prokaryotic hosts. On the other hand, the importance of glycosylation on the structural stability of antibodies has been demonstrated [64, 65]. The first aglycosylated antibody to enter clinical trials, produced in yeast, is humanized rat-derived IgG1 otelixizumab directed against CD3 which is being assessed in Phase II trials for type I diabetes mellitus.

Antibody drug conjugates (ADC)

ADC comprise one of the foremost antibody-based platforms currently being pursued for clinical implementation. Indeed, the FDA approval of brentuximab vedotin (Adcetris®) and a cytotoxin-

conjugated biobetter of trastuzumab, ado-trastuzumab emtansine (Kadcyla®) in 2011 and 2013 respectively, have eclipsed the clinical failures of first generation ADC. As of early 2016, in addition to the two ADC available in the market, over forty antibody drug conjugates are undergoing clinical trials and a plethora of such formats are in preclinical development [3]. (Table 3). The achievement of such milestones has been facilitated by the advent of novel ADC technologies and designs.

Table 3. Overview of ADC developed in recent years and their clinical status.

ADC	Format	Target	Payload	Linker	Lead indications
FDA APPROVED					
Brentuximab vedotin (Adcetris®)	IgG1 (Chimeric)	CD30	MMAE	Valine-Citrulline	Hodgkin Lymphoma, Anaplastic large cell lymphoma
Ado-trastuzumab emtansine (Kadcyla®)	IgG1 (Humanized)	HER2	DM1	Valine-Citrulline	HER2+ breast cancer
Gemtuzumab ozogamicin (Mylotarg® - withdrawn)	IgG4 (Humanized)	CD33	Calicheamicin	SS/hydrazone	Acute Myeloid Leukemia
Phase III					
Inotuzumab ozogamicin	IgG4 (Humanized)	CD22	Calicheamicin	SS/hydrazone	Acute Lymphoblastic Leukemia
Phase II					
Enfortumab vedotin (ASG-22ME)	IgG1 (Human)	Nectin-4	MMAE	Valine-Citrulline	Bladder cancer

PSMA ADC	IgG1 (Human)	PSMA	MMAE	Valine-Citrulline	Prostate cancer
Glembatumumab vedotin (CDX-011)	IgG2 (Human)	GPNMB	MMAE	Valine-Citrulline	Breast cancer
Lifastuzumab vedotin (DNIB0600A)	IgG1 (Humanized)	NaPi2b	MMAE	Valine-Citrulline	Ovarian cancer
Pinatuzumab vedotin (DCDT2980S)	IgG1 (Humanized)	CD22	MMAE	Valine-Citrulline	Non-Hodgkin's Lymphoma (NHL)
Polatuzumab vedotin (DCDS4501A)	IgG1 (Humanized)	CD79b	MMAE	Valine-Citrulline	NHL, Diffuse large B cell lymphoma
Lorvotuzumab mertansine (IMGN-901)	IgG1 (Humanized)	CD56	DM1	SPP	Hematological malignancies
IMMU-130 (Labetuzumab-SN-38)	IgG1 (Humanized)	CEACAM5	SN-38	Carbonate	Colorectal cancer
IMMU-132 (hRS7-SN38ADC)	IgG1 (Human)	TROP-2	SN-38	Carbonate	Breast cancer
Milatuzumab doxorubicin (IMMU-110)	IgG1 (Humanized)	CD74	Doxorubicin	Hydrazone	Multiple myeloma
Indatuximab ravtansine (BT-062)	IgG1 (Humanized)	CD138	DM4	SPDB	Multiple myeloma
Rovalpituzumab tesirine (SC16LD6.5)	Undisclosed	Fyn3	D6.5	Undisclosed	Small cell lung cancer

Depatuxizumab mafodotin (ABT-414)	IgG1 (Human)	EGFRvIII	MMAF	Maleimidocaproyl	Glioblastoma

Abbreviations: MMAE = monomethylauristatin; DM = maytansinoid; PSMA = prostate-specific membrane antigen; GPNMB = transmembrane glycoprotein NMB; NaPi = sodium-dependent inorganic phosphate; CEACAM = carcinoembryonic antigen-related cell adhesion molecule; EGFR = epidermal growth factor receptor.

While the targeted nature of ADC therapy is expected to reduce treatment side effects, toxicity still remains an important concern for ADC. In fact, gemtuzumab ozogamicin (Mylotarg®), a humanized anti-CD33 antibody conjugated to calicheamicin was the first ADC to receive FDA approval in 2000 for treatment of acute myeloid leukemia (AML). However, Mylotarg® was voluntarily withdrawn from the market after results of a Phase III study raised toxicity concerns and showed no benefit compared to standard therapies [66]. Brentuximab vedotin and ado-trastuzumab emtansine also present significant toxicity; both are required by the FDA to carry a black box warning due to the risk (although only seen in rare cases) of developing progressive multifocal leukoencephalopathy (brentuximab vedotin) and risk of hepatotoxicity, cardiac toxicity, and embryo-fetal toxicity (ado-trastuzumab emtansine). Consequently, there remains a challenge in the field to further validate the superior therapeutic index that ADC can deliver over traditional chemotherapy and other targeted therapies. In this regard, great efforts are being directed to implement refinements in each of the components (targeted antigen, targeting moiety, linker, payload and conjugation chemistry) to boost the therapeutic potential of ADC.

While most conjugates in clinical and preclinical development target cell surface receptors that are overexpressed in solid tumours and B-cell malignancies (Table 3), novel approaches such as targeting antigens present in neovasculature or extracellular stromal tissue are being explored. One main advantage of such approach is that perfusion into the tumor is not required since blood serum is in direct contact with vascular endothelial cells, with exposure of the conjugate to its target tissue considerably greater than for traditional ADC targeting neoplastic cells [67-69]. Another attractive feature is that vascular endothelial cells are less likely to develop resistance mechanisms. Others have also explored the possibility of targeting cancer stromal cells, aiming to suppress tumor proliferation, neovascularization, invasion, and metastasis which are typically promoted by the

tumor microenvironment [70, 71]. Overall, the factors affecting the internalization rate of ADC suggest that antigen selection is of high importance in determining the efficacy of the conjugate in a physiological environment.

Conversely, the efficacy of a conjugate is predominantly determined by its affixed payload. Current ADC feature antineoplastic agents that have an extremely high potency, usually in the sub-nanomolar range. Most of these molecules are derivatives of highly potent cytotoxic drugs that have exquisite potency but at the same time, make them unamenable for development as chemotherapeutic agents alone. The cytotoxic drugs being employed can be classified into three major groups namely, calicheamicins (DNA disruption), maytansinoids and auristatins (cell cycle interference) [72-75]. Monomethylauristatin E (MMAE) and monomethylauristatin F (MMAF) are the most widely used payloads in the current pipeline with another twenty auristatin conjugates under clinical development [76, 77]. Among the maytansine analogs, DM1 and DM4 are being pursued with more than ten ADC in clinical trials (Table 3; Figure 1b). Alternative drug classes such as duocarmycins and pyrrolobenzodiazepines may also gain popularity due to their remarkable potency [78, 79].

The linker component is a major determinant of plasma stability of a conjugate, thus impacting on the efficacy and safety profile. One of the main reasons for off-target effects is the premature release of cytotoxic activity outside of target cells. A commonly used approach for coupling the conjugate to an antibody is via a linker that contains a lysosomal-specific protease cleavage site. In this format, the linker is intended to be cleaved in the lysosome by proteases such as cathepsin B, plasmin and β-glucoronidase [80, 81]. Indeed, the valine-citrulline (Val-Cit) dipeptide linker, recognized and cleaved by cathepsin B, is currently the most widely implemented linker technology [82, 83]. A novel approach using non-cleavable linkers has gained popularity since they could substantially increase blood serum stability. In this modality, the antibody is digested inside the lysosome upon internalization, releasing the payload attached to an amino acid residue, yet still retaining its cytotoxic activity [84, 85]. For example, ado-trastuzumab emtansine, employs the hetero-bifunctional crosslinker N-succinimidyl-4-(N-maleimidomethyl) cyclohexane-1-carboxylate (SMCC), creating a non-reducible thioether linker (MCC) as a spacer between the anti-HER2 antibody and the maytansine DM1 [86]. Presumably due to increased stability, reduced toxicity has been observed with non-cleavable linker design relative to conjugates with cleavable

linker [87]. Remarkably, ado-trastuzumab emtansine has displayed superior *in vivo* activity in mouse breast cancer models compared to a similar trastuzumab-DM1 conjugate that differs only in that it contains a disulphide reducible linker [88].

The chemical reactions used to couple ADC components can also play a role in the therapeutic index. The first conjugation techniques developed to create ADC involved a chemical reaction between a functional group in the linker and a reactive moiety in native amino acid residues, predominantly the thiol side-chains of partially reduced cysteines and the epsilon-amino end of lysine residues [89, 90]. In these cases, the conjugation sites and the number of drug molecules affixed to the antibody are stochastic, resulting in heavily heterogeneous conjugates. This heterogeneity undermines the clinical potential of ADC, since it impacts severely on their toxicity and safety profiles. In terms of potency, the efficacy is compromised by the reduced subset of ADC with an optimal amount of attached drug to exert a significant cytotoxic effect. Besides the fact that conjugates with low drug-to-antibody ratios (DAR) have limited efficacy, high DAR also possess higher toxicity and reduced plasma stability due to increased clearance rates [91]. This clearly illustrates the critical importance of achieving an optimal ratio. Despite the shortcomings of stochastic attachments methods, both cysteine and lysine conjugation techniques have been utilized in the development of brentuximab vedotin and ado-trastuzumab emtansine, respectively. A set of alternate novel techniques have been developed to allow for site-specific conjugation including the THIOMAB platform [92], introduction of unnatural amino acids or enzymatic modification of native amino acid side-chains [93-95] and even glycan attachment through glyco-engineering [96].

Bispecifics

The next novel wave of therapeutic antibodies is predicted to be in the format of bispecific antibodies. The concept of bispecific antibodies was first demonstrated more than twenty years ago, initially by chemical conjugation of two antibodies [97] then by fusing two hybridoma cultures [98]. There are now more than fifty different bispecific formats in development, enabling researchers to adjust and control parameters such as size, half-life, stability, flexibility and orientation to achieve the desired therapeutic outcome. The assembly of antibody chains to accomplish the various antibody formats has been made possible with antibody engineering techniques including variations of the general approach [99-101] to novel approaches such as

'knobs-into-holes' [102], CrossMab [103], 'Dock-and-Lock' (DNL) [104, 105] and even hybrid domains derived from other immunoglobulin antibodies, via a technology referred to as strand-exchange engineered domain (SEED) [106].

The majority of bispecific antibodies are currently being assessed in clinical trials and are detailed in Table 4 with a few examples discussed below based on their mode of action. Referred to as a trifunctional or triomab is catumaxomab (Removab®), bispecific to tumor antigen EPCAM and T cell marker CD3 (Figure 1c). The antibody acts by recruiting and activating immune cells; EPCAM targets the tumor, CD3 recruits T effector cells and the Fc region recruits and activates monocytes, macrophages, dendritic cells (DC) and NK cells by FcγR binding [107]. Catumaxomab is a hybrid antibody comprised of rat IgG2b binding domains and mouse IgG2a Fc region. Catumaxomab has not yet received FDA approval (BLA submitted) but has EMA approval for the treatment of malignant ascites since 2009. The antibody is also in clinical trials for application in ovarian cancer (II), gastric cancer (II) and epithelial cancer (I). Given that catumaxomab is a rat-mouse hybrid, some anti-rat or anti-mouse IgG responses are observed in patients, though treatment does not appear to be significantly affected. In fact, development of human anti-mouse antibodies (HAMA) have been shown to contribute to greater clinical benefit [108].

Table 4. Bispecific antibodies developed in recent years and their clinical status.

Name	Company	Targets	Antibody type	Mode of Action	Indications
FDA approved					
Blinatumomab Blincyto®	Amgen	CD19/CD3	BiTE	T cell recruitment	Philadelphia chromosome-negative precursor B-cell acute lymphoblastic leukemia
Clinical Trials Completed					
Catumaxomab Removab®	Trion Pharma	EPCAM/CD3	Trifunctional/ Triomab	T cell recruitment/ Fc effector	Malignant ascites
Phase III					
Emicizumab/ RG6013/ACE910	Roche	Factors XI/X	CLC-IgG	Two factor dimerisation	Haemophilia A

MT111/MEDI565	MedImmune	CEA/CD3	BiTE	T cell recruitment	Gastrointestinal cancer
Phase II					
Vanucizumab	Roche	Angiopoietin2/VEGF	Crossmab	Two ligand inactivation	Colorectal cancer
RG7716	Roche	Angiopoietin2/VEGF	Crossmab	Two ligand inactivation	Macular degeneration
TF2	IBC Pharmaceutical/ Immunomedics	CEA/Hapten	DNL Fab3	Payload delivery	Small cell lung cancer, Colorectal cancer, Thyroid cancer
Duligotuzumab	Genentech/Roche	HER1/HER3	DAF-IgG	Two ligand inactivation	Head and neck cancer, Colorectal cancer
ABT122	Abbott Laboratories	TNFα/IL-17	DVD-IgG	Two ligand inactivation	Rheumatoid arthritis, Psoriatic arthritis
ABT981	Abbott Laboratories	IL-1α/IL-1β	DVD-IgG	Two ligand inactivation	Osteoarthritis
SAR156597	Sanofi-Aventis	IL-4/IL-13	DVD-IgG	Two ligand inactivation	Idiopathic pulmonary fibrosis
Istiratumab/ MM141	Merrimack Pharmaceuticals	IGF1R/HER3	IgG-scFv	Two ligand inactivation	Pancreatic cancer
IMCgp100	Immunocore	MHC peptide$_{280-88}$/CD3	ImmTAC	T cell recruitment	Malignant melanoma
AFM13	Affimed Therapeutics	CD30/CD16	TandAb	NK cell recruitment	Hodgkin Lymphoma
Phase I					
BI1034020	Boehringer Ingelheim Pharmaceuticals	Beta amyloid 2 epitopes	Bi-nanobody	Undisclosed	Alzheimer's Disease
ALX0761	Merck Sereno	IL-17A/IL-17F	Bi-nanobody	Two ligand inactivation	Psoriasis
LY3164530	Eli Lilly	HER1/cMET	orthoFab-IgG	Two ligand inactivation	Metastatic cancer

Pasotuxizumab	Bayer	PSMA/CD3	BiTE	T cell recruitment	Prostate cancer
MGD006	Servier	CD123/CD3	DART	T cell recruitment	Acute Myeloid Leukemia
AFM11	Affimed Therapeutics	CD19/CD3	TandAb	T cell recruitment	Acute Lymphoblastic Leukemia, Non-Hodgkin's Lymphoma
MGD007	Servier	GPA33/CD3	DART-Fc	T cell recruitment/ Fc effector	Colorectal cancer

Abbreviations: BiTE = bispecific T cell engager; CLC = common light chain; DNL= dock-and-lock; Fab = antigen binding fragment; DAF = dual acting Fab; DVD-IgG = dual variable domain immunoglobulin, scFv = single chain variable fragment; ImmTAC = immune-mobilizing monoclonal TCRs against cancer; TandAb = tandem diabody; DART = dual affinity re-targeting molecule; Fc = fragment of crystallization; EPCAM = epithelial cell adhesion molecule; CEA = carcinoembryonic antigen; VEGF = vascular endothelial growth factor; TNF = tumor necrosis factor; IGFR = insulin growth factor receptor; MHC = major histocompatibility complex; PSMA = prostate-specific membrane antigen; GP = glycoprotein; NK = natural killer.

Another example that achieves effector cell recruitment via a conceptually different format without a Fc region is bispecific T cell engager (BiTE®). BiTEs are variable regions in the form of two scFv connected by flexible linker peptides (Figure 1c) [109, 110]. One scFv is directed at a cell surface tumor antigen (with higher affinity) and the other scFv binds CD3 (with lower affinity). The first marketed BiTE was blinatumomab (Blincyto®) which targets CD19 on acute lymphoblastic leukemia (ALL), approved by the FDA in late 2014 under the accelerated approval program. Blinatumomab is currently undergoing multiple Phase II and Phase III clinical trials for other B-cell related malignancies [111]. A major setback for BiTEs is the requirement of continuous intravenous infusion due to the short half-life inherent to the small size of the molecule (55 kDa) and the lack of Fc region. Additionally, the treatment produces significant side effects, notably neurotoxicity and symptoms of cytokine-release syndrome [112]. Despite the challenges, this strategy is being investigated for other targets (CEA, EPCAM, PSMA) and indications. Other examples of molecules with immune cell recruitment are dual affinity re-targeting (DART®) [113, 114] and tandem diabodies (tandAb®) (Figure 1c) [115, 116].

Another novel class of bispecific molecules called immune-mobilizing monoclonal TCRs against cancer (ImmTAC) further expands the variety of potential tumor-specific antigens, by incorporating soluble T cell receptors (TCRs) that can target intracellular antigens through recognition of peptide-HLA antigen complexes on the cell surface (Figure 1c) [117]. Under current investigation in Phase II clinical trial for malignant melanoma is IMCgp100. The engineered TCR portion of the molecule targets the gp100 peptide280-288 antigen, which is overexpressed and presented by HLA-A2 on the surface of melanoma cells. The anti-CD3 scFv portion captures and redirects T cells to kill the melanoma cells.

With the knowledge gained on validated targets and receptor signalling of existing therapeutic antibodies, targeting two antigens to simultaneously interfere with two or more signaling pathways is being pursued to improve therapeutic efficacy. The most advanced molecule in clinical development is dugliotuzumab, a human IgG which targets the combination of HER1 and HER3 as a dual action Fab (DAF)-IgG [118]. Duligotuzumab is being evaluated in Phase II trial in patients with head and neck cancer. The dual interference can also be applied to inflammatory conditions. Dual variable domain immunoglobulin (DVD-Ig™) formats directed at TNFα + IL-17 and IL-1α + IL-1β are undergoing assessment in Phase I studies in patients with rheumatoid arthritis (Figure 1c) [119]. Other formats being investigated to interfere with signaling pathways include CrossMabs [103] and bi-nanobodies [120].

Bispecifics can also serve as vehicles to deliver payloads to tumor cells. TF2 is a DNL(Fab3) bispecific antibody that binds to CEA present on the surface of many solid tumours (Figure 1c). The antibody comprises three Fab modules that are stably coupled to each other in a triangular fashion using the 'dock-and-lock' technology. Without a Fc region, these molecules have a rather short serum half-life which is an advantage for pre-targeting approaches. TF2 is being evaluated in a Phase I trial in patients with colorectal cancer using Lutetium-177 or Indium-111 payload for imaging.

Physical and chemical degradation of antibodies

During manufacturing and storage, therapeutic antibodies are at risk of degradation via a number of pathways. Though these reactions may be kept under control by appropriate storage and

formulation conditions of the final product, degradation that occurs during culture, downstream processing and *in vivo* cannot be controlled sufficiently. These degradation events may affect antigen recognition, hamper functionality and in severe cases lead to immunogenic responses [121-125]. Each antibody molecule seems to have a unique personality related to its requirements for stability; a phenomenon derived from the fact that differences in the CDR between antibodies are primarily dictated by the surface exposed amino acids that define antigen specificity [124]. The identification of degradation prone or unstable regions early in the antibody development process would ideally permit re-engineering of these problematic areas [126-129]. This approach is aided by recent developments in computational modelling tools that predict regions of interest susceptible to physical, chemical degradation or influence other biophysical properties of antibodies. In the next section, degradation pathways commonly observed in therapeutic antibodies and an overview of predictive tools are discussed.

Aggregation

Protein aggregation is the most common and significant type of physical degradation associated with therapeutic antibodies, often leading to reduced activity and in some cases, formation of immunogenic products [130, 131]. Initial preparations of therapeutic antibodies were administered by intravenous (IV) infusion formulated at protein concentrations (1-25 mg/ml). As antibody-based therapeutics have become more widely used, high concentration formulations that allow SC injection (>50 mg/ml) became desirable giving rise to aggregation issues. Proteins are folded in such a way as to internalize hydrophobic domains and surface expose more hydrophilic domains. As protein-protein contact frequency increases at high concentrations, the opportunity for aggregation formation increases proportionally. Changes in extrinsic conditions including temperature, pH, salt, shaking, viscosity and concentration can transiently expose hydrophobic domains which in doing so promotes protein-protein interactions that lead to aggregation events [132-135]. Non-covalent aggregates can be formed via hydrophobic and/or electrostatic interactions and may be reversible, while covalent aggregates are usually formed by disulphide bonds and are difficult to reverse. Mechanisms of protein aggregation include: (1) aggregation of native state monomers; (2) aggregation of monomers with a modified conformation (non-native); (3) aggregation of chemically-modified monomers; (4) aggregation via a nucleation-dependant

process; and (5) surface-induced aggregation via adsorption of protein to glass-liquid or air-liquid interfaces [136, 137].

Denaturation

Protein denaturation refers to the partial or complete unfolding of the native three-dimensional folded protein structure. A denatured antibody often loses its tertiary and perhaps secondary structure leading to loss of binding affinity and activity if an active site domain is affected, and may expose aggregation-prone regions leading to further degradation [133, 138, 139]. Several intermediate states may exist between the folded native structure of an antibody molecule and the denatured state, with some intermediates thought to act as precursors or 'nuclei', attracting other protein species to exposed hydrophobic sites and forming irreversible aggregates. Denaturation may be induced by a number of stress conditions that arise during antibody manufacture including changes in solution pH or temperature, use of organic solvents or chaotropes, high salt concentrations, or shear force [132, 133, 140]. In general, the CH3 domain of an IgG antibody is often the most stable against denaturation at high temperatures (highest Tm) while the IgG CH2 domain is least stable and denatures first (lowest Tm) [141].

Fragmentation

Fragmentation of therapeutic antibodies can be a product of enzymatic or non-enzymatic hydrolysis that occurs at the peptide backbone of a number of regions, such as the hinge region, the CH2-CH3 interface or a region containing aspartic acid (Asp) or tryptophan (Trp) residues [132]. Asp-associated hydrolysis is affected by pH and the n+1 residue; for instance, a serine (Ser), valine (Val) or tyrosine (Tyr) adjacent to an Asp may increase the rate of Asp-hydrolysis. Hinge region hydrolysis can occur in the absence of Asp, and occurs most commonly in the IgG1 isoform [132, 142, 143]. The rate of hydrolysis is dependent on the flexibility the peptide sequence at the hinge, and occurs within a narrow range of residues. Hinge hydrolysis rates are affected by solution pH, with a minimum rate of hydrolysis observed near pH 6, and higher rates at a lower or higher pH [132, 143]. Fragmentation of full-length antibodies is a common occurrence and generally, cleaved forms are present in such low amounts that effect on efficacy would not likely be seen.

Deamidation

Deamidation is the most common chemical degradation pathway of therapeutic antibodies and results from the hydrolysis of the amide side-chain of amino acids glutamine (Gln) or asparagine (Asn) [132, 136, 144, 145]. Hydrolysis of the side-chain can occur at acidic pH (pH <4) resulting in the conversion of Asn to Asp and Gln to glutamic acid (Glu) [132]. However at higher pH, deamidation occurs predominantly (and more slowly) via the formation of a cyclic imide intermediate. For Asn, the cyclic intermediate (succinimide) leads to either the formation of Asp or an isomer of Asp. A similar process results in the deamidation of Gln to Glu; although Gln deamidation is much less frequent, due to the lower stability of the 6-membered cyclic intermediate formed. In short, deamidation events lead to more acidic forms of the antibody through the acquisition of additional carboxylic acid groups. Conversely, it is also possible for Asp residues to undergo modification to a succinimide intermediate that produces a basic form of the antibody by removal of a carboxylic acid group [144].

A number of factors can affect the rate of deamidation. For instance, Asn residues are more prone to deamidation if they are present in solvent-accessible or structurally-flexible regions, especially if followed by a small or flexible residue such as Gly, Ser, threonine (Thr) or Asn [132, 146]. Deamidation rate is also affected by extrinsic conditions including pH, temperature, buffer composition and concentration [147]. Gln deamidation is thought to be less common than Asp deamidation due to the lower stability of the 6-membered cyclic ring intermediate, which results in a much slower reaction rate [132]. Although Gln deamidation occurs less frequently, a study found that following incubation at pH 9, 7.8% of Gln82 of a recombinant IgG1 mAb had undergone deamidation, despite no deamidation of this residue occurring at neutral pH [145].

Deamidation of therapeutic antibodies is well characterised both and *in vivo*, and has been shown to decrease the potency, activity and stability of antibodies [144, 146-150]. The deamidation events appear to be highly selective for individual antibodies. For example, Harris et al. performed accelerated stability studies at elevated temperatures with rhuMAB HER2 antibody and found three labile Asn residues in the CDR region (Asn55, Asn30 and Asn102) [144]. These residues either formed aspartate, isoasparatate or a stable succinimide intermediate, resulting in a total of seven species of the antibody being resolved. Deamidation of these Asn residues was shown to significantly affect the specific *in vitro* activity and potency of rhuMAb HER2.

Oxidation

Oxidation is another common degradation pathway which can occur during antibody production, formulation or storage. A number of amino acid residues may be affected, including methionine (Met), cysteine (Cys), histidine (His), tyrosine (Tyr) and Trp [132]. Specific Met residues within the Fc region (up to four residues) are prone to oxidation resulting in production of methionine sulfoxide [136, 151, 152]. Oxidation of these residues may affect the stability of an antibody, Fc-mediated effector function or Protein A binding affinity which is often used for purification from cell culture supernatant [153]. Wang et al. demonstrated that oxidation of Met252 can result in >4-fold reduction in the half-life of an antibody in transgenic mice expressing human Fc neonatal receptor (FcRn). However, this was only observed when 80% of the antibody existed in the oxidized form, and not at 40% [154].

Oxidation can be dependent on intrinsic factors such as the degree of surface exposed residues as well as extrinsic factors including buffer composition, light exposure and pH, although Met oxidation appears to be almost pH-independent [132, 153, 155]. Oxidative stress has been observed during antibody production in mammalian expression systems where the formation of reactive oxygen species as a result of hypoxic conditions caused fragmentation of an IgG1 antibody [156].

Tryptophan oxidation of antibodies has been reported following light exposure. Sreedhara et al. found that light induced oxidation of surface exposed Trp residues (Trp53, Trp108 and Trp94) in the Fab region of an IgG1 antibody leading to a loss in potency accompanied with a solution colour change [151]. In another example, oxidation of Trp residue in the H3 CDR loop (Trp135) of a humanized anti-respiratory syncytial virus (RSV) therapeutic antibody resulted in loss of antigen binding and biological function [157].

Computational design tools

In recent years, computational methods used to simulate and develop structural models of proteins have transformed into practical design tools for the development of biobetter and next-generation antibody therapeutics [127, 158]. Current computational design tools have evolved to allow rapid identification of specific amino acid sequences or regions on a protein of interest, that contribute to its observed *in vivo* properties such as binding affinity, efficacy, stability and half-life [158].

Some of the early computational tools used for protein modelling include TANGO, PAGE, AGGRESCAN, PASTA and Zyggregator all of which rely on the sequence of the protein of interest (Table 5) [128, 159-164]. These computational tools use force fields such as CHARMM or AMBER and exploit chemical properties of the amino acids such as hydrophobicity, β-sheet propensity, charge, and aromatic content to predict aggregation hot-spots and residues susceptible to chemical degradation. In some cases, multiple tools can be used in combination to improve the predictive power. For example, Wang et al. combined TANGO and PAGE to identify aggregation-prone motifs and residues susceptible to deamidation or oxidation of 22 commercial and 20 non-commercial therapeutic antibodies [165].

Table 5. A representative list of computational tools for prediction of protein aggregation hot spots.

Name	Properties
Sequence-based methods	
TANGO [204].	Determines the secondary structure formation propensity
Aggrescan [205].	Uses amino acid aggregation propensity value
Zyggregator [207].	Compares a new peptide sequence to the database
PASTA [208].	Predicts amyloid structure aggregation by looking into sequences that are likely to stabilize the cross-beta core of fibrils
PAGE [209].	Uses physicochemical properties for prediction
Structure-based methods	
SAP [173].	Determines spatial effective surface accessible area
LIP [211].	Measures ratio of polar surface area to apolar surface area of buried interfaces
AGGRESCAN3D [212].	Based of original AGGRESCAN server with input from 3D structure and spatial arrangement of residues

Some structure-based computational tools have also been developed. One such method, Spatial Aggregation Propensity (SAP), predicts surface exposed aggregation-prone regions of a protein based on hydrophobicity, dynamic fluctuations and solvent accessibility of residues and regions [127]. The tool has been used to simulate entire antibodies and develop IgG1 antibody variants with enhanced physical stability to the wild type, by performing single or multiple mutations in either the Fab or Fc regions [127, 129].

Another method developed by Angarica and Sancho predicts aggregation propensity based on the packing density and polarity ratio (ratio of polar surface area to apolar surface area) of buried interfaces [166]. The tool was designed to characterise "Light Interfaces of high Polarity" (LIPs) considered to be intrinsically unstable cores. The technology shows promise as a tool for engineering antibody variants with increased aggregation-resistance, especially as a complimentary method to surface- or sequence-based tools mentioned above.

One of the most recent developments in computational modelling is the evolution of AGGRESCAN to AGGRESCAN3D (A3D), an improved server which addresses many of the limitations of AGGRESCAN and other sequence-based methods. A3D takes into account the three-dimensional structure of the protein and the spatial arrangement of the residues when the protein is in its native folded state [167]. With the incorporation of a mutation module that allows the easy modelling of the detected aggregation-prone and surrounding residues, A3D looks to be a promising tool for predicting problematic regions and the same time, allowing for re-design of more stable proteins.

Optimization of antibody bioavailability and delivery

Antibody-based therapies are predominantly delivered intravenously (IV), though an increasing number are now being formulated and administered subcutaneously (SC). While the IV route offers 100% bioavailability, systemic distribution and physiological barriers greatly reduce the actual concentration of antibody achieved in target tissues [168]. What is more, IV infusions are time-consuming and inconvenient. Ideally, an antibody formulation should be non-invasive and increase local bioavailability. Limited alternatives have been implemented in the clinic since formulation requirements for such delivery often pose significant hurdles. For other parenteral

administration routes, such as SC or intramuscular (IM), the most common limitation is poor antibody solubility at the high concentrations required, given that maximum volume of injection is restricted to 2 ml and 5 ml, respectively. When compared to IV formulations which range from 1-25 mg/ml, SC and IM products often require concentrations >100 mg/ml to deliver an effective dose [169]. Furthermore, these delivery routes involve an absorption step to enable systemic circulation. Two main approaches are being pursued to optimize bioavailability: 1) the design of aggregation-resistant antibodies with higher solubility to prevent precipitation at higher concentrations; 2) the use of polymer matrix systems to develop controlled release formulations and improve PK profile.

As discussed in the previous section, the design of aggregation-resistant antibodies albeit challenging, has become possible with the implementation of computational tools and increasing understanding of antibody structure and degradation pathways. Formulation stability has also been improved by using stabilizing additives such as salts (e.g. citrates, sulfates), amino acids (e.g. glycine) and sugars (e.g. sorbitol, sucrose, trehalose) [132, 170-172]. The development of SC and IM products has been successful in the last decade because of the formulation of large doses in significantly smaller volumes without aggregation issues [46]. SC and IM formulations have significantly improved patient convenience enabling self-administration through the use of pre-filled syringes, a feature that is highly advantageous for treatment of chronic diseases. A novel approach to improving SC formulation and PK has been proposed by Yang et al. whereby, crystalline antibody preparations of infliximab (Remicade®) and trastuzumab (Herceptin®) were formulated at 200 mg/ml while maintaining low viscosities suitable for this delivery route [173]. Animal studies in rats showed a 2-fold increase of antibody half-life compared to non-crystallized antibody, demonstrating the potential of crystalline preparations as controlled release systems. Alginate polymers have also been explored for controlled release. Schweizer et al. developed two polyanionic alginate matrices loaded with antibody through electrostatic interactions [174]. Both matrices were delivered to rats subcutaneously as hydrogels. After comparison with its liquid antibody counterpart, no significant differences in bioavailability were reported.

For many pathologies, local delivery could increase efficacy and reduce systemic exposure. In such cases, administration routes such as oral, topical, respiratory and intraocular become highly relevant. Controlled release systems based on polymer matrices are also being tested in preclinical

studies for these delivery routes [168, 175]. For instance, liposomes and chitosan-alginate microparticles have been employed for oral delivery in order to protect antibodies from gastric inactivation and allow release in the small intestine [176, 177]. This is being explored in combination with the conjugation of targeting ligands to improve delivery and absorption in the gastro-intestinal tract. [178]. For topical application, a hydrofiber dressing/adhesive sheet has been used to apply infliximab as a gel formulation for wound healing with improvements in 7/8 patients tested [179]. In another example, a Phase I trial has been completed with positive results for BIL-010t, a topically administered, sheep antibody therapy to treat Basal Cell Carcinoma (BCC). BIL-010t ointment was self-applied for 28 days; it was noted that 13/20 patients had decreases in the sizes of their lesions with only mild localized skin reactions reported. The respiratory route has been extensively studied for treatment of chronic obstructive pulmonary disease, lung cancer, asthma and other pulmonary pathologies. Liposomes and microspheres have shown potential to increase bioavailability of respiratory delivery by preventing proteolysis [180]. The PEGylation of antibody fragments was shown to increase lung lumen residence time in a murine model through decreased clearance of alveolar macrophages and increased mucoadhesion [181]. Other strategies being investigated to deliver antibodies via the respiratory tract include IgG-loaded lipid microparticles and nano-micelles [182-184]. The most advanced molecule in clinical development is ALX-0171, an anti-RSV nanobody administered through inhalation; demonstrating a positive safety and tolerability profile in a first-in-infant Phase I/II study with an anti-viral effect observed [185].

Overall, the IV route will likely remain the most prominent administration route in development due to ease of formulation. Still, the improvement of local bioavailability is an obvious requirement to fulfil the potential of antibody-based therapy, both in terms of efficacy and patient convenience. As such, strategies such as pursuing alternative administration routes and developing appropriate controlled release systems will gain relevance as their therapeutic potential continues to be explored in preclinical studies.

Conclusions

Antibody-based therapeutics have evolved from murine antibodies to humanized and fully human antibodies, developed with innovative technologies such as transgenic mice and phage display. In the coming years, next-generation antibodies with improved properties and formats including

ADC and bispecifics are expected to gain popularity as biobetter antibody therapeutics. Major hurdles are being overcome for biosimilar development following the marketing approval of the first biosimilar antibody by the FDA earlier this year. The advancement of next-generation biobetters and biosimilars is critical to; 1) reduce the high cost of therapeutic antibodies encountered over the last thirty years, 2) address the shortcomings confronted with the use of these antibodies such as poor efficacy and stability and most importantly, (3) provide greater patient benefit.

Acknowledgements

Disclosures

The authors declare that they have no competing financial interests.

References

[1] D.M. Ecker, S.D. Jones, H.L. Levine, The therapeutic monoclonal antibody market, MAbs, 7 (2015) 9-14.

[2] R.E. Kontermann, U. Brinkmann, Bispecific antibodies, Drug Discovery Today, 20 (2015) 838-847.

[3] P.M. Drake, D. Rabuka, An emerging playbook for antibody-drug conjugates: lessons from the laboratory and clinic suggest a strategy for improving efficacy and safety, Current Opinion in Chemical Biology, 28 (2015) 174-180.

[4] G. Kohler, C. Milstein, Continuous cultures of fused cells secreting antibody of predefined specificity, Nature, 256 (1975) 495-497.

[5] G. Kohler, C. Milstein, Derivation of specific antibody-producing tissue culture and tumor lines by cell fusion, European Journal of Immunology, 6 (1976) 511-519.

[6] W. Li, N.B. Caberoy, New perspective for phage display as an efficient and versatile technology of functional proteomics, Applied Microbiology and Biotechnology, 85 (2010) 909-919.

[7] P.T. Jones, P.H. Dear, J. Foote, M.S. Neuberger, G. Winter, Replacing the complementarity-determining regions in a human antibody with those from a mouse, Nature, 321 (1986) 522-525.

[8] L. Riechmann, M. Clark, H. Waldmann, G. Winter, Reshaping human antibodies for therapy, Nature, 332 (1988) 323-327.

[9] N. Lonberg, Human antibodies from transgenic animals, Nature Biotechnology, 23 (2005) 1117-1125.

[10] C.T. Scott, Mice with a human touch, Nature Biotechnology, 25 (2007) 1075-1077.

[11] A. Jakobovits, R. Amado, X. Yang, L. Roskos, G. Schwab, From XenoMouse technology to panitumumab, the first fully human antibody product from transgenic mice, Nature Biotechnology, 25 (2007) 1134-1143.

[12] W.D. Huse, L. Sastry, S.A. Iverson, A.S. Kang, M. Alting-Mees, D.R. Burton, S.J. Benkovic, R.A. Lerner, Generation of a large combinatorial library of the immunoglobulin repertoire in phage lambda, Science, 246 (1989) 1275-1281.

[13] J. McCafferty, A.D. Griffiths, G. Winter, D.J. Chiswell, Phage antibodies: filamentous phage displaying antibody variable domains, Nature, 348 (1990) 552-554.

[14] C.F. Barbas, 3rd, A.S. Kang, R.A. Lerner, S.J. Benkovic, Assembly of combinatorial antibody libraries on phage surfaces: the gene III site, Proceedings of the National Academy of Sciences, 88 (1991) 7978-7982.

[15] D.J. Schofield, A.R. Pope, V. Clementel, J. Buckell, S.D.J. Chapple, K.F. Clarke, J.S. Conquer, A.M. Crofts, S.R.E. Crowther, M.R. Dyson, G. Flack, G.J. Griffin, Y. Hooks, W.J. Howat, A. Kolb-Kokocinski, S. Kunze, C.D. Martin, G.L. Maslen, J.N. Mitchell, M. O'Sullivan, R.L. Perera, W. Roake, S.P. Shadbolt, K.J. Vincent, A. Warford, W.E. Wilson, J. Xie, J.L. Young, J. McCafferty, Application of phage display to high throughput antibody generation and characterization, Genome Biology, 8 (2007).

[16] J.D. Marks, H.R. Hoogenboom, T.P. Bonnert, J. McCafferty, A.D. Griffiths, G. Winter, By-passing immunization. Human antibodies from V-gene libraries displayed on phage, Journal of Molecular Biology, 222 (1991) 581-597.

[17] C.F.I. Barbas, J.D. Bain, D.M. Hoekstra, R.A. Lerner, Semisynthetic combinatorial antibody libraries: a chemical solution to the diversity problem, Proceedings of the National Academy of Sciences, 89 (1992) 4457-4461.

[18] H.R. Hoogenboom, G. Winter, By-passing immunisation. Human antibodies from synthetic repertoires of germline VH gene segments rearranged *in vitro*., Journal of Molecular Biology, 227 (1992) 381-388.

[19] H.R. Hoogenboom, A.D. Griffiths, K.S. Johnson, D.J. Chiswell, P. Hudson, G. Winter, Multi-subunit proteins on the surface of filamentous phage: methodologies for displaying antibody (Fab) heavy and light chains, Nucleic Acids Research, 19 (1991) 4133-4137.

[20] J. Davies, L. Riechmann, An antibody variable heavy domain with a lox-Cre site integrated into its coding region: bacterial recombination within a single polypeptide chain, FEBS Letters, 377 (1995) 92-96.

[21] M.M. Harmsen, H.J. De Haard, Properties, production, and applications of camelid single-domain antibody fragments, Applied Microbiology and Biotechnology, 77 (2007) 13-22.

[22] S.D. Nuttall, U.V. Krishnan, L. Doughty, K. Pearson, M.T. Ryan, N.J. Hoogenraad, M. Hattarki, J.A. Carmichael, R.A. Irving, P.J. Hudson, Isolation and characterization of an IgNAR variable domain specific for the human mitochondrial translocase receptor Tom70, European Journal of Biochemistry, 270 (2003) 3543-3554.

[23] K. Nakano, T. Kojima, K. Kasutani, C. Senoh, O. Natori, S. Ishii, H. Tsunoda, K. Hattori, Effective screening method of agonistic diabodies based on autocrine growth, Journal of Immunological Methods, 347 (2009) 31-35.

[24] Y. Mazor, T. Van Blarcom, R. Mabry, B.L. Iverson, G. Georgiou, Isolation of engineered, full-length antibodies from libraries expressed in Escherichia coli, Nature Biotechnology, 25 (2007) 563-565.

[25] L.S. Jespers, A. Roberts, S.M. Mahler, G. Winter, H.R. Hoogenboom, Guiding the selection of human antibodies from phage display repertoires to a single epitope of an antigen, Biotechnology (N Y), 12 (1994) 899-903.

[26] A.E. Nixon, D.J. Sexton, R.C. Ladner, Drugs derived from phage display: from candidate identification to clinical practice, MAbs, 6 (2014) 73-85.

[27] P.S. Daugherty, G. Chen, M.J. Olsen, B.L. Iverson, G. Georgiou, Antibody affinity maturation using bacterial surface display, Protein Engineering, 11 (1998) 825-832.

[28] M.J. Feldhaus, R.W. Siegel, L.K. Opresko, J.R. Coleman, J.M. Feldhaus, Y.A. Yeung, J.R. Cochran, P. Heinzelman, D. Colby, J. Swers, C. Graff, H.S. Wiley, K.D. Wittrup, Flow-cytometric isolation of human antibodies from a non immune Sacchromyces cerevisiae surface display library, Nature Biotechnology, 21 (2003) 163-170.

[29] D.G. Mottershead, K. Alfthan, K. Ojala, K. Takkinen, C. Oker-Blom, Baculoviral display of functional scFv and synthetic IgG-binding domains, Biochem Biophys Res Commun, 275 (2000) 84-90.

[30] J. Hanes, C. Schaffitzel, A. Knappik, A. Pluckthun, Picomolar affinity antibodies from a fully synthetic naive library selected and evolved by ribosome display, Nat Biotechnol, 18 (2000) 1287-1292.

[31] G. Georgiou, G.C. Ippolito, J. Beausang, C.E. Busse, H. Wardemann, S.R. Quake, The promise and challenge of high-throughput sequencing of the antibody repertoire, Nature Biotechnology, 32 (2014) 158-168.

[32] U. Ravn, G. Didelot, S. Venet, K.T. Ng, F. Gueneau, F. Rousseau, S. Calloud, M. Kosco-Vilbois, N. Fischer, Deep sequencing of phage display libraries to support antibody discovery, Methods, 60 (2013) 99-110.

[33] P. Mathonet, C.G. Ullman, The application of next generation sequencing to the understanding of antibody repertoires, Frontiers in Immunology, 4 (2013).

[34] W.C. Cheung, S.A. Beausoleil, X. Zhang, S. Sato, S.M. Schieferl, J.S. Wieler, J.G. Beaudet, R.K. Ramenani, L. Popova, M.J. Comb, J. Rush, R.D. Polakiewicz, A proteomics approach for the

identification and cloning of monoclonal antibodies from serum, Nature Biotechnology, 30 (2012) 447-452.

[35] S.T. Reddy, X. Ge, A.E. Miklos, R.A. Hughes, S.H. Kang, K.H. Hoi, C. Chrysostomou, S.P. Hunicke-Smith, B.L. Iverson, P.W. Tucker, A.D. Ellington, G. Georgiou, Monoclonal antibodies isolated without screening by analyzing the variable-gene repertoire of plasma cells, Nature Biotechnology, 28 (2010) 965-969.

[36] U. Ravn, F. Gueneau, L. Baerlocher, M. Osteras, M. Desmurs, P. Malinge, G. Magistrelli, L. Farinelli, M.H. Kosco-Vilbois, N. Fischer, By-passing *in vitro* screening--next generation sequencing technologies applied to antibody display and in silico candidate selection, Nucleic Acids Research, 38 (2010) e193.

[37] B.J. DeKosky, G.C. Ippolito, R.P. Deschner, J.J. Lavinder, Y. Wine, B.M. Rawlings, N. Varadarajan, C. Giesecke, T. Dorner, S.F. Andrews, P.C. Wilson, S.P. Hunicke-Smith, C.G. Willson, A.D. Ellington, G. Georgiou, High-throughput sequencing of the paired human immunoglobulin heavy and light chain repertoire, Nature Biotechnology, 31 (2013) 166-169.

[38] I. Saggy, Y. Wine, L. Shefet-Carasso, L. Nahary, G. Georgiou, I. Benhar, Antibody isolation from immunized animals: comparison of phage display and antibody discovery via V gene repertoire mining, Protein Engineering Design and Selection, 25 (2012) 539-549.

[39] K. Lehmann-Horn, H.C. Kronsbein, M.S. Weber, Targeting B cells in the treatment of multiple sclerosis: recent advances and remaining challenges, Therapeutic Advances in Neurological Disorders, 6 (2013) 161-173.

[40] A.M. Vazquez, A.M. Hernandez, A. Macias, E. Montero, D.E. Gomez, D.F. Alonso, M.R. Gabri, R.E. Gomez, Racotumomab: an anti-idiotype vaccine related to N-glycolyl-containing gangliosides - preclinical and clinical data, Frontiers in Oncology, 2 (2012) 150.

[41] P. Garrone, O. Djossou, F. Fossiez, J. Reyes, S. Ait-Yahia, C. Maat, S. Ho, T. Hauser, J.M. Dayer, J. Greffe, P. Miossec, S. Lebecque, F. Rousset, J. Banchereau, Generation and characterization of a human monoclonal autoantibody that acts as a high affinity interleukin-1 alpha specific inhibitor, Molecular Immunology, 33 (1996) 649-658.

[42] D.S. Hong, D. Hui, E. Bruera, F. Janku, A. Naing, G.S. Falchook, S. Piha-Paul, J.J. Wheler, S. Fu, A.M. Tsimberidou, M. Stecher, P. Mohanty, J. Simard, R. Kurzrock, MABp1, a first-in-class true human antibody targeting interleukin-1alpha in refractory cancers: an open-label, phase 1 dose-escalation and expansion study, The Lancet Oncology, 15 (2014) 656-666.

[43] P. Chames, M. Van Regenmortel, E. Weiss, D. Baty, Therapeutic antibodies: successes, limitations and hopes for the future, British Journal of Pharmacology, 157 (2009) 220-233.

[44] R. Niwa, M. Satoh, The current status and prospects of antibody engineering for therapeutic use: focus on glycoengineering technology, Journal of Pharmaceutical Sciences, 104 (2015) 930-941.

[45] J.B. Evans, B.A. Syed, From the analyst's couch: Next-generation antibodies, Nat Rev Drug Discov, 13 (2014) 413-414.

[46] O. Shpilberg, C. Jackisch, Subcutaneous administration of rituximab (MabThera) and trastuzumab (Herceptin) using hyaluronidase, British Journal of Cancer, 109 (2013) 1556-1561.

[47] S. Derer, C. Kellner, S. Berger, T. Valerius, M. Peipp, Fc engineering: design, expression, and functional characterization of antibody variants with improved effector function, Methods Mol Biol, 907 (2012) 519-536.

[48] A. Beck, J.M. Reichert, Marketing approval of mogamulizumab: a triumph for glyco-engineering, MAbs, 4 (2012) 419-425.

[49] M. Sachdeva, S. Dhingra, Obinutuzumab: A FDA approved monoclonal antibody in the treatment of untreated chronic lymphocytic leukemia, Int J Appl Basic Med Res, 5 (2015) 54-57.

[50] M. Ratner, Genentech's glyco-engineered antibody to succeed Rituxan, Nature Biotechnology, 32 (2014) 6+.

[51] J.M. Subramaniam, G. Whiteside, K. McKeage, J.C. Croxtall, Mogamulizumab: first global approval, Drugs, 72 (2012) 1293-1298.

[52] A.K. Kakkar, S. Balakrishnan, Obinutuzumab for chronic lymphocytic leukemia: promise of the first treatment approved with breakthrough therapy designation, J Oncol Pharm Pract, 21 (2015) 358-363.

[53] S.D. Liu, C. Chalouni, J.C. Young, T.T. Junttila, M.X. Sliwkowski, J.B. Lowe, Afucosylated antibodies increase activation of FcgammaRIIIa-dependent signaling components to intensify processes promoting ADCC, Cancer Immunol Res, 3 (2015) 173-183.

[54] T. Mizushima, H. Yagi, E. Takemoto, M. Shibata-Koyama, Y. Isoda, S. Iida, K. Masuda, M. Satoh, K. Kato, Structural basis for improved efficacy of therapeutic antibodies on defucosylation of their Fc glycans, Genes to Cells, 16 (2011) 1071-1080.

[55] S. Preithner, S. Elm, S. Lippold, M. Locher, A. Wolf, A.J. da Silva, P.A. Baeuerle, N.S. Prang, High concentrations of therapeutic IgG1 antibodies are needed to compensate for inhibition of antibody-dependent cellular cytotoxicity by excess endogenous immunoglobulin G, Mol Immunol, 43 (2006) 1183-1193.

[56] N. Zhang, L. Liu, C. Dan Dumitru, N.R.H. Cummings, M. Cukan, Y. Jiang, Y. Li, F. Li, T. Mitchell, M.R. Mallem, Y. Ou, R.N. Patel, K. Vo, H. Wang, I. Burnina, B.-K. Choi, H.E. Huber, T.A. Stadheim, D. Zha, Glycoengineered Pichia produced anti-HER2 is comparable to trastuzumab in preclinical study, MAbs, 3 (2011) 289-298.

[57] R.L. Shields, A.K. Namenuk, K. Hong, Y.G. Meng, J. Rae, J. Briggs, D. Xie, J. Lai, A. Stadlen, B. Li, J.A. Fox, L.G. Presta, High resolution mapping of the binding site on human IgG1 for Fc gamma RI, Fc gamma RII, Fc gamma RIII, and FcRn and design of IgG1 variants with improved binding to the Fc gamma R, The Journal of Biological Chemistry, 276 (2001) 6591-6604.

[58] G.A. Lazar, W. Dang, S. Karki, O. Vafa, J.S. Peng, L. Hyun, C. Chan, H.S. Chung, A. Eivazi, S.C. Yoder, J. Vielmetter, D.F. Carmichael, R.J. Hayes, B.I. Dahiyat, Engineered antibody Fc variants with enhanced effector function, Proceedings of the National Academy of Sciences, 103 (2006) 4005-4010.

[59] J.B. Stavenhagen, S. Gorlatov, N. Tuaillon, C.T. Rankin, H. Li, S. Burke, L. Huang, S. Vijh, S. Johnson, E. Bonvini, S. Koenig, Fc optimization of therapeutic antibodies enhances their ability to kill tumor cells *in vitro* and controls tumor expansion *in vivo* via low-affinity activating Fcgamma receptors, Cancer Research, 67 (2007) 8882-8890.

[60] S.T. Jung, S.T. Reddy, T.H. Kang, M.J. Borrok, I. Sandlie, P.W. Tucker, G. Georgiou, Aglycosylated IgG variants expressed in bacteria that selectively bind FcgammaRI potentiate tumor cell killing by monocyte-dendritic cells, Proceedings of the National Academy of Sciences, 107 (2010) 604-609.

[61] S.L. Sazinsky, R.G. Ott, N.W. Silver, B. Tidor, J.V. Ravetch, K.D. Wittrup, Aglycosylated immunoglobulin G1 variants productively engage activating Fc receptors, Proceedings of the National Academy of Sciences, 105 (2008) 20167-20172.

[62] M.J. Borrok, S.T. Jung, T.H. Kang, A.F. Monzingo, G. Georgiou, Revisiting the role of glycosylation in the structure of human IgG Fc, ACS Chemical Biology, 7 (2012) 1596-1602.

[63] R. Stewart, G. Thom, M. Levens, G. Guler-Gane, R. Holgate, P.M. Rudd, C. Webster, L. Jermutus, J. Lund, A variant human IgG1-Fc mediates improved ADCC, Protein Engineering Design and Selection, 24 (2011) 671-678.

[64] V. Kayser, N. Chennamsetty, V. Voynov, K. Forrer, B. Helk, B.L. Trout, Glycosylation influences on the aggregation propensity of therapeutic monoclonal antibodies, Biotechnology Journal, 6 (2011) 38-44.

[65] Y. Mimura, S. Church, R. Ghirlando, P.R. Ashton, S. Dong, M. Goodall, J. Lund, R. Jefferis, The influence of glycosylation on the thermal stability and effector function expression of human IgG1-Fc: properties of a series of truncated glycoforms, Molecular Immunology, 37 (2000) 697-706.

[66] J.L. Zaro, Mylotarg: Revisiting Its Clinical Potential Post-Withdrawal, in: J. Wang, W.-C. Shen, J.L. Zaro (Eds.) Antibody-Drug Conjugates, Springer International Publishing2015, pp. 179-190.

[67] F.J. Burrows, P.E. Thorpe, Eradication of large solid tumors in mice with an immunotoxin directed against tumor vasculature, Proceedings of the National Academy of Sciences, 90 (1993) 8996-9000.

[68] A. Palumbo, F. Hauler, P. Dziunycz, K. Schwager, A. Soltermann, F. Pretto, C. Alonso, G.F. Hofbauer, R.W. Boyle, D. Neri, A chemically modified antibody mediates complete eradication

of tumours by selective disruption of tumour blood vessels, British Journal of Cancer, 104 (2011) 1106-1115.

[69] A. Visintin, K. Knowlton, E. Tyminski, C.I. Lin, X. Zheng, K. Marquette, S. Jain, L. Tchistiakova, D. Li, C.J. O'Donnell, A. Maderna, X. Cao, R. Dunn, W.B. Snyder, A.K. Abraham, M. Leal, S. Shetty, A. Barry, L. Zawel, A.J. Coyle, H.F. Dvorak, S.C. Jaminet, Novel Anti-TM4SF1 Antibody-Drug Conjugates with Activity against Tumor Cells and Tumor Vasculature, Molecular Cancer Therapeutics, 14 (2015) 1868-1876.

[70] E. Ostermann, P. Garin-Chesa, K.H. Heider, M. Kalat, H. Lamche, C. Puri, D. Kerjaschki, W.J. Rettig, G.R. Adolf, Effective immunoconjugate therapy in cancer models targeting a serine protease of tumor fibroblasts, Clinical Cancer Research, 14 (2008) 4584-4592.

[71] D. Quail, J. Joyce, Microenvironmental regulation of tumor progression and metastasis, Nature Medicine, 19 (2013) 1423-1437.

[72] G.R. Pettit, Y. Kamano, C.L. Herald, A.A. Tuinman, F.E. Boettner, H. Kizu, J.M. Schmidt, L. Baczynskyj, K.B. Tomer, R.J. Bontems, The isolation and structure of a remarkable marine animal antineoplastic constituent: dolastatin 10, Journal of the American Chemical Society, 109 (1987) 6883-6885.

[73] W.M. Maiese, M.P. Lechevalier, H.A. Lechevalier, J. Korshalla, N. Kuck, A. Fantini, M.J. Wildey, J. Thomas, M. Greenstein, Calicheamicins, a novel family of antitumor antibiotics: taxonomy, fermentation and biological properties, The Journal of Antibiotics, 42 (1989) 558-563.

[74] J.M. Cassady, K.K. Chan, H.G. Floss, E. Leistner, Recent developments in the maytansinoid antitumor agents, Chemical and Pharmaceutical Bulletin, 52 (2004) 1-26.

[75] R.V. Chari, Targeted cancer therapy: conferring specificity to cytotoxic drugs, Accounts of Chemical Research, 41 (2008) 98-107.

[76] S.O. Doronina, B.A. Mendelsohn, T.D. Bovee, C.G. Cerveny, S.C. Alley, D.L. Meyer, E. Oflazoglu, B.E. Toki, R.J. Sanderson, R.F. Zabinski, A.F. Wahl, P.D. Senter, Enhanced activity of monomethylauristatin F through monoclonal antibody delivery: effects of linker technology on efficacy and toxicity, Bioconjugate Chemistry, 17 (2006) 114-124.

[77] T.V. Jerjian, A.E. Glode, L.A. Thompson, C.L. O'Bryant, Antibody-Drug Conjugates: A Clinical Pharmacy Perspective on an Emerging Cancer Therapy, Pharmacotherapy, 36 (2016) 99-116.

[78] R.C. Elgersma, R.G. Coumans, T. Huijbregts, W.M. Menge, J.A. Joosten, H.J. Spijker, F.M. de Groot, M.M. van der Lee, R. Ubink, D.J. van den Dobbelsteen, D.F. Egging, W.H. Dokter, G.F. Verheijden, J.M. Lemmens, C.M. Timmers, P.H. Beusker, Design, Synthesis, and Evaluation of Linker-Duocarmycin Payloads: Toward Selection of HER2-Targeting Antibody-Drug Conjugate SYD985, Molecular Pharmaceutics, 12 (2015) 1813-1835.

[79] J.A. Hartley, The development of pyrrolobenzodiazepines as antitumour agents, Expert Opinion on Investigational Drugs, 20 (2011) 733-744.

[80] J.E. Koblinski, M. Ahram, B.F. Sloane, Unraveling the role of proteases in cancer, Clin Chim Acta, 291 (2000) 113-135.

[81] S.O. Doronina, B.E. Toki, M.Y. Torgov, B.A. Mendelsohn, C.G. Cerveny, D.F. Chace, R.L. DeBlanc, R.P. Gearing, T.D. Bovee, C.B. Siegall, J.A. Francisco, A.F. Wahl, D.L. Meyer, P.D. Senter, Development of potent monoclonal antibody auristatin conjugates for cancer therapy, Nat Biotechnol, 21 (2003) 778-784.

[82] C. Vaklavas, A. Forero-Torres, Safety and efficacy of brentuximab vedotin in patients with Hodgkin lymphoma or systemic anaplastic large cell lymphoma, Ther Adv Hematol, 3 (2012) 209-225.

[83] J. Bendell, M. Saleh, A.A. Rose, P.M. Siegel, L. Hart, S. Sirpal, S. Jones, J. Green, E. Crowley, R. Simantov, T. Keler, T. Davis, L. Vahdat, Phase I/II study of the antibody-drug conjugate glembatumumab vedotin in patients with locally advanced or metastatic breast cancer, J Clin Oncol, 32 (2014) 3619-3625.

[84] H.K. Erickson, P.U. Park, W.C. Widdison, Y.V. Kovtun, L.M. Garrett, K. Hoffman, R.J. Lutz, V.S. Goldmacher, W.A. Blattler, Antibody-maytansinoid conjugates are activated in targeted cancer cells by lysosomal degradation and linker-dependent intracellular processing, Cancer Research, 66 (2006) 4426-4433.

[85] S. Alley, X. Zhang, N. Okeley, M. Anderson, E. Oflazoglu, I. Stone, C.-L. Law, P. Senter, D. Benjamin, Effects of linker chemistry on tumor targeting by anti-CD70 antibody-drug conjugates, Cancer Research, 67 (2007) 916.

[86] S. Girish, M. Gupta, B. Wang, D. Lu, I.E. Krop, C.L. Vogel, H.A. Burris Iii, P.M. LoRusso, J.H. Yi, O. Saad, B. Tong, Y.W. Chu, S. Holden, A. Joshi, Clinical pharmacology of trastuzumab emtansine (T-DM1): an antibody-drug conjugate in development for the treatment of HER2-positive cancer, Cancer Chemotherapy and Pharmacology, 69 (2012) 1229-1240.

[87] A.G. Polson, J. Calemine-Fenaux, P. Chan, W. Chang, E. Christensen, S. Clark, F.J. de Sauvage, D. Eaton, K. Elkins, J.M. Elliott, G. Frantz, R.N. Fuji, A. Gray, K. Harden, G.S. Ingle, N.M. Kljavin, H. Koeppen, C. Nelson, S. Prabhu, H. Raab, S. Ross, D.S. Slaga, J.P. Stephan, S.J. Scales, S.D. Spencer, R. Vandlen, B. Wranik, S.F. Yu, B. Zheng, A. Ebens, Antibody-drug conjugates for the treatment of non-Hodgkin's lymphoma: target and linker-drug selection, Cancer Research, 69 (2009) 2358-2364.

[88] H.K. Erickson, G.D. Lewis Phillips, D.D. Leipold, C.A. Provenzano, E. Mai, H.A. Johnson, B. Gunter, C.A. Audette, M. Gupta, J. Pinkas, J. Tibbitts, The effect of different linkers on target cell catabolism and pharmacokinetics/pharmacodynamics of trastuzumab maytansinoid conjugates, Mol Cancer Ther, 11 (2012) 1133-1142.

[89] R.P. Lyon, D.L. Meyer, J.R. Setter, P.D. Senter, Conjugation of anticancer drugs through endogenous monoclonal antibody cysteine residues, Methods Enzymol, 502 (2012) 123-138.

[90] M.P. Brun, L. Gauzy-Lazo, Protocols for lysine conjugation, Methods Mol Biol, 1045 (2013) 173-187.

[91] C.R. Behrens, E.H. Ha, L.L. Chinn, S. Bowers, G. Probst, M. Fitch-Bruhns, J. Monteon, A. Valdiosera, A. Bermudez, S. Liao-Chan, T. Wong, J. Melnick, J.W. Theunissen, M.R. Flory, D. Houser, K. Venstrom, Z. Levashova, P. Sauer, T.S. Migone, E.H. van der Horst, R.L. Halcomb, D.Y. Jackson, Antibody-Drug Conjugates (ADCs) Derived from Interchain Cysteine Cross-Linking Demonstrate Improved Homogeneity and Other Pharmacological Properties over Conventional Heterogeneous ADCs, Molecular pharmaceutics, 12 (2015) 3986-3998.

[92] J.R. Junutula, H. Raab, S. Clark, S. Bhakta, D.D. Leipold, S. Weir, Y. Chen, M. Simpson, S.P. Tsai, M.S. Dennis, Y. Lu, Y.G. Meng, C. Ng, J. Yang, C.C. Lee, E. Duenas, J. Gorrell, V. Katta, A. Kim, K. McDorman, K. Flagella, R. Venook, S. Ross, S.D. Spencer, W. Lee Wong, H.B. Lowman, R. Vandlen, M.X. Sliwkowski, R.H. Scheller, P. Polakis, W. Mallet, Site-specific conjugation of a cytotoxic drug to an antibody improves the therapeutic index, Nature Biotechnology, 26 (2008) 925-932.

[93] J.Y. Axup, K.M. Bajjuri, M. Ritland, B.M. Hutchins, C.H. Kim, S.A. Kazane, R. Halder, J.S. Forsyth, A.F. Santidrian, K. Stafin, Y. Lu, H. Tran, A.J. Seller, S.L. Biroc, A. Szydlik, J.K. Pinkstaff, F. Tian, S.C. Sinha, B. Felding-Habermann, V.V. Smider, P.G. Schultz, Synthesis of site-specific antibody-drug conjugates using unnatural amino acids, Proceedings of the National Academy of Sciences, 109 (2012) 16101-16106.

[94] E.S. Zimmerman, T.H. Heibeck, A. Gill, X. Li, C.J. Murray, M.R. Madlansacay, C. Tran, N.T. Uter, G. Yin, P.J. Rivers, A.Y. Yam, W.D. Wang, A.R. Steiner, S.U. Bajad, K. Penta, W. Yang, T.J. Hallam, C.D. Thanos, A.K. Sato, Production of site-specific antibody-drug conjugates using optimized non-natural amino acids in a cell-free expression system, Bioconjug Chem, 25 (2014) 351-361.

[95] A.M. Sochaj, K.W. Swiderska, J. Otlewski, Current methods for the synthesis of homogeneous antibody-drug conjugates, Biotechnology Advances, 33 (2015) 775-784.

[96] R. van Geel, M.A. Wijdeven, R. Heesbeen, J.M. Verkade, A.A. Wasiel, S.S. van Berkel, F.L. van Delft, Chemoenzymatic Conjugation of Toxic Payloads to the Globally Conserved N-Glycan of Native mAbs Provides Homogeneous and Highly Efficacious Antibody-Drug Conjugates, Bioconjugate Chemistry, 26 (2015) 2233-2242.

[97] A. Nisonoff, M.M. Rivers, Recombination of a mixture of univalent antibody fragments of different specificity, Arch Biochem Biophys, 93 (1961) 460-462.

[98] U.D. Staerz, M.J. Bevan, Hybrid hybridoma producing a bispecific monoclonal antibody that can focus effector T-cell activity, Proceedings of the National Academy of Sciences, 83 (1986) 1453-1457.

[99] K. Gunasekaran, M. Pentony, M. Shen, L. Garrett, C. Forte, A. Woodward, S.B. Ng, T. Born, M. Retter, K. Manchulenko, H. Sweet, I.N. Foltz, M. Wittekind, W. Yan, Enhancing antibody Fc heterodimer formation through electrostatic steering effects: applications to bispecific molecules and monovalent IgG, The Journal of Biological Chemistry, 285 (2010) 19637-19646.

[100] T.S. Von Kreudenstein, E. Escobar-Carbrera, P.I. Lario, I. D'Angelo, K. Brault, J. Kelly, Y. Durocher, J. Baardsnes, R.J. Woods, M.H. Xie, P.A. Girod, M.D. Suits, M.J. Boulanger, D.K. Poon, G.Y. Ng, S.B. Dixit, Improving biophysical properties of a bispecific antibody scaffold to aid developability: quality by molecular design, MAbs, 5 (2013) 646-654.

[101] S.M. Lewis, X. Wu, A. Pustilnik, A. Sereno, F. Huang, H.L. Rick, G. Guntas, A. Leaver-Fay, E.M. Smith, C. Ho, C. Hansen-Estruch, A.K. Chamberlain, S.M. Truhlar, E.M. Conner, S. Atwell, B. Kuhlman, S.J. Demarest, Generation of bispecific IgG antibodies by structure-based design of an orthogonal Fab interface, Nature Biotechnology, 32 (2014) 191-198.

[102] J.B. Ridgway, L.G. Presta, P. Carter, 'Knobs-into-holes' engineering of antibody CH3 domains for heavy chain heterodimerization, Protein Engineering Design and Selection, 9 (1996) 617-621.

[103] W. Schaefer, J.T. Regula, M. Bahner, J. Schanzer, R. Croasdale, H. Durr, C. Gassner, G. Georges, H. Kettenberger, S. Imhof-Jung, M. Schwaiger, K.G. Stubenrauch, C. Sustmann, M. Thomas, W. Scheuer, C. Klein, Immunoglobulin domain crossover as a generic approach for the production of bispecific IgG antibodies, Proceedings of the National Academy of Sciences, 108 (2011) 11187-11192.

[104] E.A. Rossi, D.M. Goldenberg, T.M. Cardillo, W.J. McBride, R.M. Sharkey, C.H. Chang, Stably tethered multifunctional structures of defined composition made by the dock and lock method for use in cancer targeting, Proceedings of the National Academy of Sciences, 103 (2006) 6841-6846.

[105] E.A. Rossi, D.M. Goldenberg, C.H. Chang, The dock-and-lock method combines recombinant engineering with site-specific covalent conjugation to generate multifunctional structures, Bioconjugate Chemistry, 23 (2012) 309-323.

[106] J.H. Davis, C. Aperlo, Y. Li, E. Kurosawa, Y. Lan, K.M. Lo, J.S. Huston, SEEDbodies: fusion proteins based on strand-exchange engineered domain (SEED) CH3 heterodimers in an Fc analogue platform for asymmetric binders or immunofusions and bispecific antibodies, Protein Engineering Design and Selection, 23 (2010) 195-202.

[107] R. Zeidler, J. Mysliwietz, M. Csanady, A. Walz, I. Ziegler, B. Schmitt, B. Wollenberg, H. Lindhofer, The Fc-region of a new class of intact bispecific antibody mediates activation of accessory cells and NK cells and induces direct phagocytosis of tumour cells, British Journal of Cancer, 83 (2000) 261-266.

[108] M.G. Ott, F. Marme, G. Moldenhauer, H. Lindhofer, M. Hennig, R. Spannagl, M.M. Essing, R. Linke, D. Seimetz, Humoral response to catumaxomab correlates with clinical outcome: results of the pivotal phase II/III study in patients with malignant ascites, International Journal of Cancer, 130 (2012) 2195-2203.

[109] E. Wolf, R. Hofmeister, P. Kufer, B. Schlereth, P.A. Baeuerle, BiTEs: bispecific antibody constructs with unique anti-tumor activity, Drug Discovery Today, 10 (2005) 1237-1244.

[110] P.A. Baeuerle, P. Kufer, R. Bargou, BiTE: Teaching antibodies to engage T-cells for cancer therapy, Current Opinion in Molecular Therapeutics, 11 (2009) 22-30.

[111] M.J. Newman, D.J. Benani, A review of blinatumomab, a novel immunotherapy, Journal of Oncology Pharmacy Practice, (2015).

[112] M.S. Topp, N. Gokbuget, A.S. Stein, G. Zugmaier, S. O'Brien, R.C. Bargou, H. Dombret, A.K. Fielding, L. Heffner, R.A. Larson, S. Neumann, R. Foa, M. Litzow, J.M. Ribera, A. Rambaldi, G. Schiller, M. Bruggemann, H.A. Horst, C. Holland, C. Jia, T. Maniar, B. Huber, D. Nagorsen, S.J. Forman, H.M. Kantarjian, Safety and activity of blinatumomab for adult patients with relapsed or refractory B-precursor acute lymphoblastic leukaemia: a multicentre, single-arm, phase 2 study, Lancet Oncol, 16 (2015) 57-66.

[113] S. Johnson, S. Burke, L. Huang, S. Gorlatov, H. Li, W. Wang, W. Zhang, N. Tuaillon, J. Rainey, B. Barat, Y. Yang, L. Jin, V. Ciccarone, P.A. Moore, S. Koenig, E. Bonvini, Effector cell recruitment with novel Fv-based dual-affinity re-targeting protein leads to potent tumor cytolysis and *in vivo* B-cell depletion, Journal of Molecular Biology, 399 (2010) 436-449.

[114] P.A. Moore, W. Zhang, G.J. Rainey, S. Burke, H. Li, L. Huang, S. Gorlatov, M.C. Veri, S. Aggarwal, Y. Yang, K. Shah, L. Jin, S. Zhang, L. He, T. Zhang, V. Ciccarone, S. Koenig, E. Bonvini, S. Johnson, Application of dual affinity retargeting molecules to achieve optimal redirected T-cell killing of B-cell lymphoma, Blood, 117 (2011) 4542-4551.

[115] S.M. Kipriyanov, G. Moldenhauer, J. Schuhmacher, B. Cochlovius, C.W. Von der Lieth, E.R. Matys, M. Little, Bispecific tandem diabody for tumor therapy with improved antigen binding and pharmacokinetics, J Mol Biol, 293 (1999) 41-56.

[116] F. McAleese, M. Eser, RECRUIT-TandAbs: harnessing the immune system to kill cancer cells, Future Oncology, 8 (2012) 687-695.

[117] N. Liddy, G. Bossi, K.J. Adams, A. Lissina, T.M. Mahon, N.J. Hassan, J. Gavarret, F.C. Bianchi, N.J. Pumphrey, K. Ladell, E. Gostick, A.K. Sewell, N.M. Lissin, N.E. Harwood, P.E. Molloy, Y. Li, B.J. Cameron, M. Sami, E.E. Baston, P.T. Todorov, S.J. Paston, R.E. Dennis, J.V. Harper, S.M. Dunn, R. Ashfield, A. Johnson, Y. McGrath, G. Plesa, C.H. June, M. Kalos, D.A. Price, A. Vuidepot, D.D. Williams, D.H. Sutton, B.K. Jakobsen, Monoclonal TCR-redirected tumor cell killing, Nature Medicine, 18 (2012) 980-987.

[118] G. Schaefer, L. Haber, L.M. Crocker, S. Shia, L. Shao, D. Dowbenko, K. Totpal, A. Wong, C.V. Lee, S. Stawicki, R. Clark, C. Fields, G.D. Lewis Phillips, R.A. Prell, D.M. Danilenko, Y. Franke, J.P. Stephan, J. Hwang, Y. Wu, J. Bostrom, M.X. Sliwkowski, G. Fuh, C. Eigenbrot, A two-in-one antibody against HER3 and EGFR has superior inhibitory activity compared with monospecific antibodies, Cancer Cell, 20 (2011) 472-486.

[119] C. Wu, H. Ying, C. Grinnell, S. Bryant, R. Miller, A. Clabbers, S. Bose, D. McCarthy, R.R. Zhu, L. Santora, R. Davis-Taber, Y. Kunes, E. Fung, A. Schwartz, P. Sakorafas, J. Gu, E. Tarcsa, A. Murtaza, T. Ghayur, Simultaneous targeting of multiple disease mediators by a dual-variable-domain immunoglobulin, Nature Biotechnology, 25 (2007) 1290-1297.

[120] K.E. Conrath, M. Lauwereys, M. Galleni, A. Matagne, J.M. Frere, J. Kinne, L. Wyns, S. Muyldermans, Beta-lactamase inhibitors derived from single-domain antibody fragments elicited in the camelidae, Antimicrobial Agents and Chemotherapy, 45 (2001) 2807-2812.

[121] M.K. Joubert, M. Hokom, C. Eakin, L. Zhou, M. Deshpande, M.P. Baker, T.J. Goletz, B.A. Kerwin, N. Chirmule, L.O. Narhi, V. Jawa, Highly aggregated antibody therapeutics can enhance the *in vitro* innate and late-stage T-cell immune responses, The Journal of Biological Chemistry, 287 (2012) 25266-25279.

[122] S. Hermeling, D.J. Crommelin, H. Schellekens, W. Jiskoot, Structure-immunogenicity relationships of therapeutic proteins, Pharmaceutical Research, 21 (2004) 897-903.

[123] D.S. Rehder, D. Chelius, A. McAuley, T.M. Dillon, G. Xiao, J. Crouse-Zeineddini, L. Vardanyan, N. Perico, V. Mukku, D.N. Brems, M. Matsumura, P.V. Bondarenko, Isomerization of a single aspartyl residue of anti-epidermal growth factor receptor immunoglobulin gamma2 antibody highlights the role avidity plays in antibody activity, Biochemistry, 47 (2008) 2518-2530.

[124] A.L. Daugherty, R.J. Mrsny, Formulation and delivery issues for monoclonal antibody therapeutics, Adv Drug Deliv Rev, 58 (2006) 686-706.

[125] Y. Yan, H. Wei, Y. Fu, S. Jusuf, M. Zeng, R. Ludwig, S.R. Krystek, G. Chen, L. Tao, T.K. Das, Isomerization and Oxidation in the Complementarity-Determining Regions of a Monoclonal Antibody: A Study of the Modification–Structure–Function Correlations by Hydrogen–Deuterium Exchange Mass Spectrometry, Analytical Chemistry, 88 (2016) 2041-2050.

[126] B. Moorthy, B. Xie, E. Moussa, L. Iyer, S. Chandrasekhar, J. Panchal, E. Topp, Structure of Monoclonal Antibodies, in: A. Rosenberg, B. Demeule (Eds.) Biobetters, Springer New York2015, pp. 81-89.

[127] N. Chennamsetty, V. Voynov, V. Kayser, B. Helk, B.L. Trout, Design of therapeutic proteins with enhanced stability, Proceedings of the National Academy of Sciences, 106 (2009) 11937-11942.

[128] N. Chennamsetty, V. Voynov, V. Kayser, B. Helk, B.L. Trout, Prediction of aggregation prone regions of therapeutic proteins, The Journal of Physical Chemistry B, 114 (2010) 6614-6624.

[129] F. Courtois, C.P. Schneider, N.J. Agrawal, B.L. Trout, Rational Design of Biobetters with Enhanced Stability, Journal of Pharmaceutical Sciences, 104 (2015) 2433-2440.

[130] M. Ahmadi, C.J. Bryson, E.A. Cloake, K. Welch, V. Filipe, S. Romeijn, A. Hawe, W. Jiskoot, M.P. Baker, M.H. Fogg, Small Amounts of Sub-Visible Aggregates Enhance the Immunogenic Potential of Monoclonal Antibody Therapeutics, Pharmaceutical Research, 32 (2015) 1383-1394.

[131] J. Bessa, S. Boeckle, H. Beck, T. Buckel, S. Schlicht, M. Ebeling, A. Kiialainen, A. Koulov, B. Boll, T. Weiser, T. Singer, A.G. Rolink, A. Iglesias, The Immunogenicity of Antibody Aggregates in a Novel Transgenic Mouse Model, Pharmaceutical Research, 32 (2015) 2344-2359.

[132] M.C. Manning, D.K. Chou, B.M. Murphy, R.W. Payne, D.S. Katayama, Stability of Protein Pharmaceuticals: An Update, Pharmaceutical Research, 27 (2010) 544-575.

[133] E. Sahin, A.O. Grillo, M.D. Perkins, C.J. Roberts, Comparative effects of pH and ionic strength on protein–protein interactions, unfolding, and aggregation for IgG1 antibodies, Journal of Pharmaceutical Sciences, 99 (2010) 4830-4848.

[134] P. Arosio, S. Rima, M. Morbidelli, Aggregation Mechanism of an IgG2 and two IgG1 Monoclonal Antibodies at low pH: From Oligomers to Larger Aggregates, Pharmaceutical Research, 30 (2013) 641-654.

[135] S.N. Telikepalli, O.S. Kumru, C. Kalonia, R. Esfandiary, S.B. Joshi, C.R. Middaugh, D.B. Volkin, Structural Characterization of IgG1 mAb Aggregates and Particles Generated Under Various Stress Conditions, Journal of Pharmaceutical Sciences, 103 (2014) 796-809.

[136] F. Depreter, G. Pilcer, K. Amighi, Inhaled proteins: Challenges and perspectives, International Journal of Pharmaceutics, 447 (2013) 251-280.

[137] V. Kayser, N. Chennamsetty, V. Voynov, B. Helk, K. Forrer, B.L. Trout, Evaluation of a non-Arrhenius model for therapeutic monoclonal antibody aggregation, Journal of Pharmaceutical Sciences, 100 (2011) 2526-2542.

[138] N. Kim, R.L. Remmele Jr, D. Liu, V.I. Razinkov, E.J. Fernandez, C.J. Roberts, Aggregation of anti-streptavidin immunoglobulin gamma-1 involves Fab unfolding and competing growth pathways mediated by pH and salt concentration, Biophysical Chemistry, 172 (2013) 26-36.

[139] H. Wu, R. Kroe-Barrett, S. Singh, A.S. Robinson, C.J. Roberts, Competing aggregation pathways for monoclonal antibodies, FEBS Letters, 588 (2014) 936-941.

[140] S.B. Mehta, J.S. Bee, T.W. Randolph, J.F. Carpenter, Partial Unfolding of a Monoclonal Antibody: Role of a Single Domain in Driving Protein Aggregation, Biochemistry, 53 (2014) 3367-3377.

[141] V.I. Razinkov, M.J. Treuheit, G.W. Becker, Accelerated Formulation Development of Monoclonal Antibodies (mAbs) and mAb-Based Modalities: Review of Methods and Tools, Journal of Biomolecular Screening, 20 (2015) 468-483.

[142] H. Liu, G. Gaza-Bulseco, J. Sun, Characterization of the stability of a fully human monoclonal IgG after prolonged incubation at elevated temperature, Journal of Chromatography B, 837 (2006) 35-43.

[143] J. Vlasak, R. Ionescu, Fragmentation of monoclonal antibodies, MAbs, 3 (2011) 253-263.

[144] R.J. Harris, B. Kabakoff, F.D. Macchi, F.J. Shen, M. Kwong, J.D. Andya, S.J. Shire, N. Bjork, K. Totpal, A.B. Chen, Identification of multiple sources of charge heterogeneity in a recombinant antibody, Journal of Chromatography B: Biomedical Sciences and Applications, 752 (2001) 233-245.

[145] H. Liu, G. Gaza-Bulseco, C. Chumsae, Glutamine deamidation of a recombinant monoclonal antibody, Rapid Communications in Mass Spectrometry, 22 (2008) 4081-4088.

[146] Y.T. Zhang, J. Hu, A.L. Pace, R. Wong, Y.J. Wang, Y.-H. Kao, Characterization of asparagine 330 deamidation in an Fc-fragment of IgG1 using cation exchange chromatography and peptide mapping, Journal of Chromatography B, 965 (2014) 65-71.

[147] A.L. Pace, R.L. Wong, Y.T. Zhang, Y.-H. Kao, Y.J. Wang, Asparagine deamidation dependence on buffer type, pH, and temperature, Journal of Pharmaceutical Sciences, 102 (2013) 1712-1723.

[148] L. Yi, N. Beckley, B. Gikanga, J. Zhang, Y.J. Wang, H.-W. Chih, V.K. Sharma, Isomerization of Asp–Asp motif in model peptides and a Monoclonal Antibody Fab Fragment, Journal of Pharmaceutical Sciences, 102 (2013) 947-959.

[149] V. Timm, P. Gruber, M. Wasiliu, H. Lindhofer, D. Chelius, Identification and characterization of oxidation and deamidation sites in monoclonal rat/mouse hybrid antibodies, Journal of Chromatography B, 878 (2010) 777-784.

[150] L. Huang, J. Lu, V.J. Wroblewski, J.M. Beals, R.M. Riggin, *In Vivo* Deamidation Characterization of Monoclonal Antibody by LC/MS/MS, Analytical Chemistry, 77 (2005) 1432-1439.

[151] A. Sreedhara, J. Yin, M. Joyce, K. Lau, A.T. Wecksler, G. Deperalta, L. Yi, Y. John Wang, B. Kabakoff, R.S.K. Kishore, Effect of ambient light on IgG1 monoclonal antibodies during drug product processing and development, European Journal of Pharmaceutics and Biopharmaceutics, 100 (2016) 38-46.

[152] A. Sreedhara, K. Lau, C. Li, B. Hosken, F. Macchi, D. Zhan, A. Shen, D. Steinmann, C. Schöneich, Y. Lentz, Role of Surface Exposed Tryptophan as Substrate Generators for the Antibody Catalyzed Water Oxidation Pathway, Molecular Pharmaceutics, 10 (2013) 278-288.

[153] R. Torosantucci, C. Schöneich, W. Jiskoot, Oxidation of Therapeutic Proteins and Peptides: Structural and Biological Consequences, Pharmaceutical Research, 31 (2014) 541-553.

[154] W. Wang, J. Vlasak, Y. Li, P. Pristatsky, Y. Fang, T. Pittman, J. Roman, Y. Wang, T. Prueksaritanont, R. Ionescu, Impact of methionine oxidation in human IgG1 Fc on serum half-life of monoclonal antibodies, Mol Immunol, 48 (2011) 860-866.

[155] W. Wang, S. Singh, D.L. Zeng, K. King, S. Nema, Antibody structure, instability, and formulation, Journal of Pharmaceutical Sciences, 96 (2007) 1-26.

[156] B. Yan, Z. Yates, A. Balland, G.R. Kleemann, Human IgG1 Hinge Fragmentation as the Result of H2O2-mediated Radical Cleavage, Journal of Biological Chemistry, 284 (2009) 35390-35402.

[157] Z. Wei, J. Feng, H.-Y. Lin, S. Mullapudi, E. Bishop, G.I. Tous, J. Casas-Finet, F. Hakki, R. Strouse, M.A. Schenerman, Identification of a Single Tryptophan Residue as Critical for Binding Activity in a Humanized Monoclonal Antibody against Respiratory Syncytial Virus, Analytical Chemistry, 79 (2007) 2797-2805.

[158] C.J. Wilson, Rational protein design: developing next-generation biological therapeutics and nanobiotechnological tools, Wiley Interdisciplinary Reviews: Nanomedicine and Nanobiotechnology, 7 (2015) 330-341.

[159] N. Cerda-Costa, A. Esteras-Chopo, F.X. Aviles, L. Serrano, V. Villegas, Early kinetics of amyloid fibril formation reveals conformational reorganisation of initial aggregates, Journal of Molecular Biology, 366 (2007) 1351.

[160] N. de Groot, I. Pallares, F. Aviles, J. Vendrell, S. Ventura, Prediction of "hot spots" of aggregation in disease-linked polypeptides, BMC Structural Biology, 5 (2005) 18.

[161] U. Ogmen, O. Keskin, S. Aytuna, R. Nussinoiv, A. Gursoy, PRISM: Protein interactions by structural matching, Nucleic Acids Research, 33 (2005) W331-W336.

[162] G.G. Tartaglia, M. Vendruscolo, The Zyggregator method for predicting protein aggregation propensities, Chemical Society Reviews, 37 (2008) 1395-1401.

[163] A. Trovato, F. Seno, S.C.E. Tosatto, The PASTA server for protein aggregation prediction, Protein Engineering Design and Selection, (2007) gzm042.

[164] G.G. Tartaglia, A. Cavalli, R. Pellarin, A. Caflisch, Prediction of aggregation rate and aggregation-prone segments in polypeptide sequences, Protein Science, 14 (2005) 2723-2734.

[165] X. Wang, T.K. Das, S.K. Singh, S. Kumar, Potential aggregation prone regions in biotherapeutics, MAbs, 1 (2009) 254-267.

[166] V.E. Angarica, J. Sancho, Protein Dynamics Governed by Interfaces of High Polarity and Low Packing Density, PLoS ONE, 7 (2012) e48212.

[167] R. Zambrano, M. Jamroz, A. Szczasiuk, J. Pujols, S. Kmiecik, S. Ventura, AGGRESCAN3D (A3D): server for prediction of aggregation properties of protein structures, Nucleic Acids Research, 43 (2015) W306-W313.

[168] D. Schweizer, T. Serno, A. Goepferich, Controlled release of therapeutic antibody formats, European Journal of Pharmaceutics and Biopharmaceutics, 88 (2014) 291-309.

[169] A.L. Daugherty, R.J. Mrsny, Formulation and delivery issues for monoclonal antibody therapeutics, Advanced Drug Delivery Reviews, 58 (2006) 686-706.

[170] L. Chang, D. Shepherd, J. Sun, X. Tang, M.J. Pikal, Effect of sorbitol and residual moisture on the stability of lyophilized antibodies: Implications for the mechanism of protein stabilization in the solid state, Journal of Pharmaceutical Sciences, 94 (2005) 1445-1455.

[171] L. Platts, R.J. Falconer, Controlling protein stability: Mechanisms revealed using formulations of arginine, glycine and guanidinium HCl with three globular proteins, International Journal of Pharmaceutics, 486 (2015) 131-135.

[172] S. Ohtake, Y. Kita, T. Arakawa, Interactions of formulation excipients with proteins in solution and in the dried state, Adv Drug Deliv Rev, 63 (2011) 1053-1073.

[173] M.X. Yang, B. Shenoy, M. Disttler, R. Patel, M. McGrath, S. Pechenov, A.L. Margolin, Crystalline monoclonal antibodies for subcutaneous delivery, Proceedings of the National Academy of Sciences, 100 (2003) 6934-6939.

[174] D. Schweizer, K. Schonhammer, M. Jahn, A. Gopferich, Protein-polyanion interactions for the controlled release of monoclonal antibodies, Biomacromolecules, 14 (2013) 75-83.

[175] D.W. Grainger, Controlled-release and local delivery of therapeutic antibodies, Expert Opinion on Biological Therapy, 4 (2004) 1029-1044.

[176] M. Shimizu, Y. Miwa, K. Hashimoto, A. Goto, Encapsulation of chicken egg yolk immunoglobulin G (IgY) by liposomes, Bioscience Biotechnology and Biochemistry, 57 (1993) 1445-1449.

[177] X.Y. Li, L.J. Jin, T.A. McAllister, K. Stanford, J.Y. Xu, Y.N. Lu, Y.H. Zhen, Y.X. Sun, Y.P. Xu, Chitosan-alginate microcapsules for oral delivery of egg yolk immunoglobulin (IgY), Journal of Agricultural and Food Chemistry, 55 (2007) 2911-2917.

[178] Y. Yun, Y.W. Cho, K. Park, Nanoparticles for oral delivery: Targeted nanoparticles with peptidic ligands for oral protein delivery, Advanced Drug Delivery Reviews, 65 (2013) 822-832.

[179] M. Streit, Z. Beleznay, L.R. Braathen, Topical application of the tumour necrosis factor-alpha antibody infliximab improves healing of chronic wounds, International Wound Journal, 3 (2006) 171-179.

[180] M. Smola, T. Vandamme, A. Sokolowski, Nanocarriers as pulmonary drug delivery systems to treat and to diagnose respiratory and non respiratory diseases, International Journal of Nanomedicine, 3 (2008) 1-19.

[181] S.J. Koussoroplis, G. Paulissen, D. Tyteca, H. Goldansaz, J. Todoroff, C. Barilly, C. Uyttenhove, J. Van Snick, D. Cataldo, R. Vanbever, PEGylation of antibody fragments greatly increases their local residence time following delivery to the respiratory tract, Journal of Controlled Release, 187 (2014) 91-100.

[182] L. Dellamary, D.J. Smith, A. Bloom, S. Bot, G.R. Guo, H. Deshmuk, M. Costello, A. Bot, Rational design of solid aerosols for immunoglobulin delivery by modulation of aerodynamic and release characteristics, Journal of Controlled Release, 95 (2004) 489-500.

[183] A.I. Bot, T.E. Tarara, D.J. Smith, S.R. Bot, C.M. Woods, J.G. Weers, Novel lipid-based hollow-porous microparticles as a platform for immunoglobulin delivery to the respiratory tract, Pharmaceutical Research, 17 (2000) 275-283.

[184] I.M. El-Sherbiny, N.M. El-Baz, M.H. Yacoub, Inhaled nano- and microparticles for drug delivery, Global Cardiology Science and Practice, 2015 (2015) 2.

[185] L. Detalle, T. Stohr, C. Palomo, P.A. Piedra, B.E. Gilbert, V. Mas, A. Millar, U.F. Power, C. Stortelers, K. Allosery, J.A. Melero, E. Depla, Generation and Characterization of ALX-0171, a Potent Novel Therapeutic Nanobody for the Treatment of Respiratory Syncytial Virus Infection, Antimicrobial Agents and Chemotherapy, 60 (2016) 6-13.

CHAPTER 4

Enhancing the Stability of Adalimumab by Engineering

Additional Glycosylation Motifs
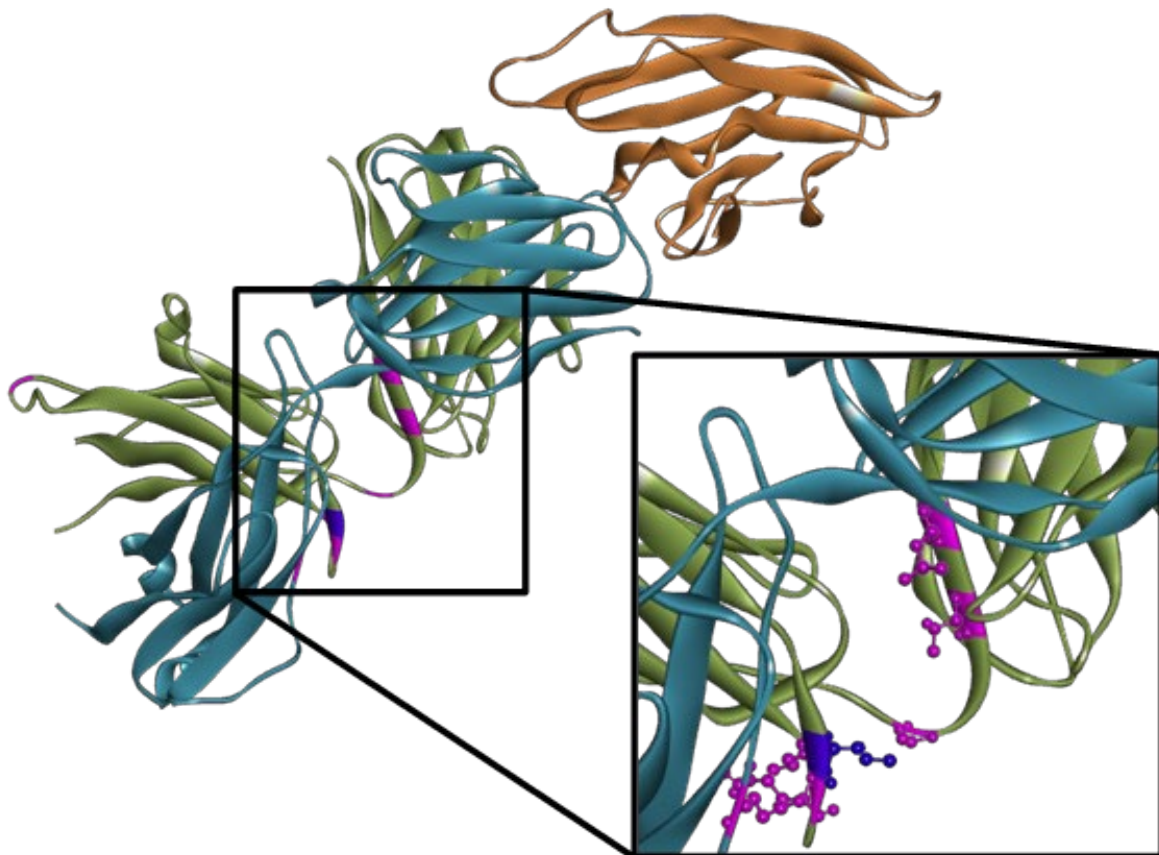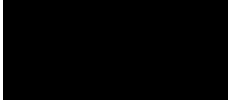
Chapter 4 – Authorship declaration statement
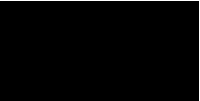
The following chapter is a manuscript prepared for submission as:

M. Reslan, V. Sifniotis, E. Cruz, Z. Sumer-Bayraktar, S. Cordwell, V. Kayser (2019). Enhancing the Stability of Adalimumab by Engineering Additional Glycosylation Motifs. E. Cruz

E. Cruz and Sumer-Bayraktar performed all mass spectrometry experiments and E. Cruz performed all mass spectrometry data analysis. E. Cruz wrote the sections in the manuscript related to the structural characterisation of the antibody mutants through mass spectrometry. E. Cruz provided critical review of the manuscript.

Esteban Cruz, Signature: 19th of August, 2019

As corresponding author and supervisor for this candidature, I hereby confirm that this authorship declaration statement is complete and accurate

Veysel Kayser, Signature: 19th of August, 2019

Abstract

Monoclonal antibodies (mAbs) are of high value in the diagnostic and treatment of many debilitating diseases such as cancers, auto-immune disorders and infections. Unfortunately, protein aggregation is one of the ongoing challenges, limiting the development and application of mAbs as therapeutic products by decreasing half-life, increasing immunogenicity and reducing activity. We engineered an aggregation-prone region of adalimumab, the top selling mAb product worldwide - with additional glycosylation sites to enhance its resistance to aggregation by steric hindrance as a next generation biologic. We found that the addition of N-glycans in the Fab domain significantly enhanced its conformational stability, with some variants increasing the melting temperature of the Fab domain by more than 6 °C. The mutations tested had minimal impact on antigen binding affinity, or affinity to Fcγ receptors responsible for effector function. Our findings highlight the significant utility of this rational engineering approach for enhancing the conformational stability of therapeutic mAbs and other next-generation antibody formats.

Introduction

Monoclonal antibodies (mAbs) are amongst the top-selling therapeutic prescription products worldwide. In 2017, Humira® (adalimumab) alone, generated over 18 billion US dollars, maintaining its position as the top-selling drug worldwide [1, 2]. Antibody therapeutics are revolutionary biopharmaceuticals used to treat cancers, auto-immune and inflammatory conditions, and even some types of asthma. Approximately 80 antibody products have been approved and marketed by the FDA and EMA with hundreds more in early and advanced clinical trials [3]. Advances in antibody engineering technology have led to the development of a multitude of novel, next-generation antibody-derived products often termed biobetters, which include bispecifics, nanobodies, antibody-drug conjugates, and nanoparticles functionalised with antibodies [3, 4].

Despite the four-decade-long progress and ever-growing interest in antibody research, one of the major challenges in the development of antibody therapeutics remains unsolved: protein aggregation [4-7]. Protein aggregation is one of the most common form of antibody degradation, having significant implications for a therapeutic product under development; aggregation can result in reduced therapeutic efficacy, and may trigger severe immunogenic side effects when

administered [8, 9]. Formulations of biologics including mAbs and other protein products are stabilized with the use of additives such as salts, sugars, amino acids and surfactants [10-12]. Some novel formulation additives have also been investigated to inhibit protein aggregation, including deuterated solvents [13], hydrogels [14, 15], peptide dendrons [16] and ionic liquids [17]. However, the type and amount of additives allowed in any given formulation is limited, especially in parenteral formulations – which are often used to administer mAbs. Thus, other approaches to enhance the aggregation-resistance of mAbs are needed.

Another approach to significantly enhance the stability of a mAb is to modify the antibody structure itself. A single amino acid mutation in an aggregation-prone region (APR) can be sufficient to significantly improve the stability of an antibody against aggregation and/or increase its melting temperature. Predictions of aggregation-prone regions are often aided by computational tools – these include TANGO, AGGRESCAN3D, SAP [18-20], docking studies and/or molecular dynamics simulations [21]. For instance, the spatial aggregation propensity (SAP) tool has previously been used to guide mutations of aggregation-prone motifs of rituximab. These motifs predicted by SAP were 'neutralised' by single-point mutations, and multiple mutations were then combined to increase the overall antibody stability [22].

A variation of this approach (single-point mutation of high SAP regions) involves engineering an additional N-glycosylation site in a spatially proximate region to an APR, to sterically hinder aggregation in that APR [23, 24]. This strategy involves the introduction of amino acid sequons containing the sequence N-X-S/T (N-glycosylation sequon), that can be recognised by oligosaccharyltransferases and result in the enzymatic attachment of a glycan to the asparagine (N) residue within the N-glycosylation sequon. Naturally occurring N-linked glycans in the Fc domain are known to significantly influence antibody stability and effector function and to increase half-life in patient serum. The introduction of extra N-linked glycosylation sites in the Fab domain may not only improve resistance to aggregation, but also enhance solubility and conformational stability of the antibody, offering additional benefits to a single-point mutation in a hydrophobic region.

Courtois, Agrawal [23] recently tested a series of Fab-glycosylated bevacizumab variants and reported significant improvements in overall stability. Nakamura, Oda-Ueda [24] also tested a glycan-introducing mutation in the Fab of adalimumab expressed in Pichia pastoris and found that

it inhibited protease digestion and precipitation under pH stress. However, its impact on soluble aggregation of the full antibody is not clear.

Table 1. Surface exposed amino acid (AA) residues identified in adalimumab Fab region for substitution.

AA Residue	Position	Region	Mutation	Proposed Function
L	178	C_H1	K	Remove APR by introducing polar amino acid [23].
			N	Remove APR and introduce glycosylation site [23].
Q	160	C_{kappa}		Sterically hinder APR by introducing glycosylation site [23].
L	116	C_{join}		
T	118			
A	122	C_H1		Improve solubility by introducing glycosylation site [25].
Q	179			Sterically hinder APR by introducing glycosylation site [23, 25].
L	183			
T	199			Improve solubility and sterically hinder self-association by introducing glycosylation site [25, 26].

In this study, we report on and discuss the stability of Fab-glycosylated adalimumab variants that have spatial proximity to a previously determined APR in the IgG1 CH1 region of rituximab [22] and bevacizumab [23]. Specifically, the amino acid of the APR transposed to the adalimumab IgG1 peptide sequence is leucine 178. The substitution of this hydrophobic amino acid to lysine in bevacizumab [23], or to serine in rituximab [22] in the equivalent position, had experimentally demonstrated increased stability. This amino acid can also be substituted with asparagine (e.g. L178N) to introduce an N-linked glycosylation site. For this study, surface exposed amino acids were identified that can be substituted to asparagine to introduce N-linked glycosylation sites i.e.

Asn-X-Ser/Thr, where X is any amino acid except proline (Fig. 1). All substitutions except T199N, were previously identified to have 10 Angstrom spatial proximity to the APR of interest [22, 23]. T199N was specifically chosen as it had been reported to dramatically increase the solubility of a poorly soluble antibody [25], however it does not have spatial proximity to the APR. This particular substitution also has the potential to sterically hinder reversible self-association [26] which warranted further investigation through this study. The substitutions that were identified and pursued for this study are listed in Table 1.
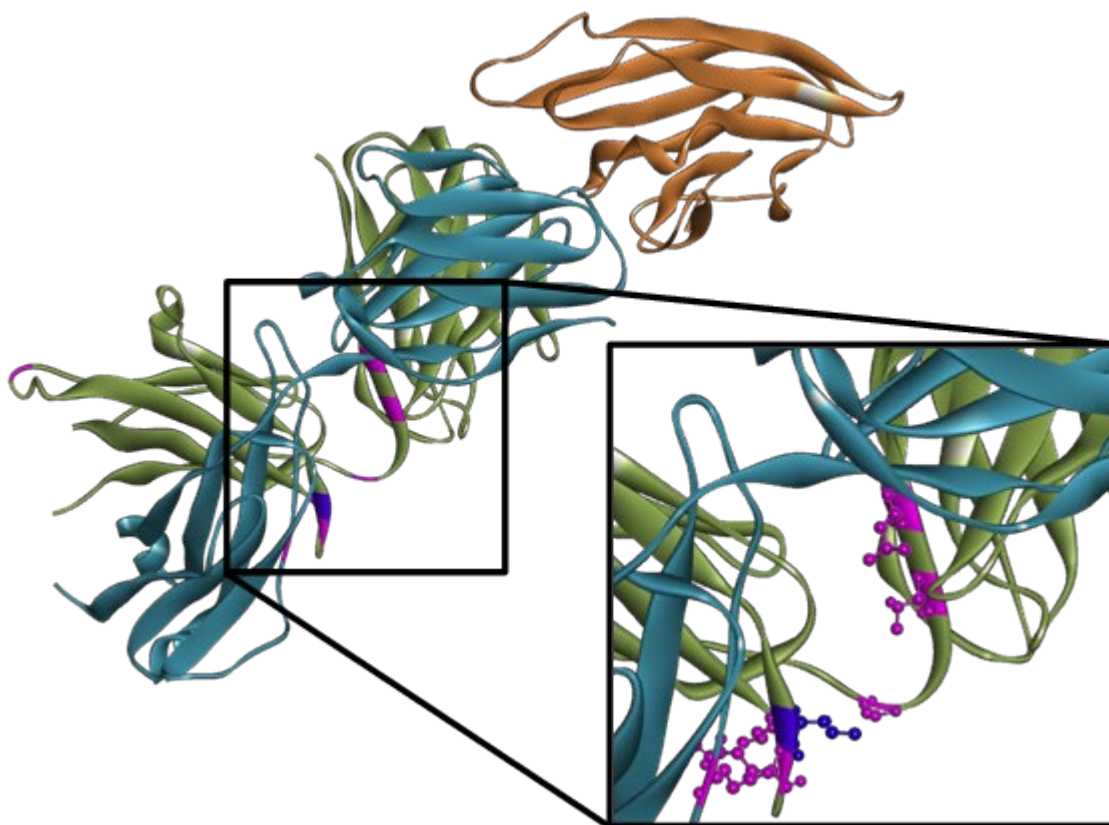
Figure 1. Crystal structure 3wd5 of adalimumab Fab fragment complexed to partial TNF-α fragment. Adalimumab VH/CH1 (green), VL/CL (aqua), TNF-α fragment (orange), APR site (purple) and surface exposed amino acids identified for substitution to an N-linked glycosylation site (pink).

In addition to studying the effect of these Fab N-linked glycosylations on the aggregation propensity of adalimumab, we also investigated the conformational stability of the variants, and

characterised their binding affinity to TNF-α, and Fcγ receptors (FcγRs) responsible for effector function, to understand the broader impact of these additional glycans.

Materials and Methods

Cloning and mutation of AdmAb WT and variants

The blank gWiz expression vector (Genlantis, P000200) was used to construct separate AdmAb IgG1 and kappa chain expression vectors. Firstly, secretion peptide genes, IgG1 and kappa chain genes were sourced from genes contained in vector pVITRO1_trastuzumab_IgG1/κ (Addgene plasmid # 61883), a kind donation from Andrew Beavil. These genes were cloned separately into the empty gWiz vector through conventional restriction cloning techniques (all materials from GeneSearch). The variable regions of AdmAb genes were designed and synthetically produced (Integrated DNA Technologies). These genes were exchanged with the trastuzumab variable regions in the gWiz vectors through In-Fusion cloning (Scientifix, 639648) to produce gWiz AdmAb IgG1 and gWiz AdmAb kappa vectors.

Mutations were then introduced to the gWiz AdmAb IgG1 and kappa vectors through high fidelity inverse PCR to produce a library of AdmAb mutant expression vectors. AdmAb WT and mutant variants were confirmed through sequencing and expressed through transfection of vector pair combinations.

Expression and Purification of AdmAb WT and variants

AdmAb WT and mutants were transiently expressed in suspension HEK293F culture. HEK293F culture was maintained and transfected in Freestyle 293F media (Life Technologies, 12338-018), 120 rpm, 37 °C, 5% CO_2, humidified incubation conditions. 24 hours prior to transfection, HEK293F culture was seeded to 6 - 7 x 10^{+5} cells/mL in a 60 mL culture and the culture was adjusted to 1 x 10^{+6} cells/mL on the day of transfection.

The complexing DNA for transfection was prepared as 1 µg total DNA per 1 x 10^{+6} cells. The gWiz AdmAb IgG1 and kappa vectors were combined in a w/w ratio of 1:1, and the complexing w/w ratio of PEI (BioScientific, 23966-2 (POL)) to total DNA was 2:1. The vector DNA and PEI were separately diluted in OptiPRO SFM (Life Technologies, 12309-050). The dilutions were combined and left to complex for 15 minutes before adding dropwise to the transfection culture.

After 24-hour incubation of the transfection culture, the culture was scaled up to 120 mL with Freestyle 293F media and supplemented to a total concentration of 0.5% tryptone w/v. After a further 24 hours of incubation, the culture was scaled up to 240 mL with Freestyle 293F media and supplemented to a total concentration of 0.5% tryptone w/v. The transfection culture remained in incubation for a total of 8 days before the media containing secreted antibody was harvested by centrifugation, and the culture supernatant was clarified by filtration.

AdmAb WT and variants were purified from the culture supernatants using protein A affinity with a 1 mL HiTrap MabSelect SuRe column (GE Healthcare, 29-0491-04). PBS pH 7.4 was used as the binding and wash buffer, and glycine-HCl pH 3 was used to elute bound antibody. Eluted antibody samples were neutralized in 1 M Tris-HCl pH 8 and concentrated to <1 mL using 50 kDa centrifugal filters (Sigma-Aldrich, Z740193). To purify the samples from any aggregates and obtain pure monomer samples, concentrated samples were fractioned using SE-HPLC (see SE-HPLC section) and the monomer fractions were collected and concentrated in 150 mM potassium phosphate buffer, pH 6.5, for analysis.

LC-MS/MS analysis of AdmAb variants

Successful mutation and introduction of glycosylation motifs of the AdmAb variants was confirmed through site-specific liquid chromatography tandem mass spectrometry (LC-MS/MS). Briefly, AdmAb variants were separated on reducing SDS-PAGE and digested with trypsin (Sigma-Aldrich, T6567) and chymotrypsin (Sigma-Aldrich, 11418467001). A fraction of the digestions was further treated with PNGase F (GeneSearch, P0708S) for glycan release. The digestion products were analysed by LC-MS/MS using higher-energy collisional dissociation (HCD), collision induced dissociation (CID) and electron transfer dissociation (ETD) methods.

The AdmAb variants (10 μg) were run on a reducing SDS-PAGE, in-gel trypsin digestion was performed on the heavy chain band (50 - 60 kDa) of variants L116N, T118N, A122N, L178K, L178N, Q179N, L183N, T199N and the light chain band (25 - 30 kDa) of Q160N. The bands were excised, diced and washed with 50% (v/v) acetonitrile in 100 mM NH4HCO3. The gel pieces were then reduced with 10 mM dithiothreitol at 56 °C for 45 minutes, followed by alkylation by addition of 55 mM iodoacetamide in 100 mM NH4HCO3, and incubation at 25 °C for 30 minutes. The samples were subsequently washed with 50% (v/v) acetonitrile in 100 mM NH4HCO3.

The alkylated polypeptides were incubated with trypsin (1 μg trypsin per 50 μg antibody) in 50 mM NH_4HCO_3, pH 6.8 at 37 °C overnight. The resulting tryptic peptides were further digested with chymotrypsin in 100 mM Tris-HCl, 10 mM $CaCl_2$, pH 7.8 at room temperature, overnight.

Glycan release was performed to confirm amino acid substitution; a fraction of the chymotryptic peptides (excluding L178K) was incubated with recombinant PNGase F (400 units per 1 μg of peptide) in 50 mM sodium phosphate buffer pH 7.5 at 37 °C, overnight. The chymotryptic peptides and the de-glycosylated fractions were desalted with C18 ZipTips (Millipore, ZTC18S096), eluted in 80% (v/v) acetonitrile, dried by vacuum centrifugation then re-dissolved in 0.1% formic acid for LC-MS/MS analysis.

Glycopeptides and de-glycosylated peptides were separated on an in-house packed 20 cm × 75 μm Reprosil-Pur C18AQ (3 μm, 120 A; Dr. Maisch GmbH) column using a Dionex 3500RS HPLC over a 90-minute 0-40% solvent B gradient at a flow rate of 300 nL/min, at 60°C (solvent A was 0.1% (v/v) formic acid; solvent B was 80% (v/v) acetonitrile and 0.1% formic acid). MS analysis was performed on an Orbitrap Fusion MS (Thermo Scientific) in positive mode. Instrument parameters were set up as follows: source voltage = 2.3 kV, S-lens RF level = 68%, and capillary temperature = 275 °C. The initial MS scan was acquired in the Orbitrap mass analyser (350–2000 m/z; MS AGC = $6 \times 10^{+5}$) with a resolution of 60,000 at 400 m/z. MS1 was followed by data-dependent HCD using top speed, where as many dependent scans as possible are acquired in a specified time. HCD fragmentation was followed by re-isolation of the top two most intense precursors, and fragmentation with CID and ETD MS/MS. HCD parameters were as follows: activation time = 0.1 ms, resolution = 30,000, maximum injection time = 200 ms, dynamic exclusion = enabled with repeat count 1, normalized energy = 40, exclusion duration = 20 s, default charge state = 2, and MSn AGC 2.0e5. CID parameters were as follows: 30,000 resolution in orbitrap, activation time = 10 ms, max injection time = 300 ms, dynamic exclusion = enabled with repeat count 1, normalized energy = 35, exclusion duration = 20 s, default charge state = 2, and MSn AGC 5.0e4. ETD parameters were as follows: 30,000 resolution in orbitrap, 5.0e4 AGC, ETD reaction time = 50 ms, Max injection time = 300 ms.

Peptide spectrum matches (PSM) were generated through a search against the corresponding FASTA file (wild-type or variant Adalimumab amino acid sequence) utilizing the search engine Byonic (Protein Metrics Inc.). Annotation of the HCD and ETD spectra were automated through

Byonic and the PSM assignments were validated by manually annotating the aforementioned spectra and the complementary CID spectrum. Further confirmation of the identity assignment was achieved through analysis of the de-glycosylated chymotryptic peptides utilizing the same LC-MS/MS approach as for the glycosylated fraction.

Accelerated stability at elevated temperatures

We performed accelerated studies at an elevated temperature as previously described [7]. Humira® 40 mg/0.8 mL subcutaneous injections (Symbion) were used for reference. Briefly, 20 µL of each AdmAb variant (1 mg/mL) was transferred to a 0.2 mL PCR vial and incubated at 65 °C for 1, 2 or 3 hours in a Thermal Cycler with heated lid (Applied Biosystems, CA, USA) to induce aggregation. Each experiment was repeated in triplicate. A thermal cycler was used to minimize sample amount and prevent evaporation of the sample and consequent changes in antibody concentration during incubation (lid/cover of thermal cycler is heated above incubation temperature). Following incubation, samples were immediately transferred to an ice bath as to halt aggregation. The aggregated samples were then characterized by size exclusion-high performance liquid chromatography (SE-HPLC).

SE-HPLC analysis of monomer loss

Size exclusion-high performance liquid chromatography (SE-HPLC) was used to quantify AdmAb monomer loss following incubation at elevated temperature as previously described [7]. Analysis was performed using an Agilent 1200 Liquid Chromatography system (Agilent Technologies) with a Zorbax GF-250 column (Agilent Technologies, 884973-701) coupled to a guard column (Agilent Technologies, 82095-911) at 22 °C, using a 150 mM potassium phosphate pH 6.5 mobile phase, and a flow rate of 0.5 mL/min. 5 µL of each incubated sample was injected in triplicate. Monomer peaks were detected using an in-line UV signal detector set at 280 nm. The area under the curve (AUC) of the monomer peak was averaged over the three runs. The percentage mean relative monomer was calculated for each sample by setting the monomer AUC of the non-incubated samples as 100% and calculating the change in monomer AUC accordingly. The standard deviations (SD) were plotted as error bars in the figures.

AdmAb melting temperature (Tm) and onset temperature of aggregation (Tagg)

The Tm and Tagg of Humira®, AdmAb WT, and variants were simultaneously measured using intrinsic tryptophan fluorescence and static light scattering (SLS), respectively, on the UNcle system (Unchained Labs). A linear temperature ramp from 15 to 95 °C at a 1 °C/minute scan rate was performed whilst measuring tryptophan fluorescence and SLS simultaneously through laser excitation at 266 nm. 8.5 µL of each AdmAb sample (1 mg/mL) was transferred undiluted in triplicate, into the UNcle sample holding unit. A holding time was not used as to maximize the frequency of measurements. Tm and Tagg were determined by the UNcle Analysis software. The barycentric mean (BCM) was used to plot the Tm curves, which is defined by the following equation:

$$\lambda_{BCM} = \frac{\sum_\lambda \lambda I(\lambda)}{\sum_\lambda I(\lambda)}$$

The equation is defined over the range 300 - 450 nm; each wavelength value (λ) is multiplied by the tryptophan fluorescence intensity (I) at that wavelength, and the sum of that value for all wavelengths from 300 - 450 is divided by the sum of the intensities at those wavelengths. This results in an 'averaged' peak wavelength (λBCM) for a given spectrum.

Binding kinetics to TNF-α and Fcγ receptors (FcγRs)

The binding kinetics of Humira®, AdmAb WT and variants were assessed to TNF-α and FcγR1A, 2B and 3A through surface plasmon resonance (SPR) to confirm that the mutations did not contribute to a loss of biological function. Briefly, a Biacore T200 system (GE Healthcare) was used, running single cycle kinetic assays. Monomeric AdmAb samples were captured on a ProA chip (GE Healthcare, 29-1275-55) and increasing dilutions of TNF-α (Sigma-Aldrich, H8916) were injected, with a 60-minute dissociation. HIS-tagged FcγR1A (Life Technologies, 10256-H08H-5), FcγR2B (Sigma-Aldrich, SRP6396) and FcγR3A (Sigma-Aldrich, SRP6436) were captured on an anti-HIS chip and increasing dilutions of monomeric AdmAb samples were injected, with a 30-minute dissociation. The sensograms were analysed to determine association rate (Ka), dissociation rate (Kd) and equilibrium dissociation constants (KD). All runs were performed at 25 °C with 10 mM HEPES, 150 mM NaCl, 0.05% v/v Tween 20 running buffer, pH adjusted to 7.4.

Soluble homotrimeric TNF-α was assayed against monomeric AdmAb samples on a ProA chip under continuous flow rate of 20 µL/min. Monomeric AdmAb samples were prepared to 10 nM and captured on the sensor chip surface with a contact time of 10 seconds. TNF-α was injected in 2-fold increasing concentrations (2.5 – 40 nM) with a contact time of 120 seconds at each concentration, then a dissociation time of 60 minutes. The chip surface was regenerated with 50 mM NaOH for 30 seconds at a flow rate of 30 µL / min.

Monomeric AdmAb samples were assayed against HIS tagged FcγRs. Anti-HIS antibody was covalently attached to a CM5 biosensor chip (GE Healthcare, 29-1049-88) using an amine coupling kit (GE Healthcare, BR-1000-50) and HIS capture kit (GE Healthcare, 28-9950-56). HIS tagged FcγR1A, 2B and 3A were prepared to 4 nM and captured to the sensor chip surface with a contact time of 300 seconds at 5 µL/min flow rate. AdmAb samples were injected on FcγR1A coated surface in 2-fold increasing concentrations (2.5 – 40 nM) at a flow rate of 20 µL/min with a contact time of 120 seconds at each concentration, followed by 30-minute dissociation time. AdmAb samples were injected on FcγR2B and FcγR3A-coated surfaces in 2-fold increasing concentrations (25 – 400 nM unless otherwise stated) at a flow rate of 10 µL/min with a contact time of 120 seconds at each concentration, followed by 1800 second dissociation time. The chip surface was regenerated with 10 mM glycine-HCl, pH 1.5 for 60 seconds at a flow rate of 30 µL/min.

The sensograms were analysed globally using a Langmuir 1:1 binding model to determine Ka, Kd and KD. All samples were conducted in duplicate to obtain average values and standard deviation. Kinetic rate and equilibrium constants determined from sensograms were accepted if the goodness of fit value (χ2) was within 5% of the maximum response level (Rmax) of the sensograms and KD was calculated as Kd/Ka.

Results

Confirmation of mutation and glycan attachment through LC-MS/MS

Detailed analysis of LC-MSMS data confirmed that all AdmAb variants had successful amino acid substitution. Incorporation of HCD, ETD and CID fragmentation techniques further provided compositional glycan information of the new N-glycosylation sites. Except for Q160N mutant, all other AdmAb glycosylation-site variants were found to contain an N-glycan (data not shown).

Here, we show the characterization of glycan site-engineered AdmAb variant T199N as a representation of the analysis performed for all AdmAb variants.
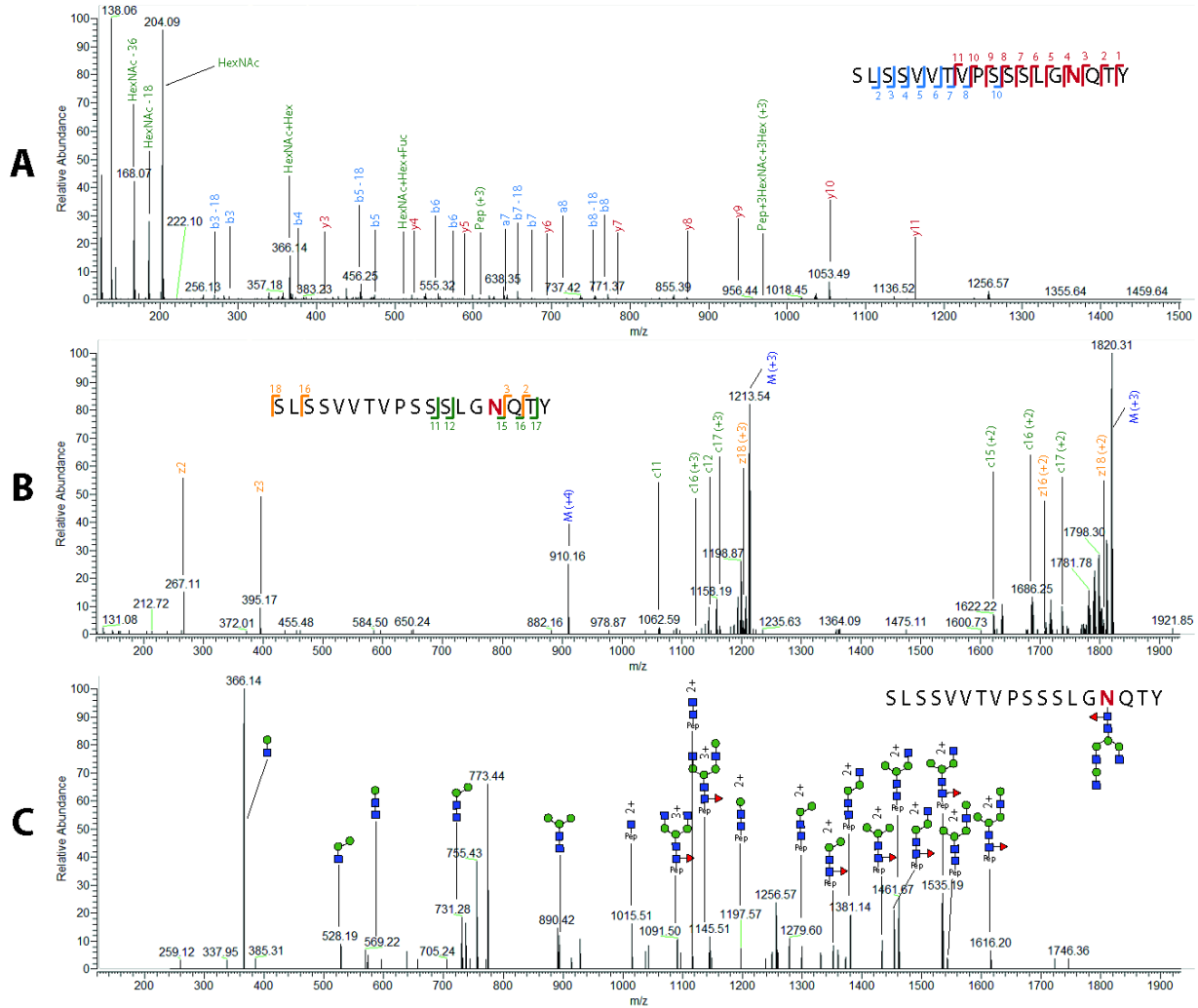
Figure 2. (A) HCD, (B) ETD and (C) CID spectra of chymotryptic T199N glycopeptide observed at m/z 909.65 (4+). Peptide sequence SLSSVVTVPSSSLGNQTY and attached complex type N-glycan HexNAc5Hex4Fuc1 are shown. Blue square; N-acetylglucosamine, red triangle; fucose, green circle; mannose, yellow circle; galactose, Hex; hexose, HexNAc; N-acetylhexosamine, M; precursor ion.

HCD spectrum of SLSSVVTVPSSSLGNQTY peptide observed at m/z 909.65(4+) showed b- and y-ion series confirming amino acid sequence and the asparagine substitution was shown specifically by y4-y11 fragment ions (Fig. 2A). HCD of T199N mutant also contained diagnostic

HexNAc (m/z 204.09) and HexNAcHex (m/z 366.14) oxonium ions, strongly indicating glycosylation on the mutant peptide (Fig. 2A). ETD further confirmed the structure of T199N glycopeptide by multiple fragment ions corresponding to dissociated peptide backbone with intact glycan (Figure 2B, c-15, c-16, c-17 and z-16 ions). Theoretical monosaccharide composition of the N-glycan was derived using Byonic (Protein Metrics) search results and GlycoMod (https://web.expasy.org). CID data in Figure 2C shows sequential loss of monosaccharides from glycopeptide fragments of T199N mutant and contains complementary oxonium ions m/z 366.14, m/z 528.19, and m/z 569.22 of the observed glycan in the low mass region. Extensive glycosidic bond cleavages (Fig. 2C, y-ions, m/z 1616.2(2+), m/z 1535.19(2+), m/z 1461.67(2+)) observed in CID confirmed that SLSSVVTVPSSSLGNQTY peptide is occupied by a complex type N-glycan with HexNAc5Hex4Fuc1 composition. CID spectra of deglycosylated T199N peptide m/z 609.64(3+) showed enhanced peptide backbone fragmentation and provided additional information for the expected mass shift from threonine to asparagine (y4-y18 ions and b17 ion, Fig. 3). Same ion series also displayed deamidation (+1Da) of the new asparagine residue which is a characteristic result of PNGaseF treatment of a formerly N-glycosylated peptide.
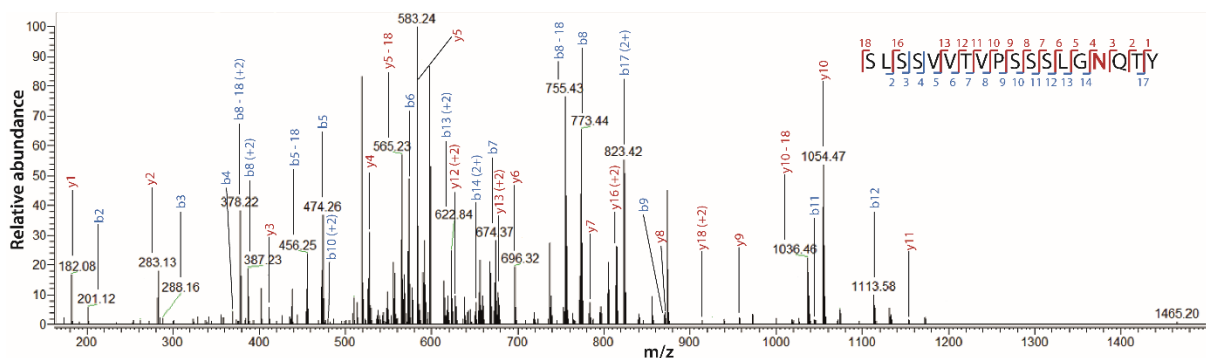
Figure 3. CID spectrum of de-glycosylated chymotryptic T199N mutant peptide SLSSVVTVPSSSLGNQTY observed at m/z 609.64(3+). b- and y- ions show CID fragments of the peptide.

Monomer loss following accelerated studies at elevated temperature

Incubation at 65 °C revealed modest differences in aggregation propensity between the reference Humira®, WT and single-mutant variants (Fig. 4). Variants L116N and T118N were completely degraded after an hour of incubation and were therefore not included in the figure (Fig. 4). Variant Q160N had very similar monomer loss data at all incubation temperatures to the WT, while L183N

had a noticeably higher monomer loss. Variants A122N, Q179N and T199N retained higher monomer content than the control at most incubation conditions, with A122N having the least monomer loss (Fig. 4). While Q179N had comparable monomer loss after 1 hour, monomer loss was lower at 2 and 3 hours, when compared to the WT. Interestingly, variants L178N and L178K had comparable monomer loss profiles which were not significantly different to the WT (Fig. 4). Humira® reference had slightly lower monomer loss than the WT.
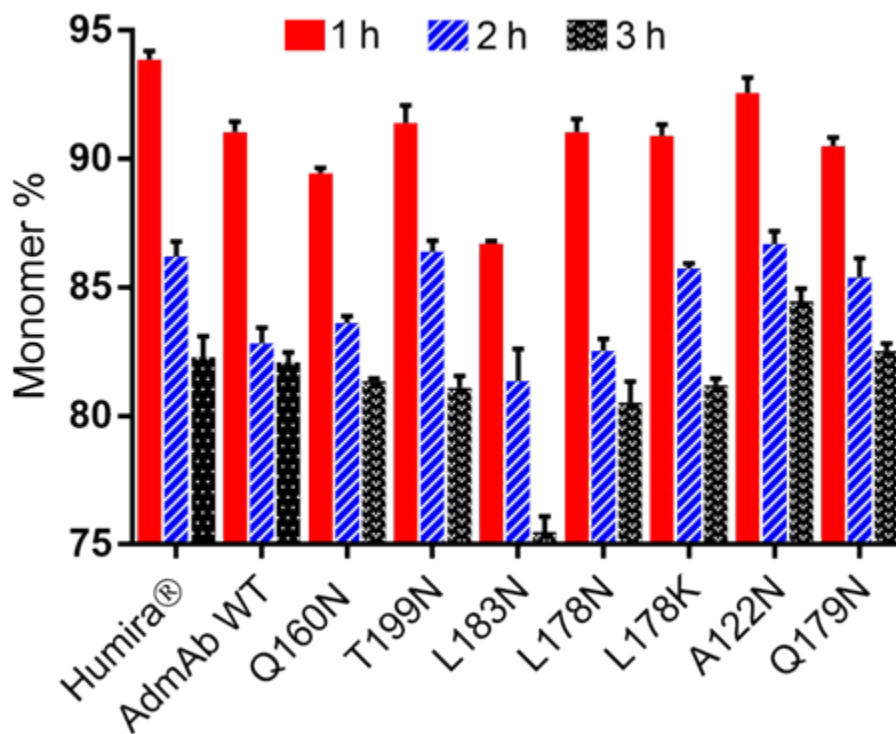
Figure 4. Monomer loss of Humira®, AdmAb wild-type (WT) and variants following incubation at 65 °C for 1, 2 and 3 hours. Error bars represent the SD.

Tm and Tagg

The WT AdmAb had a very similar Tm1 and Tm2 to the Humira® reference product; a slightly lower Tm1 was measured at 69.6 °C (WT) compared with 70.8 °C (Table 2). The Tm2 was comparable at 82 °C compared with 82.5 °C for Humira®. Variant Q160N had a similar melting profile to the WT, with an identical Tm1 and comparable Tm2 of 69.6 and 82 °C, respectively. Variants T118N and L116N had a significantly lower Tm1 at 59.7 and 63.6 °C, respectively; the

Tm2 was also lower at 68 and 78.6 °C, respectively. Interestingly, a third Tm was recorded for variants T118N and L116N at 87.8 and 88.3 °C, respectively. Variants L178K, A122N and Q179N had similar Tms and were comparable to the WT. Variants T199N and L178N had similar Tm1 values to the WT (70.6 and 69.9 °C, respectively), but significantly higher Tm2 values (88.2 and 89.3 °C, respectively). Variant L183N had a similar Tm1 to the WT, but had a consistent minor unfolding event at ~65 °C (not shown); Tm2 was higher than the WT (88.3 °C, Table 2). The Tagg of the WT and variants ranged from 70.6 to 72.5 °C, except for variants T118N and L116N, which had significantly lower Tagg values (61.7 and 64.7 °C, respectively; Table 2). Most variants had a slightly higher Tagg than the WT (70.7 °C) by approximately 1-2 °C, while the Tagg of Q160N and L178K were unchanged. Compared with L178K, the Tagg of glycosylated variant L178N was 1.7 °C higher.

Table 2. The melting (Tm) and onset of aggregation temperatures (Tagg) of the AdmAb variants compared with the wild-type (WT) and reference Humira® product (± SD). ^see discussion

AdmAb	T_m1 (°C)	T_m2 (°C)	T_m3 (°C)	T_{agg} @266 nm
Humira®	70.8 ± 0.2	82.5 ± 0.8	-	71.3 ± 0.4
WT	69.6 ± 0.5	82 ± 1.4	-	70.7 ± 0.1
Q160N	69.6 ± 0.3	81.1 ± 1.4	-	71 ± 0.4
T199N	70.6 ± 0.2	88.2 ± 2.2	-	71.7 ± 0.1
T118N	59.7 ± 0.5	68 ± 0.7	87.8 ± 2.5	61.7 ± 0.6
L178K	68.4 ± 0.6	83.5 ± 0.5	-	70.6 ± 0.3
L178N	69.9 ± 0.5	89.3 ± 0.2	-	72.3 ± 0.3
A122N	69.7 ± 0.5	83.4 ± 0.7	-	71.8 ± 0.4
Q179N	69.4 ± 0.2	82.7 ± 0.9	-	71.7 ± 0.5
L118N	63.6 ± 0.5	78.6 ± 0.5	88.3 ± 1.2	64.7 ± 0.3
L183N	70^ ± 0.5	88.3 ± 1.1	-	72.5

Binding kinetics of AdmAb to TNF-α and FcγRs

The binding kinetics of reference Humira®, monomeric AdmAb WT and variants to TNF-α and FcγR1A, 2B and 3A were assessed using SPR single cycle kinetic analysis. Samples were run in

duplicate and sensograms were fitted to a Langmuir 1:1 binding model to obtain Ka, Kd and KD values for comparison as per previous studies [27, 28]. It was determined that in general, the majority of AdmAb variants did not experience a significant loss of biological activity.

The KD range determined for monomeric AdmAb variants binding to soluble homotrimeric TNF-α spanned 36.69 – 110.27 pM, while Humira® had a mean KD of 30.77 pM (Table 3). Monomeric AdmAb WT had a KD of 66.43 ± 2.37 pM which lies within the range, with no significant outlier (Table 3). Of all variants tested, T199N had the strongest KD to TNF- α (36.69 pM) - approximately 1.8-fold stronger than the WT - while Q179N had the weakest KD (110.27 pM).

Table 3. Kinetics and binding affinity of reference (Humira®) and monomeric AdmAb mutants to soluble homotrimeric TNF-α (± SD).

AdmAb	TNF-α		
	K_a (x 10^{+5}) $M^{-1}.s^{-1}$	K_d (x 10^{-5}) s^{-1}	K_D (pM)
Humira®	11.7 ± 0.01	3.59 ± 0.80	30.77 ± 6.83
WT	6.08 ± 0.07	4.04 ± 0.10	66.43 ± 2.37
L178K	4.84 ± 0.01	4.61 ± 0.64	95.33 ± 13.3
L178N	5.33 ± 0.03	5.42 ± 0.67	101.7 ± 12.1
Q160N	6.2 ± 0.07	2.86 ± 0.05	46.05 ± 1.31
L116N	5.19 ± 0.09	2.84 ± 0.1	54.77 ± 2.87
T118N	5.04 ± 0.02	3.59 ± 0.21	71.19 ± 4.50
A122N	6.47 ± 0.03	2.87 ± 0.05	44.32 ± 0.57
Q179N	5.02 ± 0.40	5.53 ± 0.1	110.3 ± 6.56
L183N	5.58 ± 0.14	3.05 ± 0.03	55.37 ± 0.86
T199N	7.15 ± 0.69	2.62 ± 0.01	36.69 ± 3.54

The KD range determined for FcγR1A binding to monomeric AdmAb variants spanned 2.1 – 6.81 nM, while Humira® had a mean KD of 1.84 nM (Table 4). Monomeric AdmAb WT had a KD of 4.4 ± 0.01 nM which lies within the range with no significant outlier (Table 4). Of all variants tested, the strongest KD was recorded for mutant T118N (2.1 nM), while the weakest KD was recorded for L178N (6.81 nM).

Due to sample limitations, monomeric AdmAb Q160N was not tested for the cycle assays against FcγR2B (Table 4).

The KD range determined for FcγR2B binding to monomeric AdmAb variants spanned 1.81 – 9.61 nM, while Humira® had a mean KD of 2.55 nM. Monomeric AdmAb WT had a KD of 4.47 ± 0.1 nM which lies within the range with no significant outlier (Table 4). T199N had the strongest KD to FcγR2B (1.81 nM), while T118N had the weakest KD (9.61 nM). However, due to the large variation in KD values for the WT and several mutants, most differences were not deemed significant.

The KD range determined for FcγR3A binding to monomeric AdmAb variants spanned 1.48 – 18.01 nM, while Humira® had a mean KD of 1.84 nM. Monomeric AdmAb WT had a KD of 5.96 ± 1.62 nM which lies within the range with no significant outlier (Table 4). The strongest KD was recorded for L183N (1.48 nM), while the weakest KD was recorded for A122N (18.01 nM) with large ranges. Overall, all differences in KD recorded compared to the WT, were no larger or smaller than 3-fold for TNF-α and all receptors tested.

Table 4. Binding affinity of reference Humira® and monomeric AdmAb mutants to FcγR1A, FcγR2B and FcγR3A.

AdmAb	K_D (nM)		
	FcγR1A	**FcγR2B**	**FcγR3A**
Humira®	1.84 ± 0.18	2.55 ± 1.67	1.84 ± 0.68
WT	4.4 ± 0.01	4.47 ± 1.00	5.96 ± 1.62
L178K	4.14 ± 0.06	9.16 ± 6.86	2.37 ± 1.19
L178N	6.81 ± 0.45	3.67 ± 0.93	2.15 ± 0.73
Q160N	5.3 ± 0.01	N.D.	16.2 ± 3.05
L116N	3.87 ± 0.14	6.15 ± 1.10	6.71 ± 1.91
T118N	2.1 ± 0.01	9.61 ± 1.38	13.3 ± 0.45
A122N	5.58 ± 0.18	7.53 ± 2.74	18.01 ± 7.4
Q179N	2.74 ± 0.01	5.27 ± 0.11	2.92 ± 0.16
L183N	2.6 ± 0.04	2.52 ± 2.05	1.48 ± 0.84

T199N	6.49 ± 0.06	1.81 ± 1.25	11.80 ± 0.2

Discussion

We rationally designed and produced a library of glycan-engineered AdmAb variants to enhance stability through steric hindrance of an APR. Successful mutation and glycan addition was confirmed for all mutants aside from Q160N, through LC-MS/MS. Consequently, the stability and binding kinetics results for the Q160N variant are directly related to the amino acid substitution alone. Since Q160N had similar stability and antigen binding affinity to the WT, it was concluded that the amino acid substitution did not have any significant impact on the antibody properties tested. The KD values for the AdmAb WT produced in our study (Table 3 and 4) are comparable to Humira® KD values observed, and as reported in the literature; TNF-α (30-110 pM), FcγR1A (15-23 nM), FcγR2B (4.3-14.2 nM) and FcγR3A (5.8-7.9 nM) [29, 30].

Likewise, most measured KD values for the mutants tested lay within a close range to reported literature values for the reference AdmAb, showing that these mutations had minimal impact on binding properties.

The highest improvement in resistance to aggregation was observed in mutant A122N with a slight increase in Tagg and reduction in monomer loss (Table 2 and Fig. 4). The A122N mutation resulted in 1.5-fold increased binding affinity to TNF-α with slightly reduced binding to FcγRs tested and with no impact on conformational stability. Pepinsky, et al [25] reported that a mutation equivalent in position to AdmAb variant A122N significantly improved the solubility of an anti-LINGO antibody, with no impact on binding affinity or conformational stability. Improvements in solubility often correlate with reduced precipitation and insoluble aggregate formation.

This may explain the minor improvement in Tagg we observed with mutant A122N which reflects a higher resistance to precipitation at higher temperatures. Although only a minor improvement in monomer loss, the improvement is consistent at higher concentrations tested (15 mg/mL, data not shown) and is significant in a clinical setting, where typically no more than 5% of aggregates are considered acceptable by regulatory standards.

No significant improvements in monomer loss were observed with other mutants (e.g. T199N and Q179N). Courtois, et al [22] hypothesised that a mutant equivalent in position to Q179N in

bevacizumab could not be glycosylated as it was inaccessible to glycosylases. However, we confirmed that Q179N was glycosylated; likewise, Pepinsky, et al [25] were able to express a glycosylated variant with a mutation in an equivalent position to Q179N which mildly improved antibody solubility. Accessibility to glycosylases does not determine whether the initial glycan is added or not, as this addition occurs in the endoplasmic reticulum prior to the folding of the protein. Thus, it may have been possible to introduce a glycan in this position with bevacizumab as well. Nevertheless, with the additional N-glycan, Q179N was expected to sterically hinder Fab-mediated aggregation in the targeted APR; while T199N was reported to significantly improve solubility [25] and sterically hinder self-association [26], however this was not observed for AdmAb. The Q179N mutation also mildly reduced antigen binding affinity by ~1.6-fold.

Interestingly, Pepinsky, et al [25] reported no change in the Tm of the mutation equivalent in position to AdmAb variant T199N, while we observed a significant improvement in Fab Tm with variant T199N (~6 degrees higher). Additionally, T199N had 1.8-fold improved KD to TNF-α with minimal differences in KD to FcγRs. The lack of improvement in resistance to aggregation, despite the improvement in Fab stability, may be related to the mechanism of aggregation in AdmAb. Since the CH2 has the lowest Tm in most IgG1s, it is expected that most aggregation steps are at least initiated with unfolding of the CH2; thus, an improvement in Fab stability may not significantly impact overall resistance to soluble aggregation.

Similarly, we observed an improvement in Fab Tm for mutants L178N and L183N. L178N is an interesting example, because when compared to the non-glycosylated variant L178K, there is an improvement in Tagg and Fab Tm through glycosylation. This emphasises the impact of the N-glycans added via mutation on the conformational stability of the Fab and its resistance to precipitation, and highlights that these changes are not due to the amino acid substitution. The mutation significantly improved the conformational stability of the Fab domain. Furthermore, despite suppressing pH-induced precipitation when tested on the Fab alone [24], the L178N mutation had minimal impact on soluble aggregation when tested on the full AdmAb. Surprisingly, the non-glycosylated variant L178K which was reported to significantly suppress aggregation in bevacizumab [23], but enhance aggregation in rituximab [22], also had minimal impact on the stability of AdmAb. This finding highlights that framework regions differ significantly between IgG1 antibodies despite having identical sequences.

Variants L116N and T118N had multiple Tms, with a lower Tm1, higher Tm3 and a significantly reduced Tagg; additionally, they were completely degraded at 65 °C. The Tms of these mutants are harder to interpret, and do not necessarily represent the CH2, Fab and CH3 in that order. As previously reported [31], disturbances in the joining region between the Fab domains can create additional Tms for each separate domain. Thus, we expect that the Tm1 value of these mutants is representative of only part of the Fab (for e.g. the CH1 or VL); since the Tm of this part of the Fab is now less stable than the CH2, aggregation proceeded more rapidly at 65 °C. Again, our results do not correspond with findings reported for the mutation equivalent to AdmAb L116N in bevacizumab, which showed improved resistance to aggregation with no destabilization of the Fab [23]. Some perturbation in Fab stability was also observed with mutant L183N, resulting in increased monomer loss. The perturbation was minor and hard to detect; however consistently appeared in temperature ramps for Tm measurement. It is likely that the amino acid substation in this position impaired the conformational stability of part of the Fab domain as observed with mutants L116N and T118N.

Conclusion

Protein aggregation is a complex challenge hindering the development and long-term stability of therapeutic mAbs. Using advanced computational tools, we identified aggregation prone regions and engineered adalimumab, a marketed therapeutic mAb, with additional N-glycans in the Fab domain, with the aim to sterically hinder aggregation and increase long-term stability. Our glycan-engineered variants displayed a range of different stabilities, with some mutations increasing susceptibility to aggregation, others enhancing the conformational stability of the Fab domain, and one showing minor improvements in resistance to aggregation. This approach has potential application for other antibodies where the Fab domain has poor stability or is a pre-cursor to aggregation. We demonstrated that the conformational stability of blockbuster therapeutic antibodies such as AdmAb can still be improved with glycan-engineering without compromising its antigen and Fc receptor binding affinity; these findings highlight the significant value of this engineering approach in the quest for developing more stable therapeutic mAbs with improved half-lives and therapeutic outcomes.

Abbreviations

AdmAb	adalimumab
APR	aggregation-prone region
AUC	area under the curve
BCM	barycentric mean
CID	collision induced dissociation
ETD	electron transfer dissociation
HCD	higher-energy collisional dissociation
Ka	association rate constant
Kd	dissociation rate constant
KD	equilibrium dissociation constant
LC-MS/MS	liquid chromatography tandem mass spectrometry
mAb	monoclonal antibody
PEI	polyethylenimine, linear, 25 kDa
PSM	peptide spectrum matches
rpm	rotations per minute
SAP	spatial aggregation propensity
SD	standard deviation
SDS-PAGE	sodium dodecyl sulfate polyacrylamide gel electrophoresis
SE-HPLC	size exclusion-high performance liquid chromatography
SLS	static light scattering
SPR	surface plasmon resonance
Tagg	onset temperature of aggregation

Tm	melting temperature (protein)
UV	ultraviolet
v/v	volume for volume
WT	wild-type
w/v	weight for volume

Acknowledgements

Disclosure of Potential Conflicts of Interest

The authors declare no financial or commercial conflict of interest.

References

[1]. L. Urquhart, Top drugs and companies by sales in 2017, Nature Reviews: Drug Discovery, 17 (2018) 232.

[2]. D. Ecker, S. Dana Jones, H. L Levine, The Therapeutic Monoclonal Antibody Market, mAbs, 7 (2015) 9-14.

[3]. C. Klein, Special Issue: Monoclonal Antibodies, Antibodies, 7 (2018) 17.

[4]. Z. Elgundi, M. Reslan, E. Cruz, V. Sifniotis, V. Kayser, The state-of-play and future of antibody therapeutics, Advanced Drug Delivery Reviews, 122 (2017) 2-19.

[5]. M.L. Fleischman, J. Chung, E.P. Paul, R.A. Lewus, Shipping-Induced Aggregation in Therapeutic Antibodies: Utilization of a Scale-Down Model to Assess Degradation in Monoclonal Antibodies, Journal of Pharmaceutical Sciences, 106 (2017) 994-1000.

[6]. A. Beck, L. Goetsch, C. Dumontet, N. Corvaïa, Strategies and challenges for the next generation of antibody–drug conjugates, Nature Reviews: Drug Discovery, 16 (2017) 315.

[7]. V. Kayser, N. Chennamsetty, V. Voynov, B. Helk, K. Forrer, B.L. Trout, Evaluation of a Non-Arrhenius Model for Therapeutic Monoclonal Antibody Aggregation, Journal of Pharmaceutical Sciences, 100 (2011) 2526-2542.

[8]. J. Bessa, S. Boeckle, H. Beck, T. Buckel, S. Schlicht, M. Ebeling, A. Kiialainen, A. Koulov, B. Boll, T. Weiser, T. Singer, A.G. Rolink, A. Iglesias, The Immunogenicity of Antibody Aggregates in a Novel Transgenic Mouse Model, Pharmaceutical Research, 32 (2015) 2344-2359.

[9]. M. Ahmadi, C.J. Bryson, E.A. Cloake, K. Welch, V. Filipe, S. Romeijn, A. Hawe, W. Jiskoot, M.P. Baker, M.H. Fogg, Small Amounts of Sub-Visible Aggregates Enhance the Immunogenic Potential of Monoclonal Antibody Therapeutics, Pharmaceutical Research, 32 (2015) 1383-1394.

[10]. M. Reslan, Y.K. Demir, B.L. Trout, H.-K. Chan, V. Kayser, Lack of a synergistic effect of arginine–glutamic acid on the physical stability of spray-dried bovine serum albumin, Pharmaceutical Development and Technology, 22 (2017) 785-791.

[11]. J. Zhang, V. Frey, M. Corcoran, J. Zhang-van Enk, J.A. Subramony, Influence of Arginine Salts on the Thermal Stability and Aggregation Kinetics of Monoclonal Antibody: Dominant Role of Anions, Molecular Pharmaceutics, 13 (2016) 3362-3369.

[12]. R. Respaud, D. Marchand, C. Parent, T. Pelat, P. Thullier, J.-F. Tournamille, M.-C. Viaud-Massuard, P. Diot, M. Si-Tahar, L. Vecellio, N. Heuzé-Vourc'h, Effect of formulation on the stability and aerosol performance of a nebulized antibody, mAbs, 6 (2014) 1347-1355.

[13]. M. Reslan, V. Kayser, The effect of deuterium oxide on the conformational stability and aggregation of bovine serum albumin, Pharmaceutical Development and Technology, (2016) 1-7.

[14]. B.V. Sridhar, J.R. Janczy, Ø. Hatlevik, G. Wolfson, K.S. Anseth, M.W. Tibbitt, Thermal Stabilization of Biologics with Photoresponsive Hydrogels, Biomacromolecules, 19 (2018) 740-747.

[15]. J. Lee, J.H. Ko, K.M. Mansfield, P.C. Nauka, E. Bat, H.D. Maynard, Glucose-Responsive Trehalose Hydrogel for Insulin Stabilization and Delivery, Macromolecular Bioscience, 18 (2018) 1700372.

[16]. R. Bansal, S. Dhawan, S. Chattopadhyay, G.P. Maurya, V. Haridas, A.S. Rathore, Peptide Dendrons as Thermal-Stability Amplifiers for Immunoglobulin G1 Monoclonal Antibody Biotherapeutics, Bioconjugate Chemistry, 28 (2017) 2549-2559.

[17]. M. Reslan, V. Kayser, Ionic liquids as biocompatible stabilizers of proteins, Biophysical Reviews, 10 (2018) 781-793.

[18]. N. Chennamsetty, V. Voynov, V. Kayser, B. Helk, B.L. Trout, Design of therapeutic proteins with enhanced stability, Proceedings of the National Academy of Sciences, USA, 106 (2009) 11937-11942.

[19]. S. Kulshreshtha, V. Chaudhary, G.K. Goswami, N. Mathur, Computational approaches for predicting mutant protein stability, Journal of Computer-Aided Molecular Design, 30 (2016) 401-412.

[20]. R. Zambrano, M. Jamroz, A. Szczasiuk, J. Pujols, S. Kmiecik, S. Ventura, AGGRESCAN3D (A3D): server for prediction of aggregation properties of protein structures, Nucleic Acids Research, 43 (2015) W306-W313.

[21]. S. Kuyucak, V. Kayser, Biobetters From an Integrated Computational/Experimental Approach, Computational and Structural Biotechnology Journal, 15 (2017) 138-145.

[22]. F. Courtois, C.P. Schneider, N.J. Agrawal, B.L. Trout, Rational Design of Biobetters with Enhanced Stability, Journal of Pharmaceutical Sciences, 104 (2015) 2433-2440.

[23]. F. Courtois, N.J. Agrawal, T.M. Lauer, B.L. Trout, Rational design of therapeutic mAbs against aggregation through protein engineering and incorporation of glycosylation motifs applied to bevacizumab, mAbs, 8 (2016) 99-112.

[24]. H. Nakamura, N. Oda-Ueda, T. Ueda, T. Ohkuri, Introduction of a glycosylation site in the constant region decreases the aggregation of adalimumab Fab, Biochemical and Biophysical Research Communications, 503 (2018) 752-756.

[25]. R.B. Pepinsky, L. Silvian, S.A. Berkowitz, G. Farrington, A. Lugovskoy, L. Walus, J. Eldredge, A. Capili, S. Mi, C. Graff, E. Garber, Improving the solubility of anti-LINGO-1 monoclonal antibody Li33 by isotype switching and targeted mutagenesis, Protein Science, 19 (2010) 954-966.

[26]. T.F. Lerch, P. Sharpe, S.J. Mayclin, T.E. Edwards, E. Lee, H.D. Conlon, S. Polleck, J.C. Rouse, Y. Luo, Q. Zou, Infliximab crystal structures reveal insights into self-association, mAbs, 9 (2017) 874-883.

[27]. R. Karlsson, E. Pol, Å. Frostell, Comparison of surface plasmon resonance binding curves for characterization of protein interactions and analysis of screening data, Analytical Biochemistry, 502 (2016) 53-63.

[28]. J.M. Hayes, A. Frostell, R. Karlsson, S. Muller, S.M. Martín, M. Pauers, F. Reuss, E.F. Cosgrave, C. Anneren, G.P. Davey, P.M. Rudd, Identification of Fc Gamma receptor glycoforms that produce differential binding kinetics for rituximab, Mol. Cell. Proteomics, 16 (2017) 1770-1788.

[29]. Z. Kaymakcalan, P. Sakorafas, S. Bose, S. Scesney, L. Xiong, D.K. Hanzatian, J. Salfeld, E.H. Sasso, Comparisons of affinities, avidities, and complement activation of adalimumab, infliximab, and etanercept in binding to soluble and membrane tumor necrosis factor, Clinical Immunology, 131 (2009) 308-316.

[30]. L. Magnenat, A. Palmese, C. Fremaux, F. D'Amici, M. Terlizzese, M. Rossi, L. Chevalet, Demonstration of physicochemical and functional similarity between the proposed biosimilar adalimumab MSB11022 and Humira®, mAbs, 9 (2017) 127-139.

[31]. R.M. Ionescu, J. Vlasak, C. Price, M. Kirchmeier, Contribution of Variable Domains to the Stability of Humanized IgG1 Monoclonal Antibodies, Journal of Pharmaceutical Sciences, 97 (2008) 1414-1426.

CHAPTER 5

Glycan Profile Analysis of Engineered Trastuzumab with Rationally Added Glycosylation Sequons for Enhanced Physical Stability
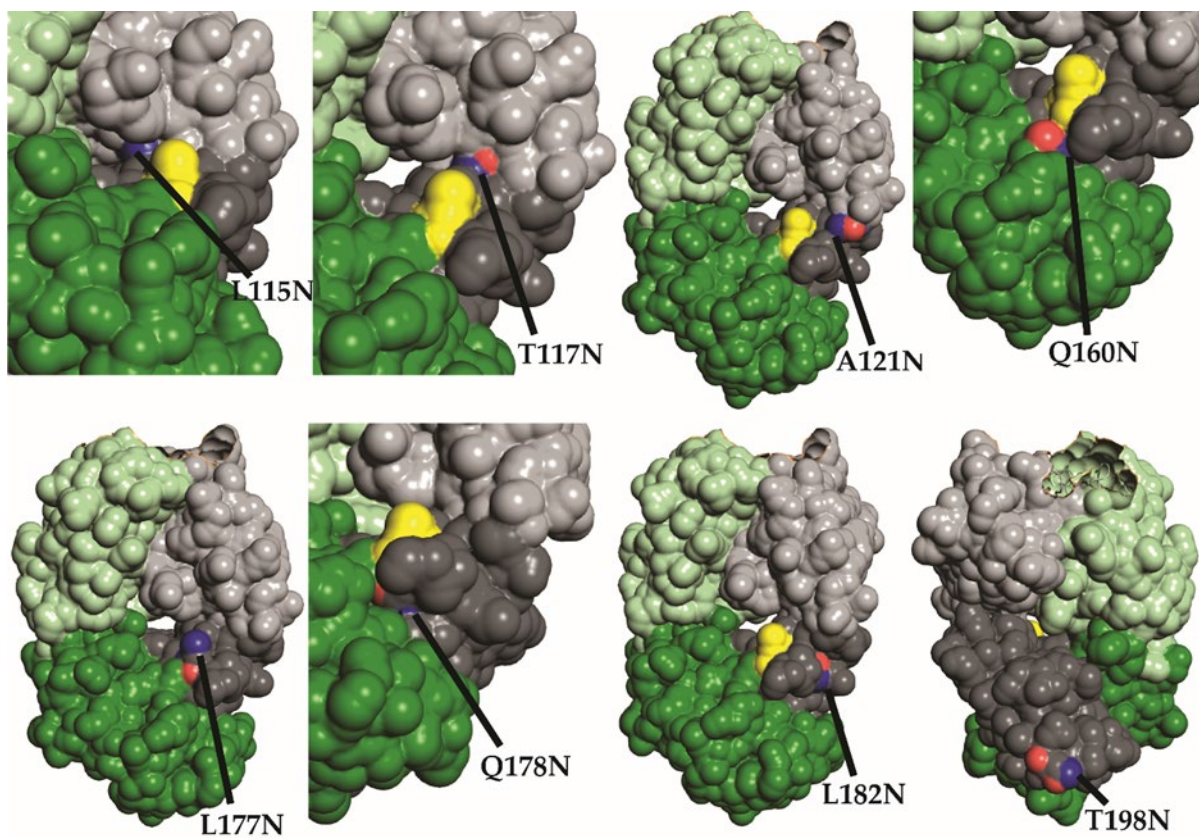
Chapter 5 – Authorship declaration statement

The following chapter is a manuscript prepared for submission as:

E. Cruz, V. Sifniotis, Z. Sumer-Bayraktar, S. Cordwell, V. Kayser. (2019). Glycan Profile Analysis of Engineered Trastuzumab with Rationally Added Glycosylation Sequons for Enhanced Physical Stability.

E. Cruz co-designed the study. E. Cruz and Z. Sumer-Bayraktar performed all mass spectrometry experiments and data analysis. E. Cruz obtained all additional results with the exception of the surface-plasmon resonance data and wrote the manuscript.

Esteban Cruz, Signature: 19th of August, 2019

As corresponding author and supervisor for this candidature, I hereby confirm that this authorship declaration statement is complete and accurate

Veysel Kayser, Signature: *Veysel Kayser*   19th of August, 2019

Abstract

Protein aggregation constitutes a recurring complication in the manufacture and clinical use of therapeutic monoclonal antibodies (mAb) and mAb derivatives. Antibody aggregates can reduce production yield, cause immunogenic reactions, decrease the shelf-life of the pharmaceutical product and impair the capacity of the antibody monomer to bind to its cognate antigen. A common strategy to tackle protein aggregation involves the identification of surface-exposed aggregation-prone regions (APR) for replacement through protein engineering. Others have shown that the insertion of *N*-glycosylation sequons on amino acids proximal to an aggregation-prone region can increase the physical stability of the protein by shielding the APR, thus preventing self-association of antibody monomers. We recently implemented this approach in the Fab region of full-size adalimumab and demonstrated that the thermodynamic stability of the Fab domain increases upon *N*-glycosite addition. Previous experimental data reported for this technique has lacked appropriate confirmation of glycan occupancy and structural characterization of the ensuing glycan profile. Here, we mutated previously identified candidate positions on the Fab domain of trastuzumab and employed tandem mass spectrometry to confirm attachment and obtain the *N*-glycosylation profile of the mutants. The trastuzumab glycomutants displayed a glycan profile with significantly higher structural heterogeneity compared to the WT antibody, which contains a single *N*-glycosylation site per heavy chain located in the CH2 domain of the Fc region. These findings suggest that Fab *N*-glycosites have higher accessibility to enzymes responsible for glycan maturation, shedding light into mAb glycobiology and potential implications in the application of this technique for the development of "biobetter" antibodies.

Introduction

The advent of therapeutic monoclonal antibodies (mAb) reshaped the pharmaceutical industry and has enabled a wide array of therapeutic avenues. Antibody therapeutics have dominated the market for the past two decades, featuring seven mAbs or mAb-based therapeutics in the top-10 list of best-selling drugs in 2018; and are now implemented in the treatment of an extensive range of pathologies, including oncological, inflammatory, cardiovascular, neurodegenerative and infectious diseases [1-3]. Moreover, mAbs comprise the largest class of molecules undergoing clinical development, thus it is forecasted that their market size will grow further as their clinical applications expand [3].

The coming of age of mAbs as therapeutics entailed substantial efforts aimed at addressing pitfalls of first-generation molecules, most notably the immunogenicity caused by their non-human origin [4]. Yet, despite the myriad advancements in antibody technology, protein aggregation is a recurring complication that continues to hinder their manufacture and clinical properties [2]. Furthermore, the physicochemical factors determining thermodynamic and colloidal stability remain poorly understood. Aggregation can have a negative impact on the therapeutic efficacy of monoclonal antibodies by compromising their biological function, increasing clearance rates, and triggering immunogenic reactions. Moreover, the shelf-life of the pharmaceutical product can be severely reduced by the accelerated formation of protein aggregates [5, 6].

Although it is believed that evolution has yielded improvements in the thermodynamic states of native antibodies relative to aggregated species, the manufacturing process and storage exposes recombinant therapeutic mAbs to a combination of "non-physiological" stress factors that hamper their physical and chemical stability [7, 8]. These factors include high protein concentrations, mechanical stress, exposure to air-water interfaces, and variations in pH, temperature, and ionic strength. To tackle this issue, numerous strategies have been developed and are the subject of intense exploration. These approaches can be broadly classified into two main categories: those that enhance the intrinsic stability of the protein to prevent aggregation throughout the manufacturing process [9-11], and those that improve the formulation of the final product by the optimization of pH, ionic strength and the incorporation of stabilizing agents [12, 13].

Excipients commonly used in protein stabilization include surfactants, sugars, amino acids, polymers, and other proteins. Recently, ionic liquids have emerged as promising additives in this context [14, 15]. Whilst highly valuable, formulation strategies are limited in their applicability in that the amount of excipient added is restricted by several factors, including toxicity and increases in viscosity and tonicity [14]. Furthermore, optimizing formulation conditions for particular proteins is challenging, given the lack of understanding of aggregation mechanisms and how excipients impact these processes. In light of these limitations, strategies to improve the intrinsic physical stability of mAbs become highly valuable as a way to avoid physical degradation in the manufacturing process and/or decrease the necessity to incorporate excipients in the final formulation. This has been particularly relevant in recent times due to the growing trend to formulate antibody therapeutics as sub-cutaneous (SC) syringes for self-injection, wherein high

protein concentrations are required to deliver effective doses in the limited injection volumes allowed by the SC route [2, 16].

Approaches to improve intrinsic aggregation resistance rely on rational modifications of the antibody structure. It is widely believed that surface-exposed hydrophobic regions in proteins can lead to self-association and initiate the formation of larger aggregates [5, 9]. Considering this, *in silico* methods have been developed to screen and identify aggregation-prone regions (APR). Exposed hydrophobic amino acids in APRs can then be replaced with more hydrophilic or charged residues through mutagenesis [7, 9, 10]. Pepinsky et al. introduced an innovative variation to this approach, wherein the mutations pursued inserted an *N*-glycosylation sequon (Asn-X-Ser/Thr) in the Fab region of an anti-LINGO antibody, enabling the attachment of an additional glycan on the antibody molecule – IgG1 molecules possess a conserved *N*-glycosylation motif in the Fc region [17]. The substantial increments (50-fold) in solubility obtained with two such mutants were attributed to the large hydrodynamic size and hydrophilic character of the glycan, preventing self-association through steric hindrance. Later, Courtois et al. employed an advanced computational tool, called Spatial Aggregation Propensity (SAP), that performs full antibody molecular dynamic simulations to identify APRs in bevacizumab; and proposed a panel of residues that could be mutated to insert a glycosylation site where the glycan can shield an aggregation prone region and deter protein-protein interactions [18]. In the latter study, significant enhancements were reported in accelerated stability studies with the glyco-engineered bevacizumab variants, reporting up to 3-fold improvements in monomer preservation. More recently, our group implemented several of the identified mutations in adalimumab and demonstrated improvements in thermodynamic stability, reflected by increments in the second melting temperature (T_m2).

Altogether, the experimental results obtained with the glycosylation site insertion approach have highlighted the potential of this technique to improve shelf-life and pharmacokinetic profiles of approved therapeutic antibodies and mAbs in preclinical development. Notwithstanding, crucial aspects neglected in the aforementioned studies have been the appropriate confirmation of glycan attachment; and more importantly, the structural analysis of the glycans attached to the engineered site. The latter is essential in the context of regulatory approval and in elucidating the molecular mechanisms that drive improvements in stability. In view of the foregoing, we sought to ascertain

differences in the glycosylation profiles of a wild-type antibody compared to its glycoengineered mutants.

Herein, we implemented several glycosite insertions in the Fab region of the blockbuster antibody trastuzumab and characterized the full glycan profile of the trastuzumab variants by glycan enzymatic release followed by LC-MS/MS analysis. In addition, we employed algorithms for prediction of successful glycan attachment to compare with experimental data in order to gain insight into structural features governing glycan transfer during translation. Furthermore, we evaluated the binding kinetics of the trastuzumab variants to its biological target (HER2) and to Fc receptors involved in eliciting effector functions to assess potential effects on therapeutic efficacy.

Materials and methods

Materials

Herceptin® was a generous donation from Genentech (San Francisco, California). The pVITRO-1-trastuzumab-IgG1/κ expression vector (containing trastuzumab heavy and light chain genes) was a generous gift from Andrew Beavil (Addgene plasmid # 61883). The gWiz expression vector was purchased from Genlantis (San Diego, USA). The primers utilized for mutagenesis and sequencing were acquired from Geneworks (Adelaide, Australia). The DpnI enzyme (R0176S) and the Phusion high-fidelity PCR kit (E0553S) were purchased from Genesearch (Gold Coast, Australia). Stellar^{TM} competent *E. coli* cells were purchased from Scientifix (Melbourne, Australia). Tryptone (LP0042B) was purchased from Thermo Fisher Scientific (Melbourne, Australia). Sodium chloride (S9888) and Kanamycin solution (K0254) were purchased from Sigma-Aldrich (Sydney, Australia). The miniprep (PLN70) and maxiprep (NA0310) kits were obtained from Sigma-Aldrich (Sydney, Australia).

Freestyle 293F cells were provided by Dr. Mario Torrado del Rey of Prof. Joel Mackay's research group, School of Life and Environmental Sciences, The University of Sydney. FreeStyle^{TM} 293 media (12338018), RPMI media (21870-076), OptiPRO^{TM} serum free media (SFM) (12309050) and other reagents used for tissue culture were purchased from Life Technologies (Melbourne, Australia). 25 kDa linear polyethylenimine (PEI) (23966-2) was purchased from BioScientific (Sydney, Australia). Disposable baffled tissue-culture flasks (CLS431405), glycine hydrochloride

(G2879), and HiTrap® Protein A HP affinity column (GE17-0403-01) were obtained from Sigma-Aldrich (Sydney, Australia). The Reprosil-Pur C18AQ (3µm, 120 A) was purchased from Dr. Maisch (Amerbuch, Germany).

PBS tablets (09-2051-100), 1 M Tris-HCl pH 9 (BIOSD814), and all chemicals employed for SDS-PAGE were acquired from Astral Scientific (Sydney, Australia). Precision Plus Protein™ Dual Color Molecular Weight Marker (1610374) was obtained from Bio-Rad Laboratories (Sydney, Australia). Trypsin (T6567), Chymotrypsin (1141847001) were purchased from Sigma-Aldrich (Sydney, Australia). C18 ZipTip® pipette tips (ZTC18S096) were obtained from Merck Millipore. PNGase F (P0708) was purchased from Genesearch (Gold Coast, Australia).

HEPES (54457), Tween 20 (P9416) and the HIS-tagged HER2 (SRP6405), $Fc_\gamma R2B$ (SRP6396), and $Fc_\gamma R3A$ (SRP6436) receptors were purchased from Sigma-Aldrich (Sydney, Australia). HIS-tagged $Fc_\gamma R1A$ (10256-H08H-5) were obtained from Life Technologies (Melbourne, Australia). The CM5 chips (29-1049-88), anti-HIS capture kit (28-9950-56), and amine coupling kit (BR-1000-50) were purchased from GE Healthcare (Sydney, Australia).

Cloning and mutation of Tmab WT and glycosylation mutants

A section of the pVITRO-1-trastuzumab-IgG1/κ expression vector containing the secretion signal and Tmab heavy chain gene, and another section containing the secretion signal and Tmab light kappa chain gene were amplified separately employing high fidelity PCR (Phusion High Fidelity PCR kit) with a 2-step PCR cycling method. These amplified sections were then inserted separately into the blank gWiz vector through restriction enzyme cloning to produce separate vectors for trastuzumab heavy chain (HC) and light chain (LC) expression. Mutagenesis was performed through high fidelity inverse PCR to obtain mutated trastuzumab expression vectors. Successful mutation was confirmed by sequencing. HEK-293F cells were co-transfected with heavy and light chain vectors for transient expression.

Expression and purification of Tmab WT and glycosylation mutants

The trastuzumab variants were expressed transiently in HEK-293F cells in suspension at 120 rpm, using Freestyle 293F media. The cell culture was maintained at 37 °C, 5% CO_2. Transfection was performed at a cell density of $1 \times 10^{+6}$ cells/mL (60 mL cultures). Vector DNA and PEI in OptiPRO SFM were added to the cells in a 2:1 PEI/DNA w/w ratio. Total DNA added per $1 \times 10^{+6}$ cells was

1 µg (1:1 w/w HC to LC ratio). Following 24 hours after transfection, the cultures were scaled up to 120 mL with Freestyle 293F media containing tryptone (0.5% w/v final concentration). At 48 hours post transfection the cultures were further scaled up to 240 mL with Freestyle 293F media containing tryptone (0.5% w/v final concentration). The cell culture supernatant was harvested by centrifugation at day 8 following transfection and subsequently clarified by filtration (0.22 µm).

Purification of the secreted antibody was performed employing a HiTrap® Protein A HP affinity column. PBS was used for the binding and washing steps. Elution of bound antibody was performed with 0.1 M glycine HCl pH 2.7 and the eluted fractions were immediately neutralized with 1 M Tris-HCl pH 9. Eluted fractions containing antibody were pooled and buffer exchanged to PBS using 50 kDa molecular weight cutoff (MWCO) centrifugal filters. Antibody concentrations were derived from absorbance readings at 280 nm using a molar extinction coefficient $\varepsilon = 2.25 \times 10^{+6} \, M^{-1} \, cm^{-1}$.

LC-MS/MS analysis of Tmab variants

Glycopeptide analysis

Tmab WT, Herceptin and Tmab mutants were run on a reducing 10% SDS-PAGE. The HC bands (Tmab WT, Herceptin and all mutants except Q160N) and the LC band (Q160N) were excised from the gel and diced. The proteins in the gel were reduced by incubation with 10 mM DTT at 56 °C for 45 minutes and then alkylated with 55 mM iodoacetamide (IAA) in 100 mM NH_4HCO_3 at 25 °C for 30 minutes. The alkylated proteins were then digested with trypsin (1 µg per 50 µg of protein) in 50 mM NH_4HCO_3 (pH 6.8) at 37 °C overnight. The tryptic peptides were subsequently treated with chymotrypsin in 100 mM Tris-HCl and 10 mM $CaCl_2$ (pH 7.8) at 25 °C overnight. C18 ZipTips were used for desalting the tryptic/chymotryptic peptides, using 80% (v/v) acetonitrile in 0.1% TFA for elution. Solvent was removed by vacuum centrifugation and the peptides were dissolved in 0.1% formic acid for LC-MS/MS analysis.

Free glycan analysis

The glycans were released from the antibody and analysed through tandem mass spectrometry as described before [19]. Briefly, antibody aliquots were reduced and alkylated using 1 M DTT and 500 mM IAA, respectively. Subsequently, 10 µg of protein was blotted on a PVDF membrane previously wetted with ethanol and left to dry overnight. The membrane was then washed with

methanol, followed by a wash with water to remove salts. The membrane was then stained briefly with Direct Blue 71 solution (1 part 0.1% direct blue 71 stain (w/v) in MilliQ water and 12 parts wash solution (40% ethanol (v/v), 10% acetic acid (v/v)) to visualize the spots. The spots were then briefly destained using wash solution and washed with water. The spots were cut from the membrane and transferred to 96-well plates and blocked with 1% (w/v) polyvinylpyrrolidone 40 (PVP40). The spots were washed three times with water and placed in new wells containing water. PNGase F was subsequently added to the wells (1 unit per 5 ug of protein) and the plate was incubated overnight at 37 °C. The resulting solution containing the released glycans was collected and transferred to a low-protein binding tube. 10 µL of 100 mM ammonium acetate pH 5 was added and incubation was done for 1 hour at 25 °C to remove glycosylamines from the reducing end. The samples were dried by vacuum centrifugation followed by reduction with 1 M NaBH$_4$ in 50 mM KOH for 3 hours at 50 °C. The reaction was neutralized with 1 µL glacial acetic acid.

An AG 50W X8 cation exchange resin loaded onto a ZipTip C18 tip for packing and was used for desalting the reduced glycans. Prior to sample loading, the columns were washed three times with 50 µL of 1 M HCl followed by three washes with 50 µL of methanol. The columns were then transferred to new collection tubes and washed three times with 50 µL of water. The samples were loaded onto the column and eluted with water. The eluted glycans were dried with a SpeedVac concentrator and redissolved in 100 µL methanol to remove residual methyl borate and dried once more. Methanol redissolution was performed three times.

Finally, a carbon cleanup step was performed with a carbon solid-phase extraction (SPE) slurry packed into a TopTip. The carbon SPE columns were initially washed three times with 50 µL of acetonitrile in 0.1% (v/v) TFA. The columns were then washed three times with 50 µL of 0.1% (v/v) TFA in water. The desalted reduced glycans were then dissolved in 0.1% (v/v) TFA in water and loaded onto the column. The columns were washed three times with 50 µL of 0.1% (v/v) TFA in water and the glycans were eluted with 50% (v/v) acetonitrile in 0.1% (v/v) TFA. The glycans were dried in a SpeedVac concentrator and dissolved in 10 mM NH$_4$HCO$_3$ for LC-MS/MS analysis.

Mass Spectrometry

Glycopeptide analysis was done using an in-house packed 20 cm x 75 µm Reprosil-Pur C18AQ (3 µm, 120 A) coupled to an Orbitrap Fusion MS (Thermo Scientific) was used for LC-MS/MS.

HPLC solvent A was 0.1% (v/v) formic acid and solvent B was 80% (v/v) acetonitrile in 0.1% formic acid. The peptides were separated running a 90-minute 0-40% solvent B gradient at 300 nL/min at 60 °C. The Orbitrap Fusion mass spectrometer was used in positive mode, with source voltage = 2.3 kV, S lens RF level = 68%, and a capillary temperature of 275 °C. Initial MS scan was acquired from 350-2000 m/z at a resolution of 60000 at 400 m/z (MS AGC = 6 x 105). Following MS1, data-dependent higher-energy collisional dissociation (HCD) was used at top speed. HCD parameters were set up as: activation time = 0.1 ms, maximum injection time = 200 ms, dynamic exclusion = enabled with repeat count 1, resolution = 30000, normalized energy = 40, exclusion duration = 20 s, default charge state = 2 and MSn AGC = 2.0 x 105. The two most intense precursors were re-isolated and subjected to collision induced fragmentation (CID). CID parameters were: resolution = 30000 in orbitrap, activation time = 10 ms, dynamic exclusion = enabled with repeat count 1, normalized energy = 35, exclusion duration = 20 s, default charge state = 2, MSn AGC = 5.0 x 104.

MS analysis of the free glycans was done on a VelosPro (Thermo) mass spectrometer with an Agilent 1260 HPLC using a Hypercarb porous graphitised carbon capillary column (3 µm particle size, 100 mm x 180 µm, pore size 250 Å, Thermo). The glycans were separated using a 60 min 5-45% (v/v) solvent B (80% (v/v) acetonitrile in 10mM NH4HCO3) gradient on a flow rate of 2 µl/min. Column was washed with 100% solvent B and equilibrated with solvent A (10mM ammonium bicarbonate) after each run. ESI–MS was performed in negative ion mode at a resolution of 30000 with a mass range of m/z 500–2000. Transfer capillary temperature was at 275 °C and the capillary voltage was at 3 kV. MS2 of the top 9 most intense ions was done using collusion induced dissociation (CID) at a normalized collision energy of 35 in the ion trap with an activation time of 10 ms.

Data Analysis

The analysis of the peptide and glycopeptide data was done using Byonic (Protein Metrics Inc.) software. Peptide spectrum matches (PSM) were obtained through a search against the FASTA files of the wild-type trastuzumab and its variants. CID spectra annotation was automated using Byonic and the spectral matches were inspected manually. The Byonic search was conducted with a semi specific digestion specificity allowing two missed cleavages. The fragment mass tolerance was 0.05 Dalton (Da). A maximum of two common modifications (Asparagine and glutamine

deamidation +0.984016 Da, Cysteine carbamidomethylation +57.021464) and one rare (Methionine oxidation +15.994915) modifications were enabled.

Free glycans were analysed manually using Thermo Xcalibur Qual Browser version 3.0.63. The theoretical monosaccharide compositions were determined using the monoisotopic masses of the detected ions using GlycoMod (http://web.expasy.org/glycomod/) with mass tolerance of ±0.5 Da. The glycan structures were manually assigned using PGC retention time and MS2 diagnostic fragment ion information. The percentage relative quantitation of each glycan structure per Tmab variant was calculated using the extracted ion chromatogram (EIC) areas upon peak smoothing using Gaussian Algorithm (15 points). The area values for the glycan structures were summed and normalised to 100% and each glycan peak was expressed as percentage of the total.

Binding affinity to HER2 and Fc receptors

The wild type trastuzumab references (Tmab WT and Herceptin) and the hyperglycosylated mutants were tested for their capacity to bind their molecular target (HER2) and Fc receptors (FcγR1A, FcγR2B, and FcγR3A). A Biacore T200 instrument (GE Healthcare, Australia) was used to obtain the binding kinetic constants through surface-plasmon resonance (SPR) using single-cycle kinetic analysis.

For HER2 binding experiments, a CM5 sensor chip was functionalized with an anti-HIS antibody through amine coupling chemistry. The HIS-tagged HER2 receptor (4 nM) was then bound to the anti-HIS at 5 µL/min flow rate for 5 minutes. The trastuzumab variants were assayed in single-cycle kinetic titrations in 2-fold serial dilutions spanning 0.5 – 8 nM using HBS-T running buffer (10 mM HEPES, 150 mM NaCl, 0.05% (v/v) Tween 20, pH 7.4). Analyte runs were performed at 20 µL/min for 2 min with 60 min dissociation times. All experiments were conducted in duplicate.

HIS-tagged Fc receptors were bound to the anti-HIS antibody on the CM5 sensor following the same procedure as for HER2. The analyte runs were performed as described above for HER2, with the exception of a 30 min dissociation time and that analyte concentrations ranged from 2.5 – 40 nM for FcγR1A, and from 25 – 400 nM for FcγR2B and FcγR3A.

The sensorgrams were fitted to a Langmuir 1:1 binding model to derive the binding kinetic constants (K_a, K_d, and K_D). The fit was deemed acceptable if χ^2 was lower than 5% of the maximum response level (R_{max}).

Results

Engineered glycosylation sites

Table 1 lists the surface exposed amino acid residues that were mutated herein in trastuzumab with the respective proposed mechanism to increase physical stability. One residue (L115) lies on the variable region of the heavy chain (V_H), five (A121, L177, Q178, L182 and T198) on the constant heavy (C_H1) and one on the constant region of the light kappa chain (C_k). The amino acid substitutions L115N, Q160N, Q178N and L182N were derived from previous studies by Courtois et al. that identified sites on the tertiary structure of the Fab region of IgG1 antibodies where the incorporation of a glycan could shield hydrophobic surface-exposed regions. These aggregation-prone regions (APRs), or aggregation hotspots, were mapped with the Spatial Aggregation Propensity (SAP) technology, wherein individual amino acids are assigned an aggregation propensity value based on side chain hydrophobicity, dynamically-exposed solvent accessible surface area (SASA), and the hydrophobic contributions of adjacent amino acids within a given radius [18]. For more details on this technique see [20].

Table 1. Surface exposed amino acid (aa) residues identified in Tmab Fab region for glycosylation sequon addition.

aa Substitution (Position)	Region	Proposed function
L115N	V_H	Mask APR by introducing glycosylation site [18].
A121N	C_H1	Improve solubility by introducing glycosylation site [17].
L177N		Mutate aa with high spatial-aggregation propensity and introduce glycosylation site [18, 21].
Q178N		Sterically hinder self-association by introducing glycosylation site and increase solubility [18, 17].
L182N		Mask APR by introducing glycosylation site [18].
T198N		Improve solubility and sterically hinder self-association by introducing glycosylation site [17].
Q160N	C_k	Mask APR by introducing glycosylation site [18].

Aside from T198, all other aforementioned substitutions were engineered to shield the APR generated by the high SAP residue L177. Mutations L115N and Q160N have previously

demonstrated to improve resistance to aggregation through accelerated stability studies in bevacizumab – a therapeutic monoclonal antibody with a pronounced tendency to aggregate through self-association [18]. Q178N and L182N were identified in the same study as positions in the vicinity of L177N that can be mutated to generate an *N*-glycosylation sequon (Asn-X-Ser/Thr) through a single amino acid substitution, however these were excluded from experimental tests in bevacizumab due to Q178 having reduced SASA and L182 not being oriented on the same face as the APR. In this work, L177 was also mutated to substitute the high SAP residue with an asparagine within a consensus motif for glycan addition. The latter mutation was recently tested in an adalimumab Fab expressed in *Pichia pastoris*, conferring improved resistance to aggregation and proteinase K digestion relative to wild-type adalimumab Fab.

A121N, Q178N and T198N were identified by Pepinsky et al. [17] as glycosite additions that could prevent self-association through steric hindrance in an anti-LINGO antibody with reduced solubility. In this case, all three modifications granted a dramatic improvement in solubility.

Glycan occupancy prediction

To assess the validity of employing existing algorithms for the prediction of glycan attachment, the primary sequence of the trastuzumab variants was subjected to an in-silico analysis using two available *N*-glycosylation prediction servers. Both servers, NetNGlyc 1.0 and NGlycPred, assign a 0-1 score, wherein values greater than 0.5 indicate a predicted glycosylated asparagine residue. Figure 1 depicts the location and surface exposure of the amino acid substitutions and the high SAP L177. Table 2 reports the predicted potential for glycan occupancy obtained with the NetNGlyc 1.0 server, which relies on adjacent primary sequence to assign a probability for N-glycan transfer during protein translation. This server has been employed successfully in various studies to predict glycosylation in identified Asn-X-Ser/Thr motifs within primary amino acid sequences [22-24]. NetNGlyc predicted all residues, except Q178N, to undergo glycosylation. Further, an additional algorithm (NGlycPred) that incorporates structural features (e.g., adjacent secondary structure, surface accessibility, local contact order) into the analysis was utilised for prediction based on fundamentally distinct inputs [25]. NGlycPred assigned a negative value (<0.5) to L115N and Q178N. Herein, all listed mutations were implemented and expressed in HEK-293F human embryonic kidney cells. The attached glycans were subsequently released by

PNGase F digestion and analysed by capillary/nanoLC-ESI-MS/MS to confirm glycan attachment and obtain structural features of the oligosaccharides.
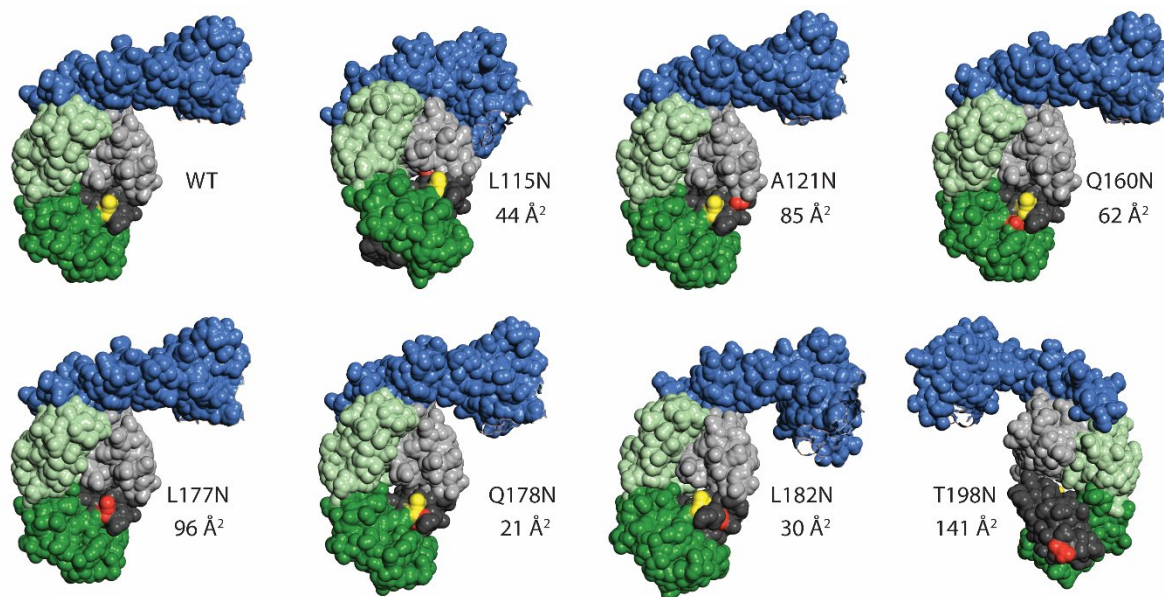
Figure 1. Location of the mutated amino acid residues for glycosite addition. Crystal structure of the HER2 extracellular domain complexed with the Fab of trastuzumab (1N8Z) visualised in PyMOL. The mutated amino acids are highlighted in red. The high SAP L177 is displayed in yellow. VH and CH1 domains are shown in light grey and dark grey respectively. VL and CL domains are shown in light green and dark green respectively. The HER2 ECD is displayed in blue.

Table 2. Estimated glycosylation potential and solvent accessible surface area (SASA) of the targeted N-glycan sequons.

aa Substitution (Position)	Region	Sequon	NetNGlyc	NGlycPred	SASA (Å^2)
Q160N	C_K	160 NESV	0.647	0.834	62.478
L115N	V_H	115 NVTV	0.679	0.462	43.709
A121N	C_H1	121 NSTK	0.547	0.686	85.338
L177N		177 NQSS	0.537	1.000	96.039
Q178N	C_H1	178 NSSG	0	0.157	20.5
L182N		182 NYSL	0.568	0.999	30.123
T198N		198 NQTY	0.592	1.000	141.149

Glycan attachment confirmation

Glycan attachment on the mutated sites was analysed through electrophoretic mobility shifts in SDS-PAGE and MS/MS glycan profile analysis. Figure 2 shows a reducing SDS-PAGE of the mutants and the in-house wild-type trastuzumab (Tmab WT) produced in the same cell line (HEK-293F) under identical expression conditions. The heavy chain (HC) band (~50 kDa) mobilities of the L115N, A121N, L177N, Q178N, L182N, and T198N mutants were retarded relative to that of WT, commercial Herceptin (Herc) and Q160N (mutated on the light chain), indicating higher levels of glycosylation on these HC mutants.

Interestingly, no matches were found for glycopeptides containing the L177N, Q178N and L182N residues. Conversely, peptides containing the non-mutated L177, Q178 and L182 amino acids were detected in WT and Tmab variants with mutations outside the region (Figures S31-S33). Assuming no missed cleavages, the tryptic/chymotryptic peptide containing L177N, Q178N or L182N has a mass of 2206.11 Da (Table 3). It is likely that glycan attachment on the side chain hindered enzymatic digestion, thus producing peptides with missed cleavages and m/z values too large for detection – glycan attachment increases the m/z further. It has also been suggested that

large glycopeptides can be missed in the workflow utilized for this analysis during peptide extraction following SDS-PAGE, as the large size could prevent them from extraction due to gel shrinkage caused by the organic solvents employed [19]. Similarly, glycan attachment in the vicinity of the cleavage sites has been shown to prevent enzymatic activity of the serine protease proteinase K in the L177N mutant in adalimumab Fab [21]. Still, successful glycosylation of L177N, Q178N, and L182N was confirmed by mobility shifts in SDS-PAGE and an increased heterogeneity observed in the released glycan profile compared to WT as discussed in the next section.
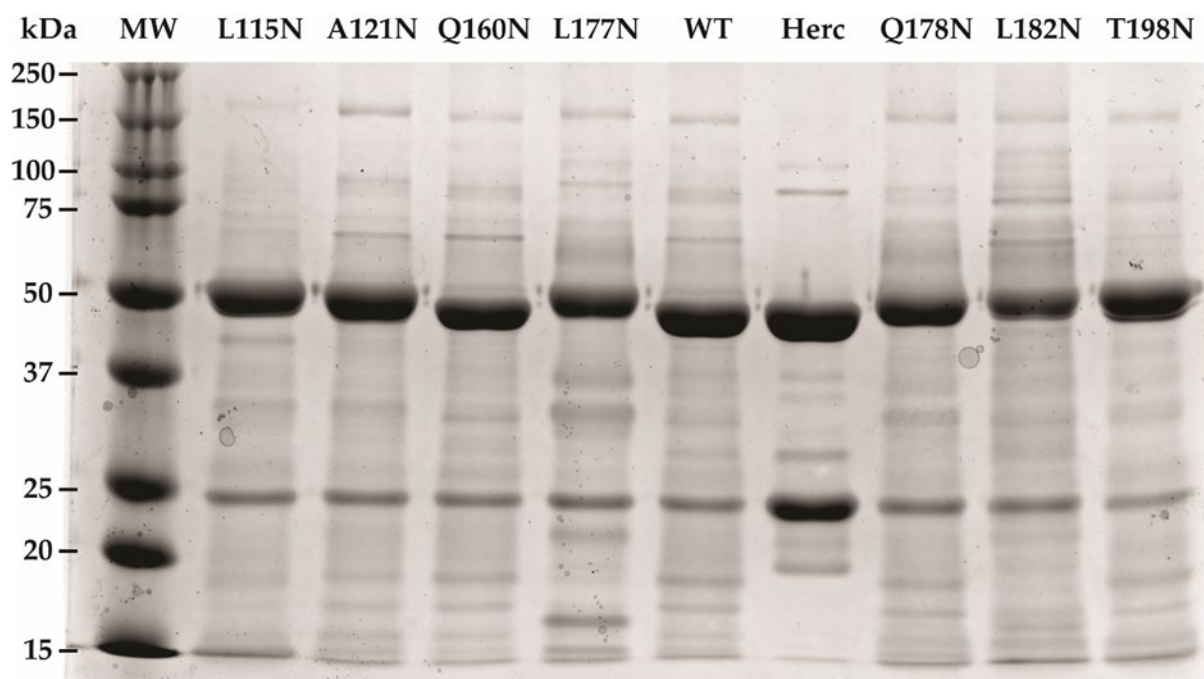
Figure 2. Reducing SDS-PAGE of the trastuzumab mutants for confirmation of glycan attachment. Commercial Herceptin (Herc) and the wild-type (non-mutated) trastuzumab produced in-house were run together with the mutants to compare electrophoretic mobility shifts in the ~50 kDa band corresponding to the heavy chain.

Despite the positive prediction from the algorithms (NGlycPred score of 0.834 (Q160N), Table 2), the light chain (LC) band (~25 kDa) of Q160N showed no apparent mobility shift compared to WT LC region, suggesting a lack of glycosylation on the mutated asparagine residue. Although the glycan profiling of the Q160N showed very similar structures to WT Tmab, the glycan release was performed on the whole protein but not on the light chain only and therefore provided an

overall glycoprofile of the protein (figure 3, table 4). While the visual similarity of the light chain gel mobilities of WT Tmab and Q160N and the information of the overall glycan profile of Q160N do not entirely exclude the possibility of glycan occupancy on the 160N, the MS analysis of the Q160N light chain peptide clearly showed the presence of a non-glycosylated LC region. To confirm the lack of glycan attachment, the Q160N mutant was subjected to trypsin and chymotrypsin digestion to generate the corresponding peptides for nanoLC-ESI-MS/MS analysis. Spectral matches were found for non-glycosylated peptides encompassing the Q160N residue, thus confirming successful Q to N conversion and reaffirming the lack of glycan attachment (Figure S34). This apparent lack of glycan attachment was also observed in the corresponding Q160N mutant when expressed in adalimumab (Q161N) (data to be published).

Table 3. Peptide sequences after trypsin/chymotrypsin digestion allowing one missed cleavage (MC) site

Mass (Da)	Position	MC	Sequence
4000.01	162-201	1	NSGALTSGVHTFPAVLQSSGLYSLSSVVTVPSSSLGTQTY
3248.63	153-183	1	FPEPVTVSWNSGALTSGVHTFPAVLQSSGLY
3148.59	184-213	1	SLSSVVTVPSSSLGTQTYIC NVNHKPSNTK
2206.11	162-183	0	NSGALTSGVHTFPAVLQSSG LY
1812.92	184-201	0	SLSSVVTVPSSSLGTQTY

Glycan profile analysis

To analyse the global glycan profile of the trastuzumab variants, the proteins were immobilized on PVDF membranes and treated with PNGase F to release glycans attached to both the conserved WT N297 and the added glycosylation site. The released oligosaccharides were run on capillary LC-ESI-MS/MS, wherein a PGC column was used for separation of distinct glycoforms and MS/MS analysis (CID fragmentation) was performed to elucidate glycan structure. Figure 3 shows the annotated full MS spectra of Tmab WT, Herceptin, Q160N, and L177N displaying the identified glycan structures found on each variant. The global glycan profile reflects contrasting differences in glycoform heterogeneity and the relative abundance of the glycans found on the glycomutants. MS1 and MS2 (where possible) spectra of all the glycomutants can be found in

supplementary materials. The released glycan profiles displayed in figure 3 and figures S1-S9 come from both the conserved Fc N-glycosylation sequon and the added N-glycosylation site. Table 4 lists the glycan structures found on all Tmab variants through this MS methodology; and Figure 4 reports the glycan relative abundances on specific Tmab variants determined by quantifying the area under the curve (AUC) of the extracted ion chromatograms.
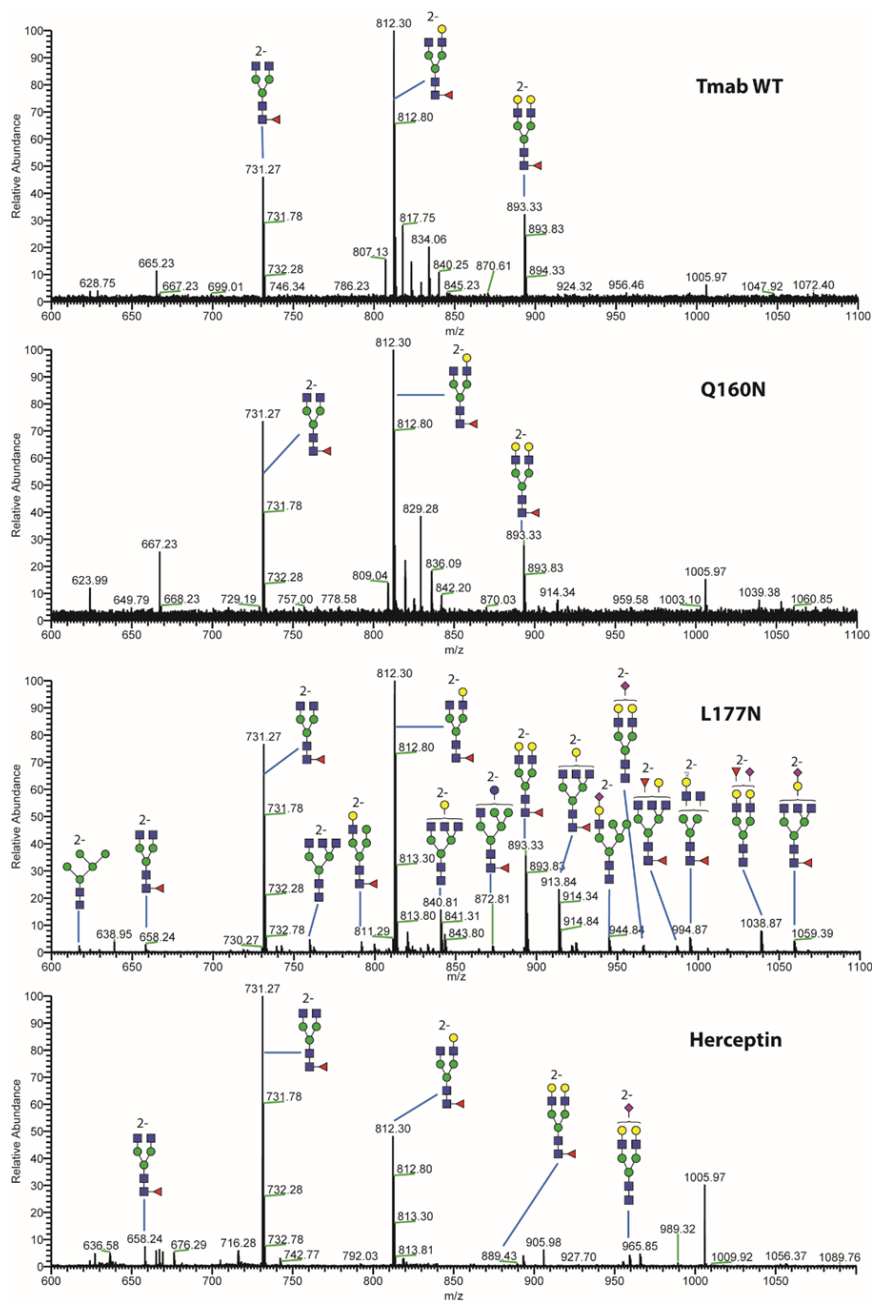
Figure 3. Full MS spectra of N-glycans released from Tmab WT, Q160N, L177N and Herceptin contrasting the heterogeneity found on the mutant.

Glycan microheterogeneity at the conserved N297 in Tmab WT is similar to that reported in previous analysis of commercial Herceptin and other monoclonal therapeutic antibodies, where complex G0F, G1F and G2F glycoforms (Figure 4 and table 4) are predominant [26, 27]. Minor species (i.e., Man5, G0 and G2S1) were detected in commercial Herceptin but not in Tmab WT (Figure 3). An important difference between commercial Herceptin and Tmab WT lies in the relative abundance of the three main glycoforms (G0F, G1F and G2F), where the originator contained the pattern G0F>G1F>G2F (60%, 31%, and 2%) and Tmab WT possessed G1F>G0F>G2F (26%, 57%, and 17%) (Figure 4). Glycosylation differences are expected between these two samples, as the originator is produced in CHO cells and our in-house Tmab in HEK-293F. Moreover, sialic acid-containing species (17a table 4) were present in the originator and not detected in Tmab WT. This observation is consistent with previous studies reporting higher sialylation of N-glycans in recombinant proteins expressed in CHO when compared to HEK cells [28].

The G1F>G0F>G2F distribution observed in Tmab WT was conserved in all the glycomutants (Figure 4), although the abundance of G1F seemed to decrease in comparison to that observed for Tmab WT. Figure 5 shows the relative abundances considering only the main complex glycoforms found on the Fc domain (G0F, G1F, and G2F). The decrease in G1F and concomitant increase in G0F was more pronounced in the Q178N mutant where G1F (40.47%) was only slightly less abundant than G0F (42.98%) (Figure 5).
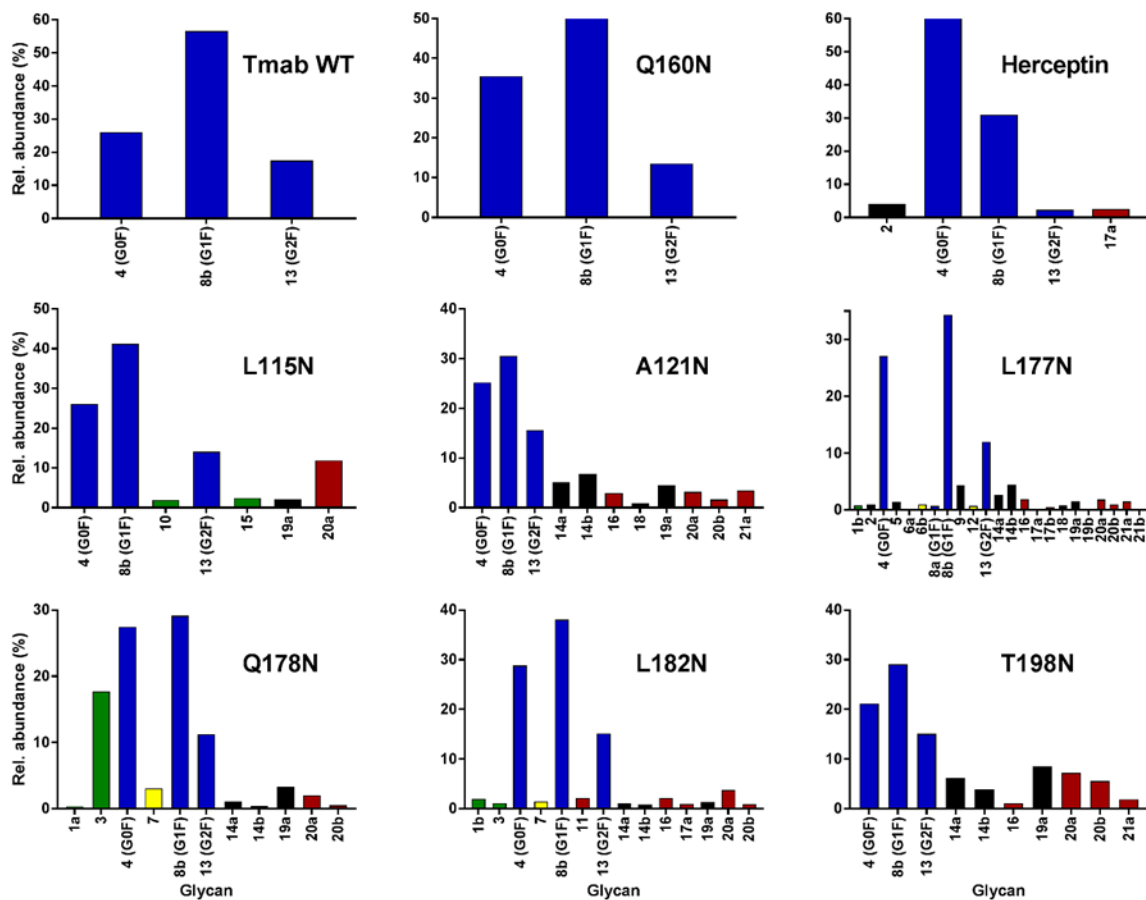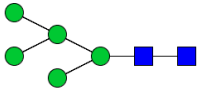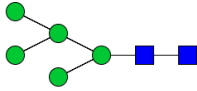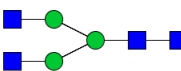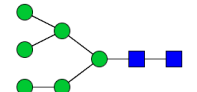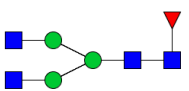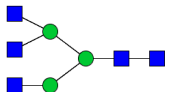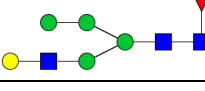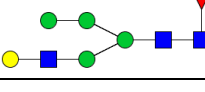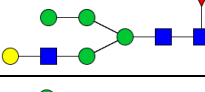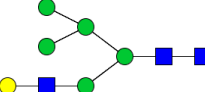
Figure 4. Relative abundances of the glycan found on each specific mutant. Highlighted in blue are G0F, G1F and G2F which were also found on the WT tmab. High mannose glycans are displayed in greed, hybrid glycans in yellow and sialic acid containing glycans in red.
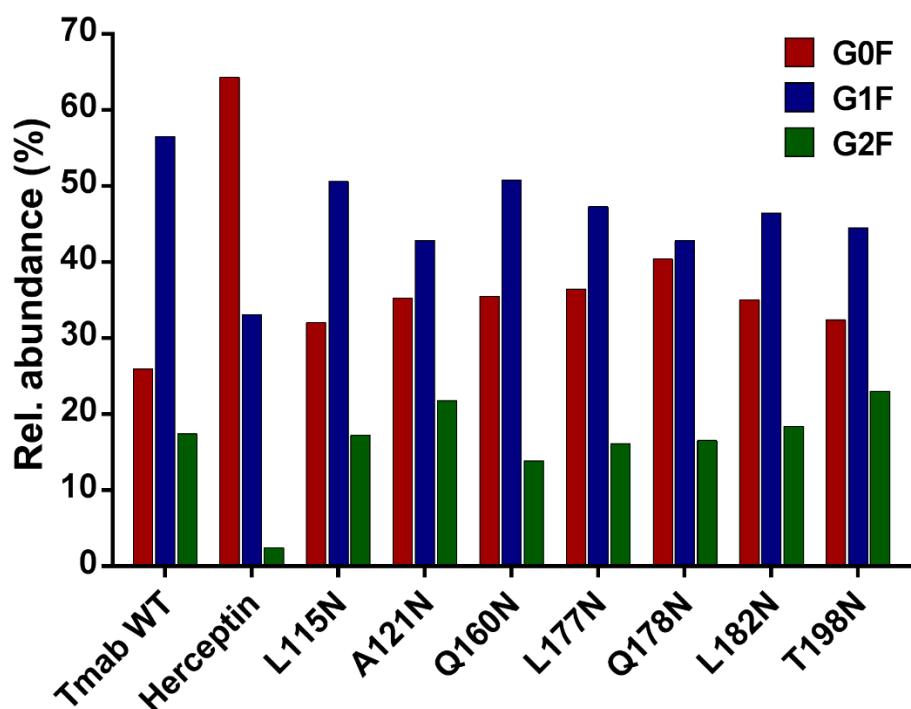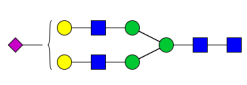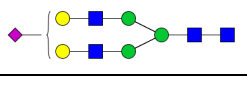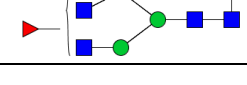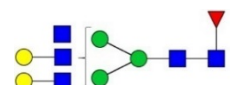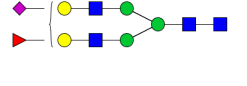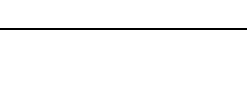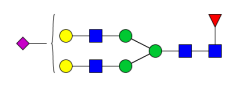
Figure 5. Relative abundances of the main glycoforms found on all Tmab variants.

Remarkably, a much wider heterogeneity of glycan structures were detected on most Tmab variants relative to wild type trastuzumab (Tmab WT and Herceptin) (Figures 3 and 4). The fact that G0F, G1F, and G2F were still the most abundant structures in all samples indicates that the increased variety of glycans come from the Fab region. The wider array of structures included high mannose, hybrid, and complex biantennary, triantennary and tetrantennary glycans with varied degrees of galactosylation and sialylation (Table 4). Variants L177N and L182N displayed the most varied sets of glycoforms with 16 and 12 different structures detected, respectively. Importantly, sialic acid-containing glycans were particularly abundant in L115N, L182N, and T198N. Q178N had a significant presence of high mannose glycans.

Table 4. Full list of glycans found on all mutants

# Structure	Type	Composition	Structure	[M-2H]²⁻	Mutants containing the glycan
1a	high mannose	HexNAc(2)Hex(5)		617.22	Q178N
1b	high mannose	HexNAc(2)Hex(5)		617.22	L177N Q178N L182N
2a (G0)	complex	HexNAc(4)Hex(3)		658.24	L177N Herceptin
2b (G0)	complex	HexNAc(4)Hex(3)		658.24	L177N
3	high mannose	HexNAc(2)Hex(6)		698.25	Q178N L182N
4 (G0F)	complex	HexNAc(4)Hex(3)Fuc(1)		731.27	All Tmab variants
5	complex	HexNAc(5)Hex(3)		759.78	L177N
6a	hybrid	HexNAc(3)Hex(4)Man(2)Fuc(1)		791.79	L177N
6b	hybrid	HexNAc(3)Hex(4)Man(2)Fuc(1)		791.79	L177N
6c	hybrid	HexNAc(3)Hex(4)Man(2)Fuc(1)		791.79	L177N
7	hybrid	HexNAc(3)Hex(5)Man(1)		799.79	Q178N L182N

8a (G1F)	complex	HexNAc(4)Hex(3)Man(1) Fuc(1)		812.3	L177N
8b (G1F)	complex	HexNAc(4)Hex(3)Man(1) Fuc(1)		812.3	All Tmab variants
9	complex	HexNAc(5)Hex(3)Man(1)		840.81	L177N
10	high mannose	HexNAc(2)Hex(8)		860.3	L115N
11	hybrid	HexNAc(3)Hex(4)Man(1) NeuAc(1)		864.31	L182N
12	hybrid	HexNAc(3)Hex(5)Man(1) Fuc(1)		872.81	L177N
13 (G2F)	complex	HexNAc(4)Hex(3)Man(2) Fuc(1)		893.33	All Tmab variants
14a	complex	HexNAc(5)Hex(3)Man(1) Fuc(1)		913.84	A121N L177N Q178N L182N T198N
14b	complex	HexNAc(5)Hex(3)Man(1) Fuc(1)		913.84	A121N L177N Q178N L182N T198N
15	high mannose	HexNAc(2)Hex(9)		941.33	L115N
16	hybrid	HexNAc(3)Hex(5)Man(1) NeuAc(1)		944.84	A121N L177N L182N T198N

17a	complex	HexNAc(4)Hex(3)Man(2) NeuAc(1)		965.84	L177N L182N
17b	complex	HexNAc(4)Hex(3)Man(2) NeuAc(1)		965.84	L177N
18	complex	HexNAc(5)Hex(3)Man(1) Fuc(2)		986.87	A121N L177N
19a	complex	HexNAc(5)Hex(3)Man(2) Fuc(1)		994.87	L115N A121N L177N Q178N L182N T198N
19b	complex	HexNAc(5)Hex(3)Man(2) Fuc(1)		994.87	L177N
20a	complex	HexNAc(4)Hex(3)Man(2) Fuc(1)NeuAc(1)		1038.87	L115N A121N L177N Q178N L182N T198N
20b	complex	HexNAc(4)Hex(3)Man(2) NeuAc(1)		1038.87	A121N L177N Q178N L182N T198N
21a	complex	HexNAc(5)Hex(3)Man(1) NeuAc(1)		1059.39	A121N L177N T198N
21b	complex	HexNAc(5)Hex(3)Man(1) NeuAc(1)		1059.39	L177N
21c	complex	HexNAc(5)Hex(3)Man(1) NeuAc(1)		1059.39	L177N

Binding affinity to HER2 and FcγR1A

To assess potential alterations in biological activity caused by the structural modifications of glycan addition, we tested the binding affinity of the Tmab variants on biologically relevant receptors in vitro. Surface-plasmon resonance (SPR) single-cycle kinetic assays were performed to determine binding kinetic constants of the Tmab variants to their molecular target HER2, and to Fc receptors FcγR1A, FcγR2B, and FcγR3A (Table 5 and Table 6). Sensorgrams displaying typical curvatures with satisfactory curve fitting were obtained across all receptors tested with the exception of mutants A121N, Q178N, L182N, and T198N on FcγR2B, thus the corresponding binding kinetic constants to this receptor were not determined (Figures S35-S38). Chi-square values and residuals were inspected to validate curve fitting.

Table 5. Binding kinetic constants of the Tmab variants to HER2 and FcγR1A

	HER2			FcγR1A		
	K_a	K_d	K_D	K_a	K_d	K_D
	$(x\ 10^{+6})\ M^{-1}.s^{-1}$	$(x\ 10^{-5})\ s^{-1}$	pM	$(x\ 10^{+5})\ M^{-1}.s^{-1}$	$(x\ 10^{-4})\ s^{-1}$	nM
Tmab WT	2.50 ± 0.03	3.03 ± 0.72	**12.11 ± 2.72**	2.11 ± 0.03	10.64 ± 0.56	**5.05 ± 0.33**
L115 > N	3.82 ± 3.80	18.16 ± 9.14	**47.56 ± 25.89**	1.79 ± 0.20	4.20 ± 0.06	**2.34 ± 0.26**
A121 > N	4.40 ± 1.71	23.84 ± 4.35	**54.24 ± 10.24**	3.83 ± 0.36	8.77 ± 1.14	**2.29 ± 0.08**
Q160 > N	0.83 ± 0.02	2.78 ± 1.26	**33.53 ± 15.86**	2.55 ± 0.02	6.62 ± 0.11	**2.59 ± 0.02**
L177 > N	1.84 ± 0.13	6.32 ± 0.08	**34.28 ± 2.01**	5.01 ± 0.18	15.04 ± 1.27	**3.00 ± 0.15**
Q178 > N	1.35 ± 0.27	4.29 ± 0.67	**31.88 ± 2.11**	7.38 ± 0.11	9.23 ± 0.30	**1.25 ± 0.02**
L182 > N	1.1 [*]	3.2 [*]	**29.1 [*]**	3.67 ± 0.55	12.37 ± 2.64	**3.37 ± 0.22**
T198 > N	6.11 ± 1.17	50.97 ± 3.23	**83.44 ± 77.77**	4.71 ± 0.02	8.09 ± 0.10	**1.72 ± 0.03**

Table 6. Binding kinetic constants of the Tmab variants to FcγR2B and FcγR3A

	FcγR2B			FcγR3A		
	K_a $(\times 10^{+4})$ $M^{-1}.s^{-1}$	K_d $(\times 10^{-4})$ s-1	K_D nM	K_a $(\times 10^{+4})$ $M^{-1}.s^{-1}$	K_d $(\times 10^{-4})$ s^{-1}	K_D nM
PBS-Herc	3.05 ± 0.04	1.99 ± 0.13	**6.55 ± 0.35**	10.51 ± 0.29	1.90 ± 0.54	**1.81 ± 0.47**
Tmab WT	5.76 ± 1.01	4.75 ± 0.41	**8.25 ± 0.69**	11.41 ± 2.06	1.29 ± 0.64	**1.13 ± 0.32**
L115 > N	0.65 ± 0.26	0.78 ± 0.44	**11.92 ± 3.57**	3.35 ± 0.85	2.74 ± 0.23	**8.17 ± 1.60**
T117 > N		ND			ND	
A121 > N		ND		2.78 ± 1.99	1.95 ± 0.43	**7.01 ± 3.84**
Q160 > N	4.01 ± 0.32	1.85 ± 0.27	**4.62 ± 0.32**	21.17 ± 4.95	8.01 ± 2.95	**3.78 ± 0.46**
L177 > N	2.95 ± 1.82	6.88 ± 4.26	**23.28 ± 44.62**	2.83 ± 0.22	3.02 ± 0.05	**10.67 ± 1.03**
Q178 > N		ND		1.95 ± 0.20	0.98 ± 0.20	**5.04 ± 1.47**
L182 > N		ND		3.12 ± 0.25	1.95 ± 0.20	**6.24 ± 1.30**
T198 > N		ND		2.25 ± 0.14	0.86 ± 0.15	**3.81 ± 0.41**

SPR-derived binding kinetic parameters of the mutants on immobilized HER2 displayed a modest decrease in the binding affinity constant (KD) compared to wild-type trastuzumab (Table 5). KD values for the Tmab variants ranged from 29.10 – 83.44 pM compared to 12.11 ± 2.72 pM for Tmab WT, which represents a 2.4 – 6.9-fold reduction in binding affinity. Most variants displayed a decrease in binding rate constant (Ka) and an increase in dissociation rate constant (Kd), with the exception of A121N and T198N that had higher Ka values, yet they also possessed the highest increase in Kd constants. Thus, the A121N and T198N mutations displayed the lowest binding affinity constants to HER2.

Conversely, binding affinity to captured FcγR1A was improved for all mutants relative to both Tmab WT and Herceptin, exhibiting KD values 1.5 – 4 times lower than Tmab WT. Mutants Q178N and T198N recorded the highest binding affinity to FcγR1A, with KD constants of 1.25 and 1.72 nM respectively. SPR assays with immobilized FcγR2B yielded curves with lower similarity to the wild-type references. Dissociation times for mutants A121N and Q178N were too long to obtain reliable kinetic binding affinity parameters. L182N showed a drastic decrease in binding affinity. Mutants L115N, Q160N, and L177N exhibited modest increases in binding affinity constants to FcγR2B. Binding affinity to FcγR3A was reduced across all mutants, displaying 3.35 – 9.44-fold increases in KD values.

Discussion

The insertion of novel N-glycosylation sites on the primary structure of IgG1 molecules is a highly promising approach to enhance the physicochemical properties of therapeutic proteins, having previously demonstrated important enhancements in solubility and physical stability in bevacizumab, adalimumab, and the Li33 anti-LINGO antibody. However, implementation of this approach in clinical development could be challenging due to the concomitant increase in structural heterogeneity. This is especially relevant when considering mAbs whose therapeutic efficacy relies, at least partially, on eliciting effector functions; given that the technique entails the incorporation of a relatively large molecule that should not alter detrimentally the binding affinity towards the various receptors involved in its biological activity (i.e., cognate antigen, Fc receptors, C1q). Further considerations include potential modifications in immunogenicity and pharmacokinetic profiles. Moreover, elucidation of the underlying mechanisms that drive improvements in stability demands thorough structural analysis of the glycan structures attached to the engineered site. In light of this, we inserted N-glycosylation motifs in trastuzumab in several amino acid positions previously identified by others on conserved regions of the IgG1 molecule and performed a detailed structural analysis of the ensuing glycan profile.

Preliminary prediction and confirmation of glycan attachment

N-glycosylation is a complex biochemical process, for which the requirements for glycan attachment are not yet fully understood. Three key factors determining glycan occupancy have been identified: (1) location of the asparagine residue within the consensus motif Asn-X-Ser/Thr, (2) location of the N residue in the ER lumen during translation, and (3) the adjacent secondary

structure of the protein must enable glycan transfer. Based on these, numerous servers have been developed to map N-glycosylation sequons and predict the probability of glycan attachment, and have been instrumental in the study of the glycosylation profile of proteomes. We thus employed two such servers to assess the validity of their prediction values applied to this antibody engineering strategy. This is particularly important considering the fact that previous studies have not pursued potential APR shielding regions experimentally due to low glycan transfer probability. Specifically, residue Q178 was deemed ineligible by Courtois et al. based on low solvent accessible surface area obtained from MD simulations. Our preliminary evaluation of glycan attachment probability on trastuzumab shed similar results (Table 2) to those obtained by Courtois et al. on their panel of glycosylation sites identified through SAP, wherein Q178N had negative predictions by both NetNGlyc and NGlycPred, and SASA was amongst the lowest calculated (20.5 Å2). Importantly, L115N also obtained a negative prediction value from NGlycPred. It was thus remarkable that our experimental data contradicted the negative prediction for residues L115N and Q178N. The Q178N mutant had previously been implemented by Pepinsky et al. in the anti-LINGO IgG1 antibody with important improvements in solubility, although no compelling data to confirm glycan attachment was reported. Moreover, our data strongly suggest that Q160N does not undergo glycan attachment, despite the high SASA and prediction values calculated for the residue. This was equally observed in the equivalent mutation in adalimumab (data to be published). These results emphasize the importance of confirming glycan attachment and performing structural analysis of the resulting structural modifications, to better interpret the results derived from aggregation experiments. Furthermore, they reveal a conspicuous need for further understanding of the factors that determine successful glycan transfer to refine this antibody engineering approach.

Glycan profile analysis

Compared to plasma proteins and other recombinant therapeutic proteins, monoclonal antibodies display limited heterogeneity in their Fc N-glycan profile, as reported herein. This observation is ascribed to the decreased surface exposure of Asn N297 and the attached glycan as it engages in several interactions with the protein backbone and residue side chains at the inner face of the domain [28, 29]. Although most plasma IgG molecules possess only the conserved N-glycosylation sequon in the Fc region, roughly 15-25% also express additional glycosylation sites

on the variable domain of the Fab region [30, 31]. Glycan profiling of Fab-glycosylated serum IgGs has revealed contrasting structural characteristics between Fc-derived and Fab-derived glycans, most notably higher overall heterogeneity and sialylation [32, 33]. All mutations evaluated in this study are located in the Fab region, although only L115N lies on a variable domain – in close proximity to the VH-CH1 interface. The global glycan profile acquired through capillary/nanoLC-ESI-MS/MS demonstrated that increased structural heterogeneity is similarly obtained when engineered glycosylation sites are incorporated through mutagenesis in the Fab region of a recombinant mAb.

There was no evident association between the degree of heterogeneity or apparent glycan maturation and the solvent accessible surface area calculated. For instance, low-SASA mutant L115N possessed a relatively high abundance of sialylated glycans, indicative of higher glycan processing. Remarkably, high mannose glycans (HexNAc(2)Man(8) and HexNAc(2)Man(9)) were also detected in L115N. Similarly, residue Q178N displayed high glycoform heterogeneity despite having the lowest SASA among the mutants, including sialylated and triantennary glycans. As the en bloc transfer of the dolichol oligosaccharide precursor occurs on nascent proteins undergoing translation, low surface exposure calculated from the WT structure might not preclude glycan attachment and the resulting orientation of the glycan could be surface-exposed for enzyme accessibility. Ideally, SASA would be calculated from the crystal structure of the mutated protein, but performing such analyses for all mutations entails prominent experimental challenges.

Overall, the degree of sialylation was markedly higher in most engineered mutants relative to both wild-type references, i.e., Tmab WT and Herceptin. Similar findings have consistently been reported for both polyclonal and recombinant monoclonal IgG proteins containing naturally-occurring N-glycosylation sequons in the Fab region [34]. The higher abundance of sialic acid glycans in Fab glycosites has been attributed to increased accessibility to enzymes involved in glycan maturation relative to the Fc glycan. In this case, however, we also found various high mannose and hybrid glycans not detected in Tmab WT. In the seminal exploration of SAP reduction by Courtois et al., a G0 glycan was selected for molecular dynamic simulations of the Fab region to shed light into the factors driving resistance to aggregation upon glycosite insertion [18]. Here, it was posited that the added glycans on some of the mutated sites produce limited APR shielding and hence the improvements in physical stability could stem from steric hindrance due

to the large hydrodynamic size and hydrophilic character of the added glycans. The diversity of glycoforms reported here indicates that this structural heterogeneity must be accounted for when performing these analyses, particularly considering the important presence of negatively charged sialic acid residues on some of the mutants.

HEK-293F cells were chosen for transient expression of the Tmab variants due to high transient transfection efficiency and yield relative to CHO cells. Comparison of the glycan profile of CHO-produced Herceptin with HEK-derived Tmab WT shows that galactosylation was more abundant in HEK-293F expression. This observation was also consistent across the mutant panel when considering uniquely Fc glycans. Galactosylation of the conserved Fc glycan is not considered to affect significantly mAb binding to FcγR receptors, yet there is consistent evidence that the presence of terminal galactose promotes activation of the classical complement route [35]. Hence, the higher content of G1F and G2F glycoforms could lead to potency advantages in mAbs with significant modulation of complement activity.

Alterations in HER2 and Fc receptor affinity

A crucial consideration in this engineering approach must be the conservation of biological activity. The proximity of the mutations to the CDRs and to regions involved in Fc receptor binding warrants examination of alterations in receptor binding affinity. Taking this into consideration, we evaluated the binding kinetics of the panel of mutants to their molecular target (HER2) and to Fc receptors involved in effector function, using single-cycle SPR.

The kinetic constants obtained indicate that HER2 binding affinity is moderately diminished for all mutants, reflected by 2.4 – 6.9-fold reductions in the binding affinity constant (KD). All KD values, however, were subnanomolar – demonstrating that strong binding to HER2 is retained despite modest decreases in affinity. Remarkably, the highest reduction in affinity was obtained with T198N, which is located farthest from the HER2 binding region. This reduction in binding affinity could have resulted from conformational changes affecting the antigen binding region. KD values derived herein for wild-type Tmab binding to HER2 were in agreement with those reported in previous literature, spanning 19 pM – 5.48 nM [36-38].

Overall, the mutant library exhibited minor modifications in Fc receptor binding affinity. Binding to FcγR1A was marginally improved in all Tmab variants. Curve fitting was less reliable for

FcγR2B, and it was not possible to calculate these parameters for mutants A121N, Q178N, L182N, and T198N. Still, sensorgram interpretation suggests that L182N binding to FcγR2B was drastically disrupted. Binding affinity to FcγR3A also showed moderate disruption across all Tmab variants, with 3.35 – 9.44-fold increases in KD values.

The affinity screening to biologically relevant receptors performed in this work served as a proof-of-principle that N-glycosylation sites can be incorporated in the Fab region of therapeutic monoclonal antibodies without major modifications in antigen and Fc receptor binding. Nonetheless, evaluation of ADCC, CDC and inhibition of cell proliferation is still required to ascertain potential variations in biological activity.

Concluding remarks

The rational addition of N-glycosylation sequons represents a highly promising strategy to improve the physical stability of therapeutic antibodies, as is highlighted by the important enhancements in physical stability obtained in previous studies with bevacizumab, adalimumab Fab, and the Li33 anti-LINGO antibody. Moreover, we have previously performed the panel of mutations reported here in full-size adalimumab and demonstrated enhancements in thermodynamic stability through this approach. However, our data established that for this strategy to move forward in the clinical development pathway, there is an evident need to control or minimize the structural heterogeneity that results from glycan addition. The latter is also required to obtain further insight into the conferred physicochemical properties responsible for the improvements in stability. Native Fc glycosylation, albeit less diverse than most glycoproteins, already constitutes a challenge concerning the assessment of critical quality attributes. This, however, could be overcome with glyco-engineering strategies to curtail glycoform heterogeneity. Technologies to reduce glycan diversity in recombinant expression are being pursued in the context of refining the production of biopharmaceuticals. Prime examples of these include engineered Pichia pastoris (GlycoSwitch) and human (GlycoDelete) cell lines. We foresee great value in combining these two glyco-engineering strategies towards the development of therapeutic antibodies with enhanced physicochemical and biological properties. Albeit introducing heterogeneity, molecular engineering approaches such as this one offer a great deal of flexibility and control over preparation of new generation therapies. This glycoengineering strategy can also

be employed to enhance the biophysical stability of other protein-based therapies with short half-life and low formulation stabilities.

References

[1] L. Urquhart, Top drugs and companies by sales in 2018, Nature Reviews Drug Discovery, 18 (2019) 245.

[2] Z. Elgundi, M. Reslan, E. Cruz, V. Sifniotis, V. Kayser, The state-of-play and future of antibody therapeutics, Advanced drug delivery reviews, 122 (2017) 2-19.

[3] H. Kaplon, J.M. Reichert, Antibodies to watch in 2019, mAbs, 11 (2019) 219-238.

[4] J.K.H. Liu, The history of monoclonal antibody development – Progress, remaining challenges and future innovations, Annals of Medicine and Surgery, 3 (2014) 113-116.

[5] V. Kayser, N. Chennamsetty, V. Voynov, B. Helk, B.L. Trout, Conformational stability and aggregation of therapeutic monoclonal antibodies studied with ANS and Thioflavin T binding, mAbs, 3 (2011) 408-411.

[6] M. Vazquez-Rey, D.A. Lang, Aggregates in monoclonal antibody manufacturing processes, Biotechnology and bioengineering, 108 (2011) 1494-1508.

[7] R. van der Kant, A.R. Karow-Zwick, J. Van Durme, M. Blech, R. Gallardo, D. Seeliger, K. Aßfalg, P. Baatsen, G. Compernolle, A. Gils, J.M. Studts, P. Schulz, P. Garidel, J. Schymkowitz, F. Rousseau, Prediction and Reduction of the Aggregation of Monoclonal Antibodies, Journal of Molecular Biology, 429 (2017) 1244-1261.

[8] J. Hernandez-Jimenez, A. Martinez-Ortega, A. Salmeron-Garcia, J. Cabeza, J.C. Prados, R. Ortiz, N. Navas, Study of aggregation in therapeutic monoclonal antibodies subjected to stress and long-term stability tests by analyzing size exclusion liquid chromatographic profiles, International journal of biological macromolecules, 118 (2018) 511-524.

[9] V. Voynov, N. Chennamsetty, V. Kayser, B. Helk, B.L. Trout, Predictive tools for stabilization of therapeutic proteins, mAbs, 1 (2009) 580-582.

[10] R. Zambrano, M. Jamroz, A. Szczasiuk, J. Pujols, S. Kmiecik, S. Ventura, AGGRESCAN3D (A3D): server for prediction of aggregation properties of protein structures, Nucleic Acids Research, 43 (2015) W306-W313.

[11] J. Van Durme, G. De Baets, R. Van Der Kant, M. Ramakers, A. Ganesan, H. Wilkinson, R. Gallardo, F. Rousseau, J. Schymkowitz, Solubis: a webserver to reduce protein aggregation through mutation, Protein engineering, design & selection : PEDS, 29 (2016) 285-289.

[12] M. Reslan, V. Kayser, The effect of deuterium oxide on the conformational stability and aggregation of bovine serum albumin, Pharmaceutical Development and Technology, 23 (2018) 1030-1036.

[13] V.I. Razinkov, M.J. Treuheit, G.W. Becker, Accelerated formulation development of monoclonal antibodies (mAbs) and mAb-based modalities: review of methods and tools, Journal of biomolecular screening, 20 (2015) 468-483.

[14] M. Reslan, V. Kayser, Ionic liquids as biocompatible stabilizers of proteins, Biophysical reviews, 10 (2018) 781-793.

[15] M. Reslan, V. Ranganathan, D.R. Macfarlane, V. Kayser, Choline ionic liquid enhances the stability of Herceptin(R) (trastuzumab), Chemical communications (Cambridge, England), 54 (2018) 10622-10625.

[16] R. Mathaes, A. Koulov, S. Joerg, H.-C. Mahler, Subcutaneous Injection Volume of Biopharmaceuticals—Pushing the Boundaries, Journal of Pharmaceutical Sciences, 105 (2016) 2255-2259.

[17] R.B. Pepinsky, L. Silvian, S.A. Berkowitz, G. Farrington, A. Lugovskoy, L. Walus, J. Eldredge, A. Capili, S. Mi, C. Graff, E. Garber, Improving the solubility of anti-LINGO-1 monoclonal antibody Li33 by isotype switching and targeted mutagenesis, Protein science : a publication of the Protein Society, 19 (2010) 954-966.

[18] F. Courtois, N.J. Agrawal, T.M. Lauer, B.L. Trout, Rational design of therapeutic mAbs against aggregation through protein engineering and incorporation of glycosylation motifs applied to bevacizumab, MAbs, 8 (2016) 99-112.

[19] P.H. Jensen, N.G. Karlsson, D. Kolarich, N.H. Packer, Structural analysis of N- and O-glycans released from glycoproteins, Nature protocols, 7 (2012) 1299-1310.

[20] N. Chennamsetty, V. Voynov, V. Kayser, B. Helk, B.L. Trout, Design of therapeutic proteins with enhanced stability, Proceedings of the National Academy of Sciences, 106 (2009) 11937.

[21] H. Nakamura, N. Oda-Ueda, T. Ueda, T. Ohkuri, Introduction of a glycosylation site in the constant region decreases the aggregation of adalimumab Fab, Biochemical and biophysical research communications, 503 (2018) 752-756.

[22] S. Chattopadhyay, P. Bagchi, D. Dutta, A. Mukherjee, N. Kobayashi, M. Chawlasarkar, Computational identification of post-translational modification sites and functional families reveal possible moonlighting role of rotaviral proteins, Bioinformation, 4 (2010) 448-451.

[23] A. Eshaghi, V.R. Duvvuri, R. Lai, J.T. Nadarajah, A. Li, S.N. Patel, D.E. Low, J.B. Gubbay, Genetic Variability of Human Respiratory Syncytial Virus A Strains Circulating in Ontario: A Novel Genotype with a 72 Nucleotide G Gene Duplication, PLOS ONE, 7 (2012) e32807.

[24] E. Cruz, J. Cain, B. Crossett, V. Kayser, Site-specific glycosylation profile of influenza A (H1N1) hemagglutinin through tandem mass spectrometry, Human vaccines & immunotherapeutics, 14 (2018) 508-517.

[25] G.-Y. Chuang, J.C. Boyington, M.G. Joyce, J. Zhu, G.J. Nabel, P.D. Kwong, I. Georgiev, Computational prediction of N-linked glycosylation incorporating structural properties and patterns, Bioinformatics, 28 (2012) 2249-2255.

[26] H. Xie, A. Chakraborty, J. Ahn, Y.Q. Yu, D.P. Dakshinamoorthy, M. Gilar, W. Chen, S.J. Skilton, J.R. Mazzeo, Rapid comparison of a candidate biosimilar to an innovator monoclonal antibody with advanced liquid chromatography and mass spectrometry technologies, MAbs, 2 (2010) 379-394.

[27] K.H. Lee, J. Lee, J.S. Bae, Y.J. Kim, H.A. Kang, S.H. Kim, S.J. Lee, K.J. Lim, J.W. Lee, S.K. Jung, S.J. Chang, Analytical similarity assessment of rituximab biosimilar CT-P10 to reference medicinal product, mAbs, 10 (2018) 380-396.

[28] A. Croset, L. Delafosse, J.P. Gaudry, C. Arod, L. Glez, C. Losberger, D. Begue, A. Krstanovic, F. Robert, F. Vilbois, L. Chevalet, B. Antonsson, Differences in the glycosylation of

recombinant proteins expressed in HEK and CHO cells, Journal of biotechnology, 161 (2012) 336-348.

[29] E. Girardi, M.D. Holdom, A.M. Davies, B.J. Sutton, A.J. Beavil, The crystal structure of rabbit IgG-Fc, The Biochemical journal, 417 (2009) 77-83.

[30] F.S. van de Bovenkamp, N.I.L. Derksen, P. Ooijevaar-de Heer, K.A. van Schie, S. Kruithof, M.A. Berkowska, C.E. van der Schoot, H. Ijspeert, M. van der Burg, A. Gils, L. Hafkenscheid, R.E.M. Toes, Y. Rombouts, R. Plomp, M. Wuhrer, S.M. van Ham, G. Vidarsson, T. Rispens, Adaptive antibody diversification through N-linked glycosylation of the immunoglobulin variable region, Proceedings of the National Academy of Sciences, 115 (2018) 1901.

[31] R. Jefferies, Glycosylation of Antibody Molecules, in: S. Dübel, J.M. Reichert (Eds.) Handbook of Therapeutic Antibodies2014, pp. 171-200.

[32] K.R. Anumula, Quantitative glycan profiling of normal human plasma derived immunoglobulin and its fragments Fab and Fc, Journal of immunological methods, 382 (2012) 167-176.

[33] A. Bondt, Y. Rombouts, M.H.J. Selman, P.J. Hensbergen, K.R. Reiding, J.M.W. Hazes, R.J.E.M. Dolhain, M. Wuhrer, Immunoglobulin G (IgG) Fab Glycosylation Analysis Using a New Mass Spectrometric High-throughput Profiling Method Reveals Pregnancy-associated Changes, Molecular &amp; Cellular Proteomics, 13 (2014) 3029.

[34] M. Holland, H. Yagi, N. Takahashi, K. Kato, C.O. Savage, D.M. Goodall, R. Jefferis, Differential glycosylation of polyclonal IgG, IgG-Fc and IgG-Fab isolated from the sera of patients with ANCA-associated systemic vasculitis, Biochimica et biophysica acta, 1760 (2006) 669-677.

[35] P.N. Boyd, A.C. Lines, A.K. Patel, The effect of the removal of sialic acid, galactose and total carbohydrate on the functional activity of Campath-1H, Molecular immunology, 32 (1995) 1311-1318.

[36] P. Dakshinamurthy, P. Mukunda, B. Prasad Kodaganti, B.R. Shenoy, B. Natarajan, A. Maliwalave, V. Halan, S. Murugesan, S. Maity, Charge variant analysis of proposed biosimilar to Trastuzumab, Biologicals, 46 (2017) 46-56.

[37] D. Lakayan, R. Haselberg, R. Gahoual, G.W. Somsen, J. Kool, Affinity profiling of monoclonal antibody and antibody-drug-conjugate preparations by coupled liquid chromatography-surface plasmon resonance biosensing, Anal Bioanal Chem, 410 (2018) 7837-7848.

[38] W.-H. Lua, S.K.-E. Gan, D.P. Lane, C.S. Verma, A search for synergy in the binding kinetics of Trastuzumab and Pertuzumab whole and F(ab) to Her2, Npj Breast Cancer, 1 (2015) 15012.

Chapter 6

Monoclonal Antibody Therapy of Solid Tumors: Clinical Limitations and Novel Strategies to Enhance Treatment Efficacy

Macrophage	Proteoglycan	Blood vessel	
Fibroblast	Collagen	Lymph vessel	
Pericyte	Tumor cell		
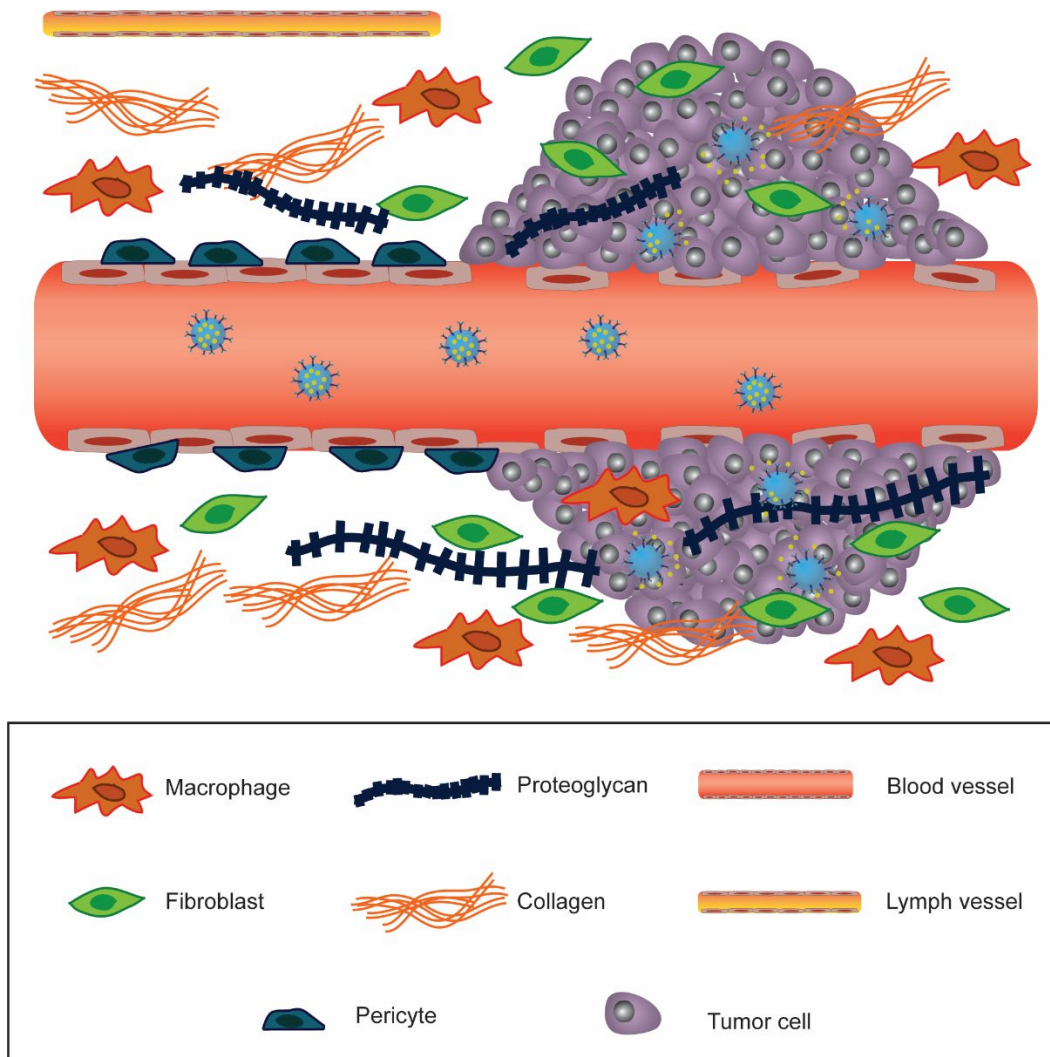
Chapter 6 – Authorship declaration statement

The following chapter is a literature review published in the journal Biologics: Targets and Therapy as:

E. Cruz, V. Kayser. Monoclonal Antibody Therapy of Solid Tumors: Clinical Limitations and Novel Strategies to Enhance Treatment Efficacy. Biologics: Targets and Therapy. 13 (2019), 33-51.

E. Cruz carried out the literature searches and wrote the review.

Permission to include the published material has been granted by the corresponding author.

Esteban Cruz, Signature: 19th of August, 2019

As corresponding author and supervisor for this candidature, I hereby confirm that this authorship declaration statement is complete and accurate

Veysel Kayser, Signature: *Veysel Kayser* 19th of August, 2019

Abstract

Abstract: Monoclonal antibodies (mAbs) have become a cornerstone in the therapeutic guidelines of a wide range of solid tumors. The targeted nature of these biotherapeutics has improved treatment outcomes by offering enhanced specificity to reduce severe side effects experienced with conventional chemotherapy. Notwithstanding, poor tumor tissue penetration and the heterogeneous distribution achieved therein are prominent drawbacks that hamper the clinical efficacy of therapeutic antibodies. Failure to deliver efficacious doses throughout the tumor can lead to treatment failure and the development of acquired resistance mechanisms. Comprehending the morphological and physiological characteristics of solid tumors and their microenvironment that affect tumor penetration and distribution is a key requirement to improve clinical outcomes and realize the full potential of monoclonal antibodies in oncology. This review summarizes the essential architectural characteristics of solid tumors that obstruct macromolecule penetration into the targeted tissue following systemic delivery. It further describes mechanisms of resistance elucidated for blockbuster antibodies for which extensive clinical data exists, as a way to illustrate various modes in which cancer cells can overcome the anticancer activity of therapeutic antibodies. Thereafter, it describes novel strategies designed to improve clinical outcomes of mAbs by increasing potency and/or improving tumor delivery; focusing on the recent clinical success and growing clinical pipeline of antibody-drug conjugates (ADC), immune checkpoint inhibitors and nanoparticle-based delivery systems.

Introduction

Therapeutic monoclonal antibodies (mAbs) successfully entered the clinic over 25 years ago and have become one of the central components of the healthcare system [1, 2]. Their arrival brought about a therapeutic revolution due to their capacity to target specific molecular components, with a large number of mAbs already approved in oncology, autoimmune disorders, chronic diseases and many more conditions. Currently, over 80 antibody therapeutics have received regulatory approval in Europe and/or the United States and just in 2017 sales of therapeutic antibodies exceeded $100 billion worldwide [3].

In oncology, therapeutic antibodies offer the possibility to treat tumors in a targeted fashion and reduce the severe side effects of conventional chemotherapy. Recent developments in cancer

biology have aided the discovery of molecular biomarkers in a wide range of solid malignancies that can be used as targets with beneficial therapeutic outcomes. At present, over 15 distinct monoclonal antibodies are indicated for the treatment of solid tumors [4]. Notwithstanding, in spite of their remarkable clinical success some patients do not benefit from the treatment due to intrinsic resistance mechanisms or the emergence of acquired resistance following treatment initialisation [5, 6].

In solid tumors, the development of acquired resistance mechanisms is thought to emerge primarily from continuous genetic alterations that modify the cellular phenotype and undermine the initial therapeutic efficacy. This capacity of cancer cells to overcome the anticancer effect of the antibody is facilitated by the exposure to subtherapeutic concentrations of the drug [7, 8]. The tumor microenvironment poses physical barriers, most notably a markedly increased hydrostatic pressure, that hinder penetration of macromolecules into the tumor following systemic administration [9, 10]. This reduces the overall amount of antibody molecules that reach the target tissue and exposes areas of the tumor that are difficult to penetrate to marginal doses of the antibody, leading to acquired resistance and treatment failure [8]. In fact, therapeutic mAbs in oncology are more commonly administered as combination therapy in conjunction with chemotherapeutics due to relatively limited efficacy as single agents [11].

Identifying and understanding primary and acquired resistance mechanisms and overcoming the barriers that impair efficient delivery of the drug into the tissue is critical to enhance therapeutic outcomes. Most of the understanding regarding primary and acquired resistance comes from the evaluation of clinical data available for early-approved blockbuster antibodies, such as trastuzumab and cetuximab. This review gives an overview of the key factors affecting tumor distribution upon systemic delivery and describes relevant mechanisms of resistance identified in trastuzumab (anti-HER2) and cetuximab (anti-EGFR) therapy. Additionally, it describes recent developments in the implementation of novel antibody-based therapeutics, such as antibody-drug conjugates, immune checkpoint inhibitors, and antibody-targeted nanoparticles that have the potential to increase therapeutic outcomes of solid tumors.

Limitations that impact clinical efficacy

Poor penetration and heterogeneous distribution in solid tumors

Therapeutic IgG antibodies must overcome pronounced physical and physiological obstacles in order to penetrate and distribute uniformly throughout the tumor. In solid malignancies, impaired lymphatic drainage due to the sparse presence of lymphatic vessels leads to the accumulation of macromolecules in the interstitial tissue and a consequent increase in hydrostatic pressure [9, 12-14]. Hence, the altered pressure differential from vascular vessels to the interstitial compartment limits convection and extravasation of macromolecules from the vascular lumen into the tumor (Figure 1) [15]. Moreover, antibody distribution following extravasation is further impeded by cellular internalization and subsequent endocytic clearance at the tumor edge (an effect coined the "binding-site barrier"), leading to poor penetration and regions of marginal antibody concentrations [10, 16, 17]. The binding-site barrier suggests that higher affinity and higher antigen expression, especially at the tumor edge, can retard mAb tumor percolation and impair homogeneous distribution; although this barrier can be overcome by increasing the administered dose.
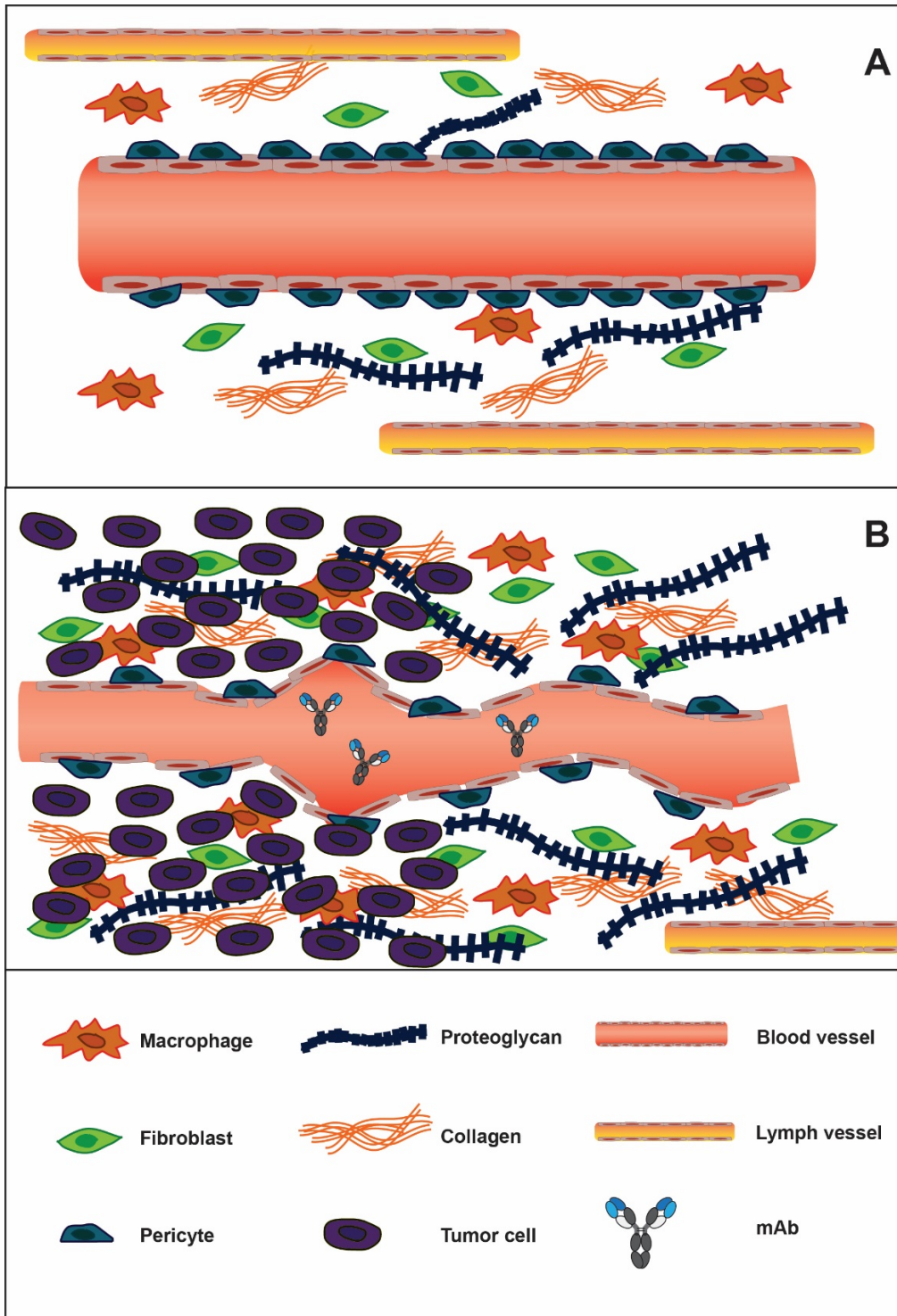
Figure 1. Structural features of the tumor microenvironment that increase interstitial pressure and hinder mAb extravasation and distribution. (A) Blood vessels that irrigate healthy normal tissue possess a continuous inner lining of endothelial cells, enveloped by perivascular cells called pericytes that grant integrity to the vascular tube. The extracellular

matrix (ECM) contains a lax network of collagen and proteoglycan fibers, and the presence of macrophages and fibroblasts is scarce. Lymph vessels efficiently remove and prevent the accumulation of macromolecules and interstitial fluid. (B) Increased demand of oxygen and nutrients in tumor tissues causes blood vessels to form defectively and irregularly shaped. The lack of pericytes makes the vascular tube unstable and leakier. The abundant presence of fibroblasts and infiltrating macrophages promote the formation of a dense extracellular matrix, with a condensed network of collagen and proteoglycan fibers. The paucity of lymph vessels leads to the accumulation of macromolecules and an increase in interstitial fluid pressure (IFP). The fibrotic nature of the ECM and the altered pressure differential between the vascular lumen and the tumor hinder antibody convection into the targeted tissue.

A vast body of research studying some of the blockbuster therapeutic mAbs has highlighted the significance of increasing tissue penetration to improve the outcome of antibody therapy [15, 18]. A study on cetuximab and trastuzumab in mouse xenografts confirmed that tumor distribution can be improved with an increase in dose; however, hypoxic areas remained difficult to reach even at higher doses. Moreover, xenografts expressing intermediate levels of ErbB1 (cognate antigen for cetuximab) displayed more homogeneous distribution of cetuximab compared to xenografts with higher ErbB1 expression [19].

An alternative approach consists in improving diffusion by employing smaller antibody fragments, such as Fab fragments (~50 kDa), single-chain variable fragments (scFv ~30 kDa) and single-domain antibodies (sdAb 12-15 kDa). Yet, while these formats indeed possess higher diffusion rates, the tumor distribution achieved in physiological settings is poor because the clearance rates for smaller fragments is markedly higher relative to full size antibody molecules [15, 20]. IgG immunoglobulins undergo salvage recycling through interaction of the Fc region with the neonatal Fc receptor (FcRn), leading to prolonged half-lives of more than 20 days for most therapeutic mAbs [21]. Conversely, antibody fragments lacking an Fc region display half-lives of hours, or even minutes for formats below the glomerular filtration cutoff (30-50 kDa). The high elimination rates upon systemic delivery prevent most antibody fragments from saturating the tumor and achieving uniform distributions [22, 23]. Increasing tumor tissue penetration thus poses significant challenges given the intricate pharmacokinetic properties of IgGs.

Resistance to monoclonal antibody therapy

Understanding the resistance mechanisms that affect monoclonal antibody therapy in cancer has proven to be a strenuous task, insofar as the antitumor activity of mAbs stems from a multiplicity of molecular mechanisms – eg, signaling pathway disruption, antibody dependent cellular cytotoxicity (ADCC), antibody dependent cellular phagocytosis (ADCP) and complement dependent cytotoxicity (CDC). To this day, the clinical contribution of the various modes of action involved in the anticancer activity of most mAbs remains controversial [24-26]. On that account, intrinsic phenotypic variations in tumor cells or tumor-related cells affecting any of the involved modes of action can compromise treatment efficacy. Moreover, adaptive phenotypic modifications can arise following repeated exposure to sub-optimal doses of the biotherapeutic resulting in acquired resistance [27, 28].

Most of the current understanding of the contributing factors in the development of intrinsic or acquired resistance and their clinical significance comes from preclinical and clinical trials of benchmark therapeutic antibodies. Notwithstanding that the modes of action of different mAbs are not identical, the vast clinical data available for these benchmark antibodies are pivotal to comprehend host response and optimize monoclonal antibody therapy. The next sections briefly discuss resistance mechanisms identified in clinical settings for trastuzumab in HER2 positive breast cancer, and for cetuximab in colorectal cancer as archetypes of solid tumor treatment.

Resistance to trastuzumab (anti-HER2 therapy)

Trastuzumab was the first therapeutic monoclonal antibody to be approved for a solid carcinoma (FDA approval in the year 1998) [29]. Trastuzumab targets the extracellular domain of the human epidermal growth factor receptor 2 (HER2/Neu or ErbB2) that is overexpressed in a broad range of malignancies. HER2 overexpression is detected in 15-20% of breast cancers and this subset is associated with poor prognosis and higher rates of recurrence [30, 31].

HER2 exists primarily as a monomeric receptor that can form heterodimers with other members of the ErbB family of receptors (HER1, HER3 and HER4) upon ligand-mediated activation of the latter. Heterodimerization activates the MAPK and PI3K/AKT/mTor intracellular pathways, inducing cell proliferation and inhibition of apoptosis, respectively [32, 33]. Direct binding of trastuzumab with HER2 can hinder heterodimerization and promote proteolysis of the receptor

through receptor-mediated endocytosis. This interaction inhibits downstream signaling and causes cell cycle arrest by accumulation of the cyclin-dependent kinase (CDK) inhibitor p27 [34]. Additionally, trastuzumab can mediate antibody-dependent cellular cytotoxicity (ADCC) [35, 36] and antibody-dependent cellular phagocytosis (ADCP) [36-38]. Induction of complement dependent cytotoxicity (CDC) has also been documented in *in vitro* experiments, but it is thought to contribute only minimally to the anticancer effect in patients [36, 39].

Intrinsic alterations of the HER2 receptor involving regions associated with the binding epitope of trastuzumab have been linked to intrinsic (or primary) resistance mechanisms. For instance, alternate transcription initiation sites can result in the expression of a truncated variant of the receptor (p95-HER2) that lacks the cognate epitope for trastuzumab [40]. Insertions and point mutations in the tyrosine kinase domain of HER2 have been identified in various cancers, some of them associated with resistance to trastuzumab and lapatinib, however evidence of such mutations in HER2 overexpressing breast cancers has not been reported to date [41, 42]. A further alteration resulting in impaired target binding comes from the overexpression of mucin-4, which has been shown to induce association with HER2 causing steric hindrance to abrogate trastuzumab binding to HER2 [43].

Additional intrinsic and acquired resistance mechanisms predominantly involve alterations in the P13K/Akt/mTOR axis, activation of other ErbB receptors (especially EGFR and HER3) by increased ligand production, and circumvention of HER2 binding by activation of the PI3K cascade through alternative pathways. Mutations in PIK3CA and function impairment of PTEN (both downstream of HER2 signaling) have been implicated in bypassing HER2 blockade [44, 45]. Overexpression of the insulin-like growth factor (IGF-IR) has been documented as an adaptive response to trastuzumab by some tumors, resulting in resistance to the antibody. IGF-IR can form heterodimers and heterotrimers with HER2 and HER3 in breast cancer cells resistant to trastuzumab [46, 47]. Similarly, increased levels of EpoR, EpHA2 and RTK MET can activate P13K/Akt/mTOR by interacting with other members of the ErbB family or through activation of intracellular kinases [47-49].

Resistance to cetuximab (anti-EGFR therapy)

The epidermal growth factor receptor (EGFR; HER1; ErbB1) forms part of the ErbB family of receptors. EGFR is pivotal in modulating proliferative mechanisms and has been implicated in a

broad range of cancers [50-52]. Cetuximab (chimeric IgG1) was the first anti-EGFR mAb to receive regulatory approval in 2004 [53]. Since then, two more anti-EGFR mAbs (panitumumab and necitumumab) and six anti-EGFR small molecule inhibitors (gefitinib, erlotinib, lapatinib, neratinib, vandetanib and osimertinib) have obtained regulatory approval for various cancers [4].

The anticancer activity of cetuximab partially resembles that of trastuzumab in that it targets another member of the ErbB family of receptors with intrinsic protein tyrosine kinase activity. Accordingly, dimerization of EGFR can activate the PI3K/AKT/mTOR, RAS/RAF/MAPK and JAK/STAT signaling pathways to promote cell growth and proliferation [54, 55]. In contrast to HER2, EGFR can undergo a conformational transition triggered by binding of specific ligands, predominantly EGF and TGFα, that promotes the formation of homodimers and heterodimers with other members of the HER family [56]. Cetuximab can block ligand activation of EGFR by binding directly to the extracellular domain III of the receptor and inducing receptor internalization and proteolysis [57]. A further contributing mechanism of action involves suppression of VEGF (a pro-angiogenic factor) production resulting in impaired angiogenesis [58]. Moreover, ADCC and CDC are also believed to contribute to cetuximab efficacy in EGFR over-expressing cancers [59, 60].

There is vast documentation of primary and acquired resistance to anti-EGFR therapy in patients with colorectal and head and neck cancer. Indeed, roughly 80% of metastatic colorectal cancer patients do not display susceptibility to EGFR blockade [61]. This low response rate has been linked to a broad spectrum of alterations in several of the components of the downstream signaling pathways. Specifically, mutations in the PIK3CA [62], NRAS, BRAF and KRAS [63]. genes that confer constitutive activation of the EGFR are amongst the best studied contributing factors in intrinsic and acquired resistance. Further alterations such as low EGFR copy numbers or low expression of specific EGFR-ligands (eg, EREG and AREG) have been implicated in resistance to EGFR therapy [64, 65].

EGFR downregulation and structural modifications in the binding region can also compromise treatment efficacy [66]. The role of mutations in the extracellular domain (ECD) of EGFR in cetuximab resistance remains unclear. Recent publications have identified several point mutations that abrogate cetuximab binding to the receptor [67]. Still, RAS mutations are found more

frequently in refractory patients than ECD mutations and have been associated with worst clinical outcomes [68].

Novel approaches to enhance efficacy

Increasing the therapeutic index with antibody drug-conjugates

Antibody drug conjugates (ADCs) were conceived as an approach to enhance the therapeutic window of its primary components, namely the targeted antibody and a cytotoxin or an immunotoxin covalently attached to the antibody. Endowing the drug with specificity towards a molecular target – by virtue of the attachment of an antibody – allows for the utilization of highly potent cytotoxic compounds, that otherwise display intolerable systemic toxicity.

ADCs increase the intrinsic potency of the targeted treatment – relative to the antibody agent, therefore lower doses are required to reach the tumor to effectively destroy the targeted cells. Moreover, depending on the chemical nature of the drug and its release in the tumor (either intracellular or extracellular), some payloads can subsequently diffuse and kill surrounding cells ('bystander killing') [69, 70]. Consequently, these features could ameliorate the drawbacks of the heterogeneous tumor distributions of therapeutic antibodies and decrease the risk of developing resistance.

Despite the potential of the concept, the clinical implementation of ADCs has met with significant challenges, mostly regarding off-target toxicity. To date, only four ADCs (Mylotarg, Adcetris, Kadcyla and Besponsa) have received regulatory approval. Gemtuzumab ozogamicin (Mylotarg) (anti-CD33) was the first to enter the market in 2000 under an accelerated approval process [71]. It was originally approved as stand-alone treatment for refractory CD33-positive acute myeloid leukemia (AML), but it was voluntarily withdrawn in 2010 after failure to display benefits relative to standard therapies in a phase III comparative controlled clinical trial (NCT00085709 or SWOG-0106) [72]. Moreover, Mylotarg caused a significantly higher rate of fatal induction toxicity in this confirmatory trial. Gentuzumab ozogamicin had previously raised hepatotoxicity concerns due to high incidence (~20%) of Grade 3 or 4 liver transaminitis and hyperbilirubinemia, and reports of hepatic veno-occlusive disease [73]. Mylotarg received FDA approval once again in 2017 following a careful review of the dosing regimen, whereby fractionated lower-dose regimens demonstrated a decrease in early mortality without compromise in complete remission rate [74,

75]. Brentuximab vedotin (Adcetris) (anti-CD30 for Hodgkin lymphoma and anaplastic large cell lymphoma) and ado-trastuzumab emtansine (Kadcyla) (anti-HER2 for HER2-positive metastatic breast cancer) gained approvals in 2011 [76] and 2013 [77], respectively. More recently, the FDA granted approval to inotuzumab ozogamicin (Besponsa) (anti-CD22) for treatment of relapsed or refractory B-cell precursor acute lymphoblastic leukemia (ALL) in 2017 [78].

The clinical development of ADCs has been hampered predominantly by systemic toxicity due to off-target release of the payload. Most adverse effects reported in clinical reports are ascribed to the potent cytotoxicity of the payload, underlining the importance of improving ADC design to enhance therapeutic index [79, 80]. On that account, the linker chemistry plays a crucial role in determining plasma stability to prevent premature release.

Linker chemistry

Earlier ADC formats carried mostly chemically-labile linkers, such as pH-labile moieties intended to be released within the cell. These linkers should be stable at the neutral pH of the blood (pH 7.3-7.5) and undergo hydrolysis once they are internalized within the cell by receptor-mediated endocytosis, where the more acidic environment of the endosome (pH 5.0-6.5) or the lysosome (pH 4.5-5.0) trigger the release of the payload [81-83]. Both Mylotarg and Besponsa employ a pH-labile hydrazone linker. Other early constructs bore reducible disulfide linkers that enable payload delivery in the intracellular reducing environment. The higher concentrations of glutathione in the intracellular compartment induce disulfide bond reduction and cytotoxin release [84].

Since then, plasma stability has been improved by the implementation of alternative release strategies. Most commonly, the linker is designed to possess a dipeptide sequence that is recognized and cleaved by lysosomal proteases following receptor-mediated endocytosis. Most ADCs currently in development employ this approach [83, 85]. Specifically, the dipeptide valine-citrulline group – recognized and cleaved by cathepsin B (lysosomal protease) – is the most widely implemented technology in the current clinical pipeline [85]. A further approach consists in utilizing non-cleavable linkers, whereby release of the drug requires cellular uptake and proteolysis (Figure 2).
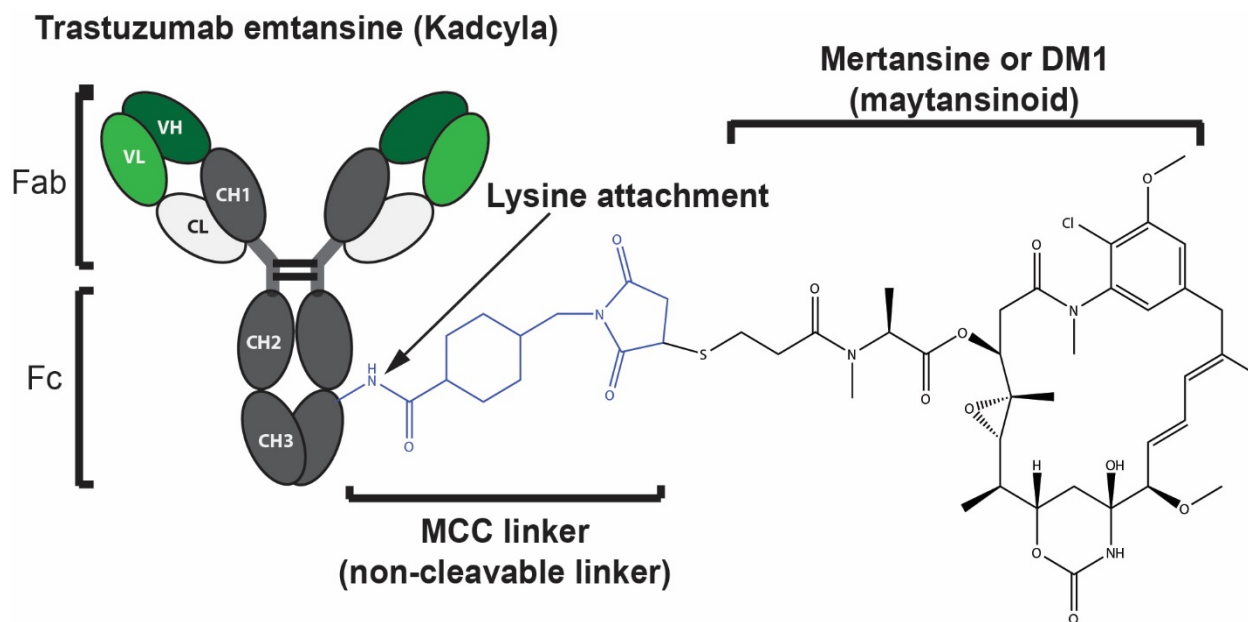
Figure 2. Structural components of an antibody drug conjugate. Trastuzumab emtansine is a commercially approved anti-Her2 antibody with a potent maytansinoid payload attached to lysines in the mAb polypeptide chain through a non-cleavable linker.

Conjugation methods

Most of the ADC formats that have entered clinical trials employ stochastic conjugation methods to lysine residues in the antibody, or to free SH groups in cysteines obtained by partial reduction of the interchain disulfide bonds. These techniques, although widely used, suffer from several disadvantages. In IgG molecules, lysine side chains are abundant and lysine conjugation yields consequently highly heterogeneous drug attachments, some of them occurring on residues where attachment can be detrimental to the physicochemical stability of the antibody [86]. Additionally, highly heterogeneous drug-to-antibody-ratios (DAR) are obtained, where the ADCs with high DARs (>8) show more narrow therapeutic indices [87]. Conjugation to free SH groups offers greater homogeneity as the maximum amount of available SH groups after partial reduction of the interchain disulfide bonds is limited to 8. Nonetheless, the disruption of these bonds can result in alterations in the quaternary structure of the IgG molecule [88]. The impact of these conjugation techniques on the physicochemical stability of ADCs is thoroughly described in [89].

Novel developments in linker technologies intend to enhance the homogeneity of ADCs by providing site-specific attachment of the drug-linker to the antibody, thereby controlling the

number of drugs affixed as well as preventing attachment to regions in the antibody that may impair binding to the cognate epitope or to Fc receptors on immune effector cells. The THIOMAB platform, developed by Genentech, was the first site-specific technique to be implemented and it consists in the insertion of engineered unpaired cysteines on protein surface [90]. Site-specific methods also include recombinant techniques to introduce unnatural amino acids – eg, p-acetylphelylalanine, N6-((2-azidoethoxy)carbonyl)-L-lysine, selenocysteine – in the primary sequence of the antibody that can be readily modified [90-92]. Furthermore, other formats have employed short peptide tags or specific attachment to the glycan moiety in the CH2 domain [93, 94]. Several preclinical studies have reported superiority in efficacy and safety of site-specific homogeneous ADCs compared to conventional lysine or cysteine-conjugation chemistry [95, 96]. Site-specific conjugates currently account for approximately 15% of ADC formats in development [97].

Cytotoxic payloads

A further increasing trend in ADC optimization focuses on the development and employment of more potent payloads. In particular, DNA alkylators – predominantly calicheamycins, pyrrolobenzodiazepines (PBDs) and duocarmycins – have seen a significant increase in popularity in the development of novel ADC platforms [98]. This strategy gained relevance after several ADCs failed to demonstrate adequate efficacy in clinical trials early in the decade. In 2013, 80% of the clinical pipeline was made up of conjugates bearing antimitotic agents, namely auristatins or maytansinoids (mostly DM1, DM4, MMAE and MMAF). Since then, this fraction has dropped by more than 15% owing to the introduction of novel formats carrying DNA alkylating agents and other novel cytotoxic compounds, e.g. trastuzumab deruxtecan [99], trastuzumab duocarmazine [100], vadastuximab talirine [101]. [102].

Further optimization of ADC design is sure to bring about major improvements to the field of antibody therapeutics and precision medicine. The field has grown dramatically in recent years and will likely continue to experience major developments in the near future as novel technologies and strategies are implemented in preclinical and clinical development. The ADC field will also benefit from advancements in the identification of novel target antigens.

Engaging the immune system

Immune checkpoint blockade

One of the most important recent developments in antibody therapy in oncology has been the introduction of immune checkpoint inhibitors (ICI) in the clinic. ICI therapy consists in the utilization of monoclonal antibodies to disrupt key signaling pathways involved in the suppression of immune effector cells [103]. Releasing the brakes of the immune system in this way can trigger potent and durable antitumor responses. One of the most advantageous features of ICI therapy is the capability of eliciting antitumor responses in a wide range of malignancies, since the treatment engages the immune machinery as opposed to traditional targeted therapy that is specific to antigens expressed in cancer cells. A further key feature of immune checkpoint blockade is the observed long-term durability of the anticancer response [104].

Two crucial inhibitory pathways have been exploited in the development of these therapeutics, namely the cytotoxic T-lymphocyte associated protein 4 (CTLA-4) and the programmed cell death (PD-1) receptor or its ligand PD-L1. The first FDA approval was granted in 2011 to ipilimumab (anti-CTLA-4) for late-stage melanoma, following the review of a phase III randomized, controlled trial that included 676 melanoma patients (stage III or IV) and demonstrated an increase in overall survival rate. This was the first drug to achieve a significant improvement in overall survival in advanced melanoma and it marked a key development in the field of cancer immunotherapy [105]. Following the first approval of ipilimumab the field has experienced a remarkable expansion. Anti-PD-1 antibodies pembrolizumab and nivolumab received regulatory approval in 2014. More recently, the anti-PD-L1 atezolizumab entered the clinic in 2016 and anti-PD-L1 mAbs avelumab and durvalumab in 2017 (table 1).

Table 1. Approved immune checkpoint inhibitors and FDA indications

Antibody	Target	FDA indications	FDA approval date
Ipilimumab (Yervoy)	CTLA-4	Unresectable or metastatic melanoma	2011

		Adjuvant treatment in cutaneous melanoma following surgery	2015
		Unresectable or metastatic melanoma in paediatric patients 12 years of age or older	2017
Nivolumab (Opdivo)	PD-1	Unresectable or metastatic melanoma	2014
		Advanced (metastatic) squamous non-small cell lung cancer (NSCLC)	2015
		Advanced (metastatic) renal cell carcinoma	2015
		Classical Hodgkin lymphoma	2016
		Metastatic squamous cell carcinoma of the head and neck (HNSCC)	2016
		Metastatic urothelial carcinoma	2017
		Microsatellite instability-high (MSI-H) or mismatch repair deficient (dMMR) metastatic colorectal cancer (mCRC)	2017
		Hepatocellular carcinoma (HCC)	2017
Pembrolizumab (Keytruda)	PD-1	Advanced or unresectable melanoma	2014
		Advanced (metastatic) NSCLC	2015
		Metastatic HNSCC	2016
		Refractory classic Hodgkin Lymphoma	2017
		Metastatic urothelial carcinoma	2017
		Metastatic solid tumors with microsatellite instability-high or mismatch repair deficient*	2017
		Metastatic gastric or gastroesophageal junction adenocarcinoma with PD-L1 expression	2017

		Metastatic cervical cancer with PD-L1 expression	2018
		Refractory primary mediastinal large B-cell lymphoma	2018
		Hepatocellular carcinoma	2018
		Metastatic Merkel cell carcinoma	2018
Atezolizumab (Tecentriq)	PD-L1	Urothelial carcinoma	2016
		Metastatic NSCLC	2016
Avelumab (Bavencio)	PD-L1	Metastatic Merkel cell carcinoma	2017
		Urothelial carcinoma	2017
Durvalumab (Imfinzi)	PD-L1	Metastatic urothelial carcinoma	2017
		Advanced NSCLC	2018
Ipilimumab + Nivolumab	CTLA-4 + PD-1	BRAF V600 wild-type unresectable or metastatic melanoma	2015
		BRAF V600 wild-type and BRAF V600 mutation-positive metastatic melanoma	2016
		Intermediate- and poor-risk advanced renal cell carcinoma	2018
		Microsatellite instability-high or mismatch repair deficient metastatic colorectal cancer	2018

*First approval based on the presence of a biomarker instead of the tissue affected

CTLA-4, cytotoxic T-lymphocyte-associated antigen; PD-1, programmed cell-death 1; programmed cell-death ligand 1; NSCLC, squamous non-small cell lung cancer; HNSCC, squamous cell carcinoma of the head and neck.

CTLA-4 therapy

The CTLA-4 and PD-1 immunosuppressive checkpoints are key regulatory mechanisms in immune response modulation and self-tolerance. In cancer, the presentation of neoantigens by antigen presenting cells (mainly dendritic cells) in the lymph nodes induces an initial activation of naïve T cells that leads to expansion and proliferation of cytotoxic and helper T cells specific to

tumor antigens. These activated T cells can subsequently infiltrate the tumor and mount a local immune response against cancer cells. The initial activation that takes place in the lymph nodes requires two co-stimulatory events: (1) T cell receptor (TCR) activation through interaction with an MHC-peptide complex on the APC and (2) co-stimulation through T cell CD28 and APC B7 ligand (CD80 or CD86) interaction [106]. Upon T cell activation, CTLA-4 (CD152), which is localized in intracellular vesicles in naïve T cells, is upregulated and translocates to the cellular membrane [107-109]. CTLA-4 is a homologue of CD28 with higher affinity towards CD80 (or B7-1) and CD86 (B7-2), therefore its exposure on the cell surface can lead to disruption of CD28-CD80 stimulation and T cell suppression through CD80-CTLA-4 signaling (Figure 3) [103, 110]. CTLA-4 works as a signal damper of T cell activation and compromises the potency of the immune antitumor response. Recent data indicate that the therapeutic efficacy of anti-CTLA-4 antibodies in oncology could also stem from a selective depletion of intratumoral regulatory T cells (Treg) through ADCC or ADCP, mediated by antibody binding to overexpressed CTLA-4 in these Tregs [111-113]. Comprehensive reviews of the mechanism of action of anti-CTLA-4 therapy can be found in [114], [115].
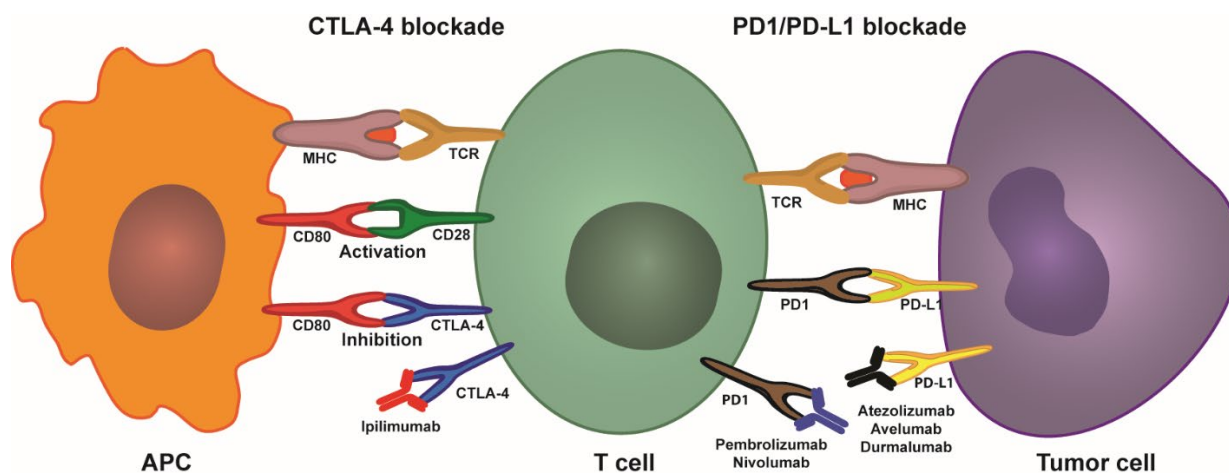
Figure 3. CTLA-4 and PD1/PD-L1 blockade using immune checkpoint inhibitors. Dendritic cells process and present tumor neoantigens through the MHC to the TCR on T-cells in the draining lymph nodes. T-cell activation further requires a co-stimulatory signal by CD80-CD28 binding. Upon T-cell activation, CTLA-4 can be upregulated in T-cells. CTLA-4 has a higher affinity towards CD80 than CD28, therefore the overexpression of CTLA-4 interferes with the co-stimulatory CD80-CD28 signal preventing T-cell activation. Ipilimumab prevents this mechanism by binding to CTLA-4 thus blocking its interaction

with CD80. Once activated T-cells migrate to the tumor to mount an immune anti-tumor response, tumor cells and macrophages can upregulate PD-L1 and suppress the immune response by interacting with the upregulated PD-1 on T-cells. Anti-PD1 and anti-PD-L1 antibodies inhibit this adaptive immune resistance mechanism.

PD-1/PD-L1 therapy

The PD-1/PD-L1 pathway plays a crucial role in adaptive immune responses. PD-1 is expressed by activated T cells, B cells, macrophages, natural killer (NK) cells and several APCs [116]. PD-1 expression on naïve T cells is induced upon TCR stimulation or TGF-β and cytokine (eg, IL-2, IL-7, IL-15, IL-21) autocrine/paracrine signaling. When activated tumor-specific T cells infiltrate the tumor, TCRs are triggered by recognition of the MHC-cognate antigen complex, resulting in the release of interferon-γ (IFN-γ) and other inflammatory cytokines. Secretion of IFN-γ can induce the expression of PD-L1, and PD-L2 to a lesser extent (PD-1 ligands), on the cell surface of tumor cells and tumor macrophages [117]. PD-1 binding to PD-L1 suppresses the T cell response of previously activated T cells at the tumor-invasive margin, leading to adaptive immune resistance (Figure 3) [118, 119]. The proposed mechanism of action of PD-1/PD-L1 inhibitors thus consists in suppression of the PD-1 regulatory signal exerted on activated tumor-infiltrating T cells [120]. Nonetheless, further mechanisms of action have been suggested and are reviewed elsewhere [120-122].

Targeting PD-1 or PD-L1 has been presumed to be a more tumor-specific approach than CTLA-4 blockade, given the involvement of the former in restoring T cell function at the effector stage which requires previous tumor specific T-cell activation. This is supported by clinical data showing improved outcomes and a lower rate of grade 3-4 adverse events with anti-PD-1 therapy compared to ipilimumab (anti-CTLA-4) [123]. The open-label, randomized, phase III clinical trial KEYNOTE-006 provided a head-to-head comparison of advanced melanoma treatment with ipilimumab or two different dose regimens of pembrolizumab (anti-PD-1). Pembrolizumab treatment achieved a more than two-fold increase in 24-month progression-free survival rates compared to ipilimumab while the 24-month overall survival rate was 55% (pembrolizumab) to 43% (ipilimumab) [123, 124]. Moreover, pembrolizumab has shown clinical efficacy in advanced melanomas refractory to ipilimumab by increasing progression-free survival [125]. A clinical trial

comparing nivolumab (anti-PD-1) to ipilimumab in advanced melanoma also reported substantial improvements in overall survival and progression free survival rates with PD-1 therapy [126].

Moving forward with ICI

Despite the remarkable clinical outcomes of ICI therapy, immune checkpoint blockade is still a relatively new concept and is undergoing extensive efforts for optimization. Key limitations being addressed include low objective response rates and primary and acquired resistance to treatment. Low objective response rates are presumably associated with primary resistance mechanisms. Achieving higher response rates will likely come from a better understanding of tumor biology and the elucidation of biomarkers that can identify patients that are more likely to respond to specific immunotherapeutics.

Moreover, since CTLA-4 and PD-1 are non-redundant inhibitory mechanisms, combination therapy targeting both pathways can significantly increase objective response rates. This was shown in a phase II trial where nivolumab plus ipilimumab therapy displayed a 61% objective response rate compared to 11% with ipilimumab mono-therapy [127]. Dual immune checkpoint inhibition has shown great promise in increasing therapeutic efficacy and nivolumab plus ipilimumab combination has already gained approval for metastatic melanoma, renal cell carcinoma and microsatellite instability-high or mismatch repair deficient metastatic colorectal cancer (table 1). Notwithstanding, combined therapy also seems to increase the frequency of immune-related toxicities [128]. Thorough reviews on strategies and novel concepts for combination therapy can be found in [129, 130]. Additionally, alternative inhibitory pathways of the antitumor immune response are also being targeted for clinical development; for example, blockade of LAG-3, TIM-3, TIGIT, VISTA, and others have started early clinical trials; and are reviewed elsewhere [131].

Bispecific antibodies (BsAbs)

A conceptually different strategy to engage the immune system in tumor cell depletion consists in the use of bispecific antibodies (BsAbs), wherein one arm of the BsAb targets a tumor cell antigen while the other arm recruits and activates T cells, or other immune effector cells. Additionally, various BsAb formats have been designed for therapeutic approaches that do not involve direct immunomodulation; eg, cross-linking or inhibition of two different receptors [132, 133]. A

plethora of bispecific antibody formats have started clinical development, and have been reviewed by others [134-136]. Nonetheless, only two bispecific formats have obtained approval by established regulatory agencies for cancer therapy. The first case – catumaxomab – comprises a hybrid rat-mouse full-size mAb with specificity towards tumor-expressed EpCAM and to the CD3 T cell co-receptor. Catumaxomab was approved by the EMA in 2009 for treatment of malignant ascites in EpCAM positive carcinomas [137]. Conversely, the other marketed BsAb – blinatumomab – comprises two scFv proteins connected by a peptide linker; a BsAb format called Bispecific T cell Engagers (BiTE). Blinatumomab binds to CD19 expressed on malignant B lymphocytes, while also engaging the CD3 co-receptor to recruit T cells. Blinatumomab was approved by the FDA in 2014 under the accelerated approval program, for use in precursor B-cell acute lymphoblastic leukemia [123].

Another flourishing strategy in cancer immunotherapy with bispecifics involves the recruitment and activation of Natural Killer (NK) cells. Analogous to BiTEs, Bispecific Killer cell Engagers (BiKEs) possess two scFv fragments; one directed towards a tumor antigen and another scFv that engages FcγRIIIa (CD16) on NK cells. Moreover, trispecific formats (TriKEs) have been created by incorporating an additional scFv fragment targeting another tumor antigen [138].; or alternatively containing IL-15 to induce NK cell expansion [139]. Several BiKEs and TriKEs are undergoing preclinical development [140, 141]. Other strategies to target NK cells for tumor eradication have been reviewed in [142].

Nanoparticle delivery vehicles to improve tumor delivery

In cancer therapy, nanoparticle (NP) delivery systems offer the possibility to modify the pharmacokinetic profile of small molecule cytotoxins and increase tumor targeting as a means to improve therapeutic indices and safety profiles. Nanoparticle delivery systems are typically in the 10-100 nm range, making them susceptible to accumulation in tumor tissues as a consequence of the EPR effect. The EPR refers to the enhanced accumulation of nanostructures in tumor tissue following extravasation through the endothelium that irrigates the neoplasm. The vasculature in these sites is formed rapidly due to an increased demand of oxygen and nutrients and secretion of vascular effectors, leaving large fenestrations or endothelial gaps that allow diffusion of nanoparticles (NPs) that are otherwise too large to penetrate through healthy capillaries [143-145]. Moreover, accumulation of NPs is further enhanced by a decrease in lymphatic drainage [143,

146]. Preferential accumulation due to the EPR effect is termed passive targeting and is an inherent property of nano-sized materials. Importantly, the contribution of the EPR effect in preclinical and clinical settings has been debated and it is known to depend on myriad factors relating to tumor characteristics, including localization, stage, vascular density, fibrotic tumor microenvironment, lymphatic drainage and vascular architecture [144, 147, 148]. Still, the EPR remains a fundamental principle behind the design and development of nanoparticle delivery strategies for solid tumors. Several nanoparticles have also been developed as imaging agents, however this section discusses only those formats intended for therapeutic purposes in oncology.

Since the first reports of the EPR effect in 1986 [143], interest in the development of nanoparticle-delivery platforms has increased substantially and has led to the approval of several NP formulations. At present, liposomal delivery systems comprise the vast majority of nanoparticle-based therapeutics approved for clinical use in oncology and those undergoing clinical development [149]. Doxil (doxorubicin encapsulated in PEGylated liposomes) was the first nano-carrier to be licensed in the US in 1995 for treatment of AIDS-related Kaposi's sarcoma. The first approval of Doxil served as a benchmark for the validation of NP systems in oncology; and the formulation is currently also FDA approved in ovarian cancer and multiple myeloma [150]. Importantly, the approval granted for the aforementioned indications was based on superior safety profiles compared to established therapy; and it also demonstrated superior efficacy in Kaposi's sarcoma [151-153]. Thereafter, ten other nanotherapeutics have entered the clinic (table 2). Except for Abraxane (albumin-bound paclitaxel) and NanoTherm (iron oxide nanoparticles), all other approved nanomedicines consist of liposomal chemotherapeutics [149, 154].

Table 2. Approved nanoparticles in oncology

Name	NP carrier	Targeting	Payload	Indications	Approval date (FDA)
Doxil/Caelyx [149].	Pegylated liposome	Passive	Doxorubicin	• HIV associated Kaposi's sarcoma • Ovarian cancer • Multiple myeloma	1995 (FDA) 1996 (EMA)

Daunoxome [171].	Non-pegylated liposome	Passive	Daunorubicin	• HIV associated Kaposi's sarcoma	1996 (FDA) Discontinued
DepoCyt [172].	Non-pegylated liposome	Passive	Cytarabine	• Lymphomatous meningitis	1999 (FDA) Discontinued
Myocet [173].	Non-pegylated liposome	Passive	Doxorubicin	• Metastatic breast cancer	2000 (EMA)
Abraxane [174].	Albumin nanoparticle	Passive	Paclitaxel	• Advanced non-small-cell lung cancer • Metastatic breast cancer • Metastatic pancreatic adenocarcinoma	2005 (FDA) 2008 (EMA)
Oncaspar [175].	PEG protein conjugate	Passive	L-Asparaginase	• Acute Lymphoblastic Leukemia	2006 (FDA)
MEPACT [176].	Non-pegylated liposome	Passive	Mifamurtide	• Non-metastatic resectable osteosarcoma	2009 (EMA)
Nanotherm [177].	Iron oxide nanoparticle	Passive	Thermal ablation*	• Glioblastoma	2010 (EMA)
Marqibo [178].	Non-pegylated liposome	Passive	Vincristine	• Philadelphia chromosome-negative acute lymphoblastic leukemia	2012 (FDA)
Onivyde [179].	Pegylated liposome	Passive	Irinotecan	• Metastatic pancreatic adenocarcinoma	2015 (FDA)

Vyxeos [180].	Non-pegylated liposome	Passive	Daonorubicin / cytarabine	• Acute myeloid leukemia	2017 (FDA)

FDA, Food and Drug Administration; EMA, European Medicines Agency; HIV, human immunodeficiency virus.

Subsequent advancements in nanoparticle synthesis and engineering have allowed for the development of multifunctional NP delivery platforms with expanded therapeutic capabilities. For instance, a highly attractive characteristic of nanoparticles is the possibility to functionalize their surface with multiple bioactive substances that can aid in tumor localization, treatment and diagnosis. A representative case is CYT-6091, a construct composed of PEGylated gold nanoparticles carrying tumor necrosis factor alpha (TNFα) on its surface that has shown promising results in a phase I clinical trial, wherein the maximum tolerated dose of nano-formulated TNFα exceeded that of native TNFα by 3-fold due to enhanced localization in tumors [155]. Furthermore, NPs can be functionalized with biomolecules that target the tumor stroma to induce changes in the extracellular matrix (ECM) and facilitate uptake. This strategy is conceptually appealing, and it is thought to hold great promise, yet it requires further understanding of the cross-talk between the multiple paracrine interactions that take place during the formation of the ECM [156, 157]. Additionally, the physicochemical properties of the NP format can be tailored to enable controlled release of a drug cargo upon exposure to tumor-specific or external stimuli. Examples of these NP vehicles include pH responsive polymeric micelles, temperature responsive polyN-isopropylacrylamide nanoparticles, light responsive mesoporous silica nanoparticles and redox responsive copolymer-based micelles [91, 158-160].

Active-targeting to increase specificity

Conceptually, the targeting capacity of nanoparticles can be further enhanced through the attachment of target-specific biomolecules, such as mAbs, antibody fragments, aptamers, affimers and peptides. In this modality, nanoparticles can initially accumulate in tumor tissue due to passive targeting and subsequently engage in high affinity interactions with tumoral targets (Figure 4) [161-163]. Most commonly, upregulated cell surface receptors (eg, HER2, EGFR, transferrin receptor, folate receptor) are targeted, wherein the multivalent presentation of targeting agent on the NP surface can cause receptor cross-linking and induce receptor-mediated endocytosis – an

advantageous feature for intracellular drug delivery [164]. Monoclonal antibodies play a pivotal role in this strategy due to their exquisite specificity; as well as to the existence of well-established techniques – primarily phage display – that allow for high-throughput development of mAbs to specific antigens. Additionally, the prevailing clinical success of monoclonal antibodies is favorable for regulatory approval.
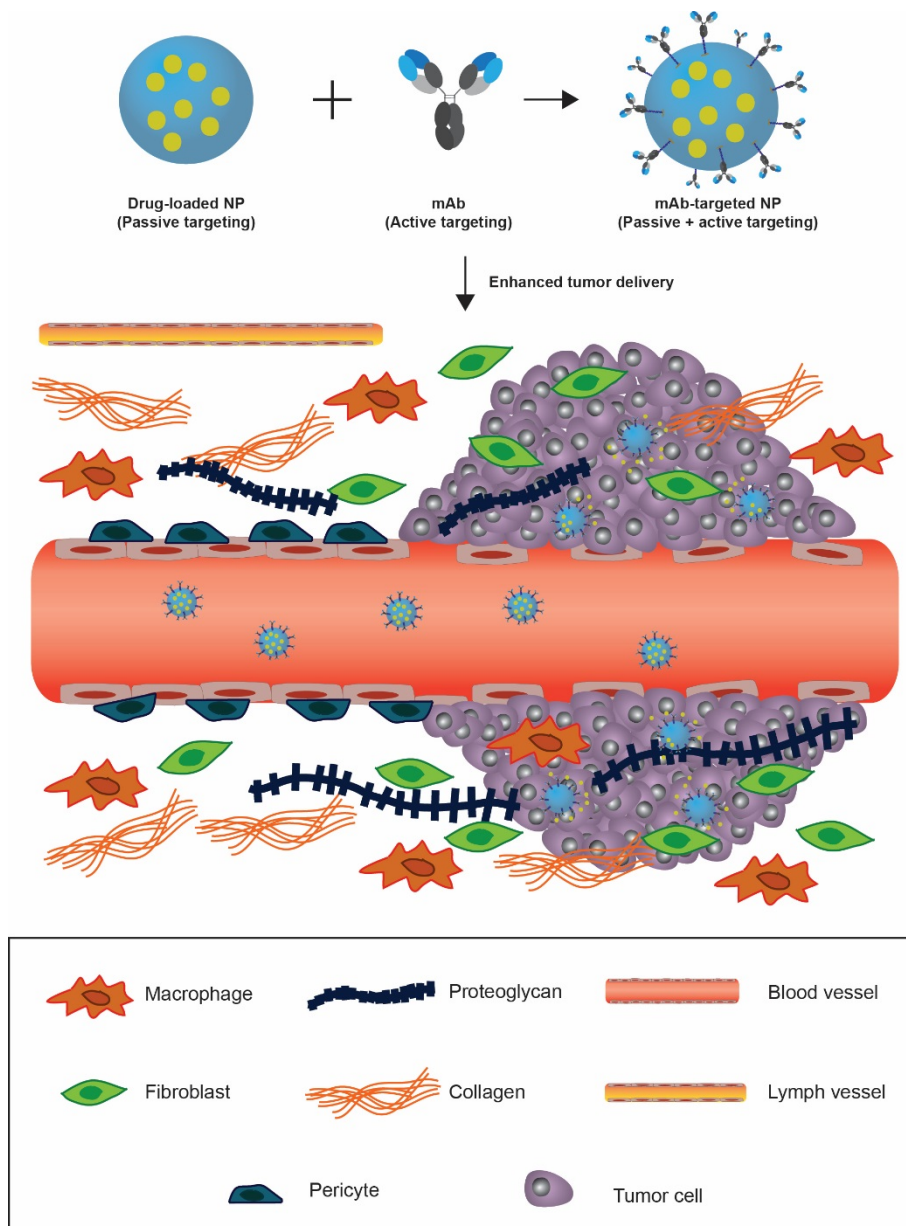
Figure 4. Harnessing the EPR effect to improve tumor delivery using nanoparticle carriers. Blood vessels that irrigate the tumor tissue are defective. The lack of pericytes and altered structural features make the vessels less stable and leakier. Larger fenestrations between the

endothelial cells allow nanoparticles to extravasate into the tumor. The fibrotic ECM lacks proper lymphatic drainage, therefore nanoparticles can accumulate in the tissue following extravasation (passive targeting). Nanoparticles can be functionalized with monoclonal antibodies, or other active targeting agents, to promote specific internalization and drug delivery into targeted cells (cancer cells or other cells in the tumor microenvironment) once they accumulate in the tumor through passive targeting.

At present, a plethora of active-targeted nanoparticles have undergone preclinical development, however only a few have initiated clinical trials. A notable example is BIND-014, a docetaxel-containing polymeric nanoparticle targeting the prostate-specific membrane antigen (PSMA) that has recently completed phase II clinical trials for various cancers, where it has demonstrated clinical efficacy and acceptable safety profiles [165]. Recently, paclitaxel solid lipid nanoparticles conjugated to various antibodies as targeting agents have demonstrated remarkable pharmacokinetic properties and efficacy in mouse models, and have started clinical development [166].

In its inception, active targeting was intended to aid tumor localization and retention in conjunction with passive targeting. Notwithstanding, experimental data has demonstrated that while engagement and internalization within cancer cells are significantly increased, tumor accumulation is only marginally improved [20, 163, 167]. An extensive analysis of *in vivo* data published from 2005-2015 showed that passive targeting results in 0.6% (median) of the injected dose accumulating in tumor tissue, compared to 0.9% with active-targeted nanoparticles [147]. It is noteworthy to underscore that these data were obtained with several different nanoparticle formats administered in a wide variety of solid tumors. Still, it suggests that accumulation via passive targeting is essential for enhanced delivery of payloads through active-targeting. Consequently, successful clinical implementation of both passive and active-targeted nanoparticles will require a better understanding of the physiological factors that determine the extent of EPR accumulation in order to identify patients that can benefit from this approach [168]. Alternatively, therapeutic strategies to increase EPR-related accumulation can be implemented, such as administration of angiotensin-II receptor blockers to increase vessel perfusion, or sonoporation to promote vascular permeability [169, 170].

Conclusion

Improving tumor penetration and distribution upon systemic delivery are crucial requirements in mAb therapy to improve clinical outcomes and prevent the emergence of acquired resistance mechanisms. Preventing treatment failure due to intrinsic resistance will require a better understanding of cancer biology and the identification of novel biomarkers for a better selection of therapeutic agents and treatment regimens. The clinical pipeline of alternative mAb based approaches to enhance clinical efficacy has experienced a marked expansion in the last decade. The formats discussed in this review – ADC, immune-checkpoint inhibitors and nanoparticle-delivery systems – are among key strategies with demonstrated clinical benefits in the treatment of solid tumors. Of note is the accelerated growth of the ICI class having obtained regulatory approval for 6 distinct antibodies since the year 2011 (first approval) and a remarkable broadening of clinical indications. Despite their clinical success, these therapeutics are based on relatively new technologies that are still undergoing extensive efforts to optimize therapeutic potential. Numerous ICI antibodies targeting alternative targets for immune inhibition (eg, LAG-3, TIM-3, TIGIT, VISTA, B7-H3) are in phase I/II clinical trials. Safety concerns inherent to the high potency and structural versatility of ADCs and nanoparticles have been prominent barriers in their implementation, but clinical validation of novel designs could bring about major breakthroughs in these fields in the coming years.

Acknowledgments

Disclosure

The authors declare no conflicts of interest in this work.

References

[1]. Z. Elgundi, M. Reslan, E. Cruz, V. Sifniotis, V. Kayser, The state-of-play and future of antibody therapeutics, Advanced drug delivery reviews, 122 (2017) 2-19.

[2]. J. Chung, Special issue on therapeutic antibodies and biopharmaceuticals, Experimental &Amp; Molecular Medicine, 49 (2017) e304.

[3]. A.L. Grilo, A. Mantalaris, The Increasingly Human and Profitable Monoclonal Antibody Market, Trends in Biotechnology, (2018).

[4]. U.S. Food and Drug Administration, Drugs@FDA: FDA Approved Drug Products, 2018.

[5]. W. De Roock, B. Claes, D. Bernasconi, J. De Schutter, B. Biesmans, G. Fountzilas, K.T. Kalogeras, V. Kotoula, D. Papamichael, P. Laurent-Puig, F. Penault-Llorca, P. Rougier, B. Vincenzi, D. Santini, G. Tonini, F. Cappuzzo, M. Frattini, F. Molinari, P. Saletti, S. De Dosso, M. Martini, A. Bardelli, S. Siena, A. Sartore-Bianchi, J. Tabernero, T. Macarulla, F. Di Fiore, A.O. Gangloff, F. Ciardiello, P. Pfeiffer, C. Qvortrup, T.P. Hansen, E. Van Cutsem, H. Piessevaux, D. Lambrechts, M. Delorenzi, S. Tejpar, Effects of KRAS, BRAF, NRAS, and PIK3CA mutations on the efficacy of cetuximab plus chemotherapy in chemotherapy-refractory metastatic colorectal cancer: a retrospective consortium analysis, The Lancet Oncology, 11 (2010) 753-762.

[6]. M.H. Jin, A.R. Nam, J.E. Park, J.H. Bang, Y.J. Bang, D.Y. Oh, Resistance Mechanism against Trastuzumab in HER2-Positive Cancer Cells and Its Negation by Src Inhibition, Molecular cancer therapeutics, 16 (2017) 1145-1154.

[7]. J.H.E. Baker, A.H. Kyle, S.A. Reinsberg, F. Moosvi, H.M. Patrick, J. Cran, K. Saatchi, U. Hafeli, A.I. Minchinton, Heterogeneous distribution of trastuzumab in HER2-positive xenografts and metastases: role of the tumor microenvironment, Clinical & experimental metastasis, 35 (2018) 691-705.

[8]. C.P. Pallasch, I. Leskov, C.J. Braun, D. Vorholt, A. Drake, Y.M. Soto-Feliciano, E.H. Bent, J. Schwamb, B. Iliopoulou, N. Kutsch, N. van Rooijen, L.P. Frenzel, C.M. Wendtner, L. Heukamp, K.A. Kreuzer, M. Hallek, J. Chen, M.T. Hemann, Sensitizing protective tumor microenvironments to antibody-mediated therapy, Cell, 156 (2014) 590-602.

[9]. L.T. Baxter, R.K. Jain, Transport of fluid and macromolecules in tumors. I. Role of interstitial pressure and convection, Microvascular Research, 37 (1989) 77-104.

[10]. M. Juweid, R. Neumann, C. Paik, M.J. Perez-Bacete, J. Sato, W. van Osdol, J.N. Weinstein, Micropharmacology of monoclonal antibodies in solid tumors: direct experimental evidence for a binding site barrier, Cancer research, 52 (1992) 5144-5153.

[11]. D. Bhutani, U.N. Vaishampayan, Monoclonal antibodies in oncology therapeutics: present and future indications, Expert opinion on biological therapy, 13 (2013) 269-282.

[12]. P.A. Netti, L.T. Baxter, Y. Boucher, R. Skalak, R.K. Jain, Time-dependent behavior of interstitial fluid pressure in solid tumors: implications for drug delivery, Cancer research, 55 (1995) 5451-5458.

[13]. J.S. Young, C.E. Llumsden, A.L. Stalker, The significance of the "tissue pressure" of normal testicular and of neoplastic (Brown-Pearce carcinoma) tissue in the rabbit, The Journal of Pathology and Bacteriology, 62 (1950) 313-333.

[14]. J.R. Less, M.C. Posner, Y. Boucher, D. Borochovitz, N. Wolmark, R.K. Jain, Interstitial hypertension in human breast and colorectal tumors, Cancer research, 52 (1992) 6371-6374.

[15]. G.M. Thurber, M.M. Schmidt, K.D. Wittrup, Antibody tumor penetration: transport opposed by systemic and antigen-mediated clearance, Advanced drug delivery reviews, 60 (2008) 1421-1434.

[16]. K. Fujimori, D.G. Covell, J.E. Fletcher, J.N. Weinstein, A modeling analysis of monoclonal antibody percolation through tumors: a binding-site barrier, Journal of nuclear medicine : official publication, Society of Nuclear Medicine, 31 (1990) 1191-1198.

[17]. T. Saga, R.D. Neumann, T. Heya, J. Sato, S. Kinuya, N. Le, C.H. Paik, J.N. Weinstein, Targeting cancer micrometastases with monoclonal antibodies: a binding-site barrier, Proceedings of the National Academy of Sciences of the United States of America, 92 (1995) 8999-9003.

[18]. G.M. Thurber, S.C. Zajic, K.D. Wittrup, Theoretic criteria for antibody penetration into solid tumors and micrometastases, Journal of nuclear medicine : official publication, Society of Nuclear Medicine, 48 (2007) 995-999.

[19]. C.M. Lee, I.F. Tannock, The distribution of the therapeutic monoclonal antibodies cetuximab and trastuzumab within solid tumors, BMC cancer, 10 (2010) 255.

[20]. M.M. Schmidt, K.D. Wittrup, A modeling analysis of the effects of molecular size and binding affinity on tumor targeting, Molecular cancer therapeutics, 8 (2009) 2861-2871.

[21]. R.J. Keizer, A.D. Huitema, J.H. Schellens, J.H. Beijnen, Clinical pharmacokinetics of therapeutic monoclonal antibodies, Clinical pharmacokinetics, 49 (2010) 493-507.

[22]. G.M. Thurber, M.M. Schmidt, K.D. Wittrup, Factors determining antibody distribution in tumors, Trends in pharmacological sciences, 29 (2008) 57-61.

[23]. A.P. Chapman, P. Antoniw, M. Spitali, S. West, S. Stephens, D.J. King, Therapeutic antibody fragments with prolonged *in vivo* half-lives, Nature Biotechnology, 17 (1999) 780.

[24]. G.J. Weiner, Monoclonal antibody mechanisms of action in cancer, Immunologic research, 39 (2007) 271-278.

[25]. R. Gennari, S. Menard, F. Fagnoni, L. Ponchio, M. Scelsi, E. Tagliabue, F. Castiglioni, L. Villani, C. Magalotti, N. Gibelli, B. Oliviero, B. Ballardini, G.D. Prada, A. Zambelli, A. Costa, Pilot Study of the Mechanism of Action of Preoperative Trastuzumab in Patients with Primary Operable Breast Tumors Overexpressing HER2, Clinical Cancer Research, 10 (2004) 5650.

[26]. R.A. Clynes, T.L. Towers, L.G. Presta, J.V. Ravetch, Inhibitory Fc receptors modulate *in vivo* cytoxicity against tumor targets, Nature Medicine, 6 (2000) 443.

[27]. L. Reslan, S. Dalle, C. Dumontet, Understanding and circumventing resistance to anticancer monoclonal antibodies, mAbs, 1 (2009) 222-229.

[28]. A. Viloria-Petit, T. Crombet, S. Jothy, D. Hicklin, P. Bohlen, J.M. Schlaeppi, J. Rak, R.S. Kerbel, Acquired resistance to the antitumor effect of epidermal growth factor receptor-blocking antibodies *in vivo*: a role for altered tumor angiogenesis, Cancer research, 61 (2001) 5090-5101.

[29]. D.J. Slamon, B. Leyland-Jones, S. Shak, H. Fuchs, V. Paton, A. Bajamonde, T. Fleming, W. Eiermann, J. Wolter, M. Pegram, J. Baselga, L. Norton, Use of chemotherapy plus a monoclonal antibody against HER2 for metastatic breast cancer that overexpresses HER2, The New England journal of medicine, 344 (2001) 783-792.

[30]. D.J. Slamon, G.M. Clark, S.G. Wong, W.J. Levin, A. Ullrich, W.L. McGuire, Human breast cancer: correlation of relapse and survival with amplification of the HER-2/neu oncogene, Science (New York, N.Y.), 235 (1987) 177-182.

[31]. S.M. Tovey, S. Brown, J.C. Doughty, E.A. Mallon, T.G. Cooke, J. Edwards, Poor survival outcomes in HER2-positive breast cancer patients with low-grade, node-negative tumours, British journal of cancer, 100 (2009) 680-683.

[32]. Z. Mitri, T. Constantine, R. O'Regan, The HER2 Receptor in Breast Cancer: Pathophysiology, Clinical Use, and New Advances in Therapy, Chemotherapy research and practice, 2012 (2012) 743193-743193.

[33]. T. Yamamoto, S. Ikawa, T. Akiyama, K. Semba, N. Nomura, N. Miyajima, T. Saito, K. Toyoshima, Similarity of protein encoded by the human c-erb-B-2 gene to epidermal growth factor receptor, Nature, 319 (1986) 230-234.

[34]. X.F. Le, F.X. Claret, A. Lammayot, L. Tian, D. Deshpande, R. LaPushin, A.M. Tari, R.C. Bast, Jr., The role of cyclin-dependent kinase inhibitor p27Kip1 in anti-HER2 antibody-induced G1 cell cycle arrest and tumor growth inhibition, The Journal of biological chemistry, 278 (2003) 23441-23450.

[35]. M. Barok, J. Isola, Z. Palyi-Krekk, P. Nagy, I. Juhasz, G. Vereb, P. Kauraniemi, A. Kapanen, M. Tanner, G. Vereb, J. Szollosi, Trastuzumab causes antibody-dependent cellular cytotoxicity-mediated growth inhibition of submacroscopic JIMT-1 breast cancer xenografts despite intrinsic drug resistance, Molecular cancer therapeutics, 6 (2007) 2065-2072.

[36]. B. Petricevic, J. Laengle, J. Singer, M. Sachet, J. Fazekas, G. Steger, R. Bartsch, E. Jensen-Jarolim, M. Bergmann, Trastuzumab mediates antibody-dependent cell-mediated cytotoxicity and phagocytosis to the same extent in both adjuvant and metastatic HER2/neu breast cancer patients, Journal of Translational Medicine, 11 (2013) 307-307.

[37]. R.A. Clynes, T.L. Towers, L.G. Presta, J.V. Ravetch, Inhibitory Fc receptors modulate *in vivo* cytotoxicity against tumor targets, Nat Med, 6 (2000) 443-446.

[38]. Y. Shi, X. Fan, H. Deng, R.J. Brezski, M. Rycyzyn, R.E. Jordan, W.R. Strohl, Q. Zou, N. Zhang, Z. An, Trastuzumab triggers phagocytic killing of high HER2 cancer cells *in vitro* and *in vivo* by interaction with Fcgamma receptors on macrophages, Journal of immunology (Baltimore, Md. : 1950), 194 (2015) 4379-4386.

[39]. S. Mamidi, M. Cinci, M. Hasmann, V. Fehring, M. Kirschfink, Lipoplex mediated silencing of membrane regulators (CD46, CD55 and CD59) enhances complement-dependent anti-tumor activity of trastuzumab and pertuzumab, Molecular oncology, 7 (2013) 580-594.

[40]. M. Scaltriti, F. Rojo, A. Ocana, J. Anido, M. Guzman, J. Cortes, S. Di Cosimo, X. Matias-Guiu, S. Ramon y Cajal, J. Arribas, J. Baselga, Expression of p95HER2, a truncated form of the HER2 receptor, and response to anti-HER2 therapies in breast cancer, Journal of the National Cancer Institute, 99 (2007) 628-638.

[41]. N.E. Ben–Baruch, R. Bose, S.M. Kavuri, C.X. Ma, M.J. Ellis, HER2 mutated breast cancer responds to treatment with single agent neratinib, a second generation HER2/EGFR tyrosine kinase inhibitor, Journal of the National Comprehensive Cancer Network : JNCCN, 13 (2015) 1061-1064.

[42]. B.N. Rexer, C.L. Arteaga, Intrinsic and Acquired Resistance to HER2-Targeted Therapies in HER2 Gene-Amplified Breast Cancer: Mechanisms and Clinical Implications, Critical Reviews in Oncogenesis, 17 (2012) 1-16.

[43]. P. Nagy, E. Friedlander, M. Tanner, A.I. Kapanen, K.L. Carraway, J. Isola, T.M. Jovin, Decreased accessibility and lack of activation of ErbB2 in JIMT-1, a herceptin-resistant, MUC4-expressing breast cancer cell line, Cancer research, 65 (2005) 473-482.

[44]. J.D. Black, S. Lopez, E. Cocco, S. Bellone, G. Altwerger, C.L. Schwab, D.P. English, E. Bonazzoli, F. Predolini, F. Ferrari, E. Ratner, D.-A. Silasi, M. Azodi, P.E. Schwartz, A.D. Santin, PIK3CA oncogenic mutations represent a major mechanism of resistance to trastuzumab in HER2/neu overexpressing uterine serous carcinomas, British Journal of Cancer, 113 (2015) 1020-1026.

[45]. C. Kim, C.-K. Lee, H.J. Chon, J.H. Kim, H.S. Park, S.J. Heo, H.J. Kim, T.S. Kim, W.S. Kwon, H.C. Chung, S.Y. Rha, PTEN loss and level of HER2 amplification is associated with trastuzumab resistance and prognosis in HER2-positive gastric cancer, Oncotarget, 8 (2017) 113494-113501.

[46]. R. Nahta, L.X. Yuan, B. Zhang, R. Kobayashi, F.J. Esteva, Insulin-like growth factor-I receptor/human epidermal growth factor receptor 2 heterodimerization contributes to trastuzumab resistance of breast cancer cells, Cancer research, 65 (2005) 11118-11128.

[47]. G. Zhuang, D.M. Brantley-Sieders, D. Vaught, J. Yu, L. Xie, S. Wells, D. Jackson, R. Muraoka-Cook, C. Arteaga, J. Chen, Elevation of receptor tyrosine kinase EphA2 mediates resistance to trastuzumab therapy, Cancer research, 70 (2010) 299-308.

[48]. K. Liang, F.J. Esteva, C. Albarracin, K. Stemke-Hale, Y. Lu, G. Bianchini, C.Y. Yang, Y. Li, X. Li, C.T. Chen, G.B. Mills, G.N. Hortobagyi, J. Mendelsohn, M.C. Hung, Z. Fan, Recombinant human erythropoietin antagonizes trastuzumab treatment of breast cancer cells via Jak2-mediated Src activation and PTEN inactivation, Cancer cell, 18 (2010) 423-435.

[49]. D.L. Shattuck, J.K. Miller, K.L. Carraway, 3rd, C. Sweeney, Met receptor contributes to trastuzumab resistance of Her2-overexpressing breast cancer cells, Cancer research, 68 (2008) 1471-1477.

[50]. J.A. Foekens, J.G.M. Klijn, P.I.M. Schmitz, P.M.J.J. Berns, The Clinical Significance of Epidermal Growth Factor Receptor (EGF-R) in Human Breast Cancer: A Review on 5232 Patients*, Endocrine Reviews, 13 (1992) 3-17.

[51]. S.H. Lu, L.L. Hsieh, F.C. Luo, I.B. Weinstein, Amplification of the EGF receptor and c-myc genes in human esophageal cancers, International journal of cancer, 42 (1988) 502-505.

[52]. A. Ochiai, A. Takanashi, N. Takekura, K. Yoshida, S. Miyamori, T. Harada, E. Tahara, Effect of human epidermal growth factor on cell growth and its receptor in human gastric carcinoma cell lines, Japanese journal of clinical oncology, 18 (1988) 15-25.

[53]. P. Kirkpatrick, J. Graham, M. Muhsin, Cetuximab, Nature Reviews Drug Discovery, 3 (2004) 549.

[54]. C.D. Andl, T. Mizushima, K. Oyama, M. Bowser, H. Nakagawa, A.K. Rustgi, EGFR-induced cell migration is mediated predominantly by the JAK-STAT pathway in primary esophageal keratinocytes, American journal of physiology. Gastrointestinal and liver physiology, 287 (2004) G1227-1237.

[55]. P. Wee, Z. Wang, Epidermal Growth Factor Receptor Cell Proliferation Signaling Pathways, Cancers, 9 (2017) 52.

[56]. F. Walker, J. Rothacker, C. Henderson, E.C. Nice, B. Catimel, H.H. Zhang, A.M. Scott, M.F. Bailey, S.G. Orchard, T.E. Adams, Z. Liu, T.P. Garrett, A.H. Clayton, A.W. Burgess, Ligand binding induces a conformational change in epidermal growth factor receptor dimers, Growth factors (Chur, Switzerland), 30 (2012) 394-409.

[57]. S. Li, K.R. Schmitz, P.D. Jeffrey, J.J.W. Wiltzius, P. Kussie, K.M. Ferguson, Structural basis for inhibition of the epidermal growth factor receptor by cetuximab, Cancer cell, 7 (2005) 301-311.

[58]. R.B. Luwor, Y. Lu, X. Li, J. Mendelsohn, Z. Fan, The antiepidermal growth factor receptor monoclonal antibody cetuximab/C225 reduces hypoxia-inducible factor-1 alpha, leading to transcriptional inhibition of vascular endothelial growth factor expression, Oncogene, 24 (2005) 4433-4441.

[59]. S. Chen, X. Li, R. Chen, M. Yin, Q. Zheng, Cetuximab intensifies the ADCC activity of adoptive NK cells in a nude mouse colorectal cancer xenograft model, Oncology Letters, 12 (2016) 1868-1876.

[60]. G.A. Milano, ADCC and treatment outcome in colorectal cancer patients receiving cetuximab-based therapy, Journal of Clinical Oncology, 34 (2016) e15085-e15085.

[61]. B. Zhao, L. Wang, H. Qiu, M. Zhang, L. Sun, P. Peng, Q. Yu, X. Yuan, Mechanisms of resistance to anti-EGFR therapy in colorectal cancer, Oncotarget, 8 (2016) 3980-4000.

[62]. J.M. Xu, Y. Wang, Y.L. Wang, Y. Wang, T. Liu, M. Ni, M.S. Li, L. Lin, F.J. Ge, C. Gong, J.Y. Gu, R. Jia, H.F. Wang, Y.L. Chen, R.R. Liu, C.H. Zhao, Z.L. Tan, Y. Jin, Y.P. Zhu, S. Ogino, Z.R. Qian, PIK3CA Mutations Contribute to Acquired Cetuximab Resistance in Patients with Metastatic Colorectal Cancer, Clinical cancer research : an official journal of the American Association for Cancer Research, 23 (2017) 4602-4616.

[63]. H.C. Hsu, T.K. Thiam, Y.J. Lu, C.Y. Yeh, W.S. Tsai, J.F. You, H.Y. Hung, C.N. Tsai, A. Hsu, H.C. Chen, S.J. Chen, T.S. Yang, Mutations of KRAS/NRAS/BRAF predict cetuximab resistance in metastatic colorectal cancer patients, Oncotarget, 7 (2016) 22257-22270.

[64]. M. Moroni, S. Veronese, S. Benvenuti, G. Marrapese, A. Sartore-Bianchi, F. Di Nicolantonio, M. Gambacorta, S. Siena, A. Bardelli, Gene copy number for epidermal growth factor receptor (EGFR) and clinical response to antiEGFR treatment in colorectal cancer: a cohort study, The Lancet. Oncology, 6 (2005) 279-286.

[65]. S. Khambata-Ford, C.R. Garrett, N.J. Meropol, M. Basik, C.T. Harbison, S. Wu, T.W. Wong, X. Huang, C.H. Takimoto, A.K. Godwin, B.R. Tan, S.S. Krishnamurthi, H.A. Burris, 3rd, E.A. Poplin, M. Hidalgo, J. Baselga, E.A. Clark, D.J. Mauro, Expression of epiregulin and amphiregulin and K-ras mutation status predict disease control in metastatic colorectal cancer patients treated with cetuximab, Journal of clinical oncology : official journal of the American Society of Clinical Oncology, 25 (2007) 3230-3237.

[66]. Y. Lu, X. Li, K. Liang, R. Luwor, Z.H. Siddik, G.B. Mills, J. Mendelsohn, Z. Fan, Epidermal growth factor receptor (EGFR) ubiquitination as a mechanism of acquired resistance escaping treatment by the anti-EGFR monoclonal antibody cetuximab, Cancer research, 67 (2007) 8240-8247.

[67]. F. Braig, M. Marz, A. Schieferdecker, A. Schulte, M. Voigt, A. Stein, T. Grob, M. Alawi, D. Indenbirken, M. Kriegs, E. Engel, U. Vanhoefer, A. Grundhoff, S. Loges, K. Riecken, B. Fehse, C. Bokemeyer, M. Binder, Epidermal growth factor receptor mutation mediates cross-resistance to panitumumab and cetuximab in gastrointestinal cancer, Oncotarget, 6 (2015) 12035-12047.

[68]. B.O. Van Emburgh, S. Arena, G. Siravegna, L. Lazzari, G. Crisafulli, G. Corti, B. Mussolin, F. Baldi, M. Buscarino, A. Bartolini, E. Valtorta, J. Vidal, B. Bellosillo, G. Germano, F. Pietrantonio, A. Ponzetti, J. Albanell, S. Siena, A. Sartore-Bianchi, F. Di Nicolantonio, C. Montagut, A. Bardelli, Acquired RAS or EGFR mutations and duration of response to EGFR blockade in colorectal cancer, Nature communications, 7 (2016) 13665.

[69]. F. Li, K.K. Emmerton, M. Jonas, X. Zhang, J.B. Miyamoto, J.R. Setter, N.D. Nicholas, N.M. Okeley, R.P. Lyon, D.R. Benjamin, C.L. Law, Intracellular Released Payload Influences Potency and Bystander-Killing Effects of Antibody-Drug Conjugates in Preclinical Models, Cancer research, 76 (2016) 2710-2719.

[70]. N.M. Okeley, J.B. Miyamoto, X. Zhang, R.J. Sanderson, D.R. Benjamin, E.L. Sievers, P.D. Senter, S.C. Alley, Intracellular activation of SGN-35, a potent anti-CD30 antibody-drug

conjugate, Clinical cancer research : an official journal of the American Association for Cancer Research, 16 (2010) 888-897.

[71]. P.F. Bross, J. Beitz, G. Chen, X.H. Chen, E. Duffy, L. Kieffer, S. Roy, R. Sridhara, A. Rahman, G. Williams, R. Pazdur, Approval summary: gemtuzumab ozogamicin in relapsed acute myeloid leukemia, Clinical cancer research : an official journal of the American Association for Cancer Research, 7 (2001) 1490-1496.

[72]. S.H. Petersdorf, K.J. Kopecky, M. Slovak, C. Willman, T. Nevill, J. Brandwein, R.A. Larson, H.P. Erba, P.J. Stiff, R.K. Stuart, R.B. Walter, M.S. Tallman, L. Stenke, F.R. Appelbaum, A phase 3 study of gemtuzumab ozogamicin during induction and postconsolidation therapy in younger patients with acute myeloid leukemia, Blood, 121 (2013) 4854.

[73]. F.J. Giles, H.M. Kantarjian, S.M. Kornblau, D.A. Thomas, G. Garcia-Manero, T.A. Waddelow, C.L. David, A.T. Phan, D.E. Colburn, A. Rashid, E.H. Estey, Mylotarg™ (gemtuzumab ozogamicin) therapy is associated with hepatic venoocclusive disease in patients who have not received stem cell transplantation, Cancer, 92 (2001) 406-413.

[74]. K.J. Norsworthy, C.W. Ko, J.E. Lee, J. Liu, C.S. John, D. Przepiorka, A.T. Farrell, R. Pazdur, FDA Approval Summary: Mylotarg for Treatment of Patients with Relapsed or Refractory CD33-Positive Acute Myeloid Leukemia, The oncologist, (2018).

[75]. E.Y. Jen, C.W. Ko, J.E. Lee, P.L. Del Valle, A. Aydanian, C. Jewell, K.J. Norsworthy, D. Przepiorka, L. Nie, J. Liu, C.M. Sheth, M. Shapiro, A.T. Farrell, R. Pazdur, FDA Approval: Gemtuzumab Ozogamicin for the Treatment of Adults with Newly Diagnosed CD33-Positive Acute Myeloid Leukemia, Clinical cancer research : an official journal of the American Association for Cancer Research, 24 (2018) 3242-3246.

[76]. C. Deng, B. Pan, O.A. Connor, Brentuximab Vedotin, Clinical Cancer Research, 19 (2013) 22.

[77]. FDA Approves Kadcyla for Breast Cancer, Cancer Discovery, 3 (2013) 366.

[78]. I.R. Yurkiewicz, L. Muffly, M. Liedtke, Inotuzumab ozogamicin: a CD22 mAb-drug conjugate for adult relapsed or refractory B-cell precursor acute lymphoblastic leukemia, Drug design, development and therapy, 12 (2018) 2293-2300.

[79]. H. Saber, J.K. Leighton, An FDA oncology analysis of antibody-drug conjugates, Regulatory toxicology and pharmacology : RTP, 71 (2015) 444-452.

[80]. J.C. Masters, D.J. Nickens, D. Xuan, R.L. Shazer, M. Amantea, Clinical toxicity of antibody drug conjugates: a meta-analysis of payloads, Investigational new drugs, 36 (2018) 121-135.

[81]. Y.-B. Hu, E.B. Dammer, R.-J. Ren, G. Wang, The endosomal-lysosomal system: from acidification and cargo sorting to neurodegeneration, Translational neurodegeneration, 4 (2015) 18-18.

[82]. R.S. Greenfield, T. Kaneko, A. Daues, M.A. Edson, K.A. Fitzgerald, L.J. Olech, J.A. Grattan, G.L. Spitalny, G.R. Braslawsky, Evaluation in Vitro of Adriamycin Immunoconjugates Synthesized Using an Acid-sensitive Hydrazone Linker, Cancer research, 50 (1990) 6600.

[83]. P.R. Hamann, L.M. Hinman, I. Hollander, C.F. Beyer, D. Lindh, R. Holcomb, W. Hallett, H.-R. Tsou, J. Upeslacis, D. Shochat, A. Mountain, D.A. Flowers, I. Bernstein, Gemtuzumab Ozogamicin, A Potent and Selective Anti-CD33 Antibody−Calicheamicin Conjugate for Treatment of Acute Myeloid Leukemia, Bioconjugate Chemistry, 13 (2002) 47-58.

[84]. G.D. Lewis Phillips, G. Li, D.L. Dugger, L.M. Crocker, K.L. Parsons, E. Mai, W.A. Blättler, J.M. Lambert, R.V.J. Chari, R.J. Lutz, W.L.T. Wong, F.S. Jacobson, H. Koeppen, R.H. Schwall, S.R. Kenkare-Mitra, S.D. Spencer, M.X. Sliwkowski, Targeting HER2-Positive Breast Cancer with Trastuzumab-DM1, an Antibody–Cytotoxic Drug Conjugate, Cancer research, 68 (2008) 9280.

[85]. Y. Wang, S. Fan, W. Zhong, X. Zhou, S. Li, Development and Properties of Valine-Alanine based Antibody-Drug Conjugates with Monomethyl Auristatin E as the Potent Payload, International journal of molecular sciences, 18 (2017).

[86]. A.A. Wakankar, M.B. Feeney, J. Rivera, Y. Chen, M. Kim, V.K. Sharma, Y.J. Wang, Physicochemical stability of the antibody-drug conjugate Trastuzumab-DM1: changes due to modification and conjugation processes, Bioconjug Chem, 21 (2010) 1588-1595.

[87]. X. Sun, J.F. Ponte, N.C. Yoder, R. Laleau, J. Coccia, L. Lanieri, Q. Qiu, R. Wu, E. Hong, M. Bogalhas, L. Wang, L. Dong, Y. Setiady, E.K. Maloney, O. Ab, X. Zhang, J. Pinkas, T.A.

Keating, R. Chari, H.K. Erickson, J.M. Lambert, Effects of Drug-Antibody Ratio on Pharmacokinetics, Biodistribution, Efficacy, and Tolerability of Antibody-Maytansinoid Conjugates, Bioconjug Chem, 28 (2017) 1371-1381.

[88]. G.W. Seegan, C.A. Smith, V.N. Schumaker, Changes in quaternary structure of IgG upon reduction of the interheavy-chain disulfide bond, Proceedings of the National Academy of Sciences of the United States of America, 76 (1979) 907-911.

[89]. P.L. Ross, J.L. Wolfe, Physical and Chemical Stability of Antibody Drug Conjugates: Current Status, Journal of pharmaceutical sciences, 105 (2016) 391-397.

[90]. J.Y. Axup, K.M. Bajjuri, M. Ritland, B.M. Hutchins, C.H. Kim, S.A. Kazane, R. Halder, J.S. Forsyth, A.F. Santidrian, K. Stafin, Y. Lu, H. Tran, A.J. Seller, S.L. Biroc, A. Szydlik, J.K. Pinkstaff, F. Tian, S.C. Sinha, B. Felding-Habermann, V.V. Smider, P.G. Schultz, Synthesis of site-specific antibody-drug conjugates using unnatural amino acids, Proceedings of the National Academy of Sciences, 109 (2012) 16101.

[91]. M.P. VanBrunt, K. Shanebeck, Z. Caldwell, J. Johnson, P. Thompson, T. Martin, H. Dong, G. Li, H. Xu, F. D'Hooge, L. Masterson, P. Bariola, A. Tiberghien, E. Ezeadi, D.G. Williams, J.A. Hartley, P.W. Howard, K.H. Grabstein, M.A. Bowen, M. Marelli, Genetically Encoded Azide Containing Amino Acid in Mammalian Cells Enables Site-Specific Antibody-Drug Conjugates Using Click Cycloaddition Chemistry, Bioconjug Chem, 26 (2015) 2249-2260.

[92]. T. Hofer, J.D. Thomas, T.R. Burke, Jr., C. Rader, An engineered selenocysteine defines a unique class of antibody derivatives, Proc Natl Acad Sci U S A, 105 (2008) 12451-12456.

[93]. P. Strop, S.H. Liu, M. Dorywalska, K. Delaria, R.G. Dushin, T.T. Tran, W.H. Ho, S. Farias, M.G. Casas, Y. Abdiche, D. Zhou, R. Chandrasekaran, C. Samain, C. Loo, A. Rossi, M. Rickert, S. Krimm, T. Wong, S.M. Chin, J. Yu, J. Dilley, J. Chaparro-Riggers, G.F. Filzen, C.J. O'Donnell, F. Wang, J.S. Myers, J. Pons, D.L. Shelton, A. Rajpal, Location matters: site of conjugation modulates stability and pharmacokinetics of antibody drug conjugates, Chemistry & biology, 20 (2013) 161-167.

[94]. X. Li, T. Fang, G.-J. Boons, Preparation of well-defined antibody-drug conjugates through glycan remodeling and strain-promoted azide-alkyne cycloadditions, Angewandte Chemie (International ed. in English), 53 (2014) 7179-7182.

[95]. C.R. Behrens, E.H. Ha, L.L. Chinn, S. Bowers, G. Probst, M. Fitch-Bruhns, J. Monteon, A. Valdiosera, A. Bermudez, S. Liao-Chan, T. Wong, J. Melnick, J.W. Theunissen, M.R. Flory, D. Houser, K. Venstrom, Z. Levashova, P. Sauer, T.S. Migone, E.H. van der Horst, R.L. Halcomb, D.Y. Jackson, Antibody-Drug Conjugates (ADCs) Derived from Interchain Cysteine Cross-Linking Demonstrate Improved Homogeneity and Other Pharmacological Properties over Conventional Heterogeneous ADCs, Molecular pharmaceutics, 12 (2015) 3986-3998.

[96]. P. Bryant, M. Pabst, G. Badescu, M. Bird, W. McDowell, E. Jamieson, J. Swierkosz, K. Jurlewicz, R. Tommasi, K. Henseleit, X. Sheng, N. Camper, A. Manin, K. Kozakowska, K. Peciak, E. Laurine, R. Grygorash, A. Kyle, D. Morris, V. Parekh, A. Abhilash, J.W. Choi, J. Edwards, M. Frigerio, M.P. Baker, A. Godwin, *In Vitro* and *In Vivo* Evaluation of Cysteine Rebridged Trastuzumab-MMAE Antibody Drug Conjugates with Defined Drug-to-Antibody Ratios, Molecular pharmaceutics, 12 (2015) 1872-1879.

[97]. J.M. Lambert, A. Berkenblit, Antibody–Drug Conjugates for Cancer Treatment, Annual Review of Medicine, 69 (2018) 191-207.

[98]. A. Beck, L. Goetsch, C. Dumontet, N. Corvaia, Strategies and challenges for the next generation of antibody-drug conjugates, Nature reviews. Drug discovery, 16 (2017) 315-337.

[99]. H. Iwata, K. Tamura, T. Doi, J. Tsurutani, S. Modi, H. Park, I.E. Krop, Y. Sagara, C.H. Redfern, R.K. Murthy, R.A. Redman, K. Shitara, Y. Fujisaki, M. Sugihara, L. Zhang, J. Shahidi, A. Yver, S. Takahashi, Trastuzumab deruxtecan (DS-8201a) in subjects with HER2-expressing solid tumors: Long-term results of a large phase 1 study with multiple expansion cohorts, Journal of Clinical Oncology, 36 (2018) 2501-2501.

[100]. C. Saura, F. Thistlethwaite, U. Banerji, S. Lord, V. Moreno, I. MacPherson, V. Boni, C.D. Rolfo, E.G.E. de Vries, C.M.L. Van Herpen, S. Rottey, J.J.J. Geenen, F. Eskens, M. Gil Martin, E. Mommers, N.P. Koper, R. Mulder, P.G. Aftimos, A phase I expansion cohorts study of SYD985 in heavily pretreated patients with HER2-positive or HER2-low metastatic breast cancer, Journal of Clinical Oncology, 36 (2018) 1014-1014.

[101]. E.M. Stein, R.B. Walter, H.P. Erba, A.T. Fathi, A.S. Advani, J.E. Lancet, F. Ravandi, T. Kovacsovics, D.J. DeAngelo, D. Bixby, S. Faderl, A.P. Jillella, P.A. Ho, M.M. O'Meara, B. Zhao, C. Biddle-Snead, A.S. Stein, A phase 1 trial of vadastuximab talirine as monotherapy in patients with CD33-positive acute myeloid leukemia, Blood, 131 (2018) 387-396.

[102]. P.M. Drake, D. Rabuka, Recent Developments in ADC Technology: Preclinical Studies Signal Future Clinical Trends, BioDrugs : clinical immunotherapeutics, biopharmaceuticals and gene therapy, 31 (2017) 521-531.

[103]. D.R. Leach, M.F. Krummel, J.P. Allison, Enhancement of antitumor immunity by CTLA-4 blockade, Science (New York, N.Y.), 271 (1996) 1734-1736.

[104]. E. Pons-Tostivint, A. Latouche, P. Vaflard, F. Ricci, D. Loirat, S. Hescot, M.-P. Sablin, R. Rouzier, M. Kamal, C. Morel, C. Lecerf, V. Servois, X. Paoletti, C. Le Tourneau, Comparative Analysis of Durable Responses on Immune Checkpoint Inhibitors Versus Other Systemic Therapies: A Pooled Analysis of Phase III Trials, JCO Precision Oncology, (2019) 1-10.

[105]. F.S. Hodi, S.J. O'Day, D.F. McDermott, R.W. Weber, J.A. Sosman, J.B. Haanen, R. Gonzalez, C. Robert, D. Schadendorf, J.C. Hassel, W. Akerley, A.J. van den Eertwegh, J. Lutzky, P. Lorigan, J.M. Vaubel, G.P. Linette, D. Hogg, C.H. Ottensmeier, C. Lebbe, C. Peschel, I. Quirt, J.I. Clark, J.D. Wolchok, J.S. Weber, J. Tian, M.J. Yellin, G.M. Nichol, A. Hoos, W.J. Urba, Improved survival with ipilimumab in patients with metastatic melanoma, The New England journal of medicine, 363 (2010) 711-723.

[106]. A.H. Sharpe, Mechanisms of costimulation, Immunological reviews, 229 (2009) 5-11.

[107]. D. Perkins, Z. Wang, C. Donovan, H. He, D. Mark, G. Guan, Y. Wang, T. Walunas, J. Bluestone, J. Listman, P.W. Finn, Regulation of CTLA-4 expression during T cell activation, Journal of immunology (Baltimore, Md. : 1950), 156 (1996) 4154-4159.

[108]. M.L. Alegre, P.J. Noel, B.J. Eisfelder, E. Chuang, M.R. Clark, S.L. Reiner, C.B. Thompson, Regulation of surface and intracellular expression of CTLA4 on mouse T cells, Journal of immunology (Baltimore, Md. : 1950), 157 (1996) 4762-4770.

[109]. J.G. Egen, J.P. Allison, Cytotoxic T lymphocyte antigen-4 accumulation in the immunological synapse is regulated by TCR signal strength, Immunity, 16 (2002) 23-35.

[110]. P.S. Linsley, J.L. Greene, W. Brady, J. Bajorath, J.A. Ledbetter, R. Peach, Human B7-1 (CD80) and B7-2 (CD86) bind with similar avidities but distinct kinetics to CD28 and CTLA-4 receptors, Immunity, 1 (1994) 793-801.

[111]. X. Du, F. Tang, M. Liu, J. Su, Y. Zhang, W. Wu, M. Devenport, C.A. Lazarski, P. Zhang, X. Wang, P. Ye, C. Wang, E. Hwang, T. Zhu, T. Xu, P. Zheng, Y. Liu, A reappraisal of CTLA-4 checkpoint blockade in cancer immunotherapy, Cell Research, 28 (2018) 416-432.

[112]. Y. Bulliard, R. Jolicoeur, M. Windman, S.M. Rue, S. Ettenberg, D.A. Knee, N.S. Wilson, G. Dranoff, J.L. Brogdon, Activating Fc gamma receptors contribute to the antitumor activities of immunoregulatory receptor-targeting antibodies, The Journal of experimental medicine, 210 (2013) 1685-1693.

[113]. J.R. Ingram, O.S. Blomberg, M. Rashidian, L. Ali, S. Garforth, E. Fedorov, A.A. Fedorov, J.B. Bonanno, C. Le Gall, S. Crowley, C. Espinosa, T. Biary, E.J. Keliher, R. Weissleder, S.C. Almo, S.K. Dougan, H.L. Ploegh, M. Dougan, Anti–CTLA-4 therapy requires an Fc domain for efficacy, Proceedings of the National Academy of Sciences, 115 (2018) 3912.

[114]. S.C. Wei, C.R. Duffy, J.P. Allison, Fundamental Mechanisms of Immune Checkpoint Blockade Therapy, Cancer Discovery, (2018).

[115]. J.A. Seidel, A. Otsuka, K. Kabashima, Anti-PD-1 and Anti-CTLA-4 Therapies in Cancer: Mechanisms of Action, Efficacy, and Limitations, Frontiers in Oncology, 8 (2018).

[116]. S. Simon, N. Labarriere, PD-1 expression on tumor-specific T cells: Friend or foe for immunotherapy?, Oncoimmunology, 7 (2017) e1364828-e1364828.

[117]. S.H. Kil, R. Estephan, J. Sanchez, J.M. Zain, M.E. Kadin, J.W. Young, S.T. Rosen, C. Querfeld, PD-L1 Is Regulated By Interferon Gamma and Interleukin 6 through STAT1 and STAT3 Signaling in Cutaneous T-Cell Lymphoma, Blood, 130 (2017) 1458.

[118]. M.E. Keir, S.C. Liang, I. Guleria, Y.E. Latchman, A. Qipo, L.A. Albacker, M. Koulmanda, G.J. Freeman, M.H. Sayegh, A.H. Sharpe, Tissue expression of PD-L1 mediates peripheral T cell tolerance, The Journal of experimental medicine, 203 (2006) 883-895.

[119]. G.J. Freeman, A.J. Long, Y. Iwai, K. Bourque, T. Chernova, H. Nishimura, L.J. Fitz, N. Malenkovich, T. Okazaki, M.C. Byrne, H.F. Horton, L. Fouser, L. Carter, V. Ling, M.R. Bowman,

B.M. Carreno, M. Collins, C.R. Wood, T. Honjo, Engagement of the PD-1 immunoinhibitory receptor by a novel B7 family member leads to negative regulation of lymphocyte activation, The Journal of experimental medicine, 192 (2000) 1027-1034.

[120]. L.T. Nguyen, P.S. Ohashi, Clinical blockade of PD1 and LAG3 — potential mechanisms of action, Nature Reviews Immunology, 15 (2014) 45.

[121]. W. Zou, J.D. Wolchok, L. Chen, PD-L1 (B7-H1) and PD-1 pathway blockade for cancer therapy: Mechanisms, response biomarkers, and combinations, Science Translational Medicine, 8 (2016) 328rv324.

[122]. M.W. LaFleur, Y. Muroyama, C.G. Drake, A.H. Sharpe, Inhibitors of the PD-1 Pathway in Tumor Therapy, Journal of immunology (Baltimore, Md. : 1950), 200 (2018) 375-383.

[123]. D. Przepiorka, C.-W. Ko, A. Deisseroth, C.L. Yancey, R. Candau-Chacon, H.-J. Chiu, B.J. Gehrke, C. Gomez-Broughton, R.C. Kane, S. Kirshner, N. Mehrotra, T.K. Ricks, D. Schmiel, P. Song, P. Zhao, Q. Zhou, A.T. Farrell, R. Pazdur, FDA Approval: Blinatumomab, Clinical Cancer Research, 21 (2015) 4035.

[124]. J. Schachter, A. Ribas, G.V. Long, A. Arance, J.J. Grob, L. Mortier, A. Daud, M.S. Carlino, C. McNeil, M. Lotem, J. Larkin, P. Lorigan, B. Neyns, C. Blank, T.M. Petrella, O. Hamid, H. Zhou, S. Ebbinghaus, N. Ibrahim, C. Robert, Pembrolizumab versus ipilimumab for advanced melanoma: final overall survival results of a multicentre, randomised, open-label phase 3 study (KEYNOTE-006), Lancet (London, England), 390 (2017) 1853-1862.

[125]. D. Schadendorf, R. Dummer, A. Hauschild, C. Robert, O. Hamid, A. Daud, A. van den Eertwegh, L. Cranmer, S. O'Day, I. Puzanov, J. Schachter, C. Blank, A. Salama, C. Loquai, J.M. Mehnert, D. Hille, S. Ebbinghaus, S.P. Kang, W. Zhou, A. Ribas, Health-related quality of life in the randomised KEYNOTE-002 study of pembrolizumab versus chemotherapy in patients with ipilimumab-refractory melanoma, European journal of cancer (Oxford, England : 1990), 67 (2016) 46-54.

[126]. M.T. Wan, M.E. Ming, Nivolumab versus ipilimumab in the treatment of advanced melanoma: a critical appraisal: ORIGINAL ARTICLE: Wolchok JD, Chiarion-Sileni V, Gonzalez

R et al. Overall survival with combined nivolumab and ipilimumab in advanced melanoma. N Engl J Med 2017; 377:1345-56, The British journal of dermatology, 179 (2018) 296-300.

[127]. J. Larkin, V. Chiarion-Sileni, R. Gonzalez, J.J. Grob, C.L. Cowey, C.D. Lao, D. Schadendorf, R. Dummer, M. Smylie, P. Rutkowski, P.F. Ferrucci, A. Hill, J. Wagstaff, M.S. Carlino, J.B. Haanen, M. Maio, I. Marquez-Rodas, G.A. McArthur, P.A. Ascierto, G.V. Long, M.K. Callahan, M.A. Postow, K. Grossmann, M. Sznol, B. Dreno, L. Bastholt, A. Yang, L.M. Rollin, C. Horak, F.S. Hodi, J.D. Wolchok, Combined Nivolumab and Ipilimumab or Monotherapy in Untreated Melanoma, New England Journal of Medicine, 373 (2015) 23-34.

[128]. J.D. Wolchok, V. Chiarion-Sileni, R. Gonzalez, P. Rutkowski, J.J. Grob, C.L. Cowey, C.D. Lao, J. Wagstaff, D. Schadendorf, P.F. Ferrucci, M. Smylie, R. Dummer, A. Hill, D. Hogg, J. Haanen, M.S. Carlino, O. Bechter, M. Maio, I. Marquez-Rodas, M. Guidoboni, G. McArthur, C. Lebbe, P.A. Ascierto, G.V. Long, J. Cebon, J. Sosman, M.A. Postow, M.K. Callahan, D. Walker, L. Rollin, R. Bhore, F.S. Hodi, J. Larkin, Overall Survival with Combined Nivolumab and Ipilimumab in Advanced Melanoma, The New England journal of medicine, 377 (2017) 1345-1356.

[129]. R. Zappasodi, T. Merghoub, J.D. Wolchok, Emerging Concepts for Immune Checkpoint Blockade-Based Combination Therapies, Cancer cell, 33 (2018) 581-598.

[130]. S.A. Patel, A.J. Minn, Combination Cancer Therapy with Immune Checkpoint Blockade: Mechanisms and Strategies, Immunity, 48 (2018) 417-433.

[131]. J.A. Marin-Acevedo, B. Dholaria, A.E. Soyano, K.L. Knutson, S. Chumsri, Y. Lou, Next generation of immune checkpoint therapy in cancer: new developments and challenges, Journal of hematology & oncology, 11 (2018) 39-39.

[132]. S. Huang, C. Li, E.A. Armstrong, C.R. Peet, J. Saker, L.C. Amler, M.X. Sliwkowski, P.M. Harari, Dual targeting of EGFR and HER3 with MEHD7945A overcomes acquired resistance to EGFR inhibitors and radiation, Cancer research, 73 (2013) 824-833.

[133]. A. Patnaik, M. Gordon, F. Tsai, K. Papadopoulous, D. Rasco, S.M. Beeram, S. Fu, F. Janku, S.M. Hynes, S.R. Gundala, M.D. Willard, W. Zhang, A.B. Lin, D. Hong, A phase I study of

LY3164530, a bispecific antibody targeting MET and EGFR, in patients with advanced or metastatic cancer, Cancer chemotherapy and pharmacology, 82 (2018) 407-418.

[134]. C. Spiess, Q. Zhai, P.J. Carter, Alternative molecular formats and therapeutic applications for bispecific antibodies, Molecular Immunology, 67 (2015) 95-106.

[135]. R.E. Kontermann, U. Brinkmann, Bispecific antibodies, Drug Discovery Today, 20 (2015) 838-847.

[136]. U. Brinkmann, R.E. Kontermann, The making of bispecific antibodies, mAbs, 9 (2017) 182-212.

[137]. M.M. Heiss, P. Murawa, P. Koralewski, E. Kutarska, O.O. Kolesnik, V.V. Ivanchenko, A.S. Dudnichenko, B. Aleknaviciene, A. Razbadauskas, M. Gore, E. Ganea-Motan, T. Ciuleanu, P. Wimberger, A. Schmittel, B. Schmalfeldt, A. Burges, C. Bokemeyer, H. Lindhofer, A. Lahr, S.L. Parsons, The trifunctional antibody catumaxomab for the treatment of malignant ascites due to epithelial cancer: Results of a prospective randomized phase II/III trial, International journal of cancer, 127 (2010) 2209-2221.

[138]. M.K. Gleason, M.R. Verneris, D.A. Todhunter, B. Zhang, V. McCullar, S.X. Zhou, A. Panoskaltsis-Mortari, L.M. Weiner, D.A. Vallera, J.S. Miller, Bispecific and trispecific killer cell engagers directly activate human NK cells through CD16 signaling and induce cytotoxicity and cytokine production, Molecular cancer therapeutics, 11 (2012) 2674-2684.

[139]. U.S. Arvindam, P. van Hauten, C. Hallstrom, D.A. Vallera, H. Dolstra, J.S. Miller, M. Felices, CD16-IL15-CLEC12A Trispecific Killer Engager (TriKE) Drives NK Cell Expansion, Activation, and Antigen Specific Killing of Cancer Stem Cells in Acute Myeloid Leukemia, Blood, 132 (2018) 1454.

[140]. A. Wiernik, B. Foley, B. Zhang, M.R. Verneris, E. Warlick, M.K. Gleason, J.A. Ross, X. Luo, D.J. Weisdorf, B. Walcheck, D.A. Vallera, J.S. Miller, Targeting natural killer cells to acute myeloid leukemia *in vitro* with a CD16 x 33 bispecific killer cell engager and ADAM17 inhibition, Clinical cancer research: an official journal of the American Association for Cancer Research, 19 (2013) 3844-3855.

[141]. H. Don Yun, M. Felices, D.A. Vallera, P. Hinderlie, S. Cooley, M. Arock, J. Gotlib, C. Ustun, J.S. Miller, Trispecific killer engager CD16xIL15xCD33 potently induces NK cell activation and cytotoxicity against neoplastic mast cells, Blood Advances, 2 (2018) 1580.

[142]. C. Guillerey, N.D. Huntington, M.J. Smyth, Targeting natural killer cells in cancer immunotherapy, Nature Immunology, 17 (2016) 1025.

[143]. Y. Matsumura, H. Maeda, A new concept for macromolecular therapeutics in cancer chemotherapy: mechanism of tumoritropic accumulation of proteins and the antitumor agent smancs, Cancer research, 46 (1986) 6387-6392.

[144]. H. Maeda, Toward a full understanding of the EPR effect in primary and metastatic tumors as well as issues related to its heterogeneity, Advanced drug delivery reviews, 91 (2015) 3-6.

[145]. F. Danhier, O. Feron, V. Préat, To exploit the tumor microenvironment: Passive and active tumor targeting of nanocarriers for anti-cancer drug delivery, Journal of Controlled Release, 148 (2010) 135-146.

[146]. K. Greish, Enhanced permeability and retention (EPR) effect for anticancer nanomedicine drug targeting, Methods in molecular biology (Clifton, N.J.), 624 (2010) 25-37.

[147]. S. Wilhelm, A.J. Tavares, Q. Dai, S. Ohta, J. Audet, H.F. Dvorak, W.C.W. Chan, Analysis of nanoparticle delivery to tumours, Nature Reviews Materials, 1 (2016) 16014.

[148]. J.W. Nichols, Y.H. Bae, EPR: Evidence and fallacy, Journal of Controlled Release, 190 (2014) 451-464.

[149]. S. Tran, P.-J. DeGiovanni, B. Piel, P. Rai, Cancer nanomedicine: a review of recent success in drug delivery, Clinical and translational medicine, 6 (2017) 44-44.

[150]. Y. Barenholz, Doxil(R)--the first FDA-approved nano-drug: lessons learned, Journal of controlled release: official journal of the Controlled Release Society, 160 (2012) 117-134.

[151]. D.W. Northfelt, B.J. Dezube, J.A. Thommes, B.J. Miller, M.A. Fischl, A. Friedman-Kien, L.D. Kaplan, C. Du Mond, R.D. Mamelok, D.H. Henry, Pegylated-liposomal doxorubicin versus doxorubicin, bleomycin, and vincristine in the treatment of AIDS-related Kaposi's sarcoma: results of a randomized phase III clinical trial, Journal of Clinical Oncology, 16 (1998) 2445-2451.

[152]. A.N. Gordon, J.T. Fleagle, D. Guthrie, D.E. Parkin, M.E. Gore, A.J. Lacave, Recurrent epithelial ovarian carcinoma: a randomized phase III study of pegylated liposomal doxorubicin versus topotecan, Journal of clinical oncology : official journal of the American Society of Clinical Oncology, 19 (2001) 3312-3322.

[153]. R.Z. Orlowski, A. Nagler, P. Sonneveld, J. Blade, R. Hajek, A. Spencer, J. San Miguel, T. Robak, A. Dmoszynska, N. Horvath, I. Spicka, H.J. Sutherland, A.N. Suvorov, S.H. Zhuang, T. Parekh, L. Xiu, Z. Yuan, W. Rackoff, J.L. Harousseau, Randomized phase III study of pegylated liposomal doxorubicin plus bortezomib compared with bortezomib alone in relapsed or refractory multiple myeloma: combination therapy improves time to progression, Journal of clinical oncology : official journal of the American Society of Clinical Oncology, 25 (2007) 3892-3901.

[154]. C.L. Ventola, Progress in Nanomedicine: Approved and Investigational Nanodrugs, P & T : a peer-reviewed journal for formulary management, 42 (2017) 742-755.

[155]. S.K. Libutti, G.F. Paciotti, A.A. Byrnes, H.R. Alexander, Jr., W.E. Gannon, M. Walker, G.D. Seidel, N. Yuldasheva, L. Tamarkin, Phase I and pharmacokinetic studies of CYT-6091, a novel PEGylated colloidal gold-rhTNF nanomedicine, Clinical cancer research : an official journal of the American Association for Cancer Research, 16 (2010) 6139-6149.

[156]. S. Yang, H. Gao, Nanoparticles for modulating tumor microenvironment to improve drug delivery and tumor therapy, Pharmacological research, 126 (2017) 97-108.

[157]. B. Zhang, Y. Hu, Z. Pang, Modulating the Tumor Microenvironment to Enhance Tumor Nanomedicine Delivery, Frontiers in Pharmacology, 8 (2017).

[158]. Z.-S. Liao, S.-Y. Huang, J.-J. Huang, J.-K. Chen, A.-W. Lee, J.-Y. Lai, D.-J. Lee, C.-C. Cheng, Self-Assembled pH-Responsive Polymeric Micelles for Highly Efficient, Noncytotoxic Delivery of Doxorubicin Chemotherapy To Inhibit Macrophage Activation: *In Vitro* Investigation, Biomacromolecules, 19 (2018) 2772-2781.

[159]. P.C. Naha, K. Bhattacharya, T. Tenuta, K.A. Dawson, I. Lynch, A. Gracia, F.M. Lyng, H.J. Byrne, Intracellular localisation, geno- and cytotoxic response of polyN-isopropylacrylamide (PNIPAM) nanoparticles to human keratinocyte (HaCaT) and colon cells (SW 480), Toxicology letters, 198 (2010) 134-143.

[160]. S. Chai, Y. Guo, Z. Zhang, Z. Chai, Y. Ma, L. Qi, Cyclodextrin-gated mesoporous silica nanoparticles as drug carriers for red light-induced drug release, Nanotechnology, 28 (2017) 145101.

[161]. A.D. Friedman, S.E. Claypool, R. Liu, The smart targeting of nanoparticles, Current pharmaceutical design, 19 (2013) 6315-6329.

[162]. R. Bazak, M. Houri, S. El Achy, S. Kamel, T. Refaat, Cancer active targeting by nanoparticles: a comprehensive review of literature, Journal of cancer research and clinical oncology, 141 (2015) 769-784.

[163]. D.B. Kirpotin, D.C. Drummond, Y. Shao, M.R. Shalaby, K. Hong, U.B. Nielsen, J.D. Marks, C.C. Benz, J.W. Park, Antibody targeting of long-circulating lipidic nanoparticles does not increase tumor localization but does increase internalization in animal models, Cancer research, 66 (2006) 6732-6740.

[164]. W. Jiang, B.Y.S. Kim, J.T. Rutka, W.C.W. Chan, Nanoparticle-mediated cellular response is size-dependent, Nature Nanotechnology, 3 (2008) 145.

[165]. K.A. Autio, R. Dreicer, J. Anderson, J.A. Garcia, A. Alva, L.L. Hart, M.I. Milowsky, E.M. Posadas, C.J. Ryan, R.P. Graf, R. Dittamore, N.A. Schreiber, J.M. Summa, H. Youssoufian, M.J. Morris, H.I. Scher, Safety and Efficacy of BIND-014, a Docetaxel Nanoparticle Targeting Prostate-Specific Membrane Antigen for Patients With Metastatic Castration-Resistant Prostate Cancer: A Phase 2 Clinical Trial, JAMA oncology, 4 (2018) 1344-1351.

[166]. J.-H. Kim, Y. Kim, K.H. Bae, T.G. Park, J.H. Lee, K. Park, Tumor-Targeted Delivery of Paclitaxel Using Low Density Lipoprotein-Mimetic Solid Lipid Nanoparticles, Molecular pharmaceutics, 12 (2015) 1230-1241.

[167]. E.A. Sykes, J. Chen, G. Zheng, W.C.W. Chan, Investigating the Impact of Nanoparticle Size on Active and Passive Tumor Targeting Efficiency, ACS Nano, 8 (2014) 5696-5706.

[168]. D. Rosenblum, N. Joshi, W. Tao, J.M. Karp, D. Peer, Progress and challenges towards targeted delivery of cancer therapeutics, Nature communications, 9 (2018) 1410.

[169]. B. Theek, M. Baues, T. Ojha, D. Mockel, S.K. Veettil, J. Steitz, L. van Bloois, G. Storm, F. Kiessling, T. Lammers, Sonoporation enhances liposome accumulation and penetration in

tumors with low EPR, Journal of controlled release : official journal of the Controlled Release Society, 231 (2016) 77-85.

[170]. V.P. Chauhan, J.D. Martin, H. Liu, D.A. Lacorre, S.R. Jain, S.V. Kozin, T. Stylianopoulos, A.S. Mousa, X. Han, P. Adstamongkonkul, Z. Popovic, P. Huang, M.G. Bawendi, Y. Boucher, R.K. Jain, Angiotensin inhibition enhances drug delivery and potentiates chemotherapy by decompressing tumour blood vessels, Nature communications, 4 (2013) 2516.

[171]. E.A. Forssen, The design and development of DaunoXome® for solid tumor targeting *in vivo*, Advanced drug delivery reviews, 24 (1997) 133-150.

[172]. M.J. Glantz, K.A. Jaeckle, M.C. Chamberlain, S. Phuphanich, L. Recht, L.J. Swinnen, B. Maria, S. LaFollette, G.B. Schumann, B.F. Cole, S.B. Howell, A randomized controlled trial comparing intrathecal sustained-release cytarabine (DepoCyt) to intrathecal methotrexate in patients with neoplastic meningitis from solid tumors, Clinical cancer research : an official journal of the American Association for Cancer Research, 5 (1999) 3394-3402.

[173]. G. Batist, J. Barton, P. Chaikin, C. Swenson, L. Welles, Myocet (liposome-encapsulated doxorubicin citrate): a new approach in breast cancer therapy, Expert opinion on pharmacotherapy, 3 (2002) 1739-1751.

[174]. E. Miele, G.P. Spinelli, E. Miele, F. Tomao, S. Tomao, Albumin-bound formulation of paclitaxel (Abraxane ABI-007) in the treatment of breast cancer, International journal of nanomedicine, 4 (2009) 99-105.

[175]. P.A. Dinndorf, J. Gootenberg, M.H. Cohen, P. Keegan, R. Pazdur, FDA drug approval summary: pegaspargase (oncaspar) for the first-line treatment of children with acute lymphoblastic leukemia (ALL), The oncologist, 12 (2007) 991-998.

[176]. J.E. Frampton, Mifamurtide, Pediatric Drugs, 12 (2010) 141-153.

[177]. K. Maier-Hauff, F. Ulrich, D. Nestler, H. Niehoff, P. Wust, B. Thiesen, H. Orawa, V. Budach, A. Jordan, Efficacy and safety of intratumoral thermotherapy using magnetic iron-oxide nanoparticles combined with external beam radiotherapy on patients with recurrent glioblastoma multiforme, Journal of Neuro-Oncology, 103 (2011) 317-324.
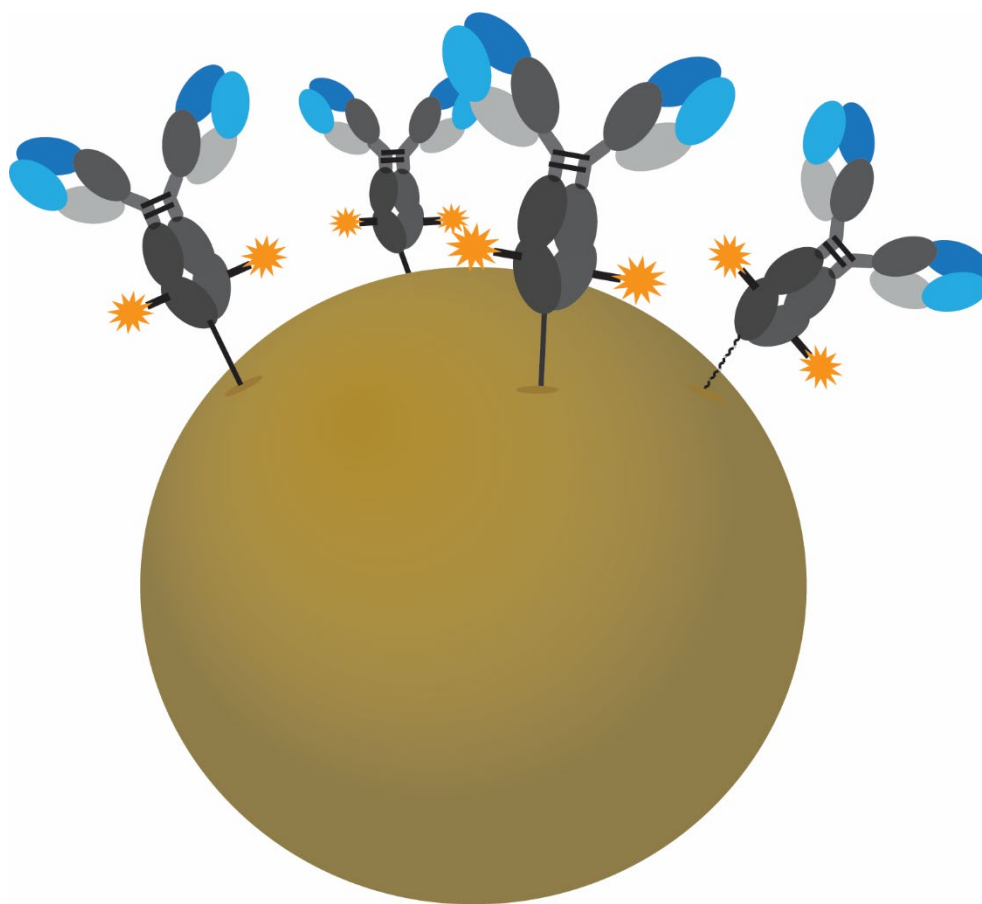
[178]. J.A. Silverman, S.R. Deitcher, Marqibo® (vincristine sulfate liposome injection) improves the pharmacokinetics and pharmacodynamics of vincristine, Cancer chemotherapy and pharmacology, 71 (2013) 555-564.

[179]. Y.N. Lamb, L.J. Scott, Liposomal Irinotecan: A Review in Metastatic Pancreatic Adenocarcinoma, Drugs, 77 (2017) 785-792.

[180]. A.C. Krauss, X. Gao, L. Li, M.L. Manning, P. Patel, W. Fu, K.G. Janoria, G. Gieser, D.A. Bateman, D. Przepiorka, Y.L. Shen, S.S. Shord, C.M. Sheth, A. Banerjee, J. Liu, K.B. Goldberg, A.T. Farrell, G.M. Blumenthal, R. Pazdur, FDA Approval Summary: (Daunorubicin and Cytarabine) Liposome for Injection for the Treatment of Adults with High-Risk Acute Myeloid Leukemia, Clinical cancer research : an official journal of the American Association for Cancer Research, (2018).

Chapter 7

Synthesis and Enhanced Cellular Uptake *In Vitro* of Anti-HER2 Multifunctional Gold Nanoparticles

Chapter 7 – Authorship declaration statement

The following chapter full research article published in the journal Cancers as:

E. Cruz, V. Kayser. Synthesis and Enhanced Cellular Uptake *In Vitro* of Anti-HER2 Multifunctional Gold Nanoparticles. Cancers, 11 (2019), 870.

E. Cruz co-designed the study and performed all experimental work and data analysis. E. Cruz wrote the manuscript.

Permission to include the published material has been granted by the corresponding author.

Esteban Cruz, Signature: 19th of August, 2019

As corresponding author and supervisor for this candidature, I hereby confirm that this authorship declaration statement is complete and accurate

Veysel Kayser, Signature: *Veysel Kayser*   19th of August, 2019

Chapter 7 – Authorship declaration statement

The following chapter full research article published in the journal Cancers as:

E. Cruz, V. Kayser. Synthesis and Enhanced Cellular Uptake *In Vitro* of Anti-HER2 Multifunctional Gold Nanoparticles. Cancers, 11 (2019), 870.

E. Cruz co-designed the study and performed all experimental work and data analysis. E. Cruz wrote the manuscript.

Permission to include the published material has been granted by the corresponding author.

Esteban Cruz, Signature: 19th of August, 2019

As corresponding author and supervisor for this candidature, I hereby confirm that this authorship declaration statement is complete and accurate

Veysel Kayser, Signature: 19th of August, 2019

Abstract

Nanoparticle carriers offer the possibility of enhanced delivery of therapeutic payloads in tumor tissues due to tumor-selective accumulation through the enhanced permeability and retention effect (EPR). Gold nanoparticles (AuNP), in particular, possess highly appealing features for development as nanomedicines, such as biocompatibility, tunable optical properties and a remarkable ease of surface functionalization. Taking advantage of the latter, several strategies have been designed to increase treatment specificity of gold nanocarriers by attaching monoclonal antibodies on the surface, as a way to promote selective interactions with the targeted cells—an approach referred to as active-targeting. Here, we describe the synthesis of spherical gold nanoparticles surface-functionalized with an anti-HER2 antibody-drug conjugate (ADC) as an active targeting agent that carries a cytotoxic payload. In addition, we enhanced the intracellular delivery properties of the carrier by attaching a cell penetrating peptide to the active-targeted nanoparticles. We demonstrate that the antibody retains high receptor-affinity after the structural modifications performed for drug-conjugation and nanoparticle attachment. Furthermore, we show that antibody attachment increases cellular uptake in HER2 amplified cell lines selectively, and incorporation of the cell penetrating peptide leads to a further increase in cellular internalization. Nanoparticle-bound antibody-drug conjugates retain high antimitotic potency, which could contribute to a higher therapeutic index in high EPR tumors.

Introduction

Most solid malignancies display a tumor microenvironment with increased interstitial fluid pressures (IFP) that significantly impairs tumor penetration of conventional anticancer agents following systemic delivery. This effect hinders movement of the therapeutic agent from the vascular lumen to the tumor tissue, requiring higher doses to achieve therapeutic efficacy [1, 2]. Consequently, the therapeutic index is reduced, and off-target side-effects compromise clinical outcomes. Moreover, inefficient localization in the target tissue can lead to tumor regions exposed to subtherapeutic doses of the drug, whereby cancer cells can undergo phenotypic alterations that render them resistant to the agent administered [3].

In this context, nanoparticles (NPs) have emerged as drug delivery vehicles that can harness the preferential accumulation of nanosized materials in the tumor due to the well-described enhanced

permeability and retention (EPR) effect [4]. Several liposome-encapsulated cytotoxic drugs have received regulatory approval on the basis of superior therapeutic indices relative to the free drug [5]. A further attractive feature of nanoparticles is their functional versatility, as their design can be tailored to confer diverse physiological and physicochemical properties to broaden treatment modalities. Myriad distinct NP formats are undergoing preclinical development for various therapeutic and diagnostic applications, e.g., gene delivery, thermal ablation therapy, magnetic resonance imaging (MRI), photoacoustic imaging [6–9].

Among the diverse range of inorganic NPs, gold nanoparticles (AuNP) have been widely appraised as attractive systems for therapeutic applications, e.g., drug delivery, photothermal therapy and radiosensitization [9, 10]. AuNPs are easy to synthesize with tunable shapes and sizes, and the strong gold-sulfur (Au-S) interaction allows for the modification of the nanoparticle surface with sulfhydryl containing linkers, through which functional groups can be incorporated to confer biological properties for therapeutic purposes [11]. An analysis of nanoparticle tumor delivery efficiency in *in vivo* models derived from published data from the year 2005 to 2015 showed that AuNPs had the highest median delivery efficiency among the analysed inorganic nanoparticle types (including iron oxide, silica, quantum dots and others) [12]. Moreover, a PEGylated AuNP format coated with TNF-α has already shown a promising safety profile and enhanced accumulation in various solid tumors in a phase I dose escalation trial, setting a clinical precedent for gold nanoparticles [13, 14].

Adding to the inherent passive accumulation of NPs in solid tumors, the targeting capacity of a nanoparticle carrier can potentially be enhanced by the incorporation of an active targeting agent on the NP surface. Active targeting moieties—e.g., antibodies, peptides, aptamers, affimers—can engage in high-affinity specific interactions with biomolecules overexpressed in cancer subtypes to increase treatment specificity [15]. Within this concept, systemic delivery of the nanocarrier results in passive accumulation in the tumor microenvironment, where the subsequent interaction of the affixed targeting agent with cancer cells can induce receptor crosslinking, receptor-mediated endocytosis and intracellular cargo delivery [16].

In this work, we employed an anti-HER2 antibody, Trastuzumab (Tmab), as an active targeting agent on spherical gold nanoparticles. Tmab is a therapeutic monoclonal antibody that binds to the human epidermal growth factor receptor 2 (HER2) and is approved for the treatment of HER2-

positive breast cancer and metastatic gastric cancer [17, 18]. Moreover, HER2 overexpression has been documented in esophageal [19], ovarian [20]. and endometrial cancer [21]. and has been identified as a negative prognostic factor in several of these malignancies [22–24]. Trastuzumab exerts its anticancer activity by binding to the extracellular domain of HER2 to prevent dimerization with other ErbB receptors, thereby inhibiting its key function in cell proliferation and migration. In addition, immune effector components can be engaged through the Fc region of the antibody to destroy cancer cells via antibody-dependent cellular cytotoxicity (ADCC), antibody-dependent cellular phagocytosis (ADCP) and complement-dependent cytotoxicity (CDC) [25, 26].

Monoclonal antibodies (mAbs) have become a cornerstone of cancer care since the first therapeutic mAb market approval in 1997 (Rituximab) by virtue of their enhanced treatment specificity. As of early 2019, more than 20 distinct mAbs are indicated for a wide array of solid malignancies, predominantly administered through systemic routes [27]. This notwithstanding, poor tumor penetration and distribution are prominent obstacles that compromise the therapeutic index of mAbs [28, 29]. To this end, enhancing drug accumulation in the tumor through the employment of enhanced delivery systems could provide major improvements in therapeutic safety and efficacy.

Conventional designs of active-targeted nanoparticles for drug delivery typically consist of nanoparticles carrying a surface-incorporated targeting agent and a cytotoxic payload either encapsulated within the NP core or loaded onto the surface. In this work, we sought to employ a novel strategy, wherein a cytotoxic drug is conjugated to the antibody initially, and the resulting antibody-drug conjugate (ADC) is employed as a targeting agent-drug carrier on the nanoparticles, thereby broadening the functionality of the active-targeting agent. Herein, we describe the synthesis and physicochemical characterization of ADC-targeted spherical gold nanoparticles. The ADC was produced by chemical attachment of monomethyl auristatin E (MMAE) to Tmab through a cathepsin-cleavable valine-citrulline linker; and further reacted with a sulfhydryl-containing linker for surface conjugation to the gold nanoparticles. We demonstrate that Trastuzumab can be chemically modified in this fashion while retaining high affinity towards its cognate receptor. Since the valine-citrulline linker must be internalized for payload release, we analysed the intracellular uptake of active-targeted AuNPs on various cancer cell lines.

Furthermore, we evaluated the effect of surface incorporation of a cell penetrating peptide to the active-targeted nanoparticle on intracellular uptake.

Materials and Methods

Materials

Herceptin® (Trastuzumab) was a generous donation from Genentech (San Francisco, CA, USA). Thiol PEG NHS (NHS-PEG-SH) (5 kDa) linker (Cat. No. PG2-NSTH-5k) was purchased from Nanocs (Boston, MA, USA). The MC-Val-Cit-PAB-MMAE (vcMMAE) linker (Cat. No. BP23969) was obtained from Broadpharm (San Diego, CA, USA). The HIV-1 TAT protein (47-57) (HIV-TAT or CPP) (Cat. No. H0292) was purchased from Sigma-Aldrich (Castle Hill, NSW, Australia). The Series S Sensor Chip CM5 (Cat. No. 29-1049-88), the amine coupling kit (Cat. No. BR-1000-50) and the anti-HIS capture kit (Cat. No. 28-9950-56) employed in the Biacore SPR instrument were purchased from GE Healthcare (Parramatta, NSW, Australia). The recombinant HIS-tagged soluble HER2 (Cat. No. SRP6405) was obtained from Sigma-Aldrich (Australia). Phosphate buffered saline (PBS) was purchased from Astral Scientific (Gymea, NSW, Australia). Amicon 3 kDa (Cat. No. Z740168) and 50 kDa (Cat. No. Z740177) cutoff centrifugal filter units were acquired from Sigma-Aldrich (Australia). Millex-GV syringe filters (0.22 µm, PVDF, Cat. No. SLGV033RS) were purchased from purchased from Sigma-Aldrich (Castle Hill, NSW, Australia). RPMI 1640 and DMEM (high glucose) media were obtained from Life Technologies (Mulgrave, VIC, Australia). All other chemicals and reagents were purchased from Sigma Aldrich (Australia).

Synthesis of Spherical Citrate-Capped Gold Nanoparticles

Spherical gold nanoparticles were synthesized by citrate reduction of gold chloride in aqueous solution as described by Turkevich [45], and revised by Frens [46]. All glassware employed in this procedure was soaked in aqua regia (3:1 HCl/HNO$_3$ molar ratio) for 3 h prior to the reaction and rinsed with double distilled H2O. Briefly, 100 mL of a 254 µM HAuCl$_4$ solution in double distilled H$_2$O was heated to boiling under stirring. Once boiling, 2 mL or 1 mL of a 1% w/v (34 µM) sodium citrate solution was added to prepare 20 nm and 50 nm, respectively. Following citrate addition, the solution was boiled for 15 min, then cooled to room temperature under stirring for 2 h. Unreacted citrate was removed by decanting after centrifugation at 10,000 g or 3,500 g for 30 min

to pellet the 20 nm and 50 nm nanoparticles. The synthesized gold nanoparticles were resuspended in double distilled water. Nanoparticle size, size distribution and morphology were assessed through transmission DLS (hydrodynamic size) electron microscopy (size, size distribution and morphology) and shifts in the surface plasmon resonance (SPR) absorption band.

Tmab PEGylation (Tmab-PEG-SH)

Trastuzumab 21 mg/mL in formulation buffer (L-histidine 4.64 mM, α,α-Trehalose 52.86 mM, polysorbate 20 concentration 73.31 μM, HCl 2.58 mM) was buffer exchanged to sodium bicarbonate (NaHCO$_3$) 0.1 M pH 8.0 using 50 kDa cutoff centrifugal filters to a final antibody concentration of 10 mg/mL (6.87×10^{-5} M). The extinction coefficient ε280 = $2.25 \times 10^{+5}$ M^{-1} cm^{-1} was used for all antibody concentration determinations. Buffer exchange was carried out thoroughly to reduce to a minimum the concentration of L-histidine in the formulation buffer, as the primary amine in L-histidine will react readily with the NHS group in the linker. A 5 mg/mL (1 mM) NHS-PEG-SH (5 kDa) linker stock solution was prepared in NaHCO$_3$ 0.1 M pH 8.0 and immediately added to Trastuzumab in 2:1, 5:1, 10:1, 20:1 and 25:1 NHS-linker/Tmab ratios and incubated at 4 °C overnight under stirring. The NHS-linker stock solution in NaHCO$_3$ pH 8.0 was prepared immediately before adding to the Trastuzumab sample, since the NHS ester can undergo rapid hydrolysis at basic pH. Following PEGylation, unreacted NHS-PEG-SH linker was removed by centrifugation through 50 kDa cutoff filters and the PEGylated Trastuzumab (Tmab-PEG-SH) was buffer exchanged to phosphate buffered saline (PBS) 0.01 M pH 7.4 with 1 mM EDTA to a final antibody concentration of 5 mg/mL. EDTA 1 mM was added to inhibit disulfide bond formation between the free SH groups in the linker [47, 48].

HIV-TAT Cell Penetrating Peptide (CPP) PEGylation (CPP-PEG-SH)

HIV-TAT (47–57) peptide was dissolved in NaHCO$_3$ 0.1 M pH 8.0 to a 1 mg/mL (641 μM) concentration. A 10 mg/mL (2 mM) NHS-PEG-SH (5 kDa) solution in NaHCO$_3$ 0.1 M pH 8.0 was added to the HIV-TAT peptide in a 4:1 NHS-linker/CPP molar ratio and incubated overnight at 4 °C under stirring. Unreacted CPP was removed by centrifugation through 3 kDa cutoff filters and the PEGylated CPP (CPP-PEG-SH) was buffer exchanged to phosphate buffered saline 0.01 M pH 7.4 with 1 mM EDTA.

Tmab-vcMMAE Conjugate Synthesis

Antibody Partial Reduction

Trastuzumab in formulation buffer was buffer exchanged to PBS 0.01 M with 10 mM EDTA in a final concentration of 5 mg/mL (34 uM). A freshly prepared 10 mM stock solution of dithiothreitol (DTT) in PBS 0.01 M EDTA 1 mM was added to the antibody in a 3:1 DTT/Tmab ratio and the reaction was incubated at 37 °C for 90 min under stirring. DTT was then removed by buffer exchanging the partially reduced Tmab with 50 kDa cutoff centrifugal filters to PBS 0.01 M containing 10 mM EDTA to a 10 mg/mL (34 µM) concentration. After partial reduction, the integrity of the full-size IgG molecule was confirmed by SE-HPLC. In addition, free sulfhydryl (SH) groups per antibody were quantified by reaction with DTNB (5, 5'-dithiobis(2-nitrobenzoic acid)) and determination of the absorbance at 412 nm for free SH concentration. The final flowthrough of the buffer exchange prior to the DTNB reaction was used as a blank to subtract the potential contribution of residual DTT in the solution. The extinction coefficient $\varepsilon 412 = 1.42 \times 10^{+5}$ M^{-1} cm^{-1} for the TNB^{2-} reaction product was employed for sulfhydryl quantification.

Conjugate Synthesis

vcMMAE was dissolved in DMSO at a 1.26 mM concentration and added to a chilled 10 mg/mL partially reduced Tmab solution in a 4.6:1 vcMMAE/Tmab ratio. The reaction mixture was incubated at 4 °C with stirring for 1 h. A 20-fold molar excess of cysteine—relative to maleimide—was added to quench the reaction. Unreacted vcMMAE and cysteine were removed by centrifugation through 50 kDa cutoff centrifugal filters and buffer exchanged to PBS 0.01 M pH 7.4 for storage, or NaHCO$_3$ 0.1 M pH 8.0 for subsequent PEGylation. The average drug-antibody ratio (DAR) was calculated based on absorbance values at 248 nm and 280 nm as has been described previously [49]. The following formula was employed:

$$DAR = \frac{\varepsilon_{248}^{Tmab} - F\varepsilon_{280}^{Tmab}}{F\varepsilon_{280}^{MMAE} - \varepsilon_{248}^{MMAE}}$$

F=A248/A280 and the extinction coefficients utilized are listed in Table 4.

Table 1. Extinction coefficients of Trastuzumab and monomethyl auristatin E (MMAE) employed for the calculation of drug-to-antibody ratio (DAR) based on UV-Vis spectroscopy

Sample	248 nm	280 nm
Trastuzumab	$7.75 \times 10^{+4}$	$2.25 \times 10^{+5}$
MMAE	$1.59 \times 10^{+4}$	$1.50 \times 10^{+3}$

PEGylation of Tmab-vcMMAE (ADC-PEG-SH) was achieved following the same procedure as for the unconjugated antibody.

Intact Mass Analysis

Trastuzumab and Tmab-vcMMAE were concentrated using 50 kDa cutoff centrifugal filters and buffer exchanged to 10% acetonitrile with 0.1% formic acid. The antibody samples were analysed through direct injection into a Triple TOF 6600 mass spectrometer (Sciex, Framingham, MA, USA). Infusion was performed at 50 µL/min. The mass range for detection was 100–5,000 m/z. Deconvolution of the raw data was achieved using SCIEX Peakview 2.2 (Concord, ON, Canada) and Bruker BioTools software packages (Billerica, MA, USA).

Binding Kinetics to Recombinant HER2 through Surface Plasmon Resonance

The binding kinetics of derivatized Trastuzumab (Tmab-PEG-SH, Tmab-vcMMAE and ADC-PEG-SH) were tested against a recombinant HER-2 protein using surface plasmon resonance (SPR) in a Biacore T200 instrument (GE Healthcare, Parramatta, NSW, Australia). Briefly, an anti-HIS antibody was bound to a CM5 sensor chip through amine coupling chemistry. Subsequently, a recombinant HIS-tagged HER-2 (4 nM) was bound to the anti-HIS antibody on the sensor chip at a 5 µL/min flow rate for 5 min. 2-fold serial dilutions of the Trastuzumab variants ranging from 8–0.5 nM in HBS-T running buffer (10 mM HEPES, 150 mM NaCl, 0.05% (v/v) Tween 20, pH 7.4) were assayed at 25 °C as single cycle kinetic titrations. The analytes were applied to the sensor surface at 20 µL/min for 2 min, followed by 60 min dissociation times. Analyses of the sensorgrams were performed by fitting a Langmuir 1:1 binding model to derive the association constant (Ka), the dissociation constant (Kd) and the binding affinity (KD— calculated as Ka/Kd). The analytes were run in duplicate to calculate average values and standard deviation. A goodness of fit ($\chi2$) value within 5% of the maximum response level (Rmax) was used as acceptance criteria.

Gold Nanoparticle Surface Functionalization

Trastuzumab-coated (Tmab-PEG-AuNP), OH-PEG coated (OH-PEG-AuNP) and CPP-coated (CPP-PEG-AuNP) gold nanoparticles were produced by incubating citrate-capped gold nanoparticles (OD = 1) with a $1 \times 10^{+5}$ molar excess of SH-PEG-Tmab, SH-PEG-OH or SH-PEG-CPP in NaHCO$_3$ 0.01 M pH for 2 h at room temperature while stirring. The unconjugated reagents were removed by pelleting the nanoparticles at 3,500 g for 30 min and removing the supernatant. The conjugated nanoparticles were centrifuged four times and resuspended in PBS 0.01 M pH 7.4 for storage at 4 °C. ADC-PEG-AuNP were produced by incubating the nanoparticles with ADC-PEG-SH following the same procedure. CPP+Tmab-PEG-AuNP were obtained by incubation with a $1 \times 10^{+5}$ molar excess of CPP-PEG-SH for 5 min followed by the addition of a $1 \times 10^{+5}$ molar excess of Tmab-PEG-SH, and further incubation under stirring for 2 h.

UV-Vis Spectroscopy

UV-Vis absorption spectra were obtained over a wavelength range of 800–200 nm for gold nanoparticles or 400–200 nm for protein samples, using a Shimadzu 2600 UV-Vis spectrophotometer (Shimadzu, Japan). AuNP samples in RPMI media were corrected by blank subtraction of the RPMI.

Size-Exclusion High-Performance Liquid Chromatography (SE-HPLC)

Size-exclusion chromatograms were obtained with a Zorbax GF-250 column connected to an Agilent 1200 Liquid Chromatography system (Agilent Technologies, Santa Clara, CA, USA), running potassium phosphate buffer 150 mM pH 6.5 as a mobile phase at a 0.5 mL/min flow rate. Peak absorption was detected at 280 nm with an in-line UV signal detector (Agilent Technologies, Santa Clara, CA, USA).

DLS and Zeta Potential Measurements

DLS and zeta potential measurements of the functionalized gold nanoparticles were conducted with a Malvern Zetasizer Nano ZS (Malvern Instruments, Worcestershire, UK) with a 633 nm Helium Neon Laser and an avalanche photo diode (APD) detector. The measurements were conducted in triplicate and the values are reported as mean Z-average ± standard deviation. For zeta potential measurements, the functionalized nanoparticles suspended in PBS 1X (phosphate

buffer 0.01 M, NaCl 0.137 M, KCl 0.0027 M, pH 7.4) were diluted 1:10 in deionized water. Cit-AuNPs were directly resuspended in PBS 0.1X. The zeta potential was derived from the Henry equation using an f(Ka) of 1.5.

Cellular Uptake Quantification through Inductively Coupled Plasma Mass Spectrometry (ICP-MS)

The SKBR-3 cell line was provided by Dr. Thomas Grewal. The DLD-1 cell line was purchased from the American Type Culture Collection (ATCC). The MDA-MB-231 and MCF-7 cell lines were obtained from Dr. Fanfan Zhou. SKOV-3 cells were provided by Dr. Pegah Varamini.

To compare the cellular uptake of gold nanoparticles coated with OH-PEG and Tmab-PEG, SKBR-3 cells were seeded at density of $1 \times 10^{+5}$ cells/well in 24-well plates in RPMI media containing 10% FBS. Following incubation at 37 °C for 48 h, the cell media was removed, the cells were washed twice with PBS, and fresh RPMI media (10% FBS) containing 50 µg/mL 20 nm and 50 nm gold nanoparticles (coated with OH-PEG or Tmab-PEG) was added, using 6 wells per AuNP sample. The cells were further incubated for 24 h. The AuNP containing media was removed and the cell monolayer washed 4 times with PBS. The cells were detached from the plate using 0.05% trypsin and collected in 1.5 mL centrifuge tubes. Trypsin was removed by pelleting the cells at 300 g for 5 min and the cells were washed twice more with PBS. The cell pellet was digested with 200 µL concentrated HNO_3 (15.9 M) overnight at room temperature. 800 µL concentrated HCl (12.1 M) was then added to dissolve the gold nanoparticles. A 1:4 dilution in Milli-Q water was performed for quantification of gold content through ICP-MS. ICP-MS measurements were carried out with a Perkin Elmer Nexion 300× ICP-MS instrument (Perkin-Elmer, Waltham, MA, USA), calibrated with 5, 10 and 20 parts per billion (ppb) gold standard solutions.

To compare cellular uptake in SKBR-3, DLD-1, MDA-MB-231 and MCF-7 cells, the uptake assays were carried out following the same procedure as described above albeit with the following modifications: (1) 25 µg/mL AuNP concentrations were used, (2) DLD-1, MDA-MB-231 and MCF-7 cells were seeded at $3 \times 10^{+4}$ cells/well, (3) MDA-MB-231 and MCF-7 cell lines were cultured in DMEM media containing 10% FBS, (4) each nanoparticle sample was run in triplicate.

The concentration of the gold nanoparticles was determined based on their absorbance at 450 nm using $\varepsilon 450 = 5.41 \times 10^{+8}$ M^{-1} cm^{-1} and $\varepsilon 450 = 9.92 \times 10^{+9}$ M^{-1} cm^{-1} for 20 nm and 50 nm, respectively, according to previous determinations [32]. ICP-MS quantification of gold content in the AuNP suspensions was utilized to corroborate that the extinction coefficients used in this method provide appropriate estimations of gold concentrations. The nanoparticles in cell culture medium were filter sterilized through 0.22 µM filters prior to addition to the cells.

Cellular Uptake Evaluation by Transmission Electron Microscopy (TEM)

SKBR-3 cells were seeded at a density of $1 \times 10^{+5}$ cells/well on collagen-coated Thermanox plastic coverslips placed inside each well (24-well plates) and incubated at 37 °C for 48 h in RPMI media containing 10% FBS. Fresh RPMI containing 50 ug/mL 50 nm OH-PEG-AuNP or Tmab-PEG-AuNP was added to the wells and further incubated at 37 °C for 24 h. The wells were washed thrice with PBS. The cells were fixed with 2.5% glutaraldehyde in 0.1 M phosphate buffer pH 7.4. The cell monolayers were subsequently fixed with osmium tetroxide 1% (w/v) in phosphate buffer 0.1 M pH 7.4, then embedded into an epon resin. The monolayers were microtomed into 70 nm sections and stained with uranyl acetate 2% and Reynold's lead citrate. TEM images were obtained with a JEOL JEM-1400 (Tokyo, Japan) microscope with an accelerating voltage of 120 kV.

Cell Cytotoxicity Evaluation

SKBR-3 and SKOV-3 cells were seeded at $5 \times 10^{+3}$ and $3 \times 10^{+3}$ cells/well on 96-well plates and incubated at 37 °C for 24 h in RPMI media containing 10% FBS. Fresh RPMI media containing free MMAE, ADC, ADC-PEG-AuNP, Trastuzumab or OH-PEG-AuNP were added to the wells at the corresponding concentrations in triplicates. RPMI media was replenished for negative control samples. Images (10x magnification) of four different regions per well were acquired at 2-h intervals for 72 h after addition of the antimitotic or control sample using an Incucyte® ZOOM Live-cell Analysis System (Essen BioScience, Ann Arbor, MI, USA). Cell confluence was analysed with the Incucyte® ZOOM integrated analysis software (v2016A) to generate cell growth curves over time. Growth rate inhibition metrics were employed to assess the antimitotic effect of the samples. Growth rate inhibition metrics have been developed recently to provide more robust and biologically relevant drug response parameters [50]. GR values were calculated as:

$$GR(d) = 2^{log_2\left(\frac{x(d)_f}{x(d)_0}\right)/log_2\left(\frac{x(c)_f}{x(c)_0}\right)} - 1$$

Where $x(d)_0$ and $x(d)_f$ are the confluence values of cells treated with a cytotoxic agent at time t = 0 h and t = 72 h, respectively. $x(c)_0$ and $x(c)_f$ are confluence values of control wells at t = 0 h and t = 72 h.

GR values were plotted against treatment concentration and the data was fitted to a four-parameter dose-response curve. GR50 was obtained by interpolating the treatment concentration at which GR = 0.5.

Statistical Analysis

Gold uptake quantification was analysed with a two-tailed, unpaired Student t-test. Values are denoted as mean ± standard deviation, and $p < 0.05$ was established as statistical significance.

Results

Nanoparticle Design

Figure 1 displays an outline of the nanoparticle design and conjugation strategy. Attachment of the bioactive moieties—anti-HER2 mAb and HIV-TAT cell penetrating peptide (CPP)—to the gold surface was achieved through the covalent thiol-gold interaction using a bifunctional 5 kDa poly ethylene glycol (PEG) linker with a thiol (SH) and an N-hydroxysuccinimide (NHS) ester end groups (NHS-PEG-SH). The NHS group reacts with ε-amines in lysine residues (and with α-amines present at the N-terminals to a lesser extent) under slightly alkaline conditions to produce stable amide bonds with the protein or peptide [30]. The 5 kDa PEG linker was employed to increase exposure of the functional groups and prevent non-specific interactions between the bioactive groups and the gold surface. Furthermore, PEGylation of gold nanoparticles has proven to be highly beneficial in increasing circulation half-life by preventing adhesion of serum proteins that facilitate uptake by the reticuloendothelial system (RES)—an effect that drastically decreases the amount of nanoparticles that can eventually reach the tumor site [31].

Trastuzumab (anti-HER2 mAb) was employed as an active targeting agent to confer specificity towards HER2 overexpressing cancer cell lines. To enhance the anticancer potency of the antibody, MMAE was attached to Trastuzumab (Tmab) through a valine-citrulline dipeptide cleavable linker (vcMMAE) to produce Tmab-vcMMAE (Figure 1). The valine-citrulline moiety is cleaved by the lysosomal protease cathepsin B; thus, MMAE release occurs primarily following

endocytosis and subsequent localization into endosomes or lysosomes. The HIV-TAT cell penetrating peptide was further added onto the surface via the same NHS-PEG-SH linker to increase cellular uptake for intracellular release of the drug cargo (Figure 2B, C).
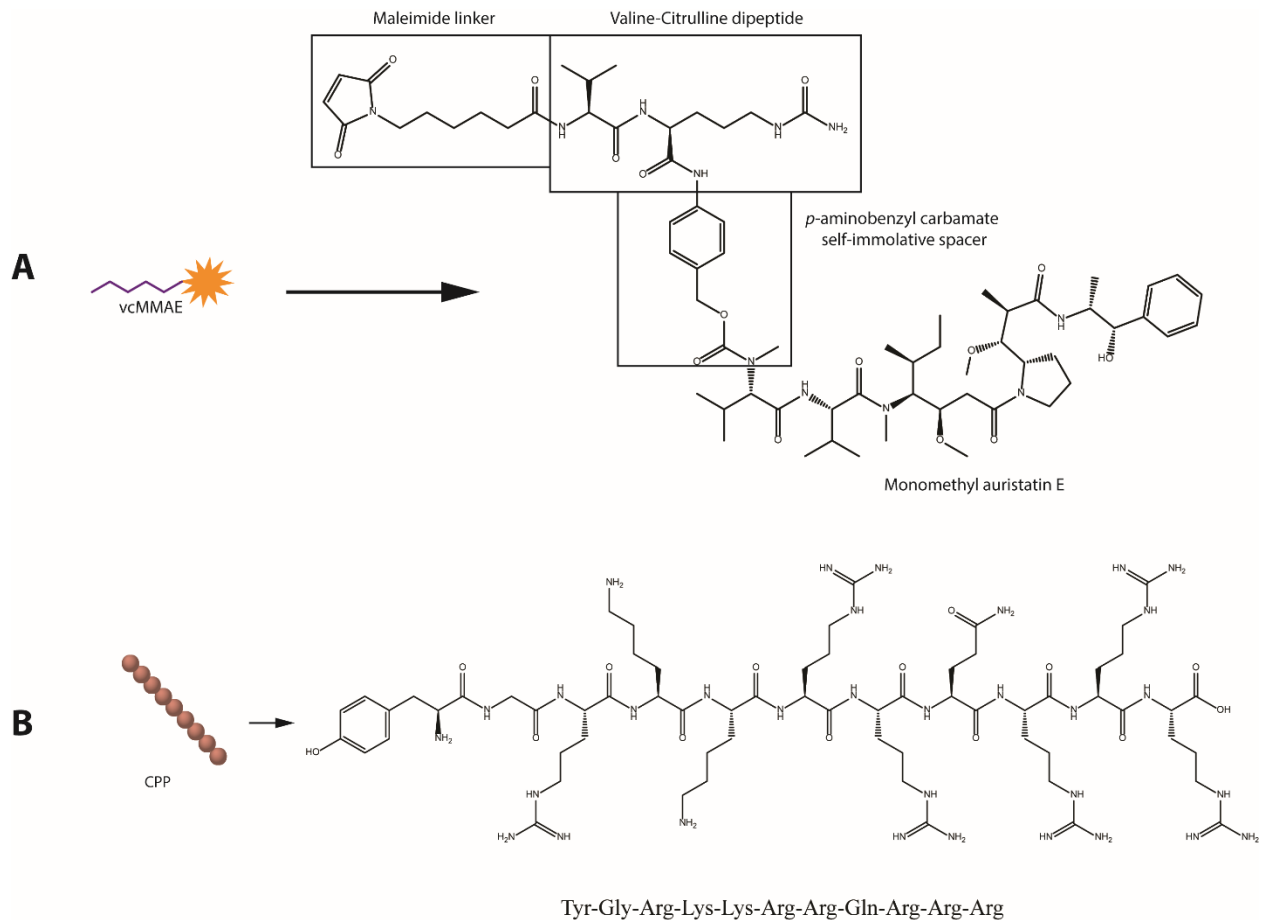
Figure 1. Molecular structures of the bioactive agents utilized for gold nanoparticle (AuNP) surface functionalization. (A) Valine-citrulline momomethyl auristatin E (vcMMAE) linker for antibody-drug conjugate (ADC) construction. (B) Human immunodeficiency virus twin-arginine translocation (HIV-1 TAT 47–57) protein.
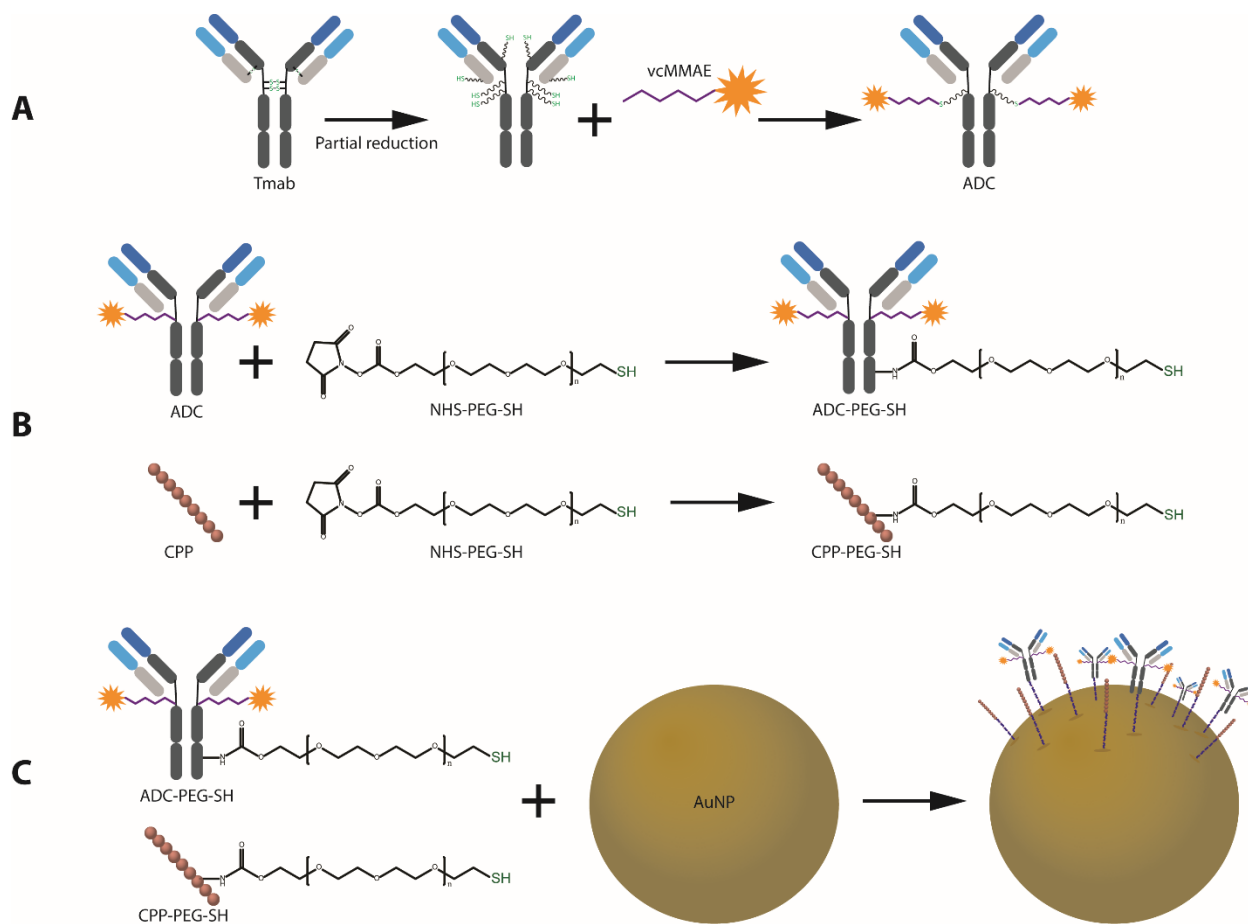
Figure 2. Schematic outline of the design and synthesis of ADC-coated gold nanoparticles with enhanced cell penetrating properties. (A) ADC synthesis. (B) Trastuzumab and CPP PEGylation for AuNP attachment. (C) Conjugation of bioactive agents onto the surface of AuNPs.

Antibody-Drug Conjugate (Tmab-vcMMAE) Synthesis

MMAE was conjugated to free sulfhydryl groups in Trastuzumab via reaction with the maleimide group in the vcMMAE linker (Figure 2A). To enable protein attachment, Trastuzumab was partially reduced by incubation with dithiothreitol (DTT) at 37 °C in a 3:1 DTT:Tmab molar ratio. Partial reduction produces cleavage of the inter-heavy chain disulfide bonds while preserving non-covalent inter-heavy chain (HC) and heavy-light chain (LC) interactions to conserve full IgG structure.

A colorimetric reaction with 5, 5′-Dithiobis(2-nitrobenzoic acid) (DTNB) was performed to confirm the presence of free SH groups following partial reduction. DTNB reacts with SH in a 1:1

molar ratio to produce 2-nitro-5-thiobenzoic acid (TNB2−). Absorption at 412 nm (λ max of TNB2−) can be utilized to calculate the amount of free SH groups per antibody monomer (Figure S1A).

After confirmation and quantification of the presence of free SH groups, the intact structure (no chain dissociation) was confirmed through size exclusion–high performance liquid chromatography (SE-HPLC), whereby the elution time of the reduced antibody shifted by 0.0128 min but did not display peaks at longer elution times indicative of chain dissociation (Figure S1B).

The drug-linker (vcMMAE) was then attached to free SH groups in the partially reduced Tmab as described in the methods section. Successful attachment of vcMMAE was confirmed through intact protein mass spectrometry analysis (Figure 3). The deconvoluted mass spectrum of the ADC displayed up to 3 vcMMAE attachments per antibody heavy chain in the G0F or G1F glycoforms (Figure 3A). Light chain analysis (Figure 3B) showcased a single attachment per LC monomer, consistent with a single free SH in LC obtained from partial reduction of the interchain disulfide bonds.
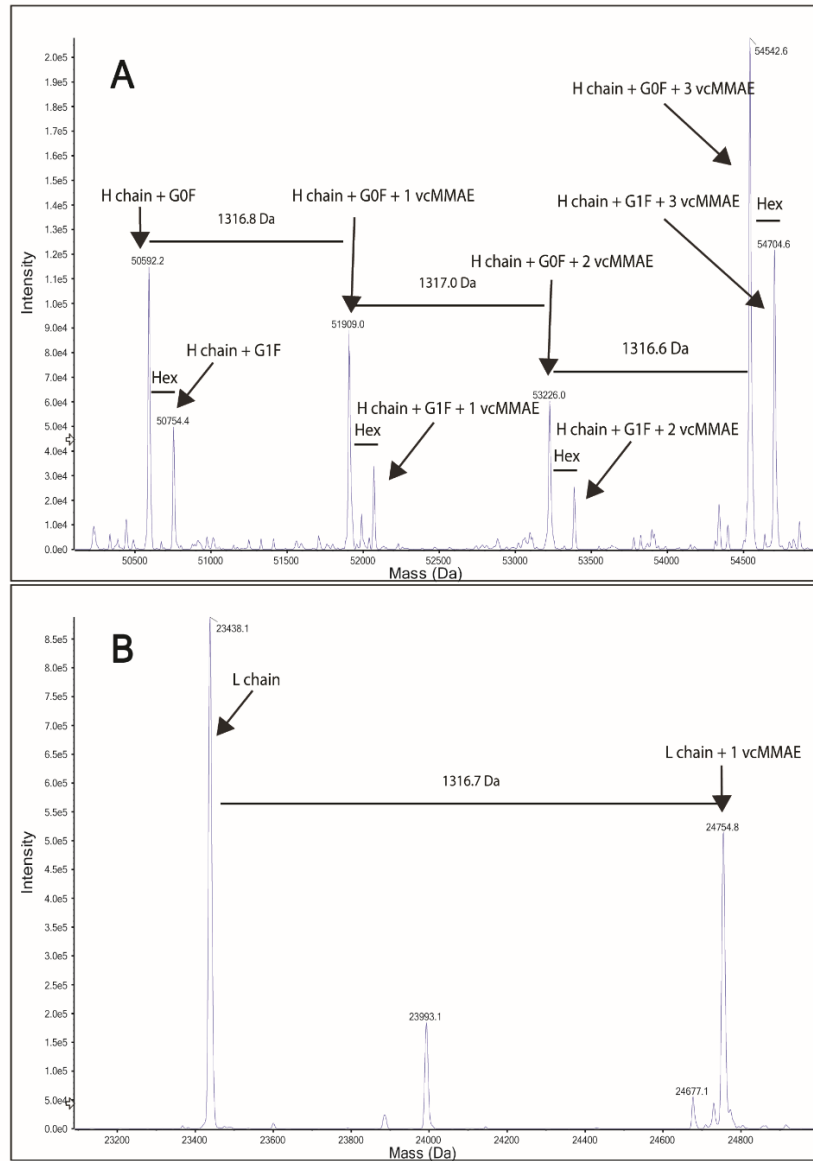
Figure 3. Protein intact mass analysis of Tmab-vcMMAE. (A) Deconvoluted spectrum of Tmab-vcMMAE heavy chain. (B) Deconvoluted spectrum of Tmab-vcMMAE light chain.
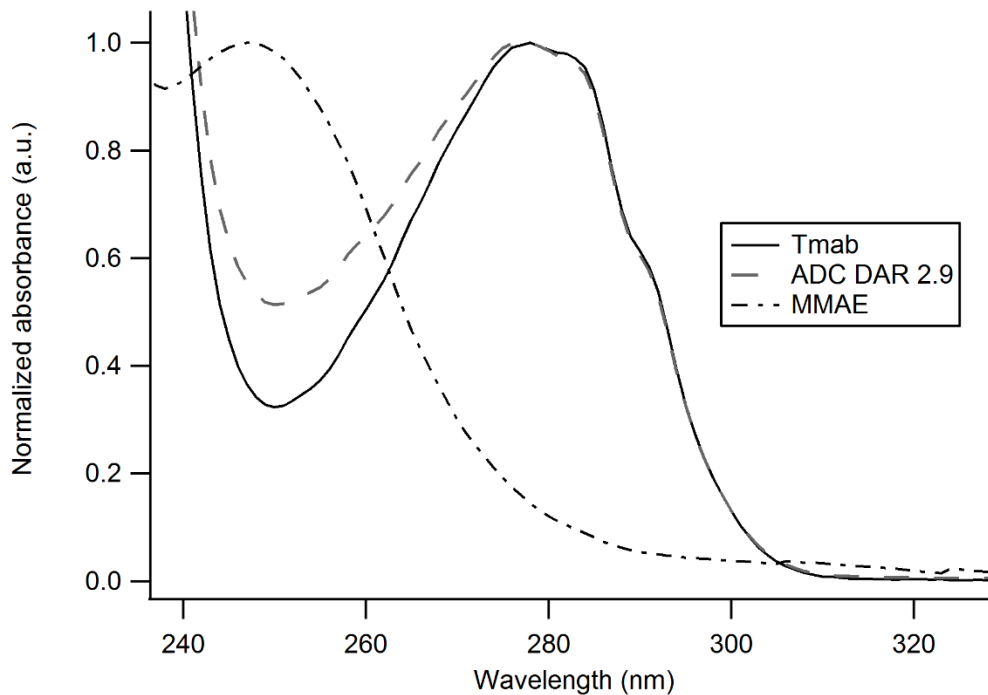
Figure 4. UV-Vis spectra of unmodified Trastuzumab, Tmab-vcMMAE (ADC) and MMAE. The contribution of MMAE to the absorption spectrum of the antibody-drug conjugate enables an estimation of the DAR based on the distinct A280/A248 ratios obtained with the unmodified antibody and the ADC.

An average drug-to-antibody ratio (DAR) of 2.91 was obtained from analysis of the UV-Vis spectrum of the ADC as described in the methods section (Figure 4).
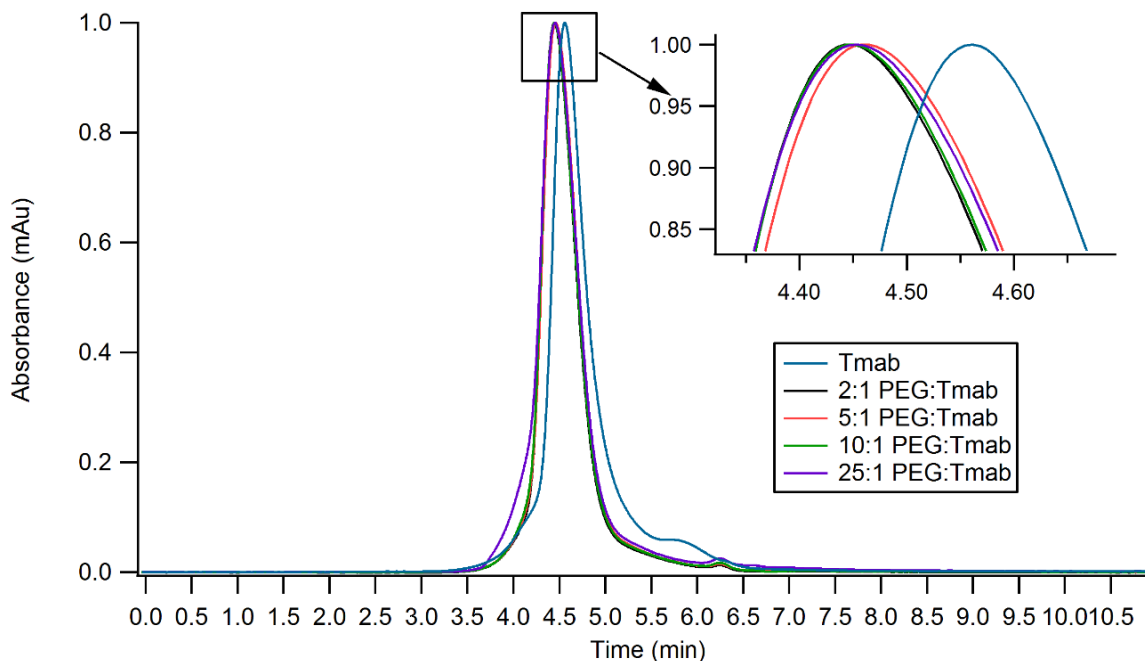
Figure 5. SE-HPLC chromatograms of PEGylated Trastuzumab variants obtained by employing varying ratios of PEG:Tmab ratios. Inset shows the zoomed region displaying small shifts in elution time.

Antibody and CPP PEGylation

Structural Characterization

Trastuzumab and HIV-TAT were PEGylated via lysine conjugation chemistry (Figure 1). Antibody PEGylation was confirmed through SE-HPLC (Figure 5). The SE-HPLC chromatograms of the PEGylated Trastuzumab show an increasing shift towards earlier elution times as the PEG-linker/tmab ratio increases (Figure 5). Resolving the exact number of PEG polymers attached per antibody molecule through SE-HPLC separation and other standard protein characterization techniques is challenging, given that the expected molecular weight (MW) increment per individual attachment corresponds to less than 4% of the MW of unmodified Trastuzumab, namely 5 kDa increments to the ~148 kDa expected MW of the antibody. Moreover, PEG molecules display heterogeneity in the number of ethylene glycol units—albeit with only small differences in MW—adding to the ensuing heterogeneity. Nonetheless, detailed characterization and homogeneity are not crucial for subsequent use as targeting agents, as long as the bulk of the protein monomers have been modified and functionality is conserved. A single

Trastuzumab monomer possesses 88 lysine residues and 4 amino-terminal groups available for reaction with the NHS group. Hence, reaction with a large number of linkers can potentially impair receptor binding. Consequently, conservation of the functionality of the PEGylated derivative was assessed prior to subsequent surface functionalization of the nanoparticles.

Binding Kinetics of Functionalized Trastuzumab

The chemically modified Trastuzumab variants (Tmab-PEG-SH, ADC and ADC-PEG-SH) were tested for their capacity to retain the binding affinity and binding kinetics to a recombinant HER2 protein after functionalization through surface plasmon resonance (SPR) single cycle kinetic analysis Figure S5).

The binding kinetics to the HER2 receptor were not significantly altered under the assay conditions. The affinity constant (KD) of the PEGylated antibodies, ranging from 5.46–6.91 pM, showed only minor differences compared to the mean KD of unmodified Trastuzumab—6.07 pM (Table 1). Kinetic constants for the antibody drug conjugate were also highly similar to the unmodified Trastuzumab. The PEGylated ADC, on the other hand, recorded a slight increase in binding rate constant (Ka) accompanied by a 32-fold increase in the dissociation rate constant (Kd), for a net 14-fold decrease KD.

The varying molar ratios of PEG-linker utilized for derivatization were deemed appropriate for subsequent attachment to the surface of gold nanoparticles, as the modified antibody did not display significant alterations in binding affinity to the cognate receptor. Henceforth, the highest molar excess (25:1 PEG-mAb ratio) for reaction was employed in order to maximize Trastuzumab attachment to AuNPs. PEGylation of Tmab-vcMMAE caused a significant decrease in KD; however, the affinity constant remains in the picomolar range, thus it is still expected to exert active targeting capacity.

Table 2. Kinetics and affinity analysis of functionalized Trastuzumab variants.

Trastuzumab Variant	K_a ($\times 10^{+6}$) $M^{-1}{\cdot}s^{-1}$	K_d ($\times 10^{+5}$) s^{-1}	K_D (pM)
Tmab	3.24 ± 0.15	1.98 ± 0.50	6.07 ± 1.27
Tmab-PEG-SH 2X	3.53 ± 0.15	2.47 ± 0.24	6.83 ± 0.68

Tmab-PEG-SH 5X	2.86 ± 0.03	1.97 ± 0.20	6.91 ± 0.78
Tmab-PEG-SH 10X	2.87 ± 0.11	1.98 ± 0.14	6.89 ± 0.21
Tmab-PEG-SH 25X	2.05 ± 0.03	1.12 ± 0.11	5.46 ± 0.44
ADC	2.25 ± 0.01	1.58 ± 0.09	7.05 ± 0.41
ADC-PEG-SH	7.45 ± 0.07	61.80 ± 0.05	85.01 ± 10.92

Gold Nanoparticle Surface Functionalization

The surface of 50 nm citrate-capped gold nanoparticles (Cit-AuNP) was functionalized with OH-PEG-SH (OH-PEG-AuNP), Tmab-PEG-SH (Tmab-PEG-AuNP), CPP-PEG-SH (CPP-PEG-AuNP), or a combination of CPP-PEG-SH and Tmab-PEG-SH (CPP+Tmab-PEG-AuNP) through a sequential addition of the bioactive agents.

Transmission electron micrograph (TEM) analysis of the synthesized Cit-AuNPs displayed a mean diameter of 48.29 ± 5.58 nm showing a narrow size distribution and uniform spherical morphology (Table 2). The mean hydrodynamic diameter obtained by DLS was 60.62 ± 0.19 nm (Z-average) with a polydispersity index (PDI) of 0.29. The SPR absorption band of the AuNPs had an absorption maximum (λ max) at 530.5 nm, consistent with the expected λ max for ~50 nm gold nanoparticles according to previously reported determinations of SPR bands of spherical AuNPs [32]. Upon surface functionalization, the λ max shifted towards longer wavelengths (red-shift)—a well-described spectral shift caused by an increase in the local refractive index on the NP surface. In increasing order, the λ max shifts were +1.9 nm for OH-PEG-AuNPs, +2.7 nm for CPP-PEG-AuNP, +3.3 nm for CPP+Tmab-PEG-AuNPs and +3.7 for Tmab-PEG-AuNPs.

The change in SPR absorption maximum was accompanied by an increase in hydrodynamic diameter (Table 2), where Tmab-PEG functionalization showed the highest increment (87.35 ± 0.41 nm). The PDIs of all surface-functionalized samples decreased relative to Cit-AuNP, indicative of enhanced colloidal stability and a consequent reduction of nanoparticle aggregation. Surface functionalization caused marked alterations in the zeta potential (ζ) of the colloidal dispersions (Table 2). Citrate-capped AuNPs displayed a mean ζ of -34.60 ± 0.91 mV, consistent with a negatively charged surface due to the negatively charged OH- groups of the citrate moiety.

Conjugation with the PEGylated-CPP yielded a mean ζ of $+6.17 \pm 071$ mV, causing a charge reversal attributable to the abundant positively charged arginine residues in HIV-TAT. The combination of cell penetrating peptide and Tmab on the AuNP surface (CPP+Tmab-PEG-AuNP) also had a slightly positively charged zeta potential ($+1.5 \pm 0.46$ mV).

Table 3. Size (Z-average), zeta potential (ζ) and absorption maximum (λ max) of surface-functionalized gold nanoparticles.

NP	Z-ave (nm)	PDI	ζ (mV)	λ max (nm)	TEM (nm)
Cit-AuNP	60.62 ± 0.19	0.29	-34.60 ± 0.91	530.5	48.29 ± 5.58
OH-PEG-AuNP	86.61 ± 0.12	0.17	-14.37 ± 0.12	532.4	
Tmab-PEG-AuNP	87.35 ± 0.41	0.17	-1.10 ± 0.46	534.2	
CPP+Tmab-PEG-AuNP	83.42 ± 2.14	0.20	1.5 ± 0.46	533.8	
CPP-PEG-AuNP	81.22 ± 0.39	0.17	6.17 ± 0.71	533.2	
ADC-PEG-AuNP	85.45 ± 1.34	0.19	-2.3 ± 0.37	534.1	

NP: nanoparticle format, PDI: polydispersity index, TEM: transmission electron microscope.

Cellular Uptake in Various Breast Cancer Cell Lines

Active Targeting in HER2-Positive SBKR-3 Cells

To evaluate the active targeting capacity of Trastuzumab-conjugated gold nanoparticles (Tmab-PEG-AuNPs), SKBR-3 cells (HER-2 positive) were incubated with 20 nm and 50 nm AuNPs coated with Tmab-PEG-SH or OH-PEG-SH. All reported values for gold uptake were obtained from ICP-MS quantification, as described in the methods section. Mean gold nanoparticle uptake per cell was significantly higher for 20 nm Tmab-PEG-AuNP ($t (10) = 6.61$, $p > 0.001$) and 50 nm Tmab-PEG-AuNPs ($t (10) = 6.96$, $p > 0.001$) compared to the OH-PEG functionalized AuNPs counterparts (Figure 6A). Qualitative assessment of cellular internalization through TEM microscopy showed localization into vesicular structures for both nanoparticles formats (Figure 6B, C).

Trastuzumab coated AuNPs did not display enhanced uptake in two other breast cancer cell lines (MCF-7 and MDA-MB-231) that are not reported to upregulate HER-2 expression (Figure 7) [33]. Uptake into DLD-1 cells (colorectal cancer HER-2 negative cell lines) showed a small increase in mean uptake per cell with no statistical significance. ADC conjugated gold nanoparticles were not employed for cellular uptake assays as the high potency of the drug can cause significant cell death at the concentrations used; thus, evaluation of cellular uptake is not comparable to the other formats.
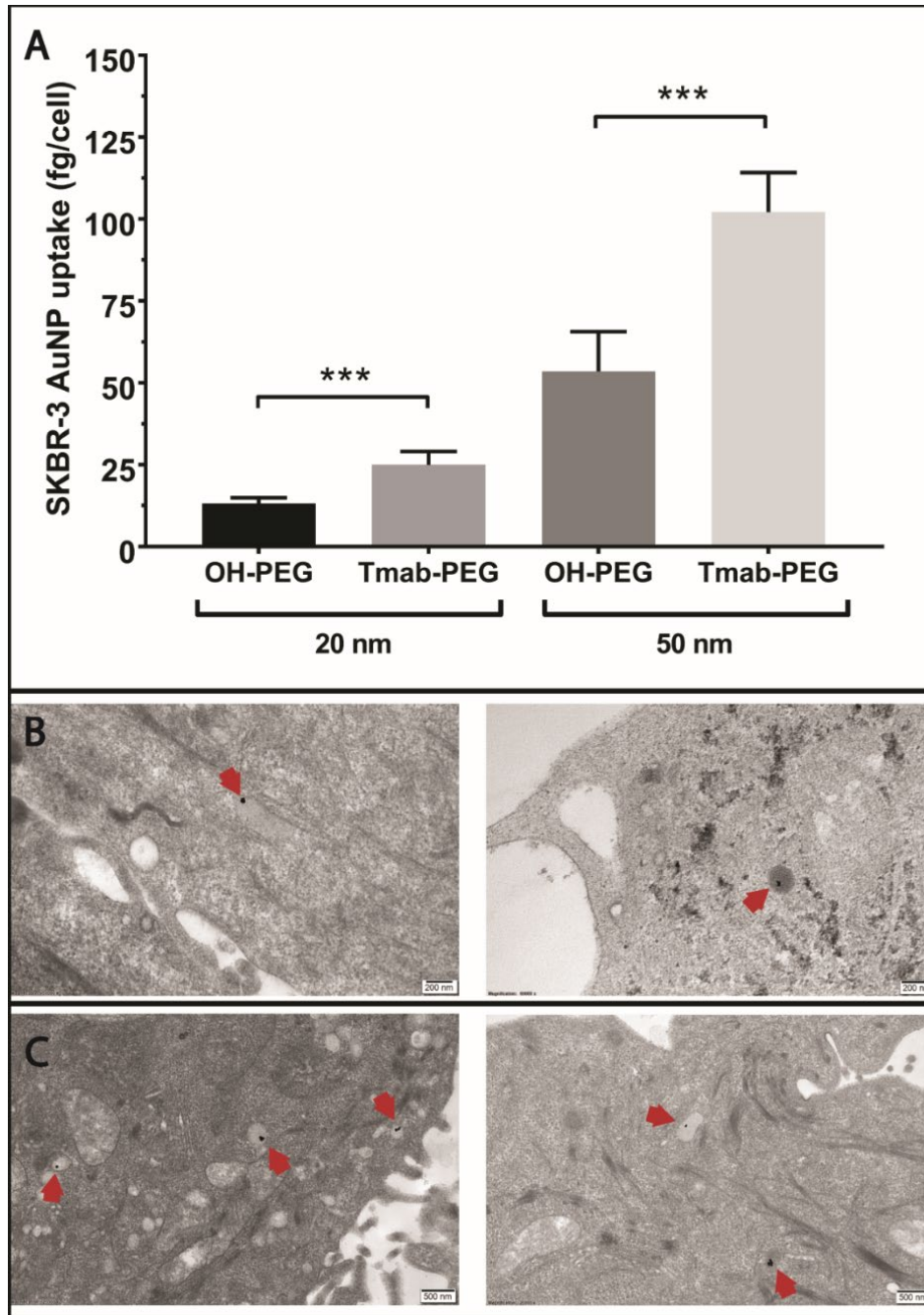
Figure 6. Evaluation of the active targeting capacity of Trastuzumab-functionalized gold nanoparticles. (A) ICP-MS quantification of OH-PEG-AuNP and Tmab-PEG-AuNP uptake into SKBR-3 cells after 24 h incubation. Uptake data are reported as means ± SD. *** $p < 0.001$ (Student's t-test). (B) TEM micrographs of OH-PEG-AuNPs internalized into SKBR-3 cells. Scale bar 200 nm (C) TEM micrographs of Tmab-PEG-AuNPs internalized into SKBR-3 cells. Scale bar: 500 nm.
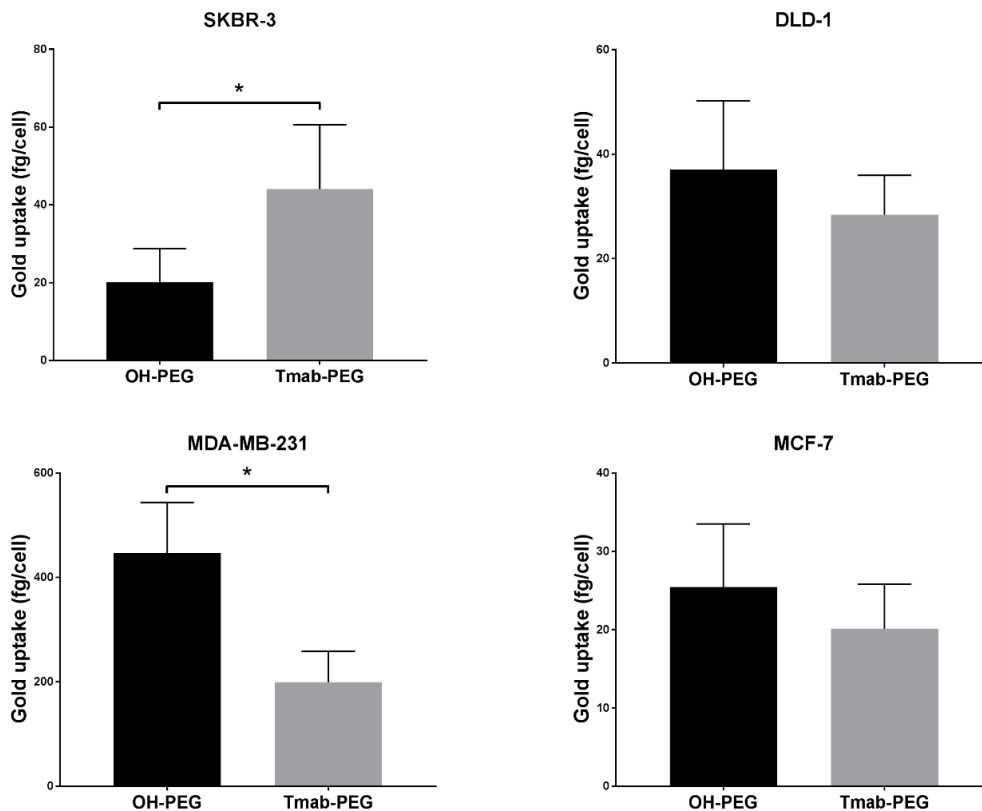
Figure 7. Active targeting of Trastuzumab functionalized gold nanoparticles in various cancer cell lines. Uptake data are reported as means ± SD. * p < 0.05 (Student's t-test). Differences between OH-PEG and Tmab-PEG functionalised gold nanoparticle uptake in DLD-1 and MCF-7 cell lines were not significant.

CPP-Driven Enhanced Internalization

To assess the effect on cell internalization using the HIV-TAT cell penetrating peptide as a coating functional group on the surface of the nanoparticles, 4 different cancer cell lines (SKBR-3, DLD-1, MDA-MB-231 and MCF-7) were treated with 25 μg/mL 50 nm gold nanoparticles functionalized with OH-PEG-SH, Tmab-PEG-SH, CPP-PEG-SH, or a combination of Tmab-PEG-SH and CPP-PEG-SH (CPP+Tmab-PEG-AuNP).

A significant increase in uptake, relative to OH-PEG-AuNP, obtained by attachment of the anti-HER2 antibody (Tmab-PEG-AuNP) was recorded for the SKBR-3 cell line (t (4) = 2.22, p > 0.05) only (Figure 7). In the same SKBR-3 cell line, AuNP functionalized with the cell penetrating peptide (CPP-PEG-AuNPs) showed approximately 1000-fold increase compared to the Tmab-

PEG-AuNP (Figure 8). Similarly, CPP-PEG-AuNPs displayed a high increase in cell uptake relative to OH-PEG-Tmab in all cell lines tested (Figure 8). CPP+Tmab-PEG-AuNP also recorded markedly higher uptake across all cell lines compared to OH-PEG-AuNP. CPP-PEG-AuNP displayed significantly higher internalization than the combination of CPP+Tmab-PEG-AuNP in SKBR-3 and MCF-7 cells, and no statistical difference was observed between these two formats in the DLD-1 and MDA-MB-231 cell lines.
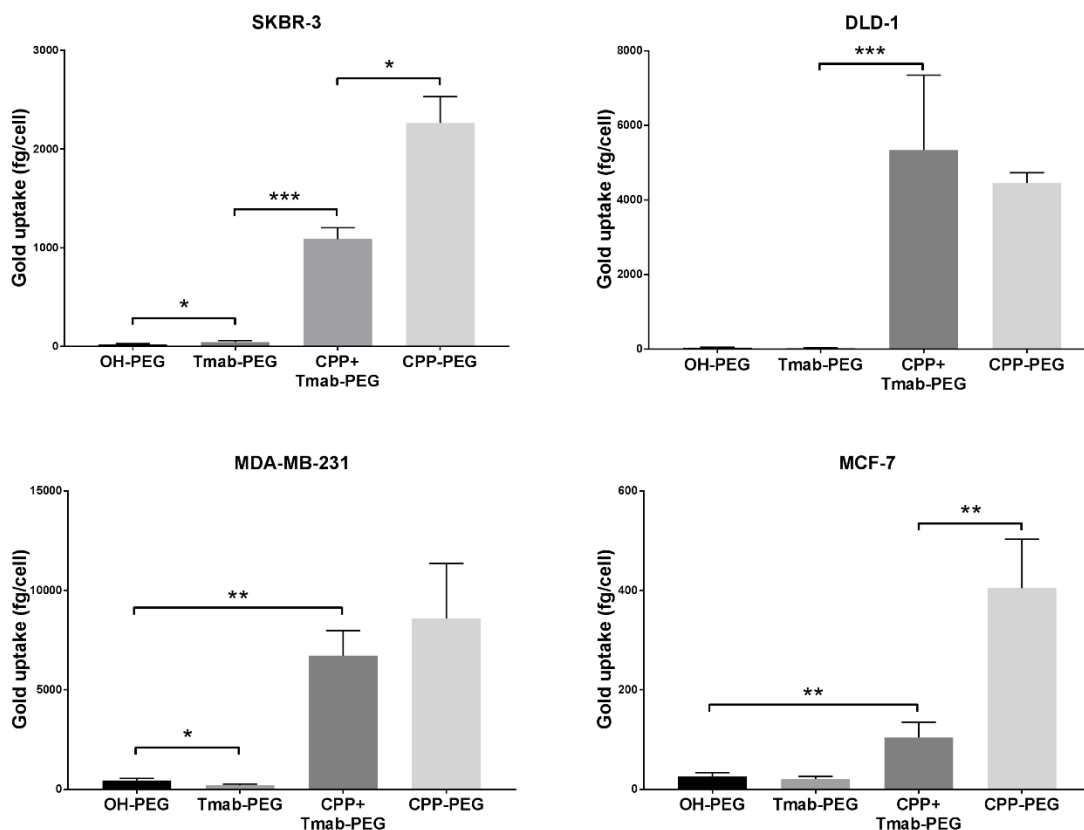
Figure 8. Cellular uptake of cell penetrating peptide (CPP) functionalized gold nanoparticles into various cancer cell lines. Uptake data are reported as means ± SD. * $p < 0.05$, ** $p < 0.01$, *** $p < 0.001$ (Student's t-test).

In Vitro Cytotoxicity of ADC-PEG-AuNP in HER2 Overexpressing Cancer Cell Lines

To assess the capacity for intracellular release of the drug payload, the *in vitro* cytotoxic activity of the antibody-drug conjugate bound to the nanoparticles (ADC-PEG-AuNP) was evaluated in two HER2 amplified cell lines: (1) SKBR-3 and (2) SKOV-3 (ovarian adenocarcinoma). Growth rate inhibition (GR) metrics derived from cell growth curves were determined to compare the

GR50 value of free MMAE, Tmab-vcMMAE, ADC-PEG-AuNP and Trastuzumab (Figure 9 and Figure S6). Growth rate calculations are specified in the methods section. GR50 corresponds to the concentration at which $GR(c) = 0.5$. ADC and ADC-PEG-AuNP concentrations reported in Figure 9 correspond to MMAE concentrations based on DAR and antibody per AuNP estimations.

The *in vitro* cytotoxic activity of free MMAE was higher in both cell lines relative to ADC and ADC-PEG-AuNP (Table 3). MMAE GR50 values were subnanomolar for both cell lines. SKOV-3 displayed slightly higher sensitivity to MMAE (GR50 = 0.14 nM) compared to SKBR-3 cells (GR50 = 0.33 nM). ADC and ADC-PEG-AuNP displayed similar GR50 values for both cell lines. Trastuzumab showed a dramatically decreased potency relative to MMAE containing formats, particularly in SKOV-3. Hence, the GR50 value was not determined for this cell line due to the high concentration of antibody required to obtain an appropriate dose-response curve. The effect on growth rate inhibition was also determined for OH-PEG-AuNP as a control. The stabilized gold nanoparticles only caused small reductions in growth rate at high nanoparticle concentrations (Figure 9).
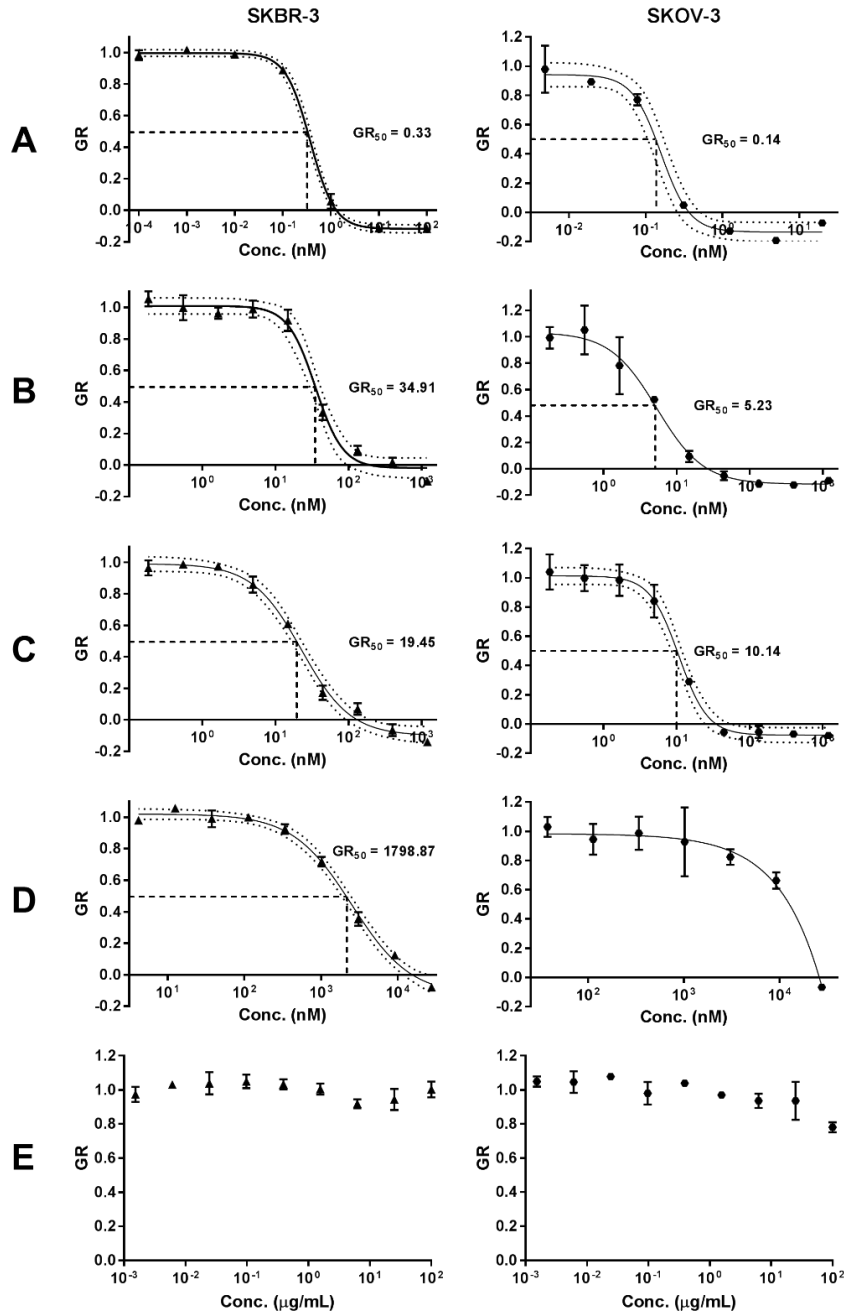
Figure 9. Growth rate (GR) inhibition of (A) free MMAE, (B) ADC, (C) ADC-PEG-AuNP, (D) Trastuzumab and (E) OH-PEG-AuNP in SKBR-3 and SKOV-3 cell lines. Data are reported as means ± SD. 95% confidence bands are displayed as dotted lines. Concentration of ADC and ADC-PEG-PEG are reported as molar concentrations of MMAE according to the estimated DAR and number of ADC per AuNP, respectively.

Table 4. GR50 values with confidence intervals (CI) obtained from dose-response curves in Figure 9.

Sample	SKBR-3			SKOV-3		
Agent	GR_{50} (nM)	GR_{50} 95% CI	R^2	SKOV-3	GR_{50} 95% CI	R^2
Free MMAE	0.33	(0.28–0.37)	0.9986	0.14	(0.11–0.17)	0.9851
ADC	34.91	(29.04–41.02)	0.9847	4.81	(3.56–6.32)	0.9636
ADC-PEG-AuNP	19.45	(16.52–22.80)	0.9913	10.14	(8.55–11.83)	0.9878
Tmab	2118.36	(1849.27–2426.61)	0.9931	N.D.	N.D.	N.D.

N.D.: not defined, CI: confidence intervals, GR50: concentration required to achieve a growth rate inhibition of 0.5.

Discussion

The lack of clinical precedent for inorganic nanoparticles has hindered their implementation in cancer therapy. However, the results of the Phase I clinical trial (NCT00356980) of CYT-6091 (PEGylated colloidal gold-rhTNF) published in 2009 were highly promising with regards to safety profile and the capacity to accumulate effectively in a wide range of solid tumors [34]. Considering the remarkable therapeutic potential of gold nanoparticles and the validation of the EPR effect for colloidal gold in human patients, we were prompted to assess three strategies; or a combination thereof, to further enhance the potential of AuNPs for clinical implementation: (1) surface attachment of PEGylated Trastuzumab for targeted treatment of HER2-positive tumors (active targeting), (2) employment of an antibody-drug conjugate as targeting agent to increase the anticancer potency of the system, and (2) surface coating with the cationic HIV-TAT cell penetrating peptide to enhance intracellular delivery.

Trastuzumab and HIV-TAT PEGylation

Attachment of poly ethylene glycol has become a conventional strategy to increase circulation times and distribution of nanosized structures. PEGylation prevents opsonization and uptake by the RES system—a biological mechanism that severely impedes tumor localization by premature clearance [35, 36]. Herein, our results support that Trastuzumab PEGylation for subsequent gold surface attachment can be readily achieved without significant modifications in HER-2 affinity or

binding kinetics as was reflected by SPR binding measurements to a recombinant HER2 protein. The same NHS-linker was used for HIV-TAT PEGylation, taking advantage of the two lysine residues in its amino acid composition (Figure 1).

ADC Construction

MMAE is a cytotoxic payload with exceptionally high potency that has frequently been employed in the construction of antibody drug conjugates. Under our experimental conditions, we obtained an average drug-to-antibody ratio of 2.91, as per UV-Vis spectroscopy analysis, consistent with DARs reported for similar ADC synthesis methods [37, 38]. For further structural characterization and confirmation of vcMMAE attachment, the ADC was analysed through intact protein mass spectrometry analysis. The ADC was buffer exchanged to MeCN 10% v/v to induce inter-heavy and heavy-light chain dissociation, in order to analyse the number of drugs attached to each polypeptide chain. Chain dissociation in MeCN 10% v/v was confirmed by SE-HPLC chromatograms showing the appearance of two peaks at longer elution times (Figure S2). The deconvoluted mass spectra confirmed that vcMMAE can attach to all possible free sulfhydryl groups formed upon partial reduction, i.e., a maximum of three attachments on the heavy chain and one attachment on the light chain.

Herein, our results report on the feasibility of combining two common bioconjugation techniques (lysine and cysteine attachment) to PEGylate Tmab-vcMMAE for nanoparticle attachment. Furthermore, our data show that HER-2 binding affinity decreases by an order or magnitude with ADC PEGylation; yet, the binding affinity remains within the picomolar range. Several studies have combined targeting agents and cytotoxic drugs on nanoparticles; however, the added complexity of the systems also complicates appropriate characterization for implementation, especially in regard to dosage determination as the amount of each individual component requires quantification. To this end, the use of antibody-drug conjugates as targeting agents carrying the payload could simplify this—provided that the DAR is determined, quantification of protein content would be sufficient to estimate drug dosage per nanoparticle.

Gold Nanoparticle Surface Functionalization

Adding to improved biodistribution and tumor targeting, PEGylation also increases the colloidal stability of gold nanoparticles—a key requirement for long-term storage. Attachment of the

bioactive groups was achieved through the thiol moiety of the PEG linker, which, at high pH, can form covalent gold-sulfur (Au-S) bonds, providing stable conjugation to the surface [11]. Indeed, surface functionalization had a pronounced enhancement in nanoparticle stability upon addition of 1% NaCl and cell culture media (Figure S3). Attachment was confirmed by an increase in hydrodynamic size (DLS) and SPR absorption maxima, and most importantly by alterations in the zeta potential that allow to discriminate the presence of the bioactive groups. For instance, the positively charged HIV-TAT caused a charge reversal in zeta potential (+6.17 ± 0.71 mV) for a +40.77 mV shift compared to the citrate-capped gold nanoparticles (−34.60 mV). In contrast, coating with the neutral OH-PEG caused a smaller +20.23 mV shift. Zeta potential values closer to the isoelectric point are generally detrimental to colloidal stability; however, the hydrophilic PEG polymer on the surface impedes nanoparticle aggregation by steric hindrance to prevent surface interactions between AuNPs. The large exclusion volume of the hydration cloud of the PEG linkers is known to prevent interactions between nanoparticle surfaces that lead to aggregation [35].

Quantification of the average number of antibodies that coat individual nanoparticles is challenging, insofar as common colorimetric methods for protein quantitation are difficult to perform due to the much stronger absorption coefficients of gold nanoparticles throughout the wavelength ranges used for protein concentration measurements. Instead, we quantified the amount of antibody by accounting for the ensuing decrease in antibody concentration following attachment, after removal of the functionalized nanoparticles through centrifugation. According to these measurements, an average of 156 antibodies covered the surface of 50 nm AuNPs and 40 antibodies on 20 nm AuNPs (Figure S4).

Active Targeting and Cellular Uptake

The multivalent presentation of Trastuzumab on gold nanoparticles has been shown previously to promote HER2 receptor crosslinking, leading to enhanced cellular internalization in HER2 overexpressing cell lines [39]. In our experimental setup, Trastuzumab-coated gold nanoparticles were compared to the AuNPs coated with the SH-linker without antibody derivatization, to maximize the similarity in physicochemical properties, excluding the presence of protein. Indeed, the mean hydrodynamic diameter of both formats differed by less than 1 nm according to DLS measurements (Table 2). Electrophoretic mobility determinations, on the other hand, recorded

negative zeta potential values for OH-PEG-AuNPs and close to neutral values for Tmab-PEG-AuNP. The drift towards more neutral values—relative to citrate-capped nanoparticles—is consistent with antibody attachment, as Trastuzumab (isoelectric point (pI) 8.7) possesses a net positive charge when dissolved in PBS. A small net positive charge is also expected when suspended in cell culture media (pH 7.4). The effect of nanoparticle surface charge on cellular uptake is well-documented, whereby positively charged nanoparticles have consistently displayed higher uptake rates in nonphagocytic cells [40]. The increase in internalization with positively charged surfaces has generally been ascribed to favorable electrostatic nanoparticle/cell interactions due to the net negative charge of the plasma membrane [40]. In view of the foregoing, it is difficult to rule out a contribution of the more neutral zeta potential of Tmab-PEG-AuNP in enhancing cellular uptake. This notwithstanding, the observation that internalization enhancement was only recorded in a HER2 overexpressing cell line (SKBR-3)—and not in the HER2 basal counterparts (DLD-1, MDA-MB-231 and MCF-7)—supports cellular uptake increase through Trastuzumab-mediated HER2 receptor crosslinking. Interestingly, TEM micrographs of SKBR-3 cells did not show clear distinction between both formats in subcellular localization—i.e., both AuNP designs were primarily localized within vesicular structures, presumably coated preendosomal and carrier vesicles (early endosomes and lysosomes). Alternatively, it is possible that some of these structures are autophagosomes, as gold nanoparticles have been shown to induce autophagosome accumulation [41]. This observation warrants further elucidation of the effect of surface functionalization on uptake mechanism and localization.

Cellular Uptake Enhancement with HIV-TAT

Due to the relatively low loading capacity of spherical gold nanoparticles, it is essential to ensure maximum cellular internalization when developed as drug delivery vehicles. Having improved selective uptake into HER2 overexpressing cell lines through active targeting, we sought to evaluate the effect of combining a cell penetrating peptide with the antibody targeting agent. HIV-TAT internalization mechanism remains a topic of debate; however, evidence of uptake saturability and energy dependency suggest an endosomal pathway [42]. Endosomal and subsequent lysosomal localization is required for effective drug release of cathepsin B-cleavable linkers, such as those containing the valine-citrulline dipeptide. Enhancing uptake is thus paramount in HER2-targeted conjugates for intracellular release, considering that most ErbB

receptors have shown impaired ligand-induced receptor trafficking [43]. To this end, functionalization with the cell penetrating peptide caused a dramatic increase in cellular uptake across all cell lines tested. This enhancement was considerably more significant than that obtained by antibody functionalization only. Conversely, our results did not show improvement in uptake upon combination of both bioactive agents compared to CPP-PEG-AuNP. In fact, uptake was significantly higher with CPP functionalization in SKBR-3 and MCF-7 cells. We presume that this observation stems from the more positive zeta potential of CPP-PEG-AuNPs, in which case engagement through cell membrane/nanoparticle electrostatic interactions is a stronger determinant of uptake rate than antibody-mediated receptor cross-linking.

These findings warrant further investigation into the effect of the highlighted physicochemical and physiological attributes in a more physiological setting. While higher uptake may be desirable in delivery applications, internalization must be specific to the targeted tumor cells. Previous studies have reported that uptake, rather than diffusion, could be the primary mechanism for nanoparticle tumor delivery. Consequently, surface charge has been proposed as a major determinant in tumor distribution upon systemic administration [44]. If indeed transcellular transport has a crucial impact in tumor penetration, then enhancing cellular internalization through strategies such as the attachment of a cell penetrating peptide might provide improved tumor tissue distribution, thus enhancing efficacy and therapeutic index.

In Vitro Cytotoxicity of ADC-PEG-AuNP in HER2 Overexpressing Cancer Cell Lines

Growth rate inhibition sensitivity in SKOV-3 and SKBR-3 cell lines was markedly higher for free MMAE than for the antibody-drug conjugate and for ADC-carrying gold nanoparticles (Figure 8). It is plausible that the requirement of linker cleavage and self-immolation of the p-aminobenzyl carbamate group in the antibody-drug conjugate hinders conjugated vcMMAE activity compared to the free drug. Additionally, although HER2 binding and cross-linking can induce receptor-mediated endocytosis, free MMAE likely penetrates more readily into the intracellular compartment. Nonetheless, the structural characteristics that presumably hinder conjugated vcMMAE cytotoxicity in isolated carcinoma cells are expected to provide selectivity advantages in more physiological settings.

Comparison of the cytotoxic activity of free ADC and nanoparticle-conjugated ADC displayed similar GR50 for both SKBR-3 and SKOV-3 cells (Table 3). GR50 values for ADC-PEG-AuNP

were lower for SKBR-3 cells and higher for SKOV-3 cells relative to free ADC; however, due to the degree of uncertainty in the estimation of antibodies per nanoparticle it is difficult to establish a significant improvement in MMAE intracellular release and antimitotic activity for either one of the formats. Still, concentrations of ADC-PEG-AuNP required to achieve a 50% growth rate inhibition were extremely low in both HER2 amplified cell lines. As expected, the antimitotic activity of MMAE-containing formats is dramatically higher than that of the unmodified Trastuzumab and PEG-stabilized gold nanoparticles. OH-PEG-AuNPs only caused small reductions in growth rate at high gold concentrations (100 µg/mL) in SKOV-3, which is higher than the equivalent gold concentrations required to achieve a 50% growth rate inhibition in ADC-PEG-AuNPs (> 20 µg/mL). These results confirm that MMAE antibody-drug conjugate retain a highly potent cytotoxic activity when bound to the surface of gold nanoparticles. These findings warrant further investigation in animal models, as increased accumulation in high EPR tumors could confer potency and safety advantages over the free ADC.

Conclusions

The results presented herein report on the feasibility of utilizing multiple bioactive agents to construct gold nanoparticles with broader therapeutic capabilities. The construction of a thiol-functionalized PEGylated antibody drug-conjugate (PEGylated Trastuzumab-vcMMAE) proved to yield ADCs with conserved high affinity towards the HER2 receptor; thereby enabling coupling to gold nanoparticles to function as targeting agents carrying a cytotoxic payload. ADCs attached to the surface of gold nanoparticles demonstrated to retain similar *in vitro* cytotoxic potency against HER2 overexpressing cancer cell lines relative to the free ADC. Notwithstanding, enhanced accumulation in high EPR tumors could results in wider therapeutic indices.

Cellular uptake of AuNPs in a HER2 amplified cell line was significantly improved upon covalent attachment of the Trastuzumab targeting agent through the PEGylated-SH linker. Internalization into different cancer cell lines was further enhanced by employing the HIV-1 TAT protein (47–57) as a cell penetrating peptide. Yet, the combination of the antibody targeting agent and the penetrating peptide did not provide improvements in uptake—relative to the penetrating peptide only—in the conditions tested. Our results support previous observations with different nanoparticle formats with regards to the prominent role of surface charge on determining uptake rate into cells, insofar as the charge reversal obtained by incorporating the cell penetrating peptide

had a more pronounced impact than the addition of the antibody targeting agent. Efficient cleavage of the valine-citrulline moiety for drug release requires cellular internalization for exposure to cathepsin B in lysosomes or endosomes; therefore, incorporation of the CPP might provide improved intracellular delivery of the MMAE payload in this format.

Supplementary Materials: The following are available online at www.mdpi.com/xxx/s1, Figure S1: Analysis of the presence of sulfhydryl groups and conservation of intact structure of Trastuzumab after partial reduction with DTT, Figure S2: SE-HPLC chromatograms of partially reduced Trastuzumab in 1 mM EDTA, Tmab-vcMMAE in H2O and Tmab-vcMMAE in acetonitrile 10% with formic acid 1%, Figure S3: AuNP stability upon surface functionalization with Tmab-PEG-SH. Addition of 1% NaCl to citrate capped AuNPs caused aggregation as evidenced by a broad absorption band in the 700–800 nm range, Figure S4: Representative tryptophan fluorescence emission spectra for the estimation of Trastuzumab:AuNP ratio for 20 nm AuNPs, Figure S5: Representative sensorgrams of (A) Trastuzumab, (B) Tmab-PEG-SH 25X and (C) Tmab-vcMMAE binding to recombinant HER2 receptor, Figure S6: Representative SKBR-3 cell growth curves employed to analyse growth rate inhibition activity of MMAE-containing agents at equivalent MMAE concentrations.

Author Contributions

E.C. and V.K. conceived the design. E.C. designed the study, performed all experimental work and data analysis and wrote the manuscript. V.K. supervised the development of the study, contributed to data interpretation and manuscript evaluation and editing.

Funding

Conflicts of Interest

The authors declare no conflict of interest

References

[1]. Heldin, C.H.; Rubin, K.; Pietras, K.; Ostman, A. High interstitial fluid pressure-an obstacle in cancer therapy. Nat. Rev. Cancer, 4 (2004), 806–813, doi:10.1038/nrc1456.

[2]. Netti, P.A.; Baxter, L.T.; Boucher, Y.; Skalak, R.; Jain, R.K. Time-dependent behavior of interstitial fluidpressure in solid tumors: Implications for drug delivery. Cancer Res, 55 (1995) 5451–5458.

[3]. Tredan, O.; Galmarini, C.M.; Patel, K.; Tannock, I.F. Drug resistance and the solid tumor microenvironment. J Natl Cancer Inst, 99 (2007), 1441–1454, doi:10.1093/jnci/djm135.

[4]. Matsumura, Y.; Maeda, H. A new concept for macromolecular therapeutics in cancer chemotherapy: Mechanism of tumoritropic accumulation of proteins and the antitumor agent smancs. Cancer Res, 46 (1986), 6387–6392.

[5]. Tran, S.; DeGiovanni, P.-J.; Piel, B.; Rai, P. Cancer nanomedicine: A review of recent success in drug delivery. Clin Transl Med, 6 (2017), 44–44, doi:10.1186/s40169-017-0175-0.

[6]. Jin, S.; Leach, J.C.; Ye, K. Nanoparticle-mediated gene delivery. Methods Mol. Biol. 544 (2009), 547–557, doi:10.1007/978-1-59745-483-4_34.

[7]. Manthe, R.L.; Foy, S.P.; Krishnamurthy, N.; Sharma, B.; Labhasetwar, V. Tumor ablation and nanotechnology. Mol Pharm, 7 (2010), 1880–1898, doi:10.1021/mp1001944.

[8]. Will, O.; Purkayastha, S.; Chan, C.; Athanasiou, T.; Darzi, A.W.; Gedroyc, W.; Tekkis, P.P. Diagnostic precision of nanoparticle-enhanced MRI for lymph-node metastases: A meta-analysis. Lancet Oncol, 7 (2006), 52–60, doi:10.1016/s1470-2045(05)70537-4.

[9]. Lukianova-Hleb, E.Y.; Ren, X.; Sawant, R.R.; Wu, X.; Torchilin, V.P.; Lapotko, D.O. On-demand intracellular amplification of chemoradiation with cancer-specific plasmonic nanobubbles. Nat Med, 20 (2014), 778, doi:10.1038/nm.3484.

[10]. Kyriazi, M.-E.; Giust, D.; El-Sagheer, A.H.; Lackie, P.M.; Muskens, O.L.; Brown, T.; Kanaras, A.G. Multiplexed mRNA Sensing and Combinatorial-Targeted Drug Delivery Using DNA-Gold Nanoparticle Dimers. ACS Nano, 12 (2018), 3333–3340, doi:10.1021/acsnano.7b08620.

[11]. Xue, Y.; Li, X.; Li, H.; Zhang, W. Quantifying thiol–gold interactions towards the efficient strength control. Nat Commu, 5 (2014), 4348, doi:10.1038/ncomms5348.

[12]. Wilhelm, S.; Tavares, A.J.; Dai, Q.; Ohta, S.; Audet, J.; Dvorak, H.F.; Chan, W.C.W. Analysis of nanoparticle delivery to tumours. Nat Rev Mater 1 (2016), 16014, doi:10.1038/natrevmats.2016.14.

[13]. Alkilany, A.M.; Murphy, C.J. Toxicity and cellular uptake of gold nanoparticles: What we have learned so far? J. Nanopart. Res. Interdiscip. Forum Nanoscale Sci Technol, 12 (2010), 2313–2333, doi:10.1007/s11051-010-9911-8.

[14]. Goel, R.; Shah, N.; Visaria, R.; Paciotti, G.F.; Bischof, J.C. Biodistribution of TNF-alpha-coated gold nanoparticles in an *in vivo* model system. Nanomedicine, 4 (2009), 401–410, doi:10.2217/nnm.09.21.

[15]. Byrne, J.D.; Betancourt, T.; Brannon-Peppas, L. Active targeting schemes for nanoparticle systems in cancer therapeutics. Adv Drug Deliv Rev, 60 (2008), 1615–1626, doi:10.1016/j.addr.2008.08.005.

[16]. Rosenblum, D.; Joshi, N.; Tao, W.; Karp, J.M.; Peer, D. Progress and challenges towards targeted delivery of cancer therapeutics. Nat Commu, 9 (2018), 1410, doi:10.1038/s41467-018-03705-y.

[17]. Slamon, D.J.; Leyland-Jones, B.; Shak, S.; Fuchs, H.; Paton, V.; Bajamonde, A.; Fleming, T.; Eiermann, W.; Wolter, J.; Pegram, M.; et al. Use of Chemotherapy plus a Monoclonal Antibody against HER2 for Metastatic Breast Cancer That Overexpresses HER2. N Engl J Med, 344 (2001), 783–792, doi:10.1056/NEJM200103153441101.

[18]. Bang, Y.J.; Van Cutsem, E.; Feyereislova, A.; Chung, H.C.; Shen, L.; Sawaki, A.; Lordick, F.; Ohtsu, A.; Omuro, Y.; Satoh, T.; et al. Trastuzumab in combination with chemotherapy versus chemotherapy alone for treatment of HER2-positive advanced gastric or gastro-oesophageal junction cancer (ToGA): A phase 3, open-label, randomised controlled trial. Lancet, 376 (2010), 687–697, doi:10.1016/s0140-6736(10)61121-x.

[19]. Fléjou, J.F.; Paraf, F.; Muzeau, F.; Fékété, F.; Hénin, D.; Jothy, S.; Potet, F. Expression of c-erbB-2 oncogene product in Barrett's adenocarcinoma: Pathological and prognostic correlations. J Clin Pathol, 47 (1994), 23, doi:10.1136/jcp.47.1.23.

[20]. Berchuck, A.; Kamel, A.; Whitaker, R.; Kerns, B.; Olt, G.; Kinney, R.; Soper, J.T.; Dodge, R.; Clarke-Pearson, D.L.; Marks, P.; et al. Overexpression of HER-2/neu Is Associated with Poor Survival in Advanced Epithelial Ovarian Cancer. Cancer Res, 50 (1990), 4087.

[21]. Rolitsky, C.D.; Theil, K.S.; McGaughy, V.R.; Copeland, L.J.; Niemann, T.H. HER-2/neu amplification and overexpression in endometrial carcinoma. Int J Gynecol Pathol, 18 (1999), 138–143, doi:10.1097/00004347-199904000-00007.

[22]. Nakajima, M.; Sawada, H.; Yamada, Y.; Watanabe, A.; Tatsumi, M.; Yamashita, J.; Matsuda, M.; Sakaguchi, T.; Hirao, T.; Nakano, H. The prognostic significance of amplification and overexpression of c-met and c-erb B-2 in human gastric carcinomas. Cancer, 85 (1999), 1894–1902, doi:10.1002/(SICI)1097-0142(19990501)85:9<1894:AID-CNCR3>3.0.CO;2-J.

[23]. Santin, A.D.; Bellone, S.; Van Stedum, S.; Bushen, W.; Palmieri, M.; Siegel, E.R.; De Las Casas, L.E.; Roman, J.J.; Burnett, A.; Pecorelli, S. Amplification of c-erbB2 oncogene. Cancer, 104 (2005), 1391–1397, doi:10.1002/cncr.21308.

[24]. Yonemura, Y.; Ninomiya, I.; Yamaguchi, A.; Fushida, S.; Kimura, H.; Ohoyama, S.; Miyazaki, I.; Endou, Y.; Tanaka, M.; Sasaki, T. Evaluation of Immunoreactivity for erbB-2 Protein as a Marker of Poor Short Term Prognosis in Gastric Cancer. Cancer Res, 51 (1991), 1034.

[25]. Hudis, C.A. Trastuzumab--mechanism of action and use in clinical practice. N Engl J Med, 357 (2007), 39–51, doi:10.1056/NEJMra043186.

[26]. Liu, M.; Yang, Y.J.; Zheng, H.; Zhong, X.R.; Wang, Y.; Wang, Z.; Wang, Y.G.; Wang, Y.P. Membrane-bound complement regulatory proteins are prognostic factors of operable breast cancer treated with adjuvant trastuzumab: A retrospective study. Oncol Rep, 32 (2014), 2619–2627, doi:10.3892/or.2014.3496.

[27]. Elgundi, Z.; Reslan, M.; Cruz, E.; Sifniotis, V.; Kayser, V. The state-of-play and future of antibody therapeutics. Adv Drug Deliv Rev, 122 (2017), 2–19, doi:10.1016/j.addr.2016.11.004.

[28]. Thurber, G.M.; Schmidt, M.M.; Wittrup, K.D. Antibody tumor penetration: Transport opposed by systemic and antigen-mediated clearance. Adv Drug Deliv Rev, 60 (2008), 1421–1434, doi:10.1016/j.addr.2008.04.012.

[29]. Lee, C.M.; Tannock, I.F. The distribution of the therapeutic monoclonal antibodies cetuximab and trastuzumab within solid tumors. BMC Cancer, 10 (2010), 255–255, doi:10.1186/1471-2407-10-255.

[30]. Hermanson, G.T. Chapter 18-PEGylation and Synthetic Polymer Modification. In Bioconjugate Techniques, 3rd ed.; Hermanson, G.T., Ed.; Academic Press: Boston, MA, USA, 2013, doi:10.1016/B978-0-12-382239-0.00018-2pp. 787-838.

[31]. Gustafson, H.H.; Holt-Casper, D.; Grainger, D.W.; Ghandehari, H. Nanoparticle Uptake: The Phagocyte Problem. Nano Today, 10 (2015), 487–510, doi:10.1016/j.nantod.2015.06.006.

[32]. Haiss, W.; Thanh, N.T.K.; Aveyard, J.; Fernig, D.G. Determination of Size and Concentration of Gold Nanoparticles from UV−Vis Spectra. Anal Chem, 79 (2007), 4215–4221, doi:10.1021/ac0702084.

[33]. Holliday, D.L.; Speirs, V. Choosing the right cell line for breast cancer research. Breast Cancer Res, 13 (2011), 215, doi:10.1186/bcr2889.

[34]. Libutti, S.K.; Paciotti, G.F.; Byrnes, A.A.; Alexander, H.R., Jr.; Gannon, W.E.; Walker, M.; Seidel, G.D.; Yuldasheva, N.; Tamarkin, L. Phase I and pharmacokinetic studies of CYT-6091, a novel PEGylated colloidal gold-rhTNF nanomedicine. Clin Cancer Res, 16 (2010), 6139–6149, doi:10.1158/1078-0432.ccr-10-0978.

[35]. Suk, J.S.; Xu, Q.; Kim, N.; Hanes, J.; Ensign, L.M. PEGylation as a strategy for improving nanoparticle-based drug and gene delivery. Adv Drug Deliv Rev, 99 (2016), 28–51, doi:10.1016/j.addr.2015.09.012.

[36]. Gref, R.; Minamitake, Y.; Peracchia, M.T.; Trubetskoy, V.; Torchilin, V.; Langer, R. Biodegradable long-circulating polymeric nanospheres. Science, 263 (1994), 1600–1603.

[37]. Adem, Y.T.; Schwarz, K.A.; Duenas, E.; Patapoff, T.W.; Galush, W.J.; Esue, O. Auristatin Antibody Drug Conjugate Physical Instability and the Role of Drug Payload. Bioconj Chem, 25 (2014), 656–664, doi:10.1021/bc400439x.

[38]. Li, F.; Emmerton, K.K.; Jonas, M.; Zhang, X.; Miyamoto, J.B.; Setter, J.R.; Nicholas, N.D.; Okeley, N.M.; Lyon, R.P.; Benjamin, D.R.; et al. Intracellular Released Payload Influences Potency and Bystander-Killing Effects of Antibody-Drug Conjugates in Preclinical Models. Cancer Res, 76 (2016), 2710–2719, doi:10.1158/0008-5472.can-15-1795.

[39]. Jiang, W.; Kim, B.Y.S.; Rutka, J.T.; Chan, W.C.W. Nanoparticle-mediated cellular response is size-dependent. Nat Nanotechnol, 3 (2008), 145, doi:10.1038/nnano.2008.30. https://www.nature.com/articles/nnano.2008.30#supplementary-information.

[40]. Cho, E.C.; Xie, J.; Wurm, P.A.; Xia, Y. Understanding the Role of Surface Charges in Cellular Adsorption versus Internalization by Selectively Removing Gold Nanoparticles on the Cell Surface with a I2/KI Etchant. Nano Lett, 9 (2009), 1080–1084, doi:10.1021/nl803487r.

[41]. Ma, X.; Wu, Y.; Jin, S.; Tian, Y.; Zhang, X.; Zhao, Y.; Yu, L.; Liang, X.-J. Gold Nanoparticles Induce Autophagosome Accumulation through Size-Dependent Nanoparticle Uptake and Lysosome Impairment. ACS Nano, 5 (2011), 8629–8639, doi:10.1021/nn202155y.

[42]. Tkachenko, A.G.; Xie, H.; Liu, Y.; Coleman, D.; Ryan, J.; Glomm, W.R.; Shipton, M.K.; Franzen, S.; Feldheim, D.L. Cellular Trajectories of Peptide-Modified Gold Particle Complexes: Comparison of Nuclear Localization Signals and Peptide Transduction Domains. Bioconj. Chem, 15 (2004), 482–490, doi:10.1021/bc034189q.

[43]. Baulida, J.; Kraus, M.H.; Alimandi, M.; Di Fiore, P.P.; Carpenter, G. All ErbB receptors other than the epidermal growth factor receptor are endocytosis impaired. J Biol Chem, 271 (1996), 5251–5257.

[44]. Kim, B.; Han, G.; Toley, B.J.; Kim, C.-k.; Rotello, V.M.; Forbes, N.S. Tuning payload delivery in tumour cylindroids using gold nanoparticles. Nat. Nanotechnol, 5 (2010), 465, doi:10.1038/nnano.2010.58. https://www.nature.com/articles/nnano.2010.58#supplementary-information.

[45]. Turkevich, J.; Stevenson, P.C.; Hillier, J. The Formation of Colloidal Gold. J Phys Chem, 57 (1953), 670–673, doi:10.1021/j150508a015.

[46]. Frens, G. Controlled Nucleation for the Regulation of the Particle Size in Monodisperse Gold Suspensions. Nat Phys Sci, 241 (1973), 20, doi:10.1038/physci241020a0.

[47]. Kelly, S.T.; Zydney, A.L. Effects of intermolecular thiol–disulfide interchange reactions on bsa fouling during microfiltration. Biotechnol Bioeng, 44 (1994), 972–982, doi:10.1002/bit.260440814.

[48]. Trivedi, M.V.; Laurence, J.S.; Siahaan, T.J. The role of thiols and disulfides on protein stability. Curr Protein Pept Sci, 10 (2009), 614–625.

[49]. Hamblett, K.J.; Senter, P.D.; Chace, D.F.; Sun, M.M.; Lenox, J.; Cerveny, C.G.; Kissler, K.M.; Bernhardt, S.X.; Kopcha, A.K.; Zabinski, R.F.; et al. Effects of drug loading on the antitumor activity of a monoclonal antibody drug conjugate. Clin Cancer Res, 10 (2004), 7063–7070, doi:10.1158/1078-0432.ccr-04-0789.

[50]. Hafner, M.; Niepel, M.; Chung, M.; Sorger, P.K. Growth rate inhibition metrics correct for confounders in measuring sensitivity to cancer drugs. Nat Methods, 13 (2016), 521–527, doi:10.1038/nmeth.3853.

CONCLUDING REMARKS AND FUTURE DIRECTIONS

Landmark discoveries in the field of molecular biology in the 1990's ushered in a new era in the biomedical field with the introduction of a plethora of recombinant products into the pharmaceutical market. Biotherapeutics have since experienced tremendous growth, best exemplified by the current dominance of antibody therapeutics in the pharmaceutical market. The field continues to capitalize on these discoveries, as novel bio-engineering approaches are sought to improve established therapies based on further advancements in molecular biology and other disciplines. While the latter provide manifold opportunities, these also entail prominent challenges towards clinical development and regulatory approval. The experimental work contained in this thesis reports on various novel approaches that make use of recent progress in the field aimed towards the improvement of biological therapies, showcasing the application of state-of-the-art mass spectrometry techniques to address key aspects in various stages of preclinical development.

The first aim of this thesis consisted in exploiting recently developed methodologies in mass spectrometry to study a structural feature of influenza hemagglutinin that has recently gained notoriety in the study of viral evolution, namely the alterations in the number and position of N-glycosylation sequons on the viral glycoprotein. Remarkably, the implementation of rationally-designed vaccines for influenza and other infectious diseases has remained elusive, despite myriad advancements in recombinant technologies and an imminent need to improve currently available options. This, in many cases, stems from insufficient understanding of immune response mechanisms, antigenic determinants, and viral adaptation mechanisms. Thus, we sought to apply a targeted workflow on whole viruses of a specific H1N1 strain to obtain the glycan profile of influenza hemagglutnin as a proof-of-concept. Notably, the MS experimental setup employs complementary activation modes that enable the determination of glycan structures on specific sites of the protein. Hence, not only does it provide identification of glycosylation sites, but by deriving structural features of the glycans it allows to assess the impact of localisation on glycan maturation. Through this method, we acquired extensive site-specific structural data on H1 hemagglutinin without the need for protein purification or complex sample preparation. This work

prompts implementation of such analytical workflows to obtain glycosylation profiles of further relevant influenza glycoproteins. This information will contribute to the study of influenza antigenicity and serve as an important complement to biological activity and comprehensive sequence-data based studies for this aim. Notably, understanding the role of N-glycans in antigenicity provides opportunities for glycoprotein engineering towards the development of optimized vaccines platforms. For instance, protein glycoengineering strategies, such as the one covered in chapters 4 and 5, could be employed to modulate the antigenicity of recombinant vaccine formats.

The succeeding sections of this thesis address further facets in the rational design of biomolecules for therapeutic purposes. The second aim of this thesis – addressed in chapters 3, 4, and 5 – sought to put forward and evaluate an innovative approach to alter the physicochemical properties of the conserved structural regions of IgG1 molecules, with the intent of developing a generalised strategy to enhance the clinical potential of antibody therapeutics by increasing their physical stability. Chapter 3 serves as an introductory chapter to the subsequent research manuscripts (chapters 4 and 5), presenting an overview of the complications that physical degradation poses on the development and manufacture of antibody therapeutics. The chapter provides a brief description of various computational tools that have been developed to enable in silico identification of aggregation-prone regions. The structural modifications implemented in chapters 4 and 5 were derived from one such tool, namely the Spatial Aggregation Propensity (SAP) prediction.

Chapters 4 and 5 report on the targeted insertion of glycosylation sites on monoclonal antibodies to deter aggregation propensity and enhance solubility by shielding aggregation-prone regions identified by SAP. Rationally designed mutations were introduced on the primary structure of blockbuster therapeutic antibodies – adalimumab in chapter 4 and trastuzumab in chapter 5 – to explore the possibility of enhancing the clinical properties of established therapeutics mAbs. Naturally, this technique can equally be applied to mAb leads in preclinical development. We demonstrated in chapter 4 that the hyperglycosylation strategy can confer important improvements in the thermodynamic stability of the Fab region, reflected by increases in the corresponding melting temperature. Importantly, this was achieved without compromising the high binding affinity to the molecular target of adalimumab (TNF-α) or to Fc-receptors involved in effector

functions, indicating that the biological activity of an IgG molecule is unlikely to be impaired by glycosylation of the targeted sites. Contrary to previous reports employing this technique in other antibodies, it was not possible to establish enhancements in aggregation resistance in accelerated stability studies when incorporated in adalimumab. To understand these seemingly contradictory observations, further insight is needed into the mechanisms that drive antibody aggregation and into the structural modifications that emerge upon glycosite addition. Moreover, additional long-term experiments evaluating the physicochemical stability of the protein at lower temperatures are needed to ascertain the colloidal stability of the protein under conditions that better reflect the storage of antibody therapeutics in a clinical context.

Hyperglycosylation of trastuzumab in chapter 5 revealed an important consequence of the technique: the overall structural heterogeneity of the protein increases markedly due to extensive glycan maturation in the Fab glycosylation sites. In comparison, glycan heterogeneity in the conserved Fc-region is relatively limited as a result of the atypical orientation of these glycans towards the core of the protein. Although controlling Fc glycosylation is presumably more important, due to the well-studied interactions that glycoforms in this position establish with Fc-receptors, the large increase in heterogeneity obtained through hyperglycosylation is likely to have important implications for regulatory approval if this strategy is to be pursued in therapeutic antibodies. These findings prompt further study of the impact of individual glycoforms on self-association mechanisms and enhancements in thermodynamic stability of the domain.

Altogether, the experimental data reported herein for the glycosite insertion strategy highlight the potential of this method to enhance the physical stability of therapeutic antibodies, yet it also underscores aspects of the technique that require further refinement for implementation. We presume that combining this approach with other glycoengineering technologies that minimise glycan heterogeneity could have great potential. It is important to note that inserting engineered glycosylation sites can be employed to enhance the biophysical properties of further therapeutic proteins. Moreover, the method enables protein functionalisation in a targeted fashion, since the glycan can be used as a chemical handle with a predetermined localisation that grants site-specificity and homogeneity relative to stochastic protein labelling chemistry. For instance, this could be advantageous for the construction of site-specific protein-drug conjugates.

The third aim of this thesis involved the exploration of alternative applications of protein engineering in the design of novel therapeutic agents. Chapter 7 showcases the feasibility of chemically modifying an IgG molecule (trastuzumab) to expand the versatility of the protein. The two most common protein labelling techniques (i.e., lysine and native cysteine chemistry) were employed concomitantly on trastuzumab to produce an antibody-drug conjugate capable of binding covalently to the surface of gold nanoparticles. We showed that the antibody retains its antigen binding capacity upon chemical functionalisation, and that it is capable of enhancing targeting to tumor cells *in vitro*. The antibody-targeted nanocarriers synthesized in this chapter are expected to improve selective tumour delivery by harnessing the preferential accumulation of nanosized materials combined with the active-targeting capacity of the antibodies exposed on its surface. The utilisation of an antibody-drug conjugate as a targeting agent provides several advantages, including better control of drug loading and the use of commercially available "smart" linkers that enable localised release of the payload to diminish off-target toxicity. Future work will involve the assessment of safety and efficacy in mouse xenograft models with overexpression of HER2. Furthermore, the nanoparticle system presented in chapter 7 provides remarkable versatility. A promising possibility consists in tagging the nanoparticle surface with two (or more) antibodies with distinct specificities. This "multispecific" format could conceptually allow circumvention of resistance mechanisms that evoke downregulation of one of the molecular targets.

Various mass spectrometry methodologies were employed to tackle the different aims of this thesis, highlighting the numerous applications that novel MS tools offer in protein engineering. Data-dependent acquisition employing HCD and CID activation modes was utilised to derive site-specific structural information of influenza hemagglutinin glycosylation. For the second aim, a combination of workflows and activation modes, including CID, HCD, and ETD, were performed to confirm unambiguously the amino acid mutations and the attachment of glycans on the inserted asparagine residues, and were subsequently focused on the structural analysis of the glycan molecules. In the last aim, intact protein mass analysis was used to confirm the chemical attachment of the drug-linker moiety to trastuzumab in the construction of the antibody-drug conjugate. The latter also provided information concerning the number of drug molecules attached per antibody chain. Mass spectrometry has stood out as a key analytical technique in the current era of biopharmaceuticals; and constant technological advancements will continue to extend the

capabilities of these techniques to address crucial considerations in the development of novel biotherapeutics.

Appendices

Supplementary information from Chapter 2: Site-specific Glycosylation Profile of Influenza A (H1N1) Hemagglutinin through Tandem Mass Spectrometry

Supplementary table 1. Influenza protein coverage across all bands obtained by SDS-PAGE fractionation (Fig. 2) and subsequent mass spectrometry analysis.

Description	Coverage (%)	# Peptides	# PSMs	# Unique Peptides	# AAs	MW [kDa].	FDR A2
hemagglutinin	71.50	62	2, 018	62	565	63.2	0%
nucleocapsid protein	79.72	59	1, 050	59	498	56.2	0%
polymerase PB2	65.88	64	251	63	759	86	0%
matrix protein 1	78.57	29	1, 238	29	252	27.9	0%
neuraminidase	38.59	19	217	19	469	51.5	0%
polymerase PB1	44.85	50	231	49	758	86.6	0%
polymerase PA	58.66	57	196	57	716	82.5	0%
nonstructural protein 1	64.35	15	69	15	230	25.8	0%
PB1-F2 protein	24.44	4	20	4	90	10.8	23.10 %
nuclear export protein	24.79	3	9	3	121	14.4	21.40 %
matrix protein 2	38.14	2	9	2	97	11.1	50%

Supplementary table 2. Influenza protein coverage for band 4 (Fig. 2) obtained by SDS-PAGE fractionation and subsequent mass spectrometry analysis.

Description	Coverage (%)	# Peptides	# PSMs	# Unique Peptides	# AAs	MW [kDa].	FDR A2
hemagglutinin	56.81	48	855	48	565	63.2	0%
nucleocapsid protein	71.08	49	121	49	498	56.2	0%

matrix protein 1	78.17	27	104	27	252	27.9	0%
neuraminidase, partial	26.44	16	76	16	469	51.5	0%
polymerase PB1	32.59	27	42	27	758	86.6	0%
polymerase PA	37.29	23	31	23	716	82.5	0%
polymerase PB2	32.81	24	28	24	759	86	0%
PB1-F2 protein	8.89	1	4	1	90	10.8	20%
nonstructural protein 1	24.78	3	3	3	230	25.8	0%
matrix protein 2	38.14	2	3	2	97	11.1	18.80%

Supplementary table 3. Influenza protein coverage for band 5 (Fig. 2) obtained by SDS-PAGE fractionation and subsequent mass spectrometry analysis.

Description	Coverage (%)	# Peptides	# PSMs	# Unique Peptides	# AAs	MW [kDa].	FDR A2
nucleocapsid protein	80.12	56	556	56	498	56.2	0%
hemagglutinin	48.85	37	162	37	565	63.2	0%
matrix protein 1	66.67	22	123	22	252	27.9	0%
neuraminidase	20.64	12	45	12	470	51.6	0%
polymerase PB2	31.62	21	23	21	759	86	0%
polymerase PB1	16.36	14	39	14	758	86.6	0%
polymerase PA	19.55	11	12	11	716	82.5	0%
polymerase PB1	3.83	3	5	3	757	86.4	18.80%

matrix protein 2	10.31	1	1	1		97	11.1	23.50 %
PB1-F2 protein	8.89	1	1	1		90	10.8	22.20 %

Supplementary table 4. Influenza protein coverage for band 6 (Fig. 2) obtained by SDS-PAGE fractionation and subsequent mass spectrometry analysis.

Description	Coverage (%)	# Peptides	# PSMs	# Unique Peptides	# Protein Groups	# AAs	MW [kDa].	FDR A2
hemagglutinin	37.35	34	429	34	1	565	63.2	0%
nucleocapsid protein	51.81	34	59	34	1	498	56.2	0%
matrix protein 1	59.52	19	80	19	1	252	27.9	0%
nonstructural protein 1	36.52	8	10	8	1	230	25.8	0%
polymerase PA	11.73	10	11	10	1	716	82.5	0%
neuraminidase	17.87	8	15	8	1	470	51.6	0%
polymerase PB2	7.11	5	5	5	1	759	85.9	0%
nuclear export protein	5.79	1	1	1	1	121	14.3	16.70 %
matrix protein 2	10.31	1	1	1	1	97	11.1	15.40 %
polymerase	1.98	2	3	2	1	757	86.4	14.30 %

Supplementary information from Chapter 4: Enhancing the stability of adalimumab by engineering additional glycosylation motifs
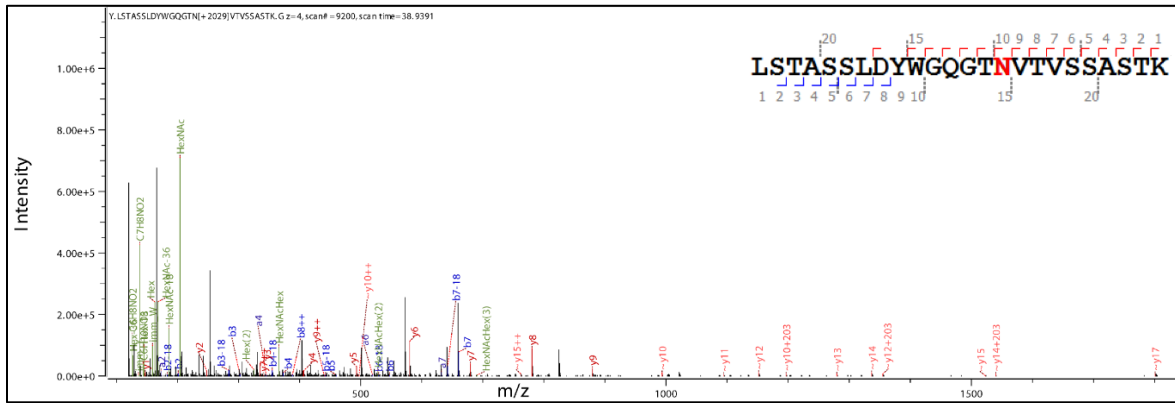
Figure S1. HCD spectrum of the chymotryptic peptide LSTASSLDYWGQGTNVTVSSASTK for the L116N mutant.
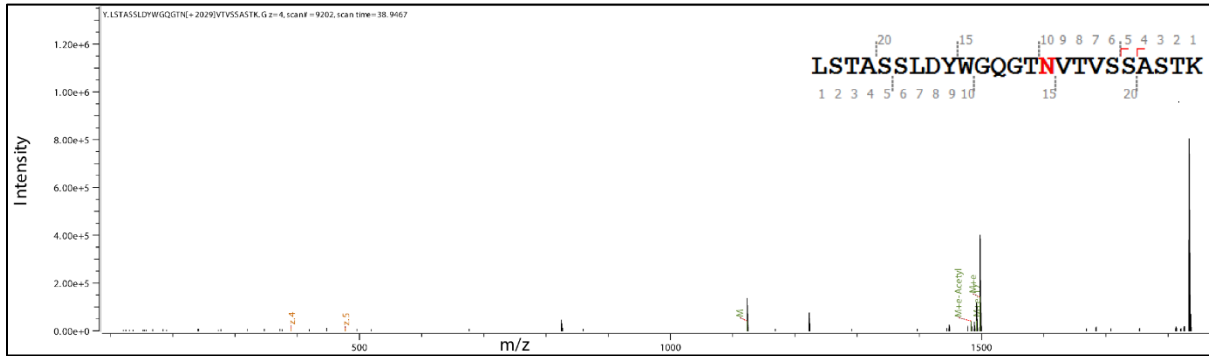
Figure S2. ETD spectrum of the chymotryptic peptide LSTASSLDYWGQGTNVTVSSASTK for the L116N mutant.
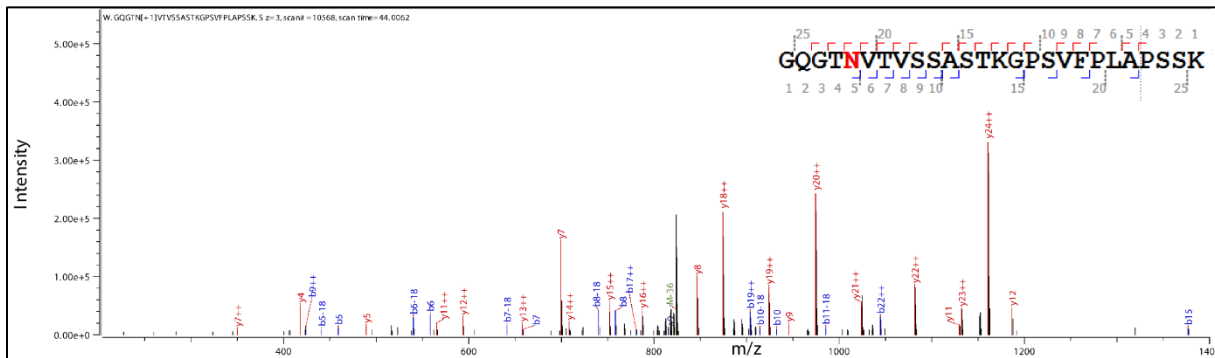
Figure S3. HCD spectrum of the de-glycosylated chymotryptic peptide GQGTNVTVSSASTKGPAVFPLAPSSK for the L116N mutant.
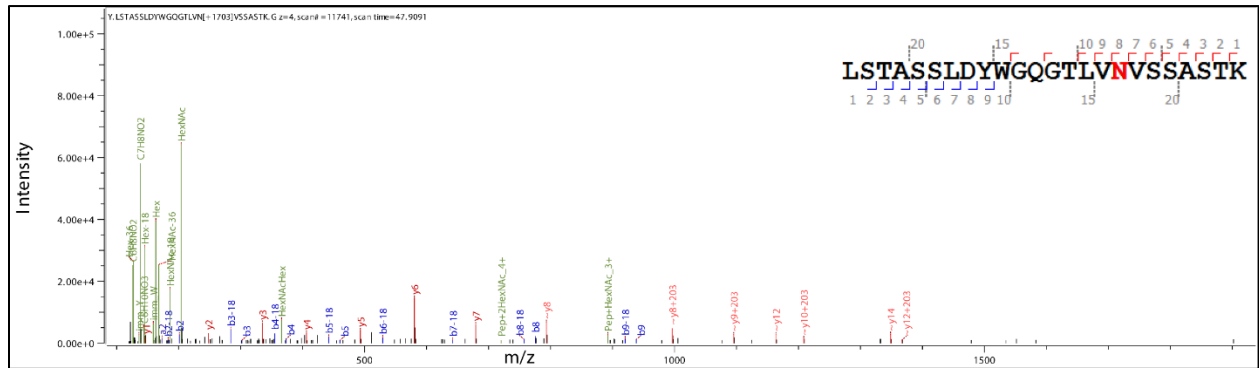
Figure S4. HCD spectrum of the chymotryptic peptide LSTASSLDYWGQGTLVNVSSASTK for the T118N mutant.
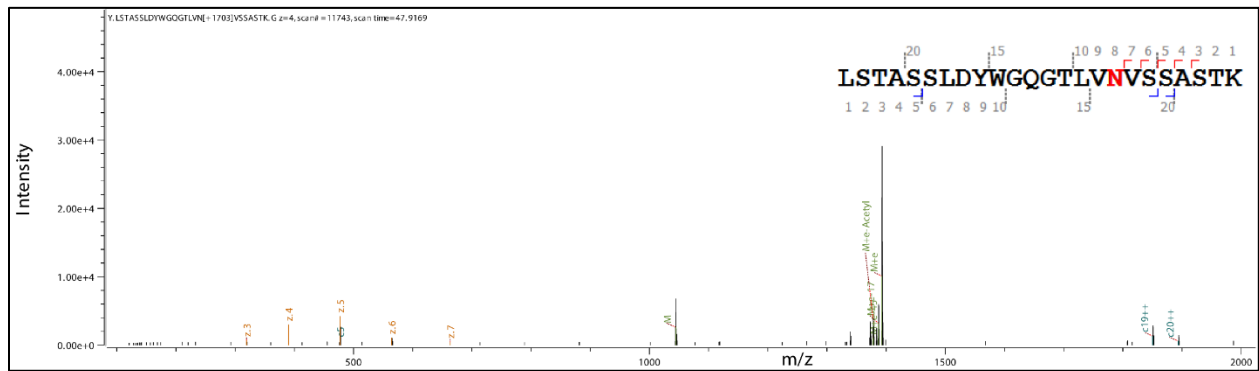
Figure S5. ETD spectrum of the chymotryptic peptide LSTASSLDYWGQGTLVNVSSASTK for the T118N mutant.
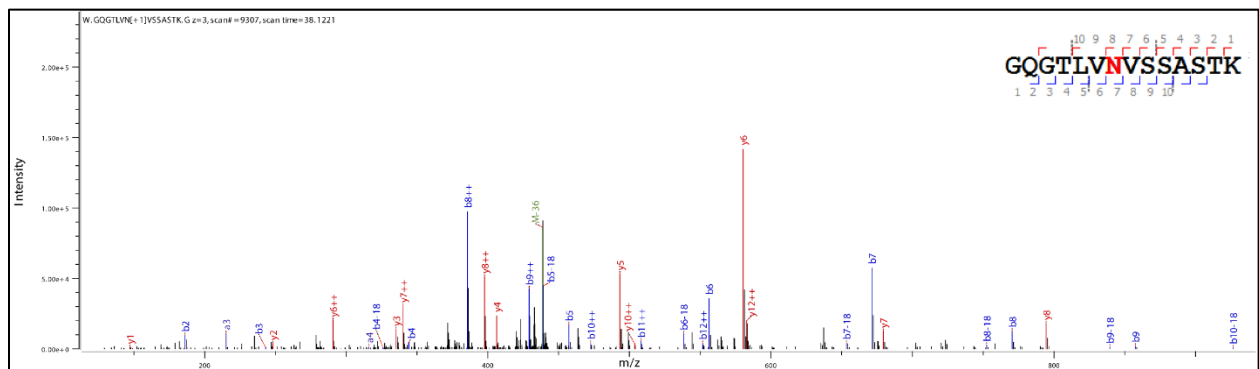
Figure S6. CID spectrum of the de-glycosylated chymotryptic peptide LSTASSLDYWGQGTLVNVSSASTK for the T118N mutant.
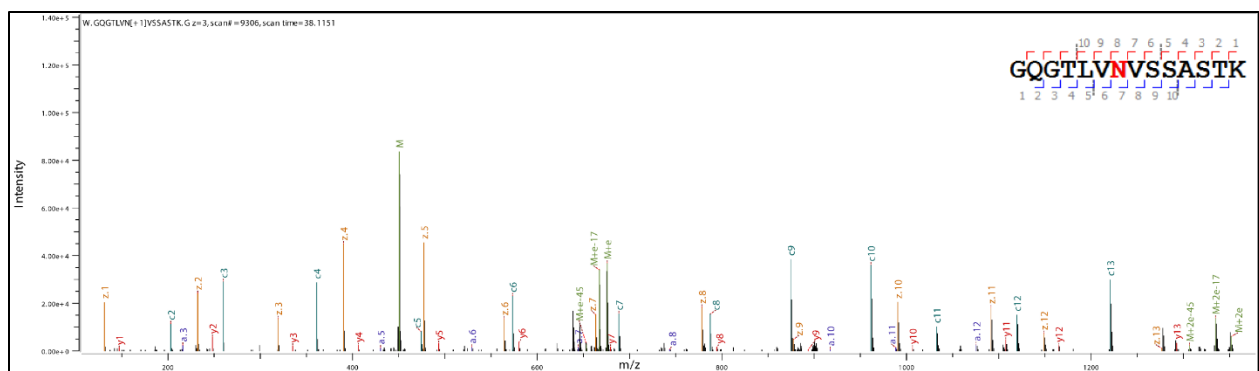
Figure S7. ETD spectrum of the de-glycosylated chymotryptic peptide LSTASSLDYWGQGTLVNVSSASTK for the T118N mutant.
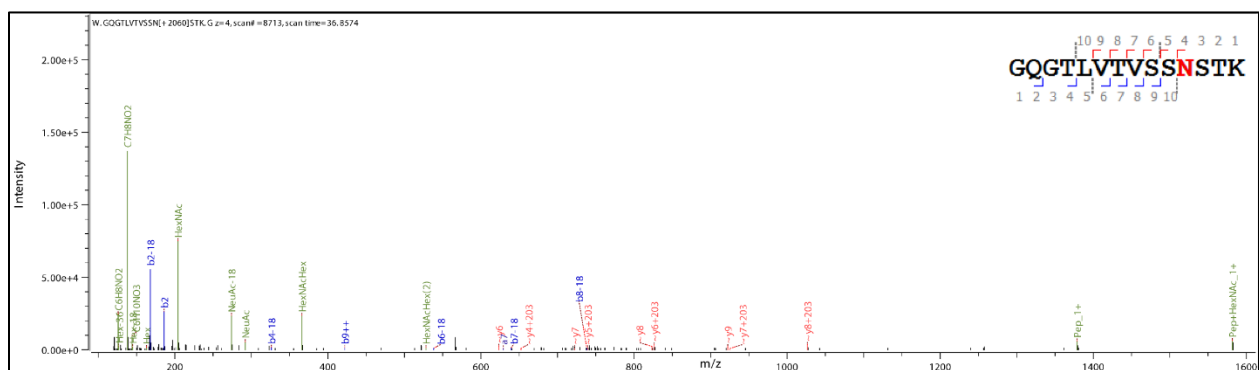
Figure S8. HCD spectrum of the chymotryptic peptide GQGTLVTVSSNSTK for the A122N mutant.
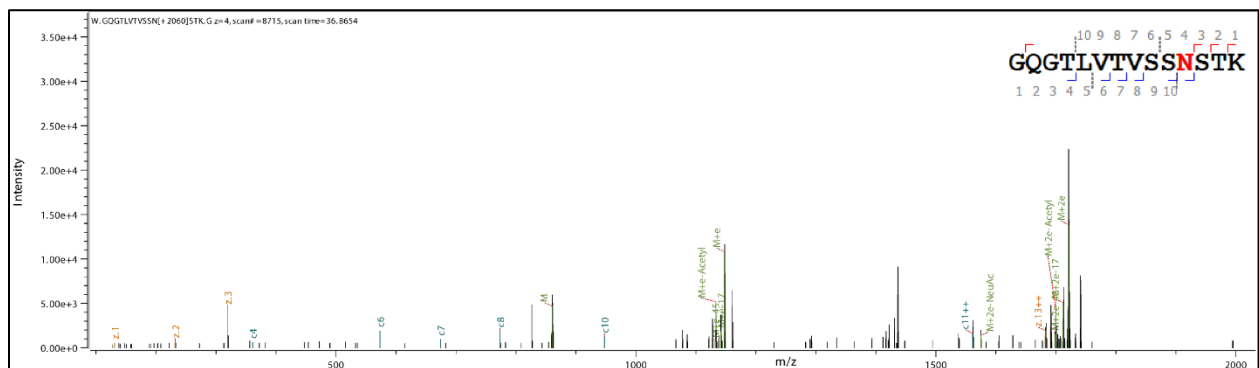
Figure S9. ETD spectrum of the chymotryptic peptide GQGTLVTVSSNSTK for the A122N mutant.
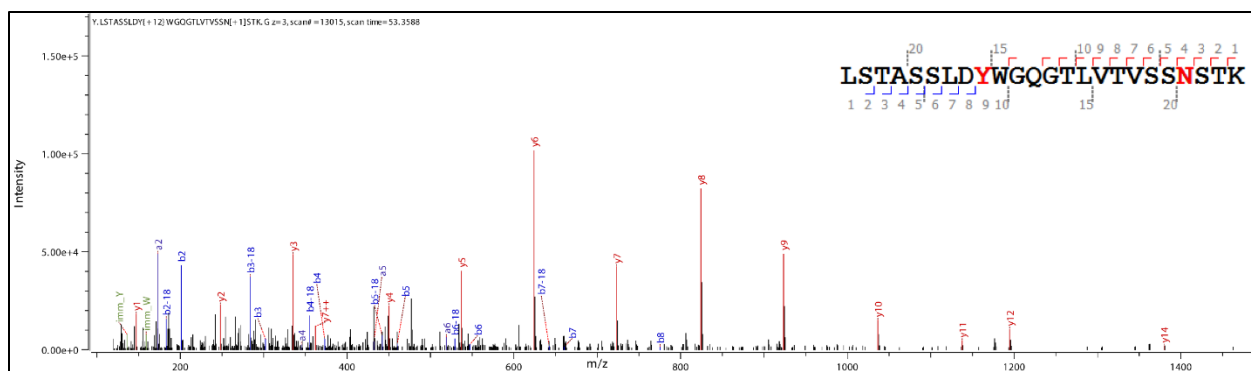
Figure S10. CID spectrum of the de-glycosylated chymotryptic peptide LSTASSLDYWGQGTLVTVSSNSTK for the A122N mutant.
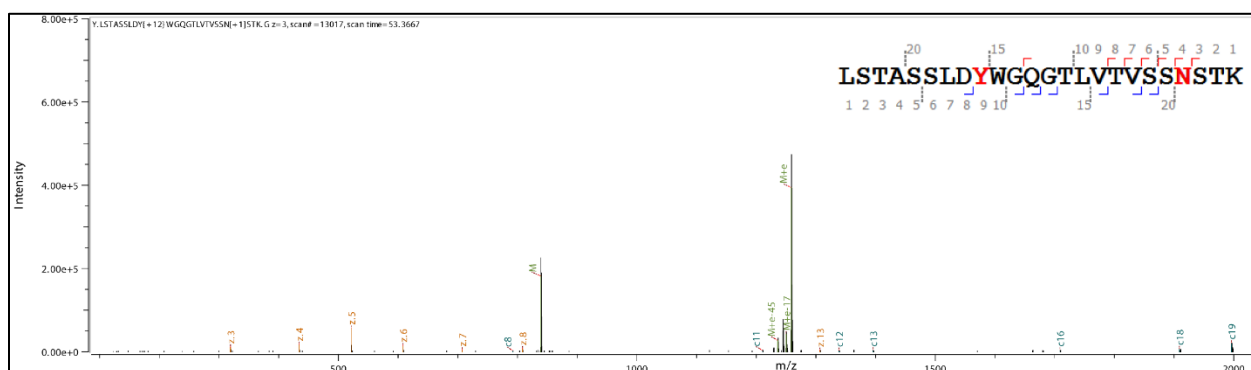
Figure S11. ETD spectrum of the de-glycosylated chymotryptic peptide LSTASSLDYWGQGTLVTVSSNSTK for the A122N mutant.
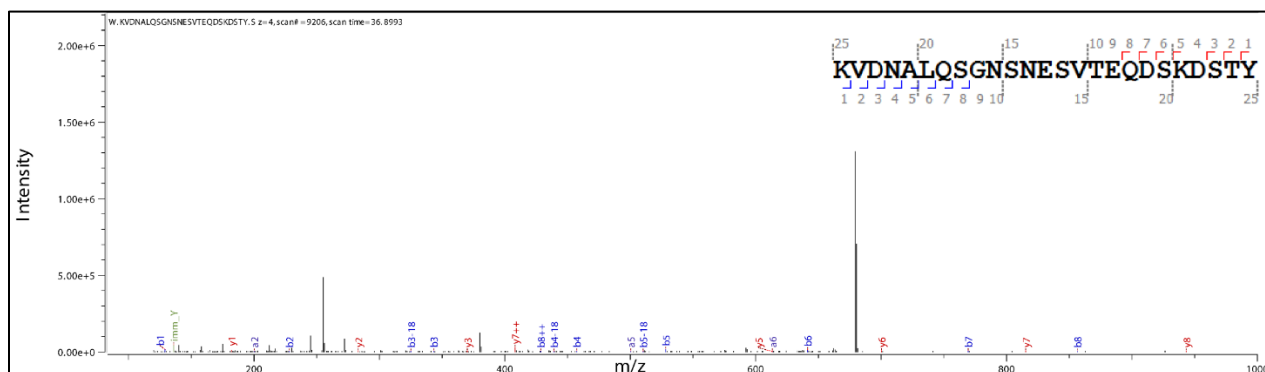
Figure S12. HCD spectrum of the chymotryptic peptide KVDNALQSGNSNESSVTEQDSKDSTY for the Q160N mutant

Figure S13. ETD spectrum of the chymotryptic peptide KVDNALQSGNSNESSVTEQDSKDSTY for the Q160N mutant

Figure S14. CID spectrum of the chymotryptic peptide NSGALTSGVHTFPAVK for the L178K mutant.

Figure S15. ETD spectrum of the chymotryptic peptide NSGALTSGVHTFPAVK for the L178K mutant.
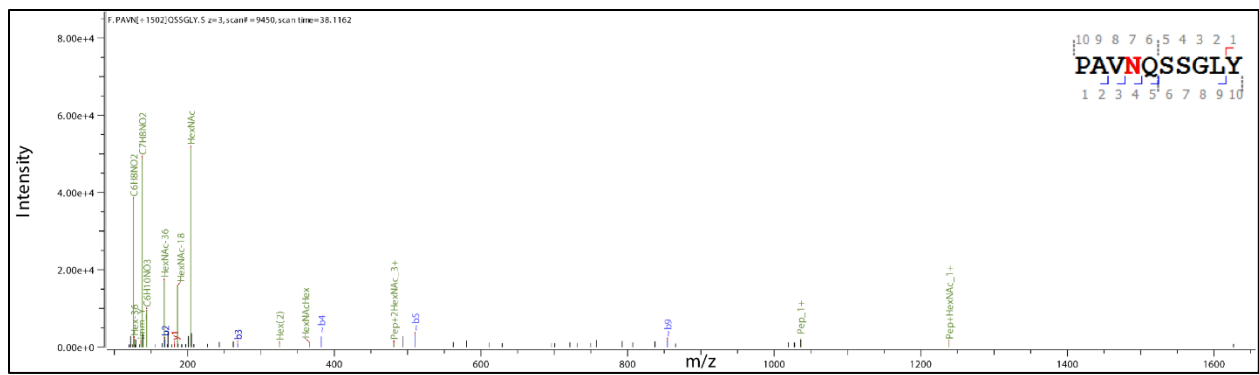
Figure S16. SHCD spectrum of the chymotryptic peptide PAVNQSSGLY for the L178N mutant.
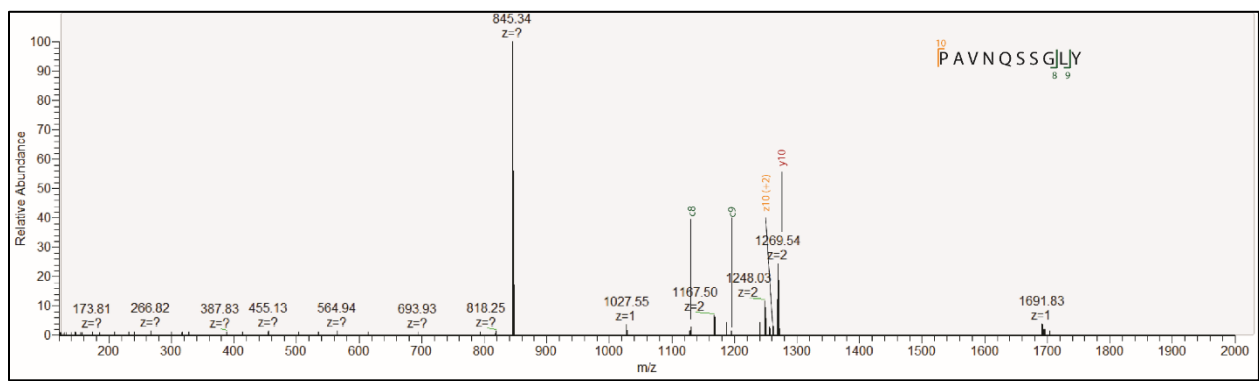
Figure S17. ETD spectrum of the chymotryptic peptide PAVNQSSGLY for the L178N mutant.
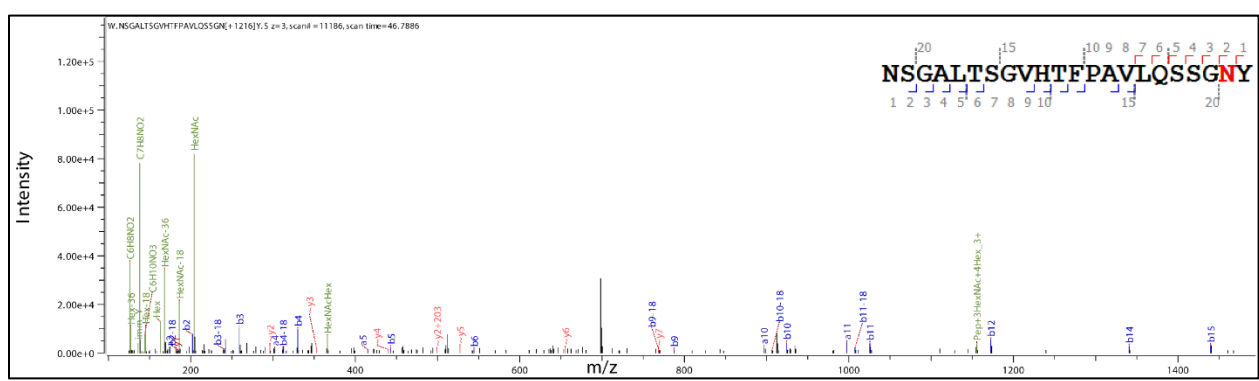
Figure S18. HCD spectrum of the chymotryptic peptide NSGALTSGVHTFPAVLQSSGNY for the L183N mutant.
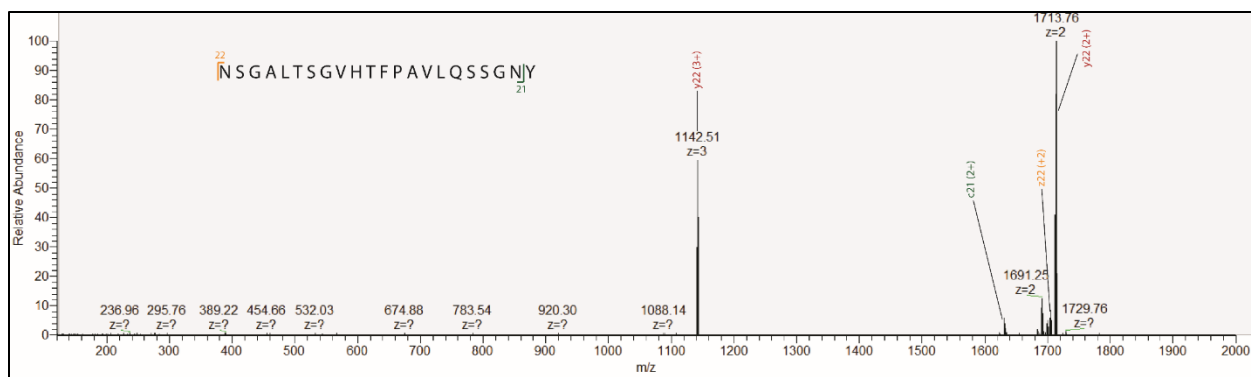
Figure S19. ETD spectrum of the chymotryptic peptide NSGALTSGVHTFPAVLQSSGNY for the L183N mutant.
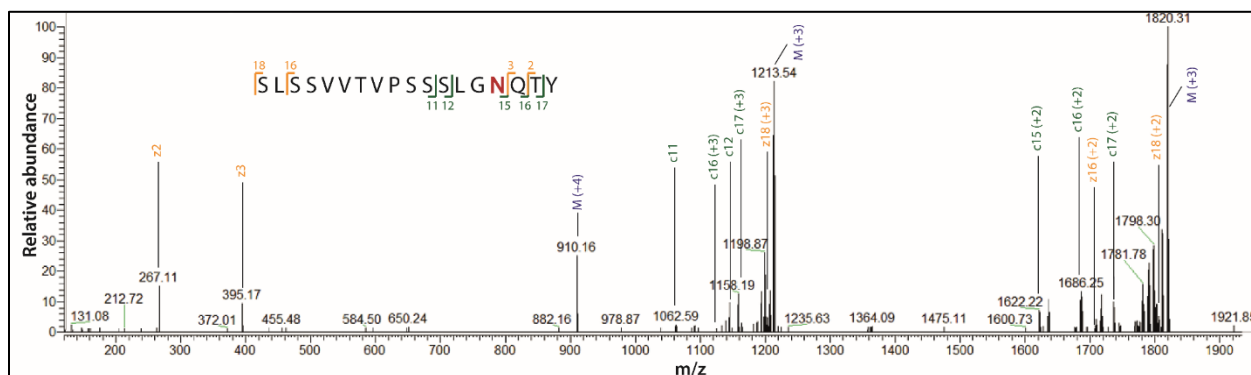
Figure S20. ETD spectrum of the chymotryptic peptide SLSSVVTVPSSSLGNQTY for the T198N mutant.
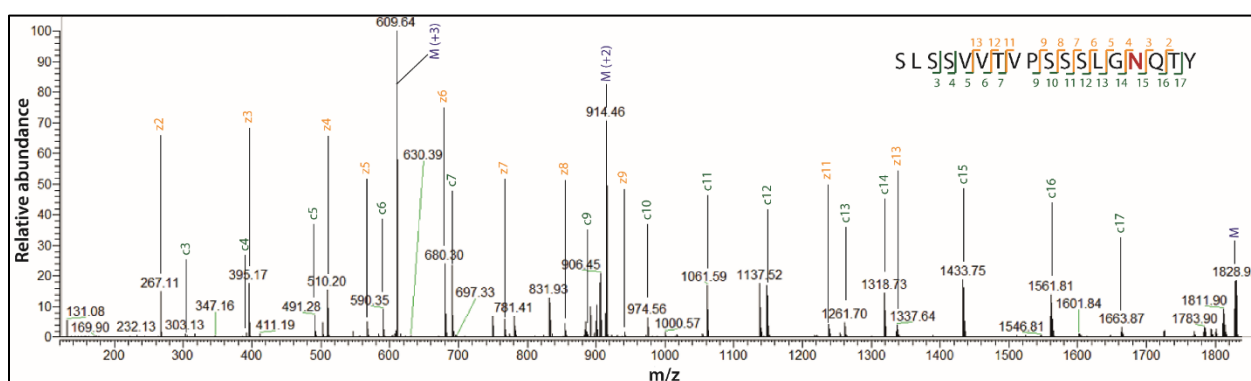
Figure S21. ETD spectrum of the de-glycosylated chymotryptic peptide SLSSVVTVPSSSLGNQTY for the T198N mutant.

263

Supplementary information from Chapter 5: Glycan profile analysis of engineered trastuzumab with rationally added glycosylation sequons for enhanced stability

Full MS spectra of the Tmab variants
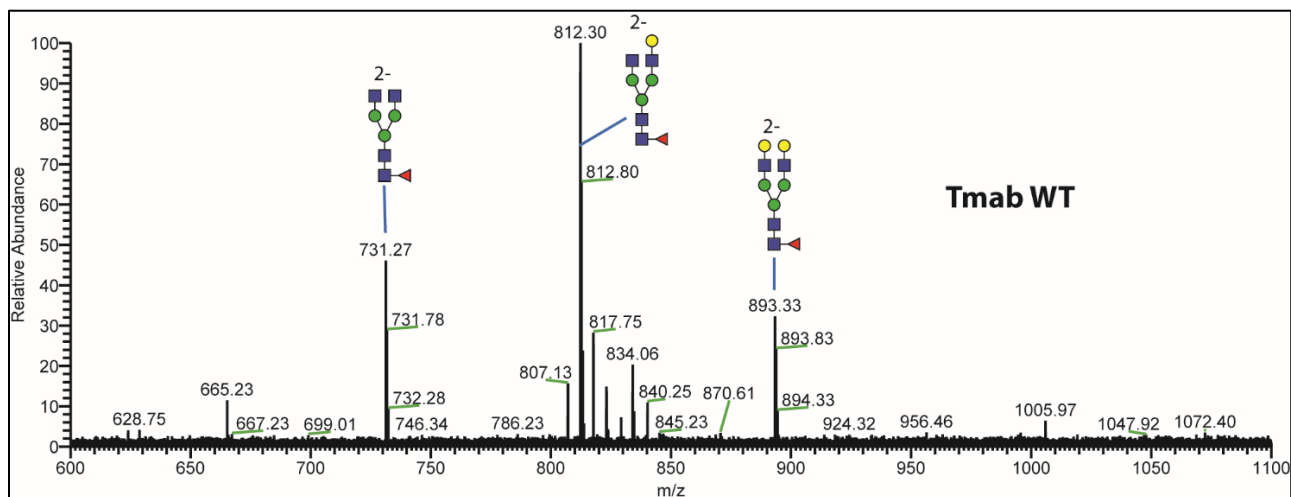
Figure S1. Full MS spectra of released glycans from Tmab WT.
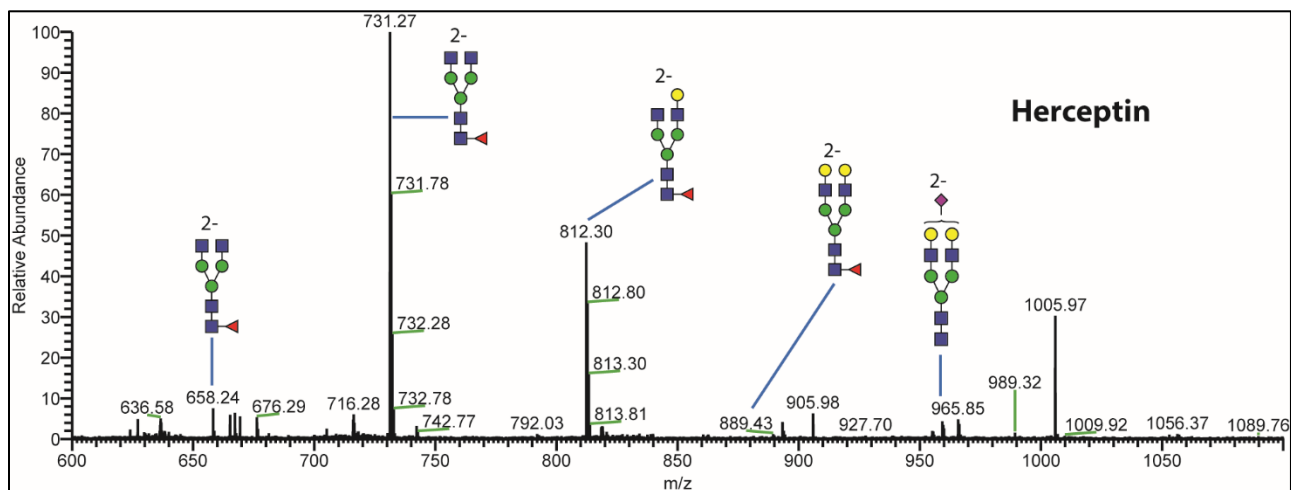
Figure S2. Full MS spectra of released glycans from Herceptin.
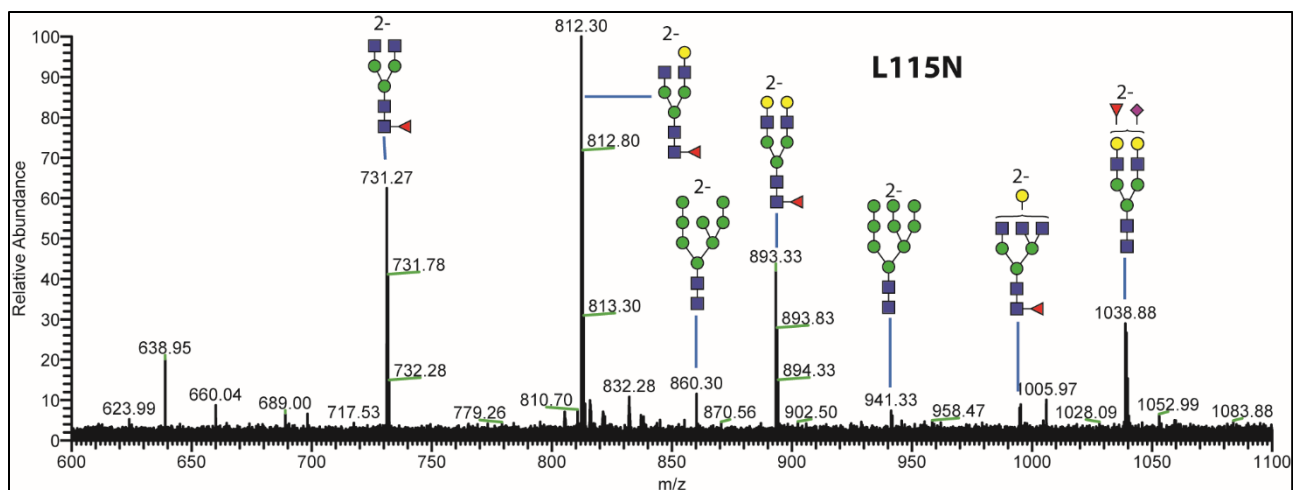
Figure S3. Full MS spectra of released glycans from L115N.
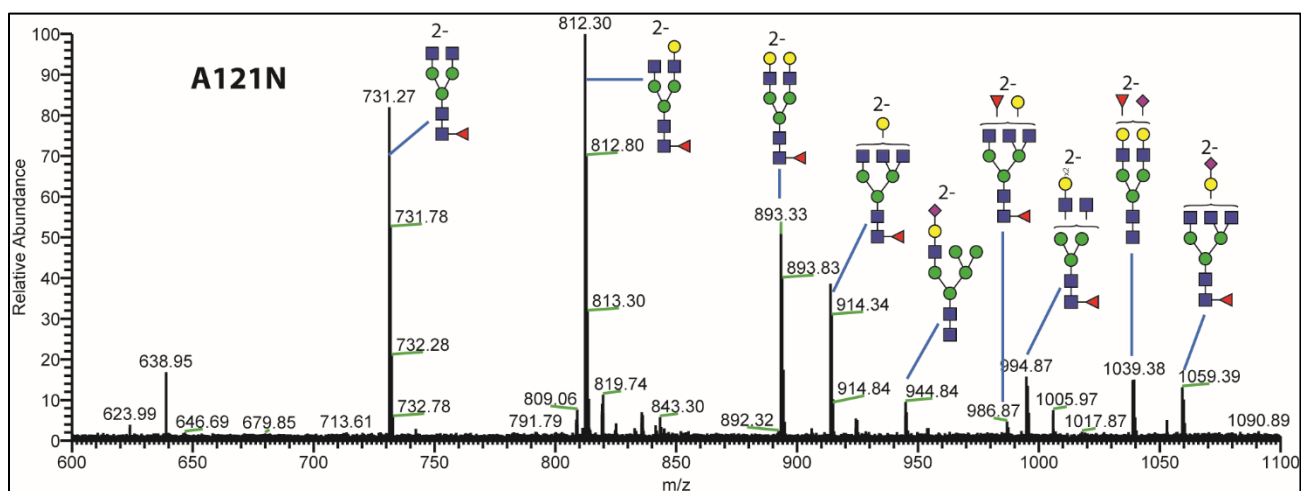
Figure S4. Full MS spectra of released glycans from A121N.
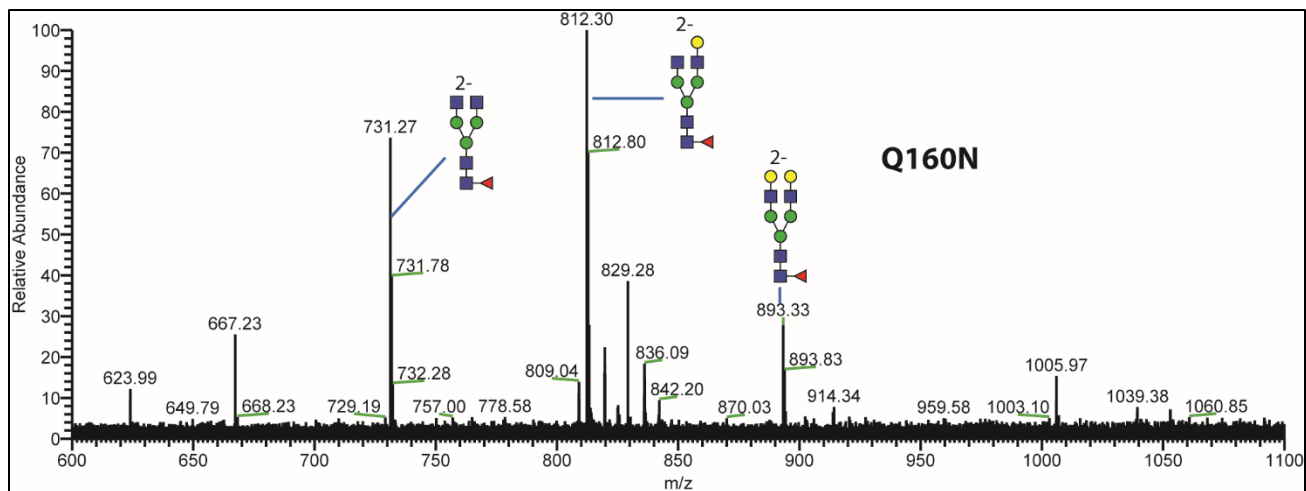
Figure S5. Full MS spectra of released glycans from Q160N.
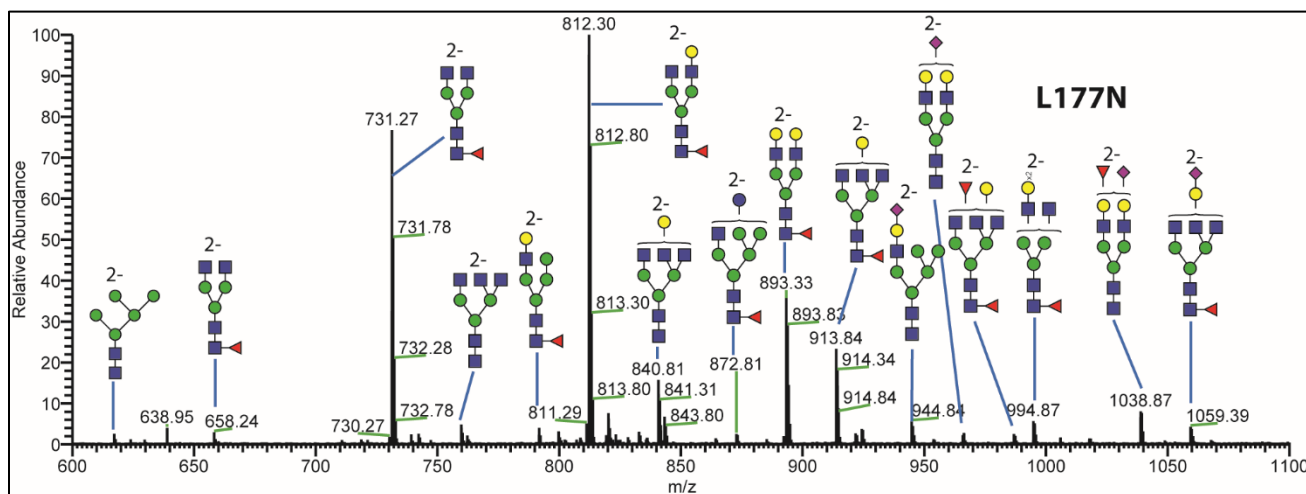
Figure S6. Full MS spectra of released glycans from L177N.
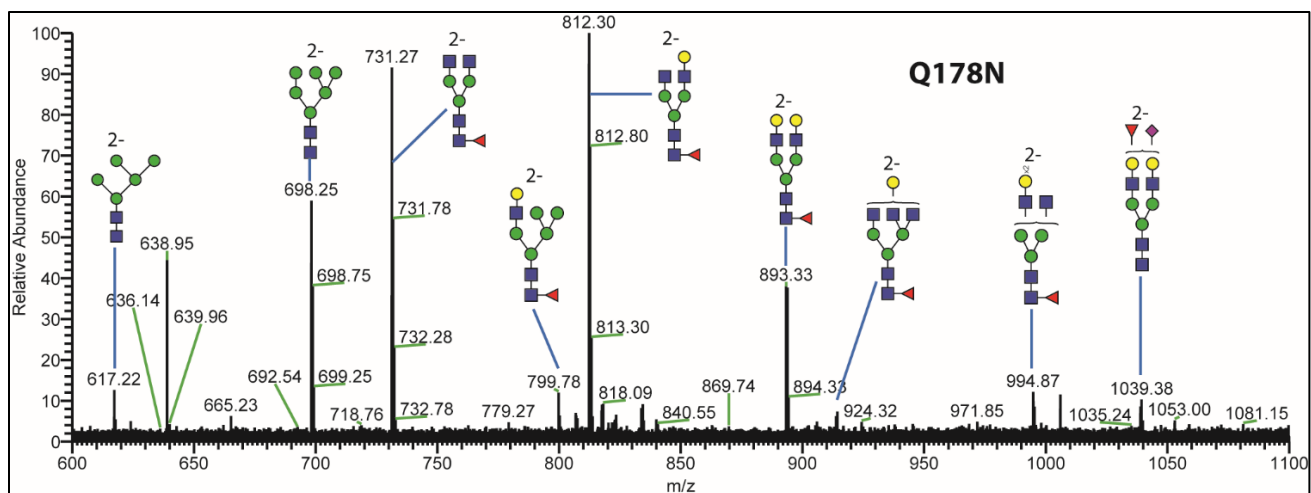
Figure S7. Full MS spectra of released glycans from Q178N.
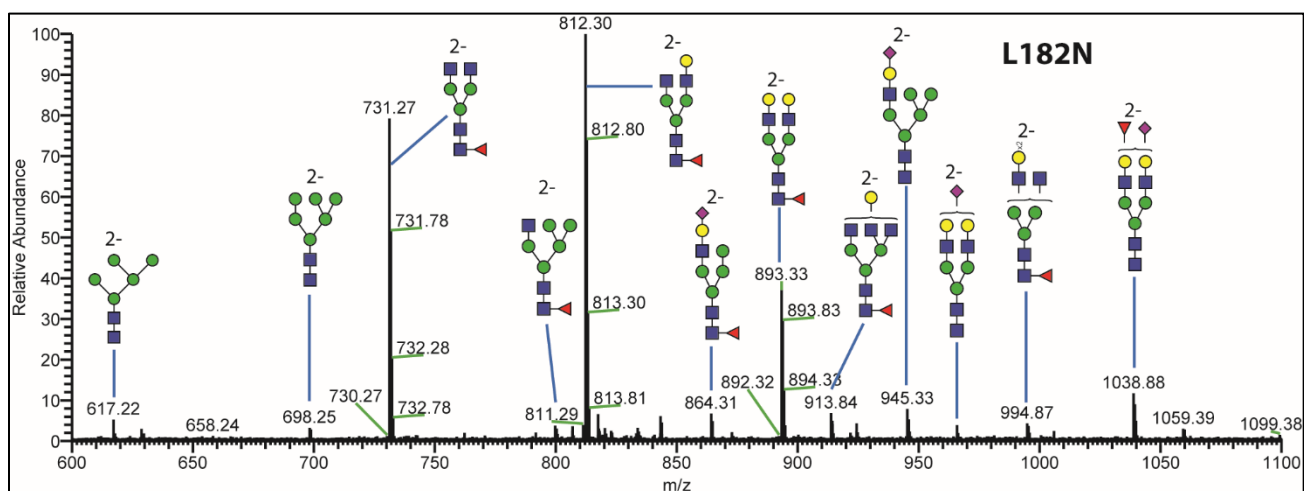
Figure S8. Full MS spectra of released glycans from L182N.

267
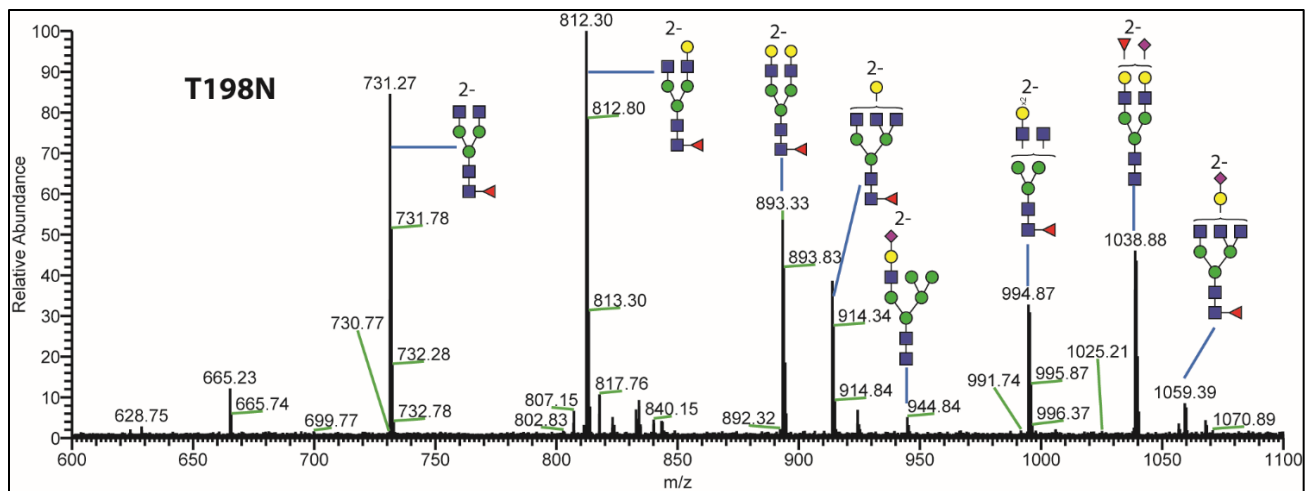
Figure S9. Full MS spectra of released glycans from T198N.

MS2 spectra
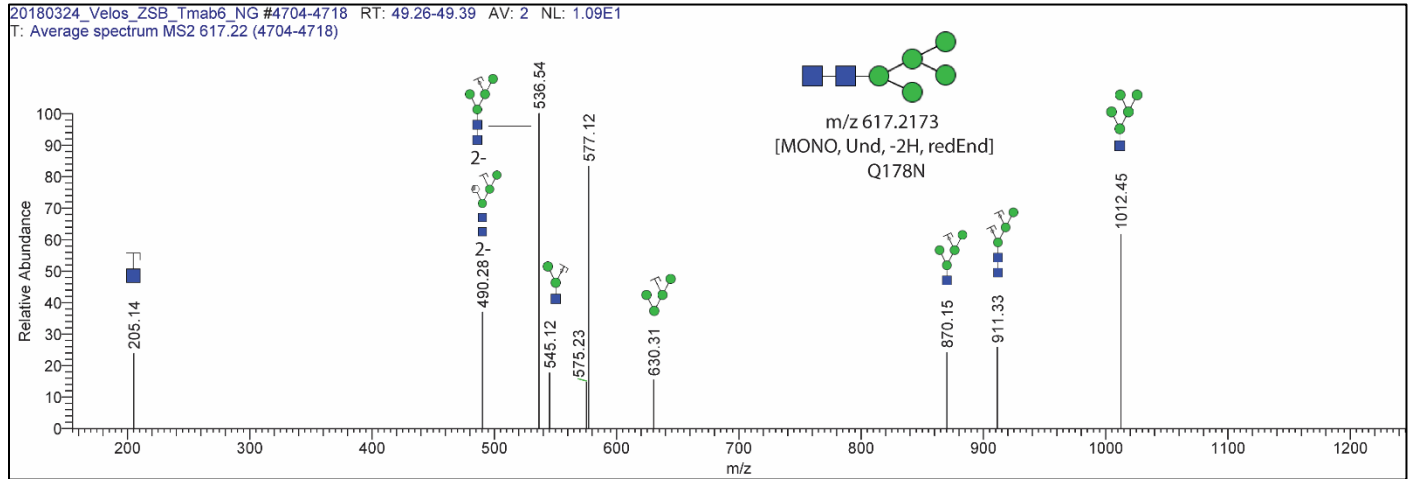
Figure S10. MS2 spectra of glycan 1 (table 4).
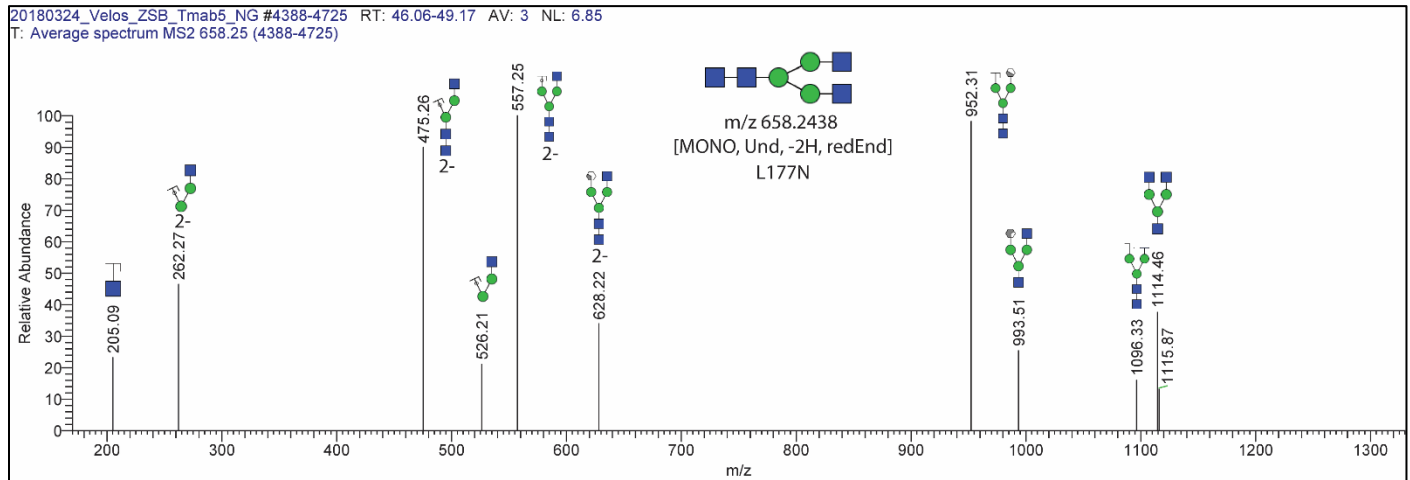

Figure S11. MS2 spectra of glycan 2 (table 4).
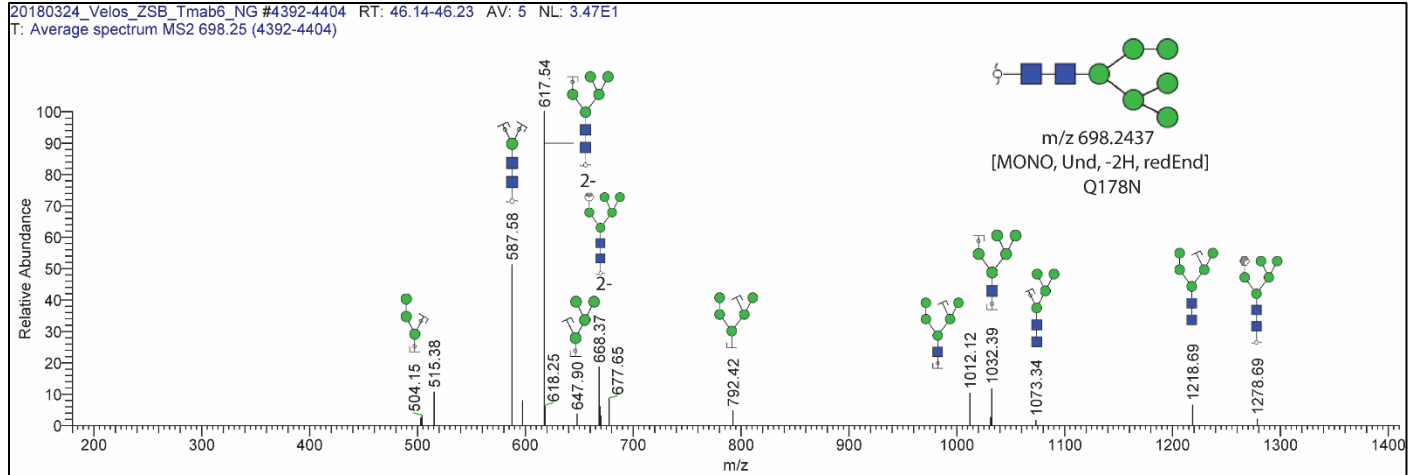
Figure S12. MS2 spectra of glycan 3 (table 4).
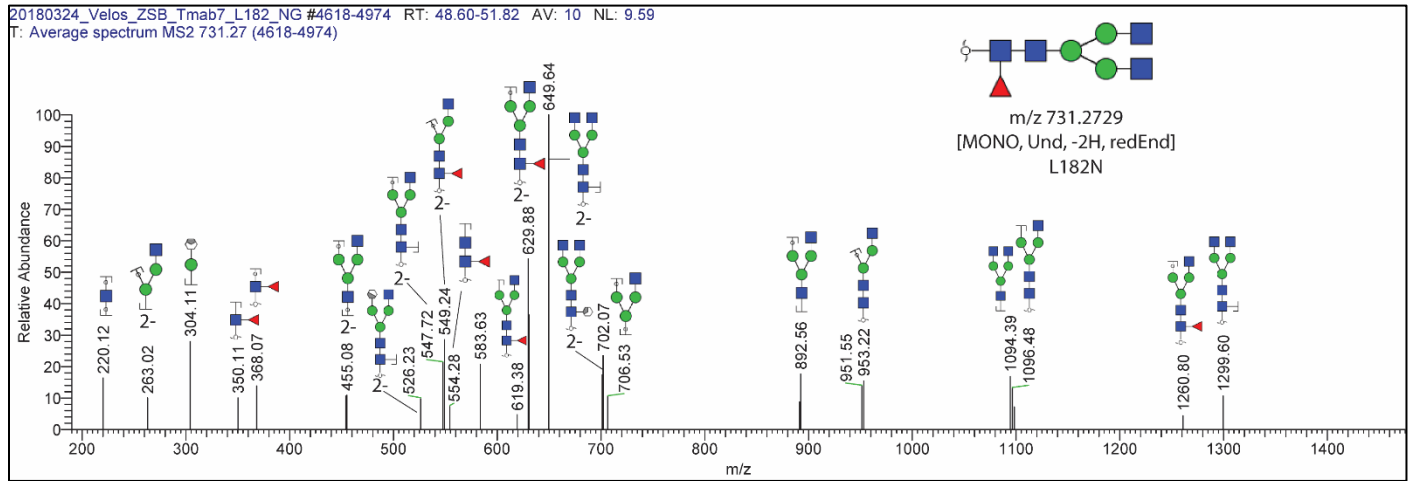
Figure S13. MS2 spectra of glycan 4 (table 4).
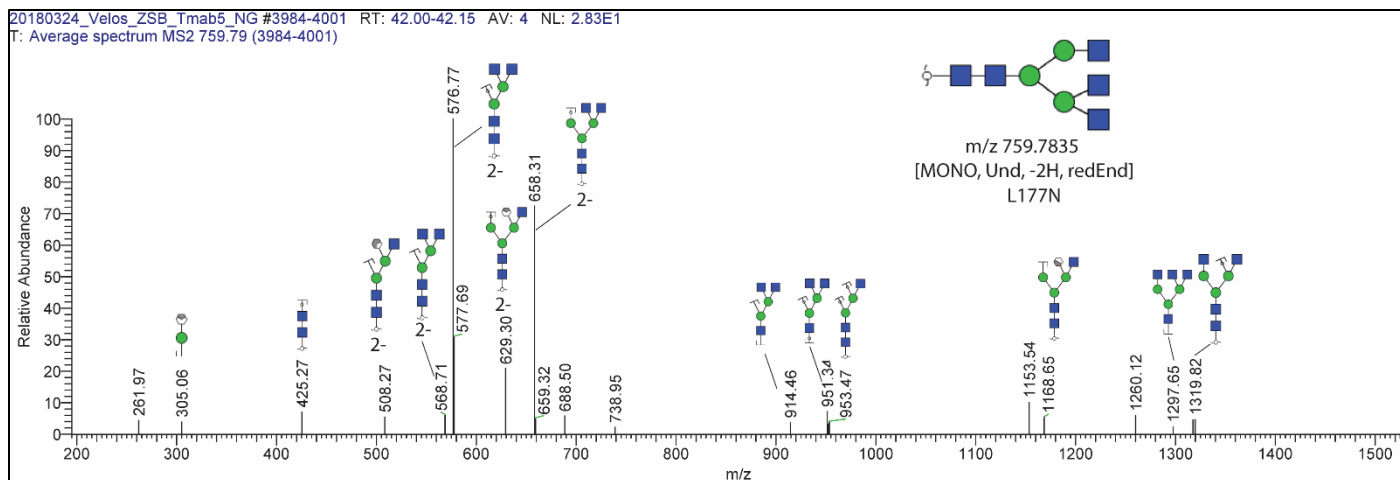
Figure S14. MS2 spectra of glycan 5 (table 4).
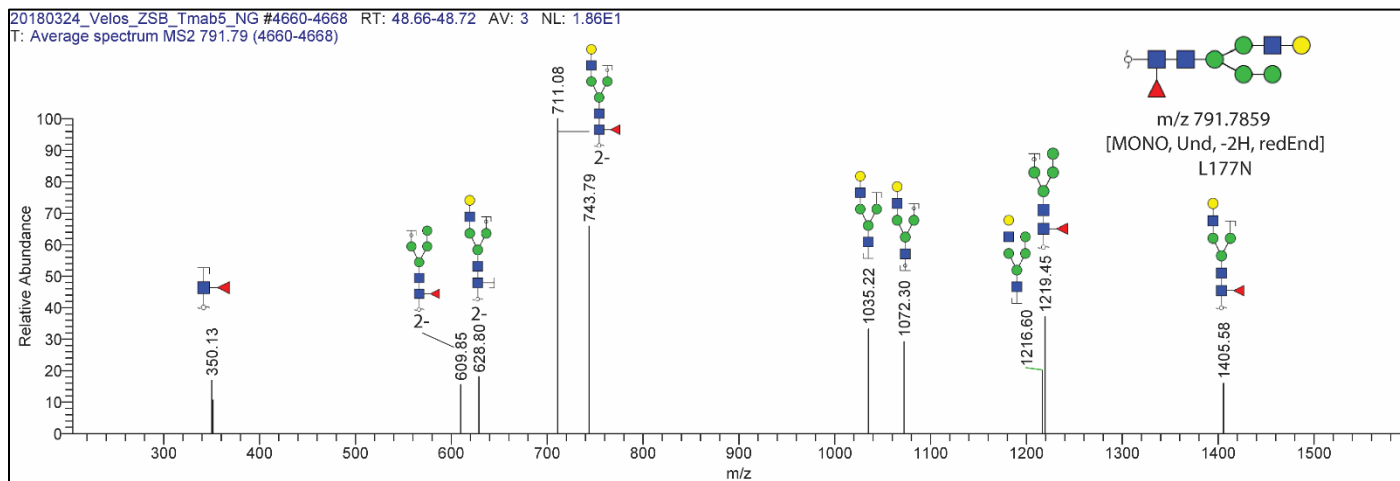
Figure S15. MS2 spectra of glycan 6 (table 4).
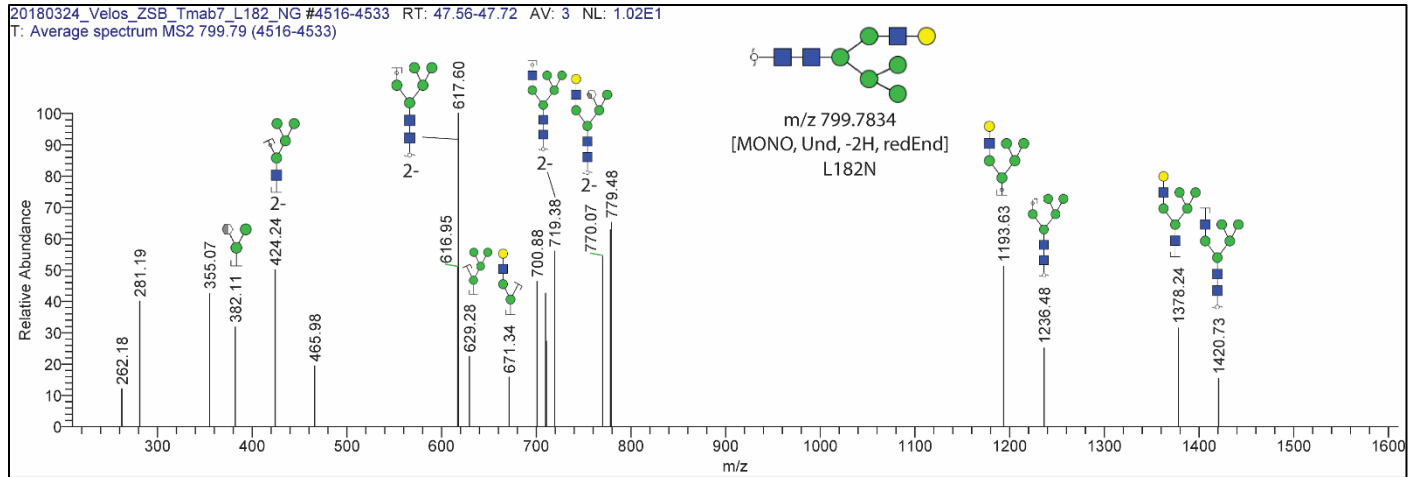
Figure S16. MS2 spectra of glycan 7 (table 4).
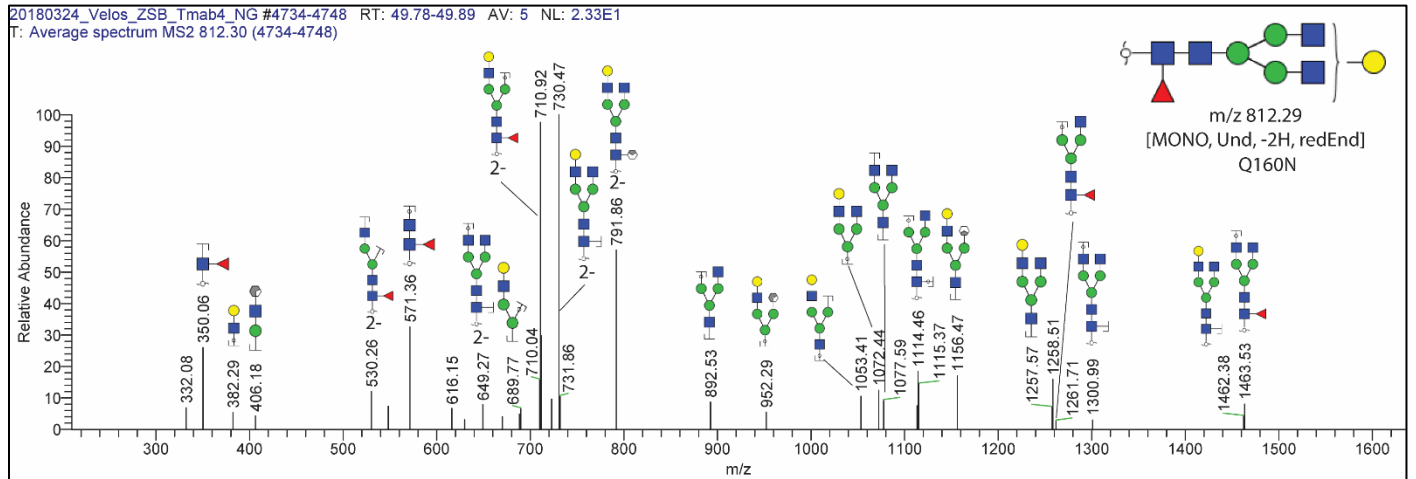
Figure S17. MS2 spectra of glycan 8 (table 4).
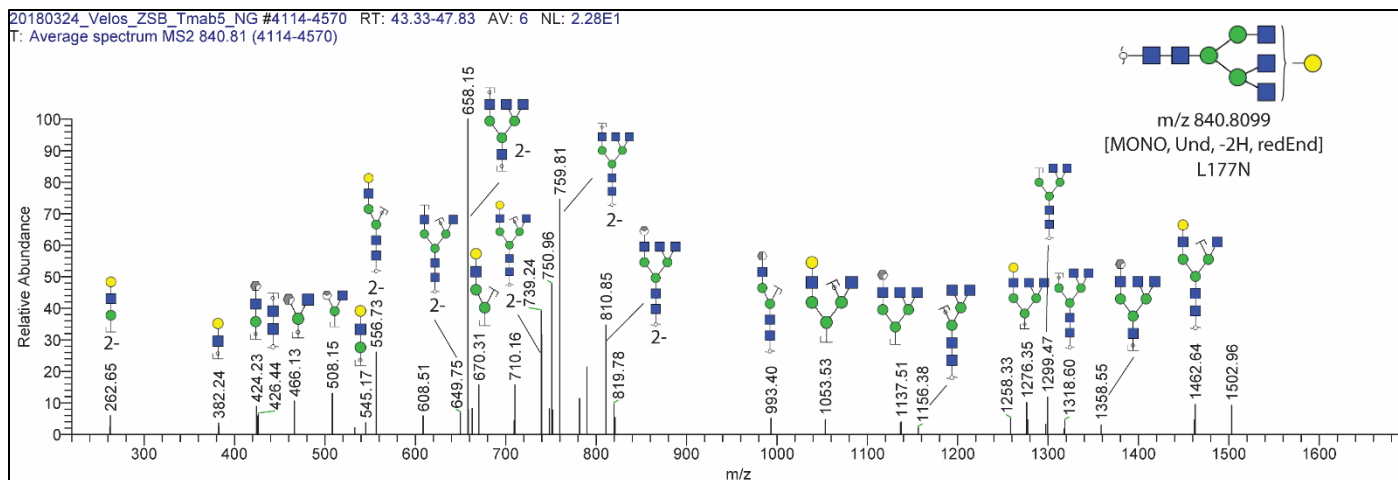
Figure S18. MS2 spectra of glycan 9 (table 4).
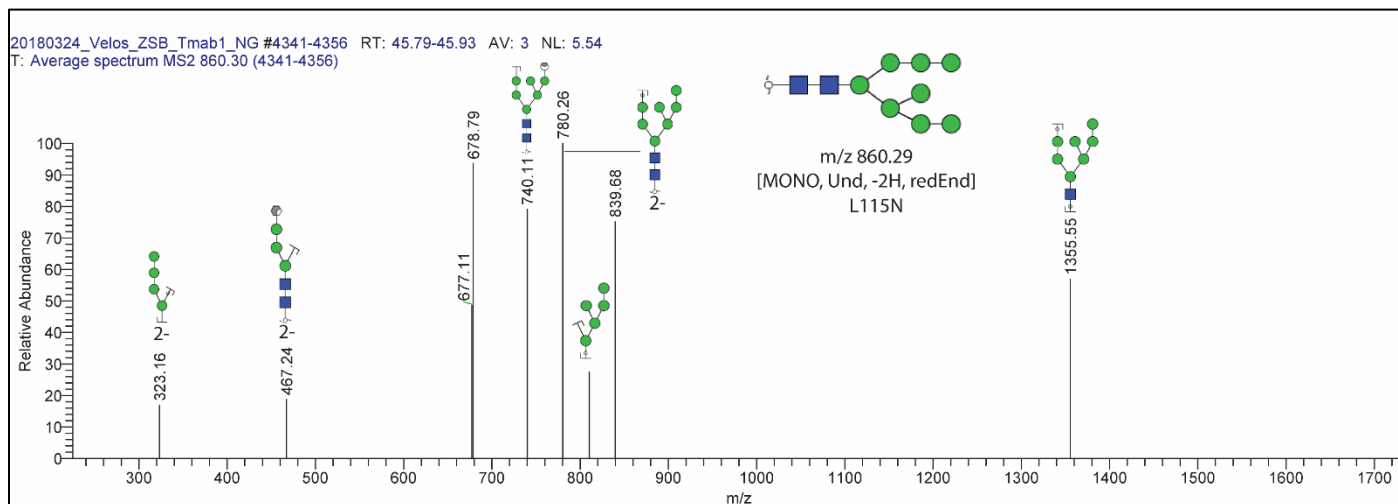
Figure S19. MS2 spectra of glycan 10 (table 4).
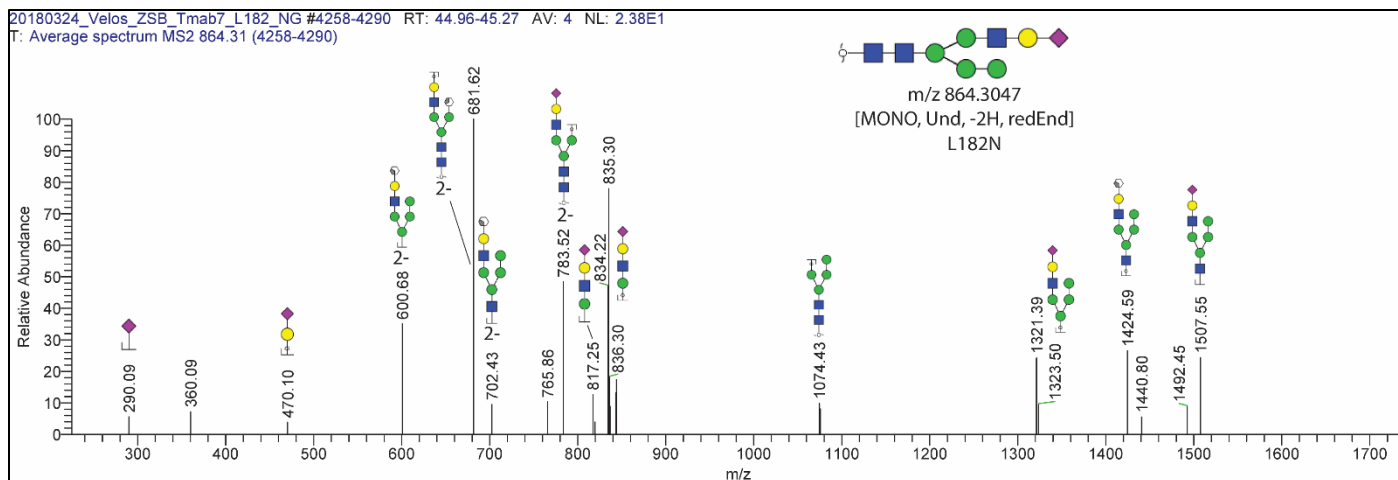
Figure S20. MS2 spectra of glycan 11 (table 4).
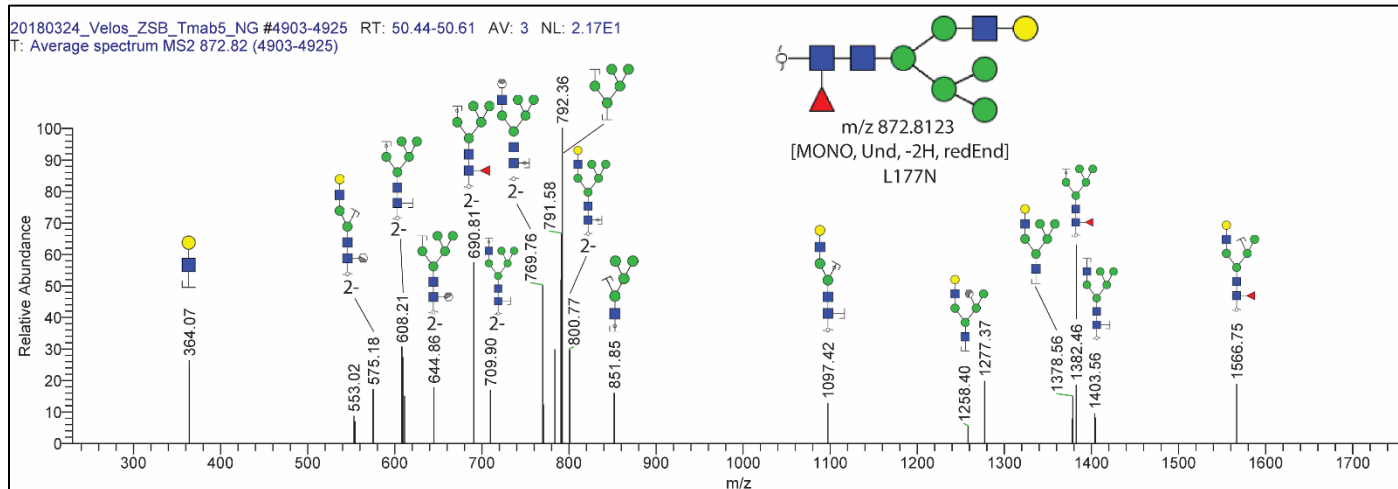
Figure S21. MS2 spectra of glycan 12 (table 4).
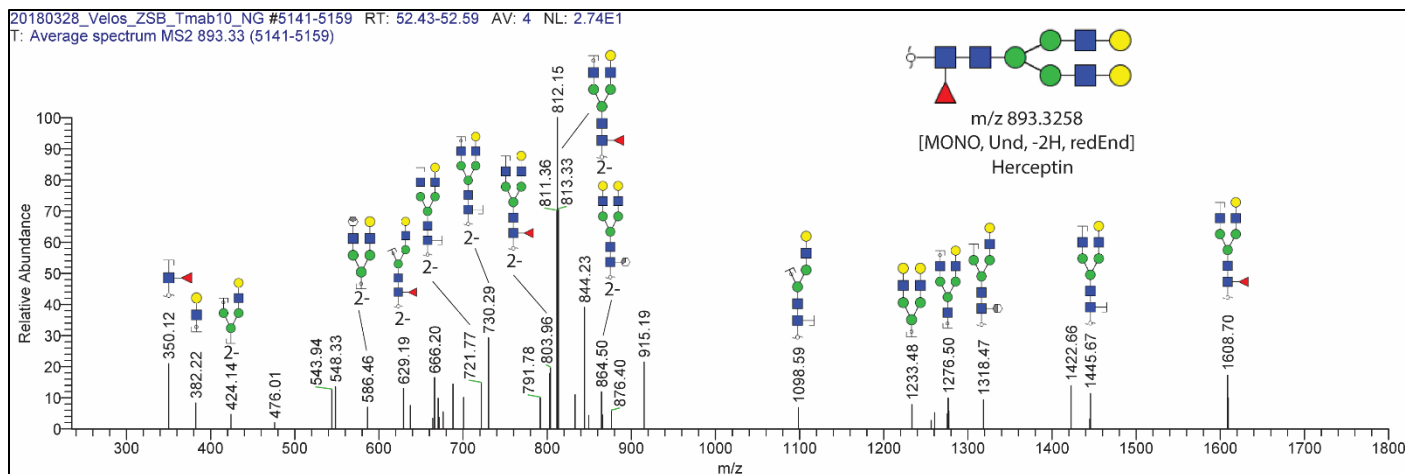
Figure S22. MS2 spectra of glycan 13 (table 4).
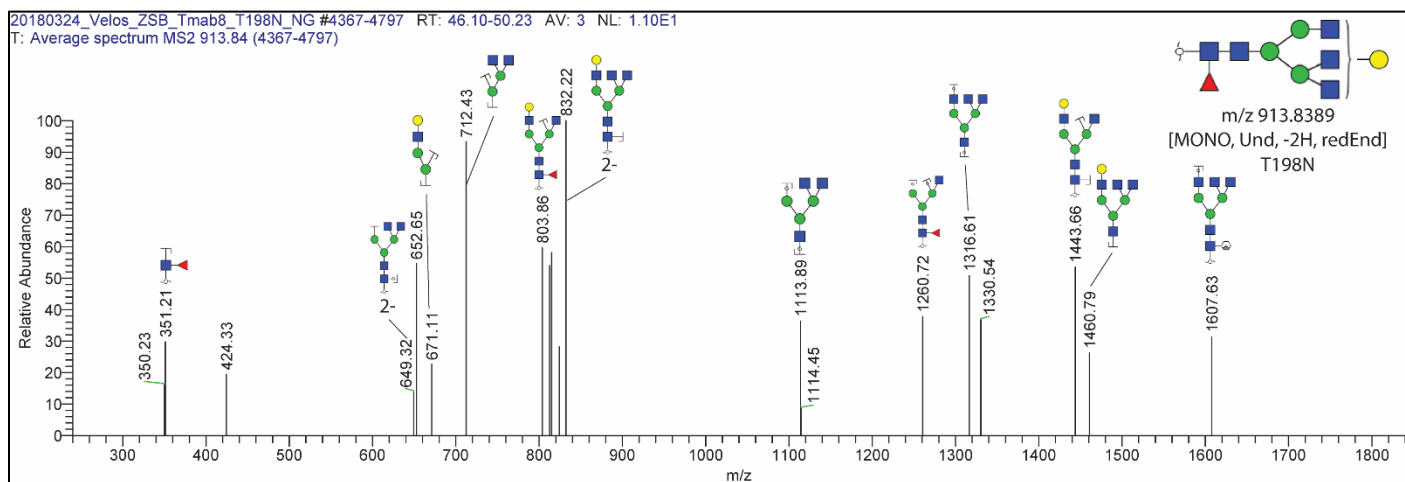
Figure S23. MS2 spectra of glycan 14 (table 4).
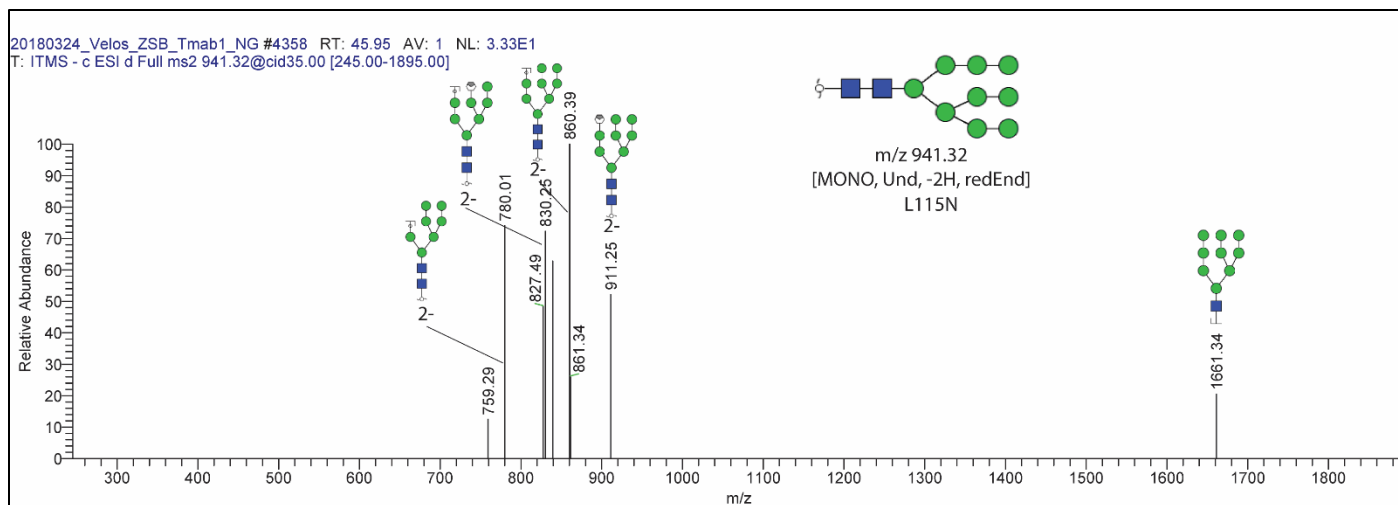
Figure S24. MS2 spectra of glycan 15 (table 4).
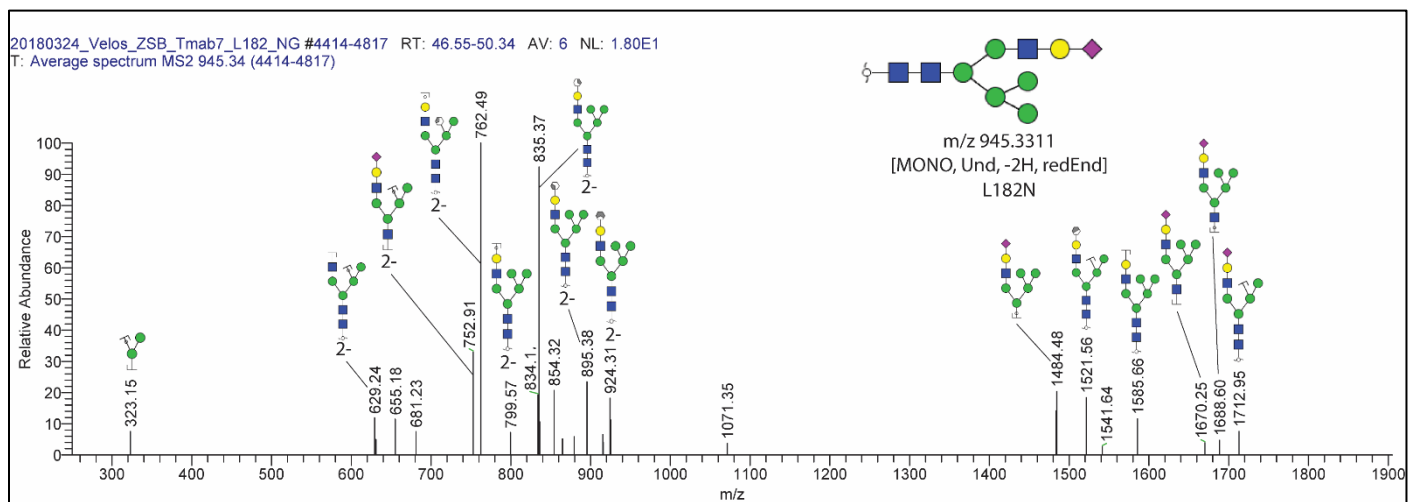
Figure S25. MS2 spectra of glycan 16 (table 4).
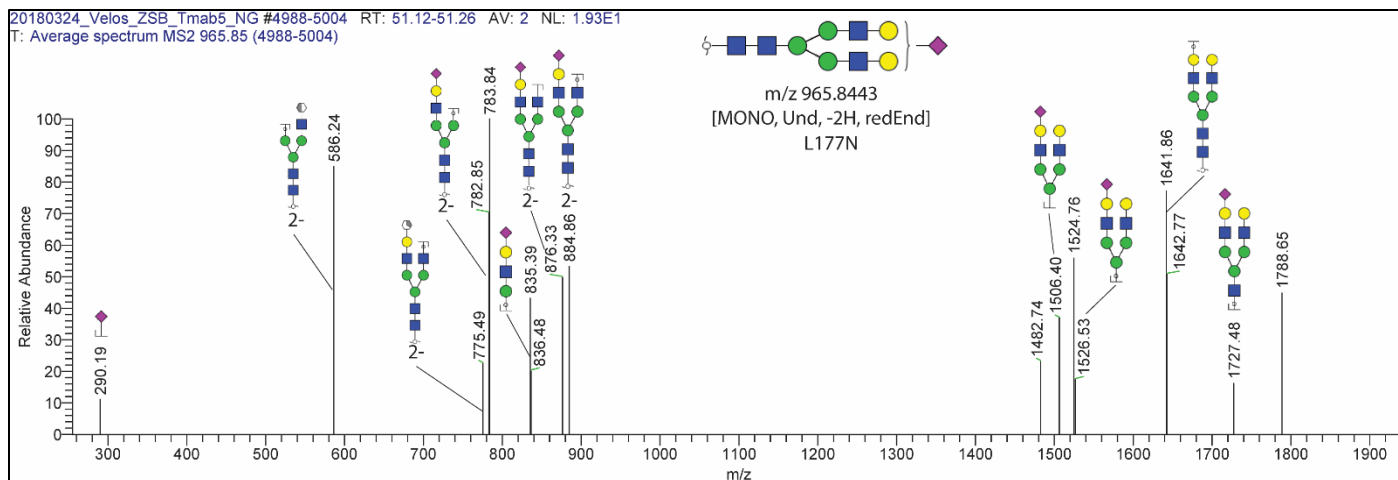
Figure S26. MS2 spectra of glycan 17 (table 4).
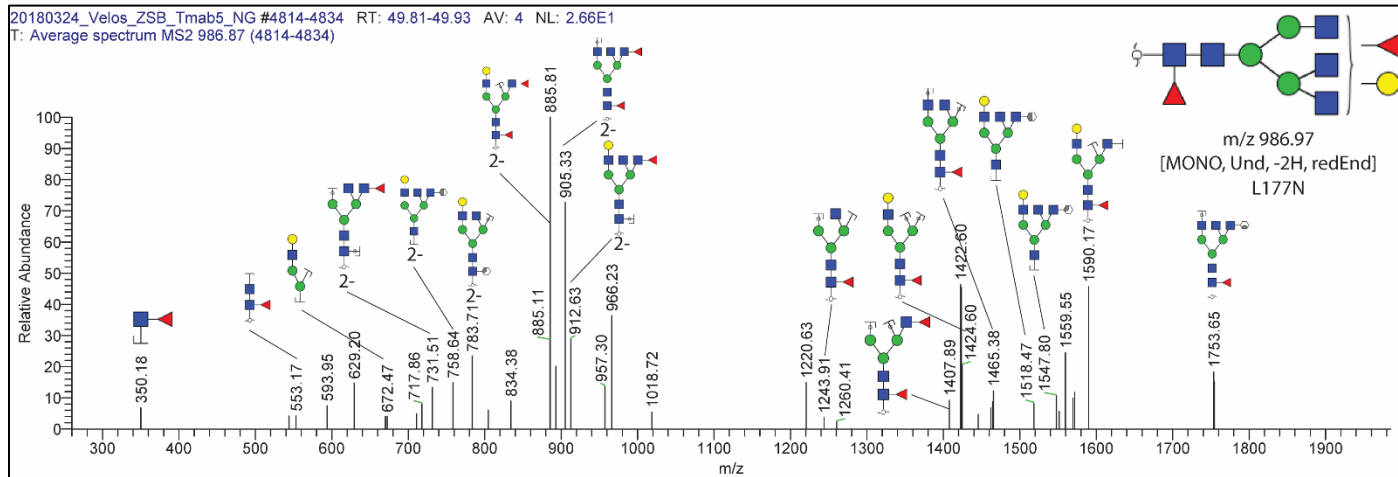
Figure S27. MS2 spectra of glycan 18 (table 4).
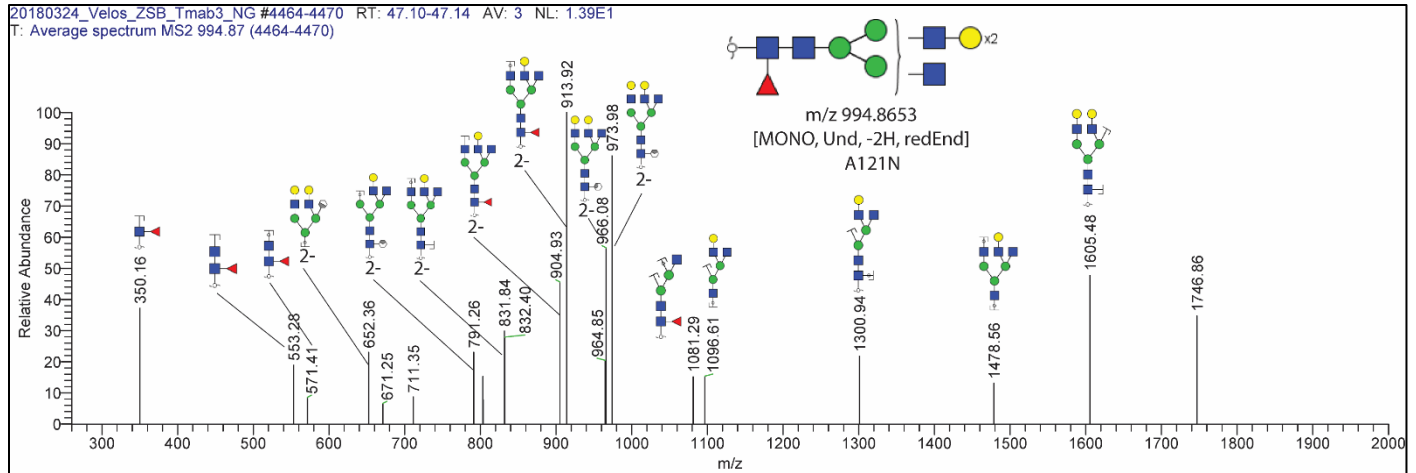
Figure S28. MS2 spectra of glycan 19 (table 4).
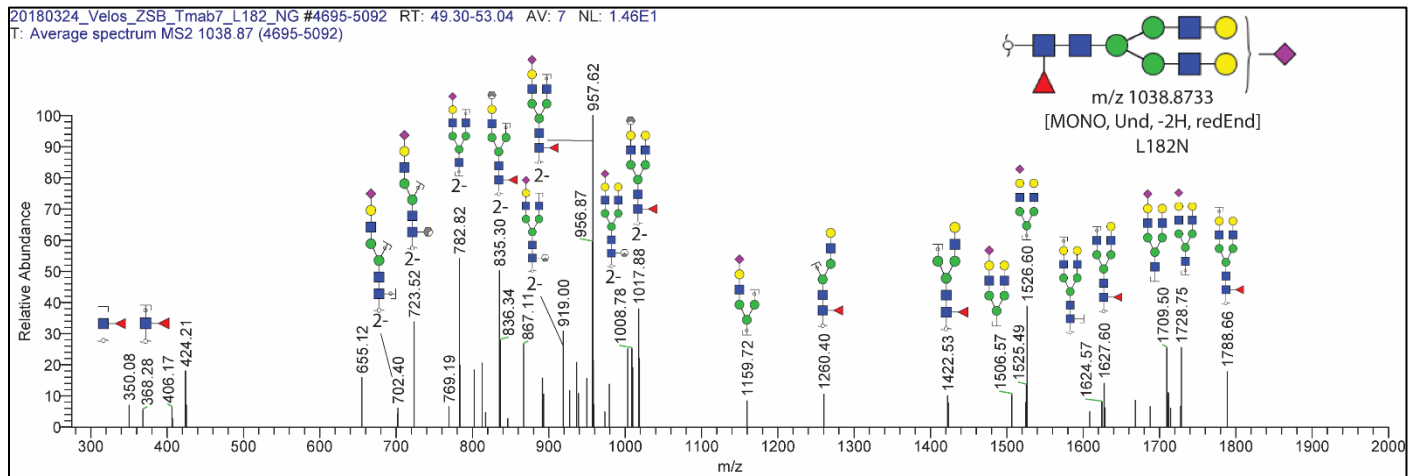
Figure S29. MS2 spectra of glycan 20 (table 4).
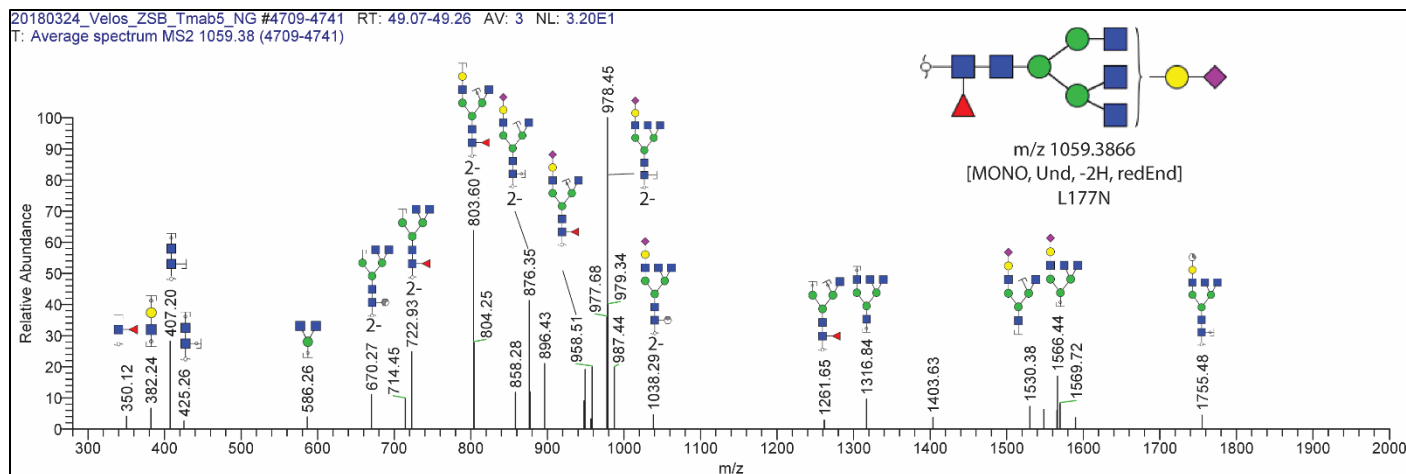
Figure S30. MS2 spectra of glycan 21 (table 4).

Glycopeptide spectra
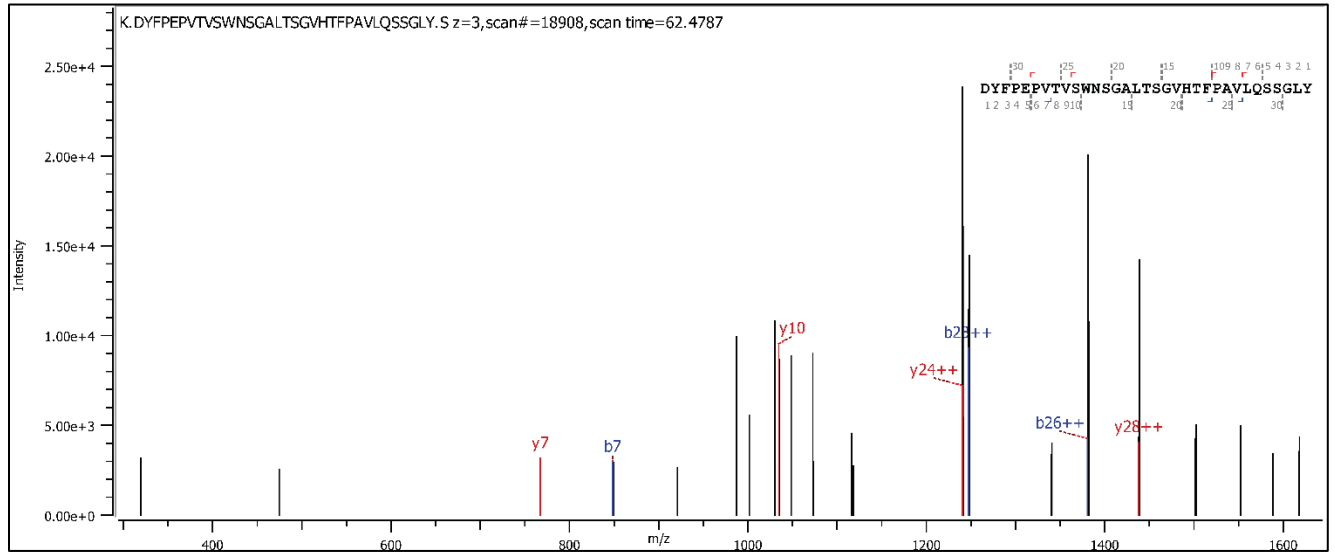
Figure S31. CID spectrum of the chymotryptic peptide DYFPEPVTVSWNSGALTSGVHTFPAVLQSSGLY from the L115N mutant containing amino acid positions 177, 178 and 182.
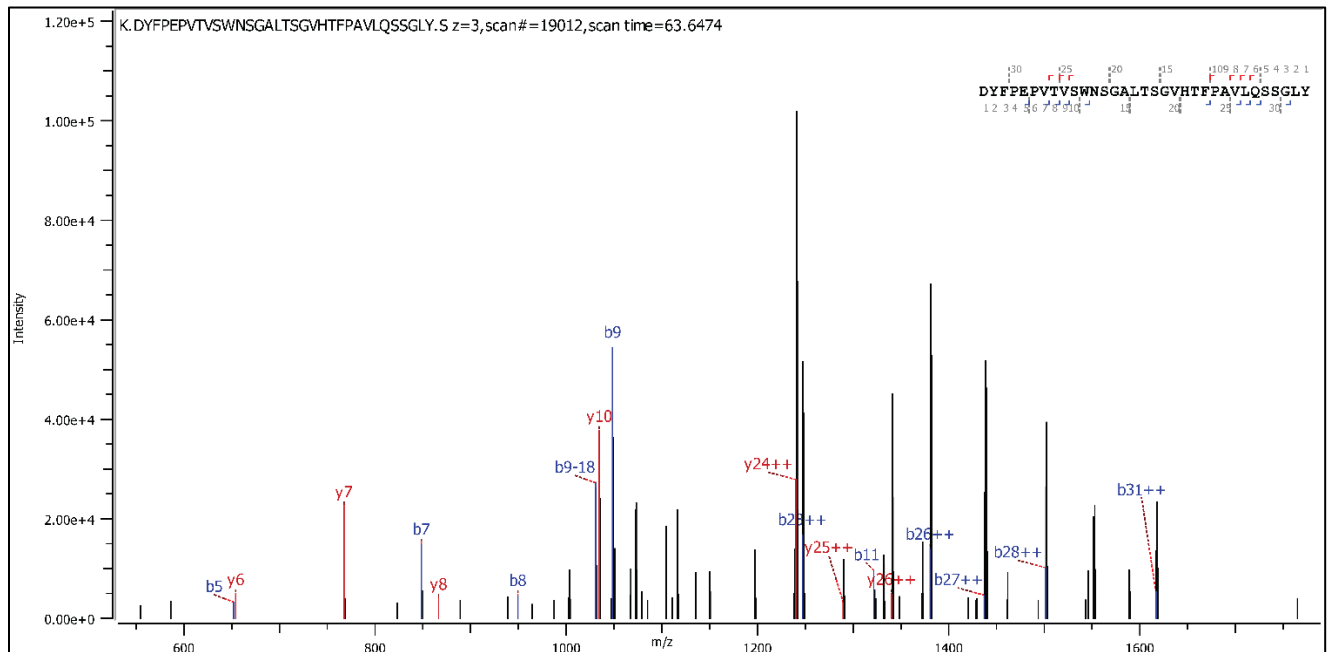
Figure S32. CID spectrum of the chymotryptic peptide DYFPEPVTVSWNSGALTSGVHTFPAVLQSSGLY from the A121N mutant amino acid positions 177, 178 and 182.
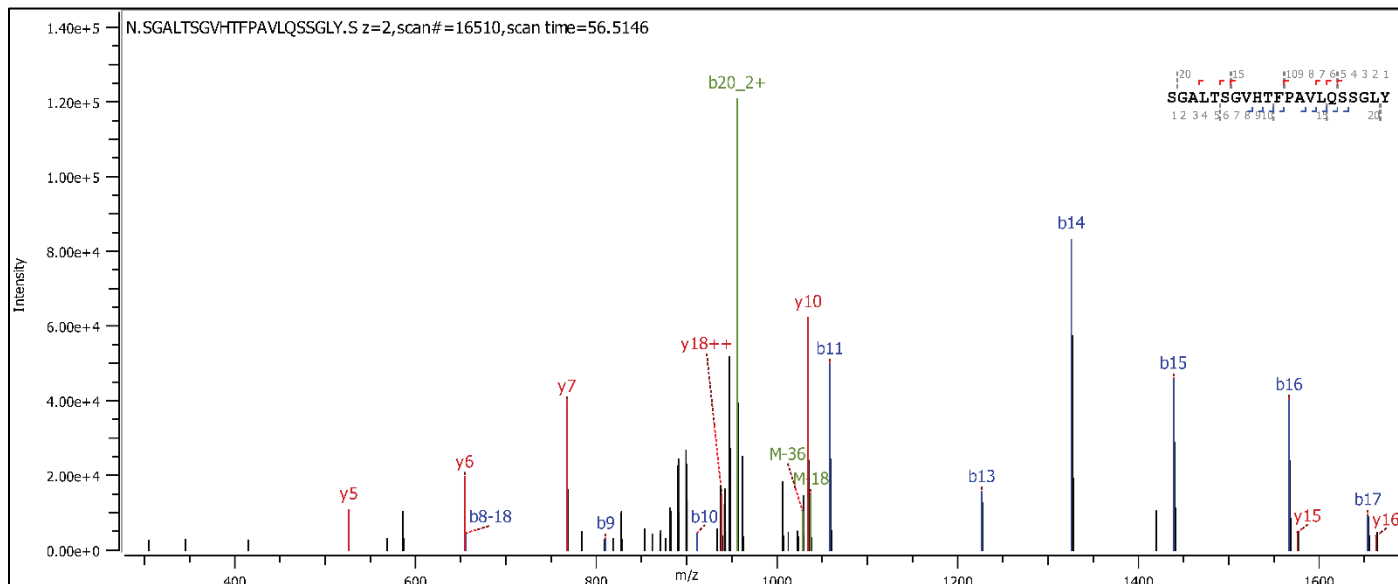
Figure S33. CID spectrum of the chymotryptic peptide SGALTSGVHTFPAVLQSSGLY from Tmab WT amino acid positions 177, 178 and 182.
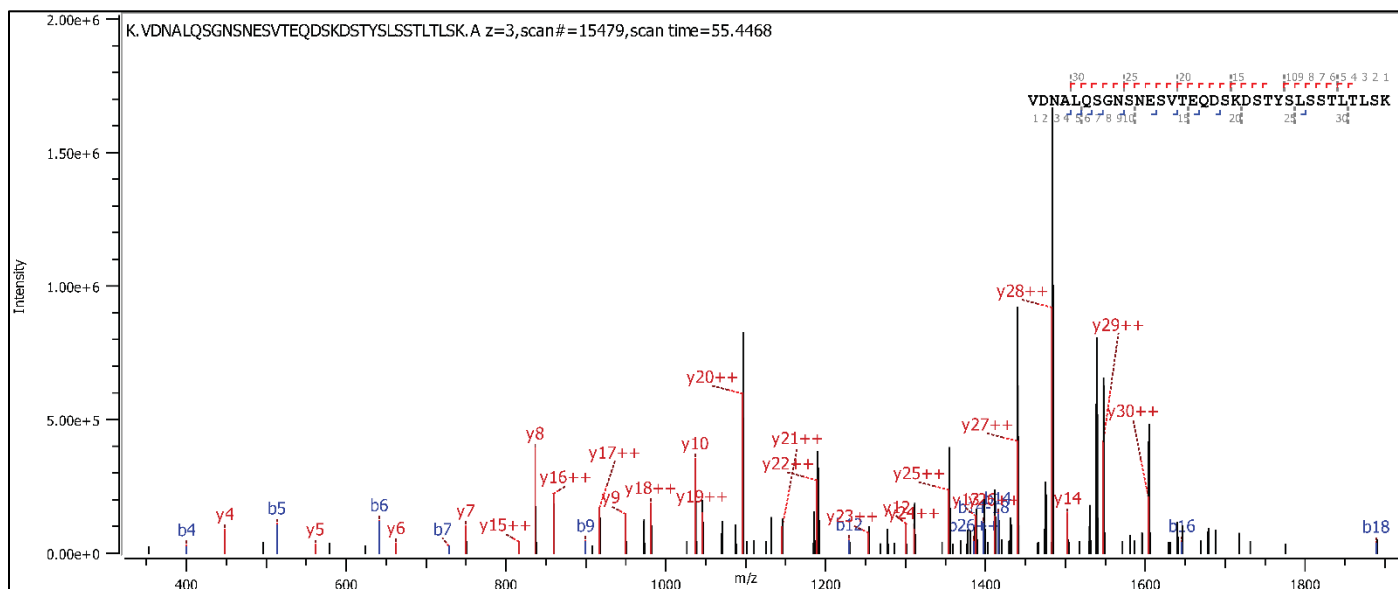
Figure S34. CID spectrum of the chymotryptic peptide VDNALQSGNSNESVTEQDSKDSTYSLSSTLTLSK from the Q160N mutant confirming the mutation at position 160.
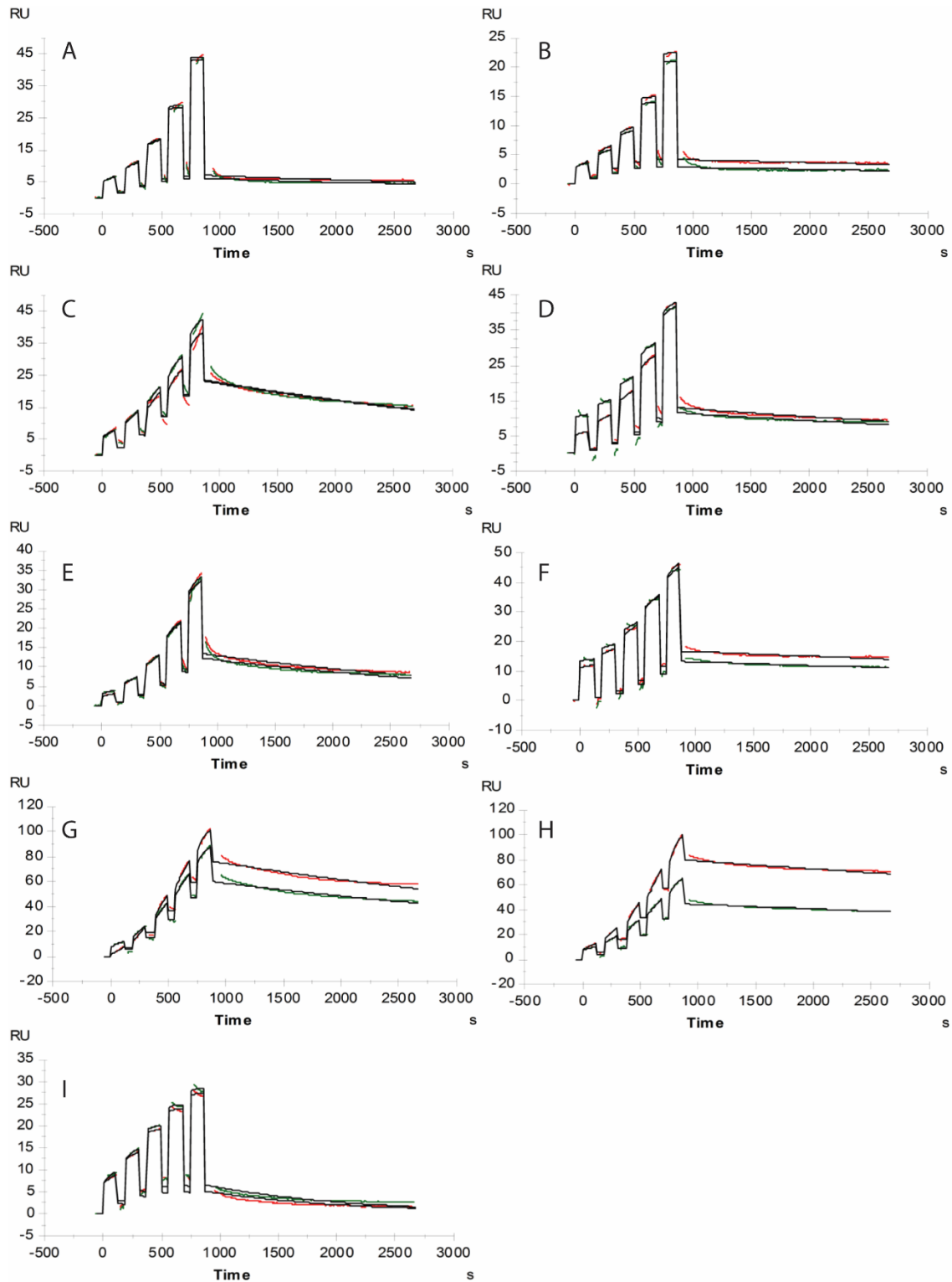
SPR sensorgrams
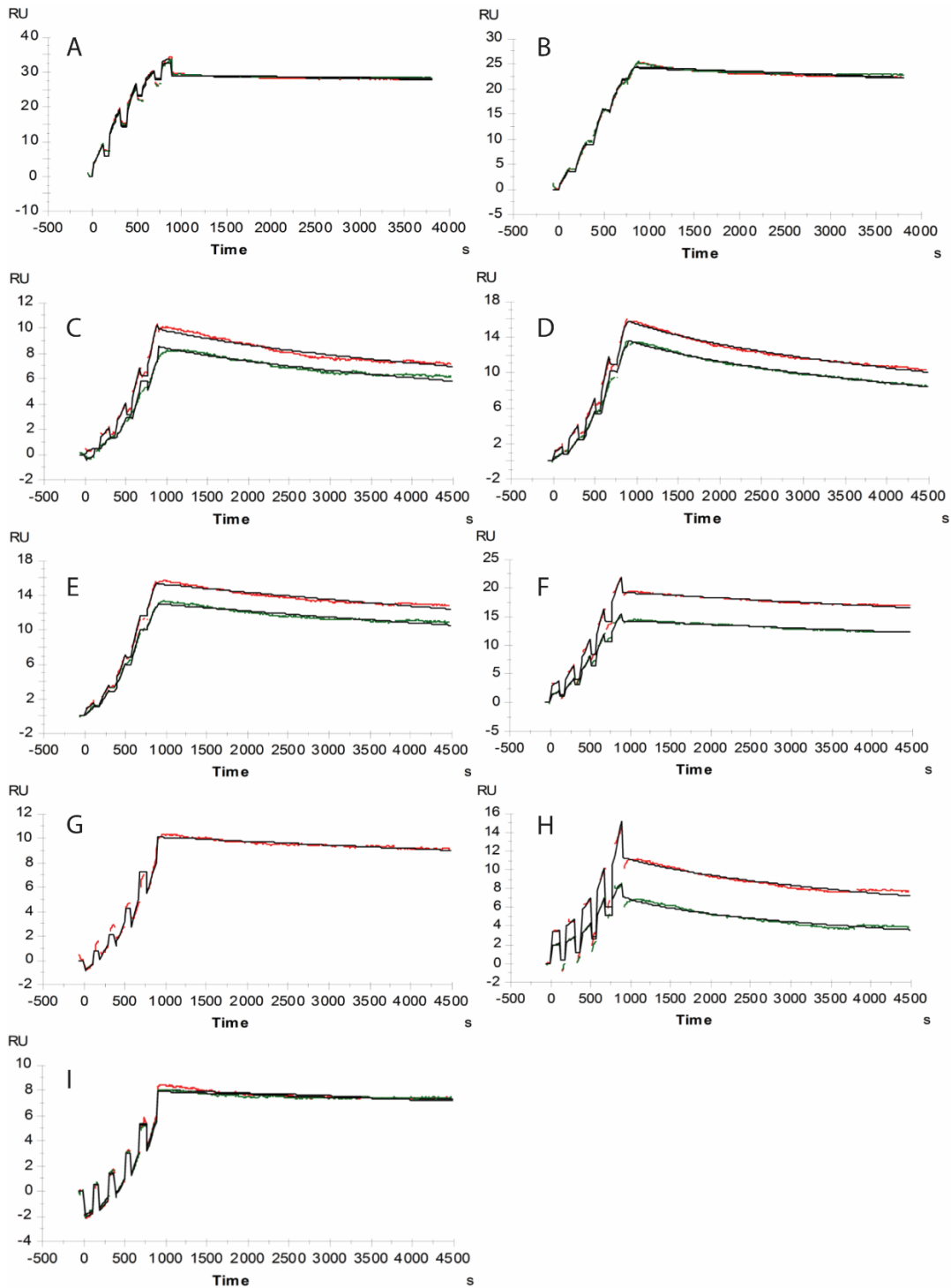
Figure S35. Analysed SPR sensorgrams of single cycle kinetic assays of Tmab variants to surface captured HER2. (A) Herceptin, (B) Tmab WT, (C) L115N, (D) A121N, (E) L177N, (F) Q178N, (G) L182N, (H) T198N, and (I) Q160N.
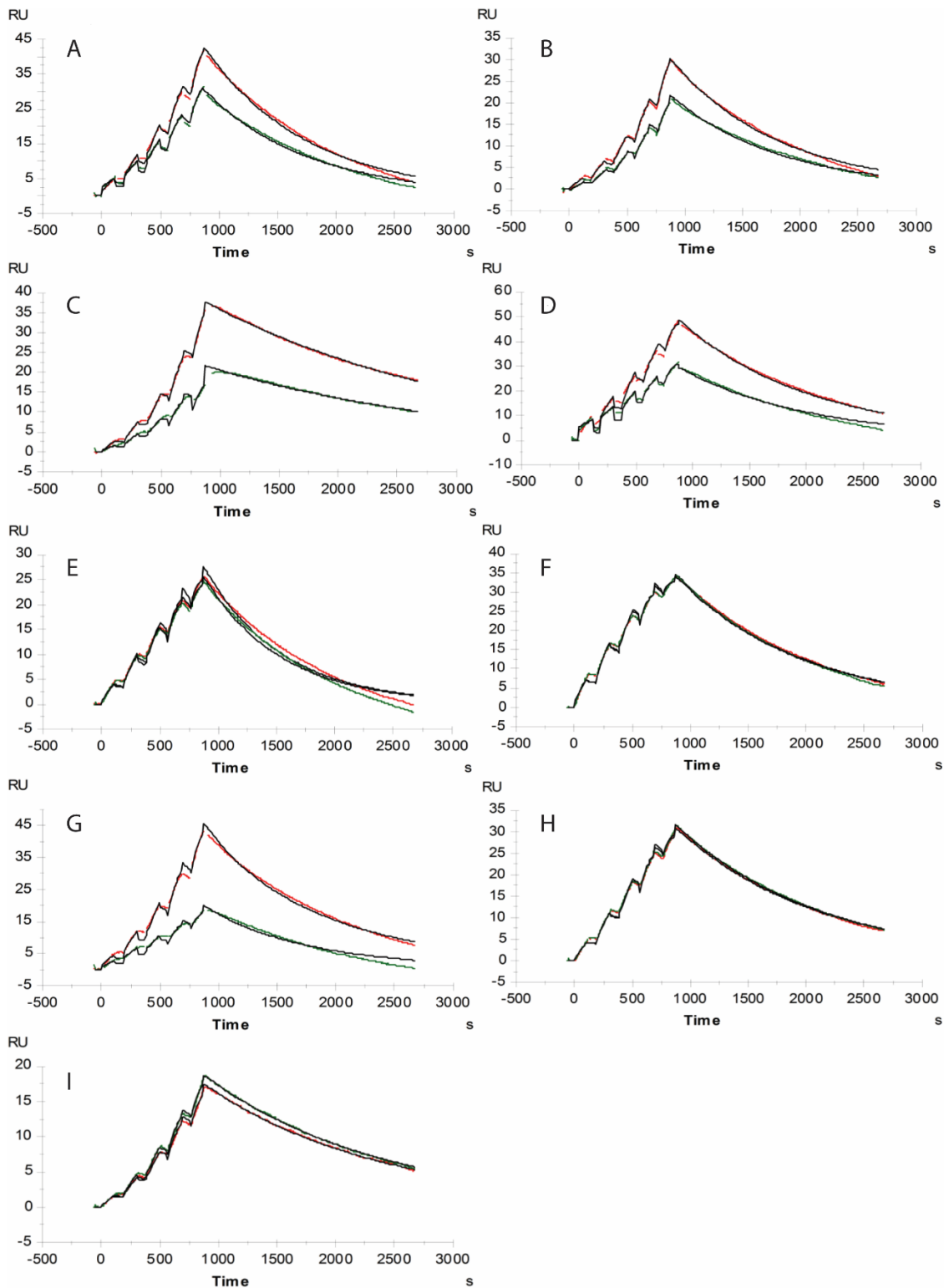
Figure S36. Analysed SPR sensorgrams of single cycle kinetic assays of Tmab variants to surface captured FcγR1A. (A) Herceptin, (B) Tmab WT, (C) L115N, (D) A121N, (E) L177N, (F) Q178N, (G) L182N, (H) T198N, and (I) Q160N.
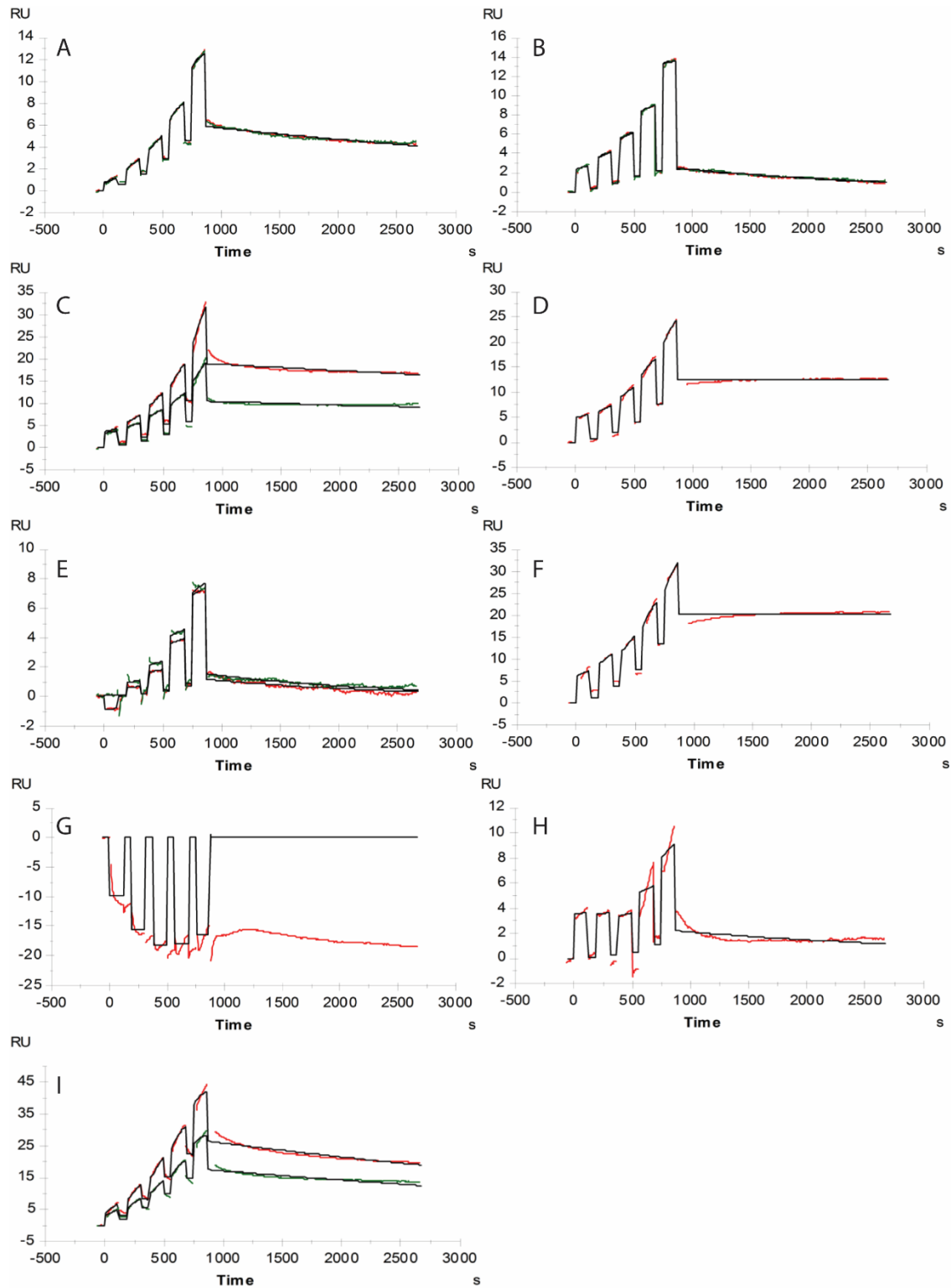
Figure S37. Analysed SPR sensorgrams of single cycle kinetic assays of Tmab variants to surface captured FcγR2A. (A) Herceptin, (B) Tmab WT, (C) L115N, (D) A121N, (E) L177N, (F) Q178N, (G) L182N, (H) T198N, and (I) Q160N.

Figure S38. Analysed SPR sensorgrams of single cycle kinetic assays of Tmab variants to surface captured FcγR3A. (A) Herceptin, (B) Tmab WT, (C) L115N, (D) A121N, (E) L177N, (F) Q178N, (G) L182N, (H) T198N, and (I) Q160N.
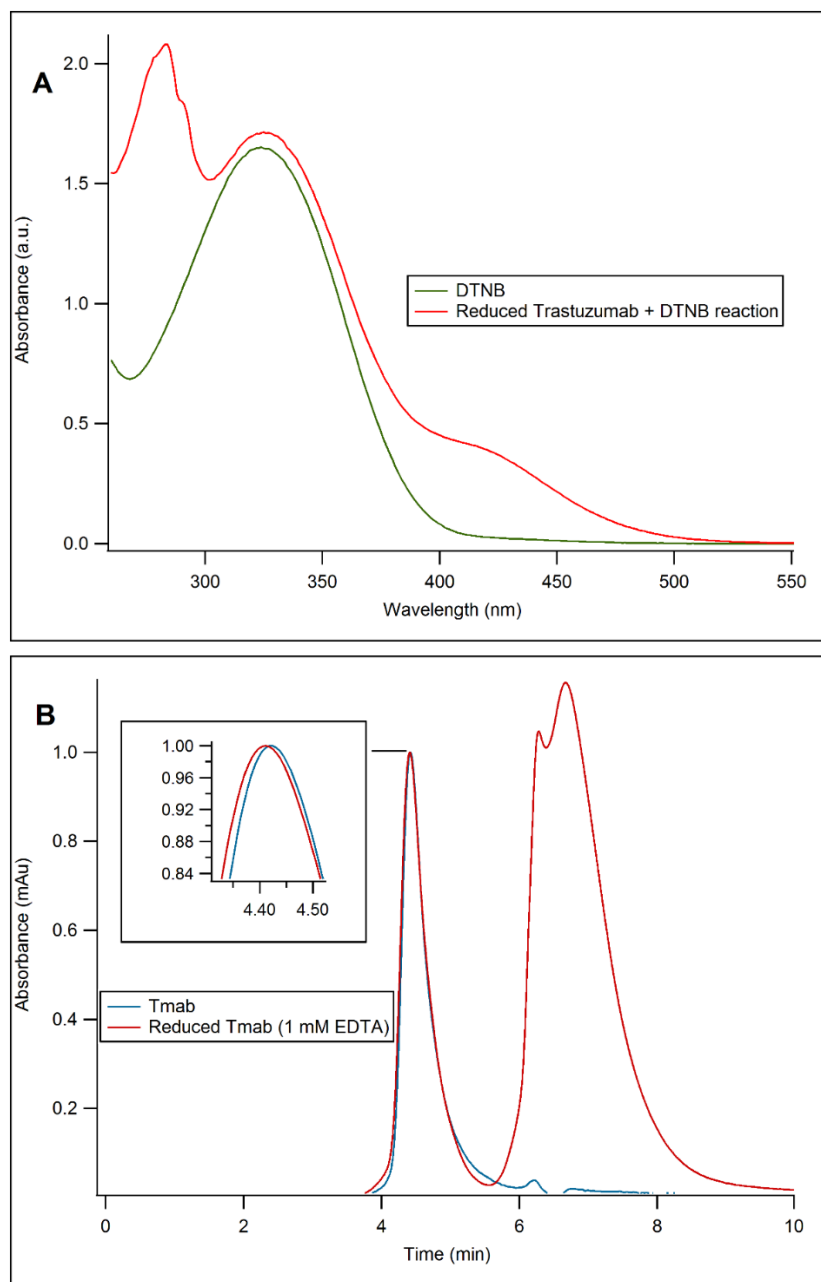
Figure S1. Analysis of the presence of sulfhydryl groups and conservation of intact structure of Trastuzumab after partial reduction with DTT. (A) UV-Vis spectra of Ellman's reagent (DTNB) and of partially reduced antibody after reaction with DTNB. (B) SE-HPLC chromatogram of intact Trastuzumab and reduced Trastuzumab.
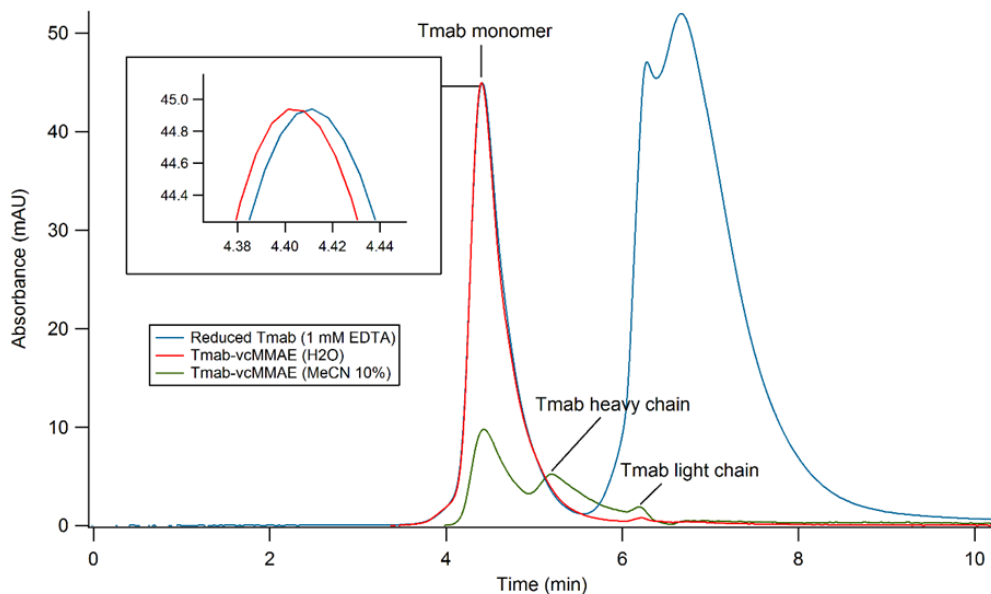
Figure S2. SE-HPLC chromatograms of partially reduced Trastuzumab in 1 mM EDTA, Tmab-vcMMAE in H2O and Tmab-vcMMAE in acetonitrile 10% with formic acid 1%.
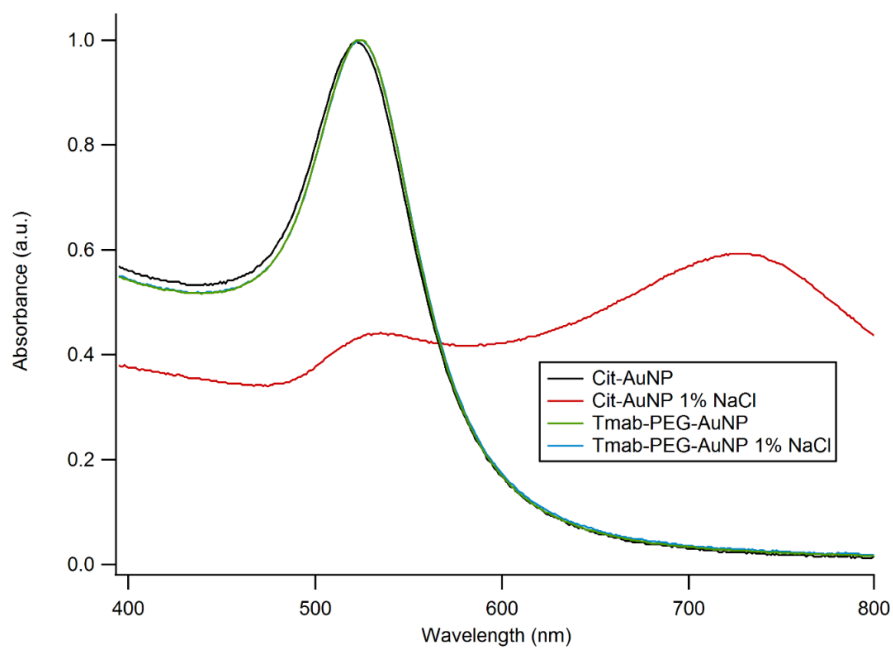
Figure S3. AuNP stability upon surface functionalization with Tmab-PEG-SH. Addition of 1% NaCl to citrate capped AuNPs caused aggregation as evidenced by a broad absorption band in the 700-800 nm range. Tmab-PEG-SH attachment prevented aggregation upon addition of NaCl.
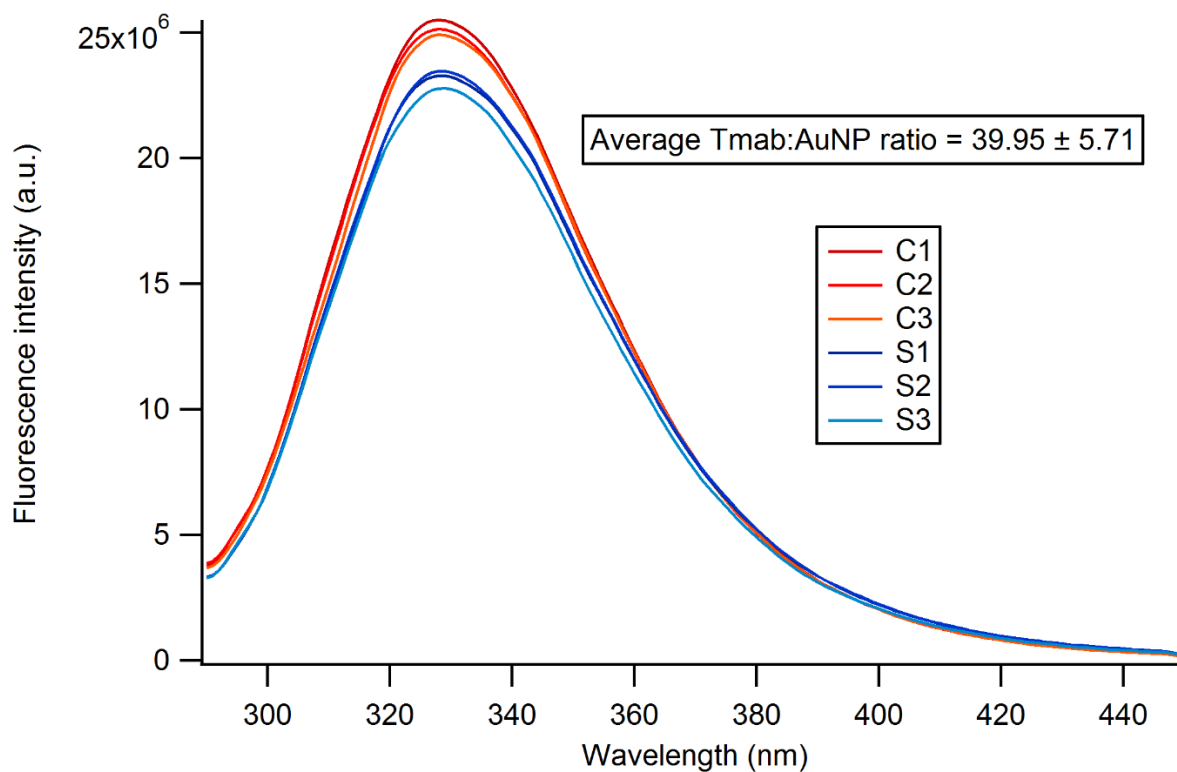
Figure S4. Representative tryptophan fluorescence emission spectra for the estimation of Trastuzumab:AuNP ratio for 20 nm AuNPs. The estimation is based on the loss of fluorescence intensity following AuNP surface attachment and centrifugation of the functionalized gold nanoparticles. The decrease in intensity is assumed to come from removal of the Trastuzumab monomers attached on AuNPs through nanoparticle sedimentation. C denotes controls and S the reacted samples. The ratio (R) is calculated as:
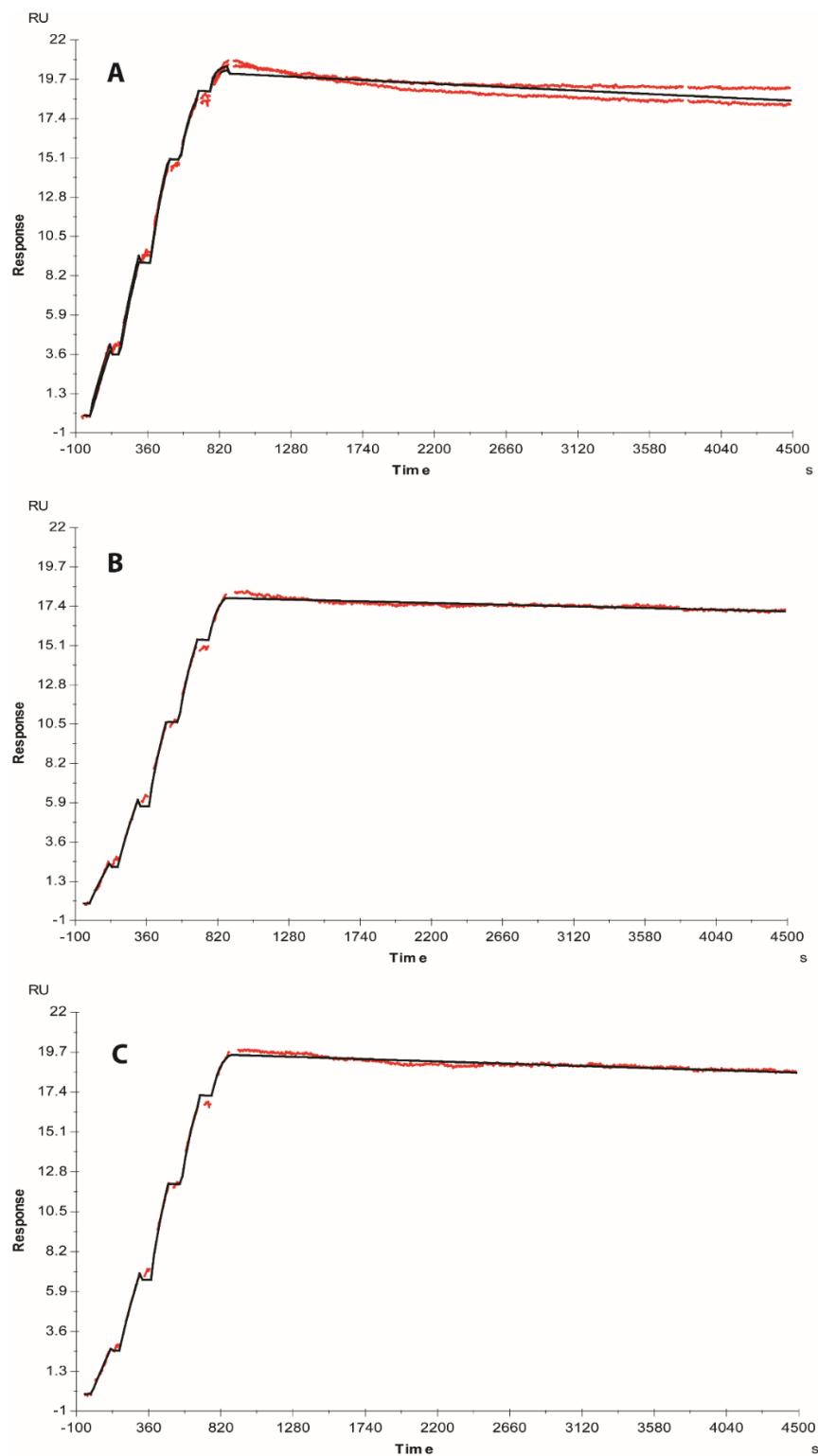
$$R = \left(1 - \frac{I_S}{I_0}\right) \times F$$

Where:

I_s = fluorescence intensity of the supernatant after AuNP removal by centrifugation post reaction

I_0 = fluorescence intensity of the control (identical original concentration of antibody as that in the reaction)

F = Tmab:AuNP molar ratio in the reaction

288

Figure S5. Representative sensorgrams of (A) Trastuzumab, (B) Tmab-PEG-SH 25X and (C) Tmab-vcMMAE binding to recombinant HER2 receptor. The sensorgram is shown in red and the derived 1:1 binding model fit in black.
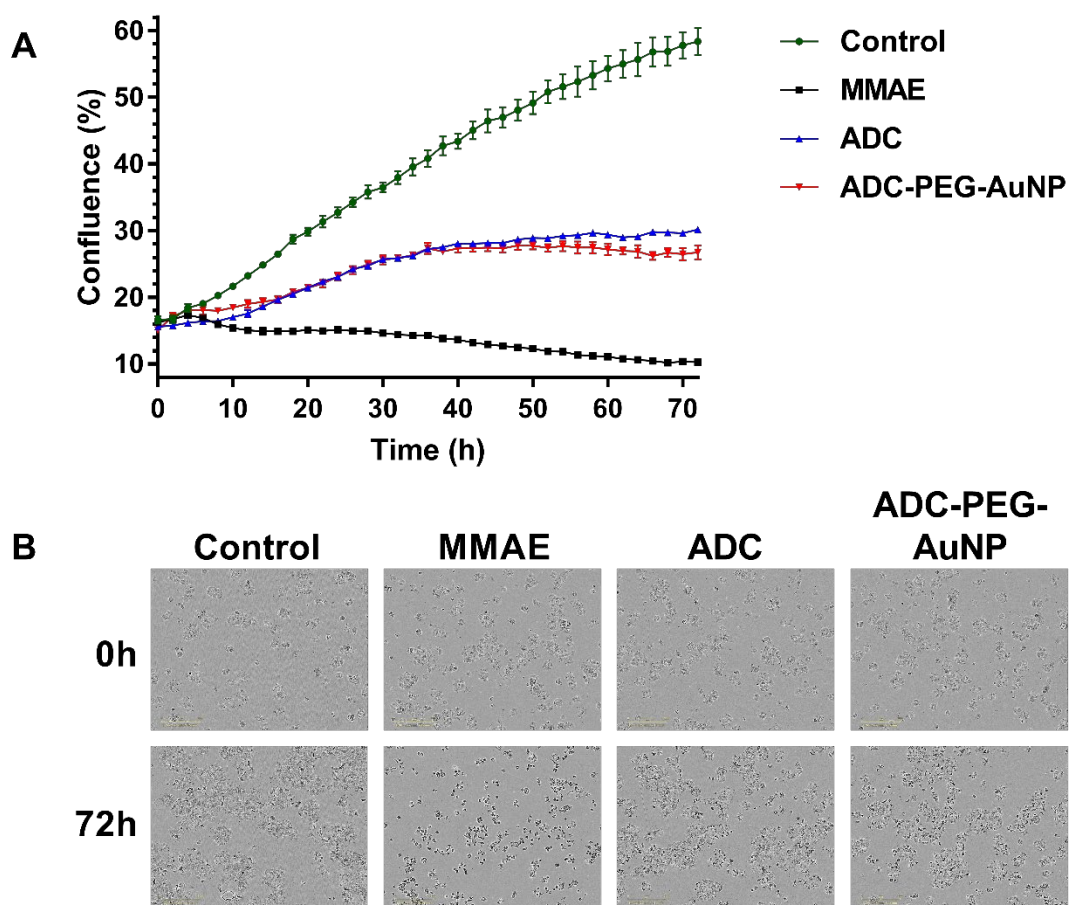
Figure S6. Representative SKBR-3 cell growth curves employed to analyse growth rate inhibition activity of MMAE-containing agents at equivalent MMAE concentrations. (A) Cell confluence change over time monitored every 2 hours. Data are reported as means ± SD. (B) Representative images of SKBR-3 cells obtained with the Incucyte® ZOOM Live-cell Analysis System showing decrease in confluence and morphological changes for MMAE treated cells.